
**Pre-Test Geological and
Geochemical Evaluation of the
Caprock, St. Peter Sandstone
and Formation Fluids
Yakley Field, Pike County,
Illinois**

March 1983

Prepared for
Pacific Northwest Laboratory
Underground Energy Storage Program
under Subcontract B-82313-A-O

Pacific Northwest Laboratory
Operated for the U.S. Department of Energy
by Battelle Memorial Institute



DISCLAIMER

This report was prepared as an account of work sponsored by an agency of the United States Government. Neither the United States Government nor any agency thereof, nor any of their employees, makes any warranty, express or implied, or assumes any legal liability or responsibility for the accuracy, completeness, or usefulness of any information, apparatus, product, or process disclosed, or represents that its use would not infringe privately owned rights. Reference herein to any specific commercial product, process, or service by trade name, trademark, manufacturer, or otherwise, does not necessarily constitute or imply its endorsement, recommendation, or favoring by the United States Government or any agency thereof. The views and opinions of authors expressed herein do not necessarily state or reflect those of the United States Government or any agency thereof.

PACIFIC NORTHWEST LABORATORY
operated by
BATTELLE
for the
UNITED STATES DEPARTMENT OF ENERGY
under Contract DE-AC06-76RLO 1830

Printed in the United States of America
Available from
National Technical Information Service
United States Department of Commerce
5285 Port Royal Road
Springfield, Virginia 22161

NTIS Price Codes
Microfiche A01

Printed Copy

Pages	Price Codes
001-025	A02
026-050	A03
051-075	A04
076-100	A05
101-125	A06
126-150	A07
151-175	A08
176-200	A09
201-225	A010
226-250	A011
251-275	A012
276-300	A013

PRE-TEST GEOLOGICAL AND GEOCHEMICAL
EVALUATION OF THE CAPROCK, ST. PETER
SANDSTONE AND FORMATION FLUIDS
YAKLEY FIELD, PIKE COUNTY, ILLINOIS

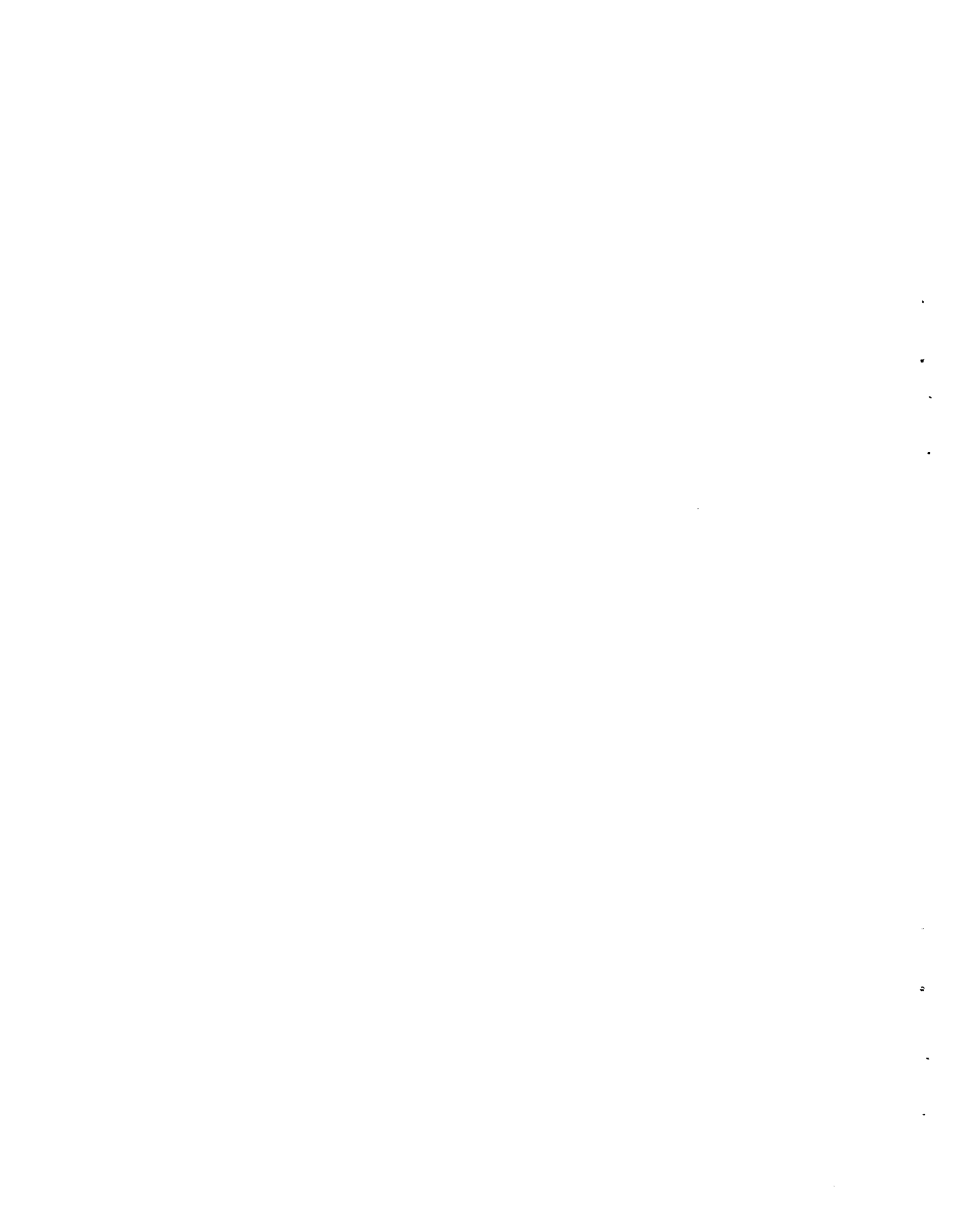
PB-KBB Inc.
Houston, Texas

David K. Davies and Associates

March 1983

Prepared for
Pacific Northwest Laboratory
Underground Energy Storage Program
under Subcontract B-82313-A-0

Pacific Northwest Laboratory
Richland, Washington 99352



PACIFIC NORTHWEST LABORATORY PERSPECTIVE

Compressed air energy storage (CAES) is a technique that transfers energy from off-peak to peak demand time for electric utility systems. It incorporates modified state-of-the-art gas turbines and underground reservoirs--aquifers, salt cavities, or mined hard rock caverns. The compressor and turbine sections of the gas turbine are alternately coupled to a motor/generator for operation during different time periods. During nocturnal and weekend off-peak periods, base load plants not using petroleum fuels provide energy to compress air, which is stored in the underground reservoirs. During the subsequent diurnal peak-load periods, the compressed air is withdrawn from storage, mixed with fuel, combusted and then expanded through the turbines to generate peak power. Because the turbine is not required to drive a compressor, this concept reduces peaking plant consumption of petroleum fuel by more than 60%. Some second-generation CAES concepts require no petroleum fuels.

Since 1975, the Pacific Northwest Laboratory (PNL) has served as the U.S. Department of Energy's lead laboratory in managing research and development efforts to support CAES technology commercialization.

A substantial part of the CAES Technology Projects is represented by the Reservoir Stability Studies. The goal of these studies is to ensure long-term stable containment of air in the underground reservoirs used in conjunction with CAES plants. The specific objective is to develop stability criteria and engineering guidelines for designing CAES reservoirs in each of the three major reservoir types, including aquifers, salt cavities, and mined hard rock caverns. Such information is essential to gain utility confidence in CAES as a viable alternative to conventional electric energy production techniques.

Three parallel studies have been performed. Each contained a survey of the state-of-the-art and numerical and experimental studies. The mined hard rock and salt studies were completed and final criteria documents have been issued. The aquifer study has also been completed as a generic study, but has been extended to include a specific field experiment, the Pittsfield Aquifer Test.

This document covers work performed in support of that field study. It was conducted by David K. Davies and Associates as a second tier subcontractor to PNL. The primary field study contractor to PNL, PB-KBB, Inc. of Houston, Texas, was responsible for design, construction, and operation of the Pittsfield Aquifer Test. Davies and Associates' analyses sought to characterize the geologic nature of porous media constituents native to the aquifer field test site near Pittsfield, Illinois. Davies subjected the geologic samples to geochemical evaluations to determine anticipated responses to cyclic air injection, heating and moisture--conditions typical of an operating CAES reservoir. This report documents the procedures used and results obtained from these analyses.

The information presented herein will be used, in conjunction with results of actual field tests and other data, as the basis for the porous media reservoir stability criteria. An interim version of this criteria and guidelines document will be issued by PNL in 1983.

T. J. Doherty
Compressed Air Energy Storage
Project
Pacific Northwest Laboratory

SUMMARY

Rock Characteristics -

The Platteville and Joachim Formations comprise the caprock in the Yakley Well Field. The Platteville Formation is a fine-grained limestone which contains thin illitic shale laminations and becomes dolomitic toward the contact with the Joachim Formation. The Joachim Formation is primarily fine-grained dolomite. Fine fraction X-ray diffraction analysis indicates that the dolomite is either ferroan or ankerite. Ankerite is a calcium-magnesium carbonate which contains a specific amount of iron in its structure.

Illite, calcite, anhydrite, pyrite, and marcasite are also present in variable quantities. The Joachim contains large open or filled vugs. Some portions are extensively fractured. Vugs and fractures are generally filled by calcite and minor amounts of galena, sphalerite, and pyrite or marcasite. Scanning electron microscope examination reveals that abundant intercrystalline pore spaces are present in the Joachim. These pores, however, are generally not interconnected, an observation which accounts for the relatively high porosities (maximum of 36%) and low permeabilities (0.03-71 md) of samples tested.

Triaxial compressive strengths under a 1000 p.s.i. confining pressure vary from 2813-17083 lb/in² and unconfined uniaxial compressive strengths vary from 3215 to 10880 lb/in². These data indicate that the Joachim Formation can withstand additional pressures to which it will be subjected during air injection and cycling. Those samples with open vugs and open vertical fractures failed under substantially lower loads than did samples of compact dolomite or limestone. Sandy dolomite samples, representative of the Joachim-St. Peter transition zone, exhibited uniaxial compressive strengths of 2140 and 2790 lb/in². These strengths, however, do not represent in situ conditions since no confining pressures were applied to the samples. The in situ strength should be greater since uniaxial testing provides data concerning minimum threshold pressures for failure.

The green St. Peter Sandstone is poorly to moderately well sorted, medium to coarse-grained (average grain diameter of the coarse mode=0.44 to 0.63 mm), and the quartz grain size is bimodally distributed. The sand is texturally immature due

to the presence of abundant fine grained detrital matrix (Tr-27%), which was co-deposited with quartz (73-86%). The fabric is variable. Quartz grains exhibit concavo-convex or point contacts and occasionally grains appear to "float" in the matrix. Fine fraction X-ray diffraction analysis reveals that illite (4-32%) occurs in all samples. Potassium feldspar (0-27%) is absent in only one sample. Calcite, marcasite, sericite, pyrite, ankerite, and anhydrite occur sporadically in samples analyzed. Barite (3%) was detected in the fine fraction of the sample from Well G. This is a new mineral phase, previously undetected, which may have formed as a result of extensive drilling in the Yakley Field. SEM examination reveals that most of the illite occurs as laminated clay (detrital clay matrix). Potassium feldspar is generally present as an authigenic precipitate on quartz grains and within the pore system. Marcasite and pyrite are distributed unevenly in the pore system. Porosities of green sand samples vary from 10.0 to 23.0%. Horizontal permeabilities vary from 2.08 to 6098 md, and vertical permeabilities vary from 0.93 to 3890 md. The permeability of the green sand appears to be controlled by depositional matrix which is laminated in a horizontal fashion. Thus, vertical permeabilities are less than horizontal permeabilities. One green sand sample was subjected to uniaxial compressive strength testing. The strength at failure of 1170 p.s.i. is the minimum of all samples tested but is not representative of in situ conditions as discussed above.

The white St. Peter Sandstone is medium grained (0.37-0.45 mm = average grain diameter) and is moderately to well sorted. The sand is texturally mature, and quartz grains exhibit concavo-convex or point contacts. Vertical fractures in the white sand are either open or are infilled by calcite. The white sand is composed dominantly of monocrystalline quartz (85-87%) and cemented by silica. Detrital clay matrix was detected in one sample. Fine fraction X-ray diffraction analysis shows that illite (17-59%) and potassium feldspar (3-17%) occur with quartz in all samples analyzed. Other mineral phases detected sporadically include marcasite, pyrite, and anhydrite. SEM examination reveals that the illite detected by X-ray diffraction analysis occurs as fibers which bridge pore throats and partially occlude porosity. The porosity of the white sand ranges from 9.7 to 20.9%. The horizontal permeability varies from 13 to 5248 md, and the vertical permeability varies from 78 to 2866 md. Permeability variations are controlled by cementation patterns with poorly cemented samples exhibiting greater permeabilities than well cemented samples. One sample was subjected to uniaxial compressive strength testing. The strength at failure was 5880 p.s.i.

The gray St. Peter Sandstone is medium grained (average grain diameter = 0.37 mm) and is moderately well sorted. The sand is texturally mature with individual grains exhibiting, generally, concavo-convex contacts. The dominant detrital grain is monocrystalline quartz (87%), and quartz grains are cemented by authigenic clay and pyrite. Gray sand samples are frequently "streaked" due to differential groundwater percolation, and some samples contain subvertical, planar fractures at high angles to the core. Fine fraction X-ray diffraction analysis indicates that, in addition to quartz, illite, pyrite, sericite, dolomite, anhydrite, and kaolinite occur in the gray sand. SEM examination reveals that illite is present in the fibrous and more compact forms and that pyrite is distributed throughout the pore system. The porosity of gray sand samples varies from 14.2 to 17.7%. Vertical permeabilities vary from 78 to 417 md. One horizontal permeability measurement (31 md) indicates that vertical permeabilities are greater than horizontal permeabilities. No samples were subjected to compressive strength testing.

Thermal Testing -

Spalling of detrital clay matrix from the surface of quartz grains is the most obvious effect of heating samples for various lengths of time and under pressure. Hand specimen examination of plugs which were heated under pressure reveals that, in some instances, pyrite has been altered to hematite and free sulfur.

Geochemical Evaluation -

The following conclusions may be drawn from the geochemical evaluation:

1. Water Quality

- a. Galena Formation water is slightly alkaline and is saturated with respect to calcite, dolomite, pyrolusite, and manganese hydroxide.
- b. St. Peter Formation water is slightly alkaline.
- c. The level of total dissolved solids, sulfate, and chloride found in the St. Peter Formation water exceeds maximum mandatory concentration limits set by the U.S. Public Health Service for drinking water.

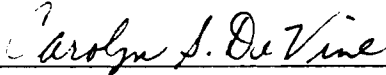
- d. St. Peter Formation waters are saturated with respect to aragonite, barite, calcite, dolomite, iron hydroxides, fluorapatite, hematite, magnesite, magnetite, manganese hydroxides, pyrolusite, and quartz. These phases are likely to precipitate from the water.

2. Effect of Air Injection on St. Peter Water

- a. Species in a reduced or partially reduced state (Fe^{2+} , Mn^{2+} , and Mn^{3+}) will be oxidized and will form insoluble residues (hydroxides or oxides).
- b. Carbon dioxide gas (CO_2) will be evolved from the formation water, and the pH will rise, shifting the water into the carbonate (CO_3^{2-}) stability field. The probability for the precipitation of carbonate mineral phase will be enhanced.

3. Effect of Air Injection on St. Peter Minerals

- a. Quartz (SiO_2) will not chemically react with air; however, in the presence of warm, humid air, and, if the pH of residual formation water rises above 9, some dissolution of quartz may occur. This effect should be greatest at the air-water interface but should be relatively insignificant.
- b. Pyrite and marcasite (FeS_2) will be oxidized. Sulfate ions and either hematite, iron (III) hydroxide ($\text{Fe}(\text{OH})_3$), or iron hydroxyoxide ($\text{FeO}(\text{OH})$) will be produced.
- c. Detrital and authigenic illite may be recrystallized.



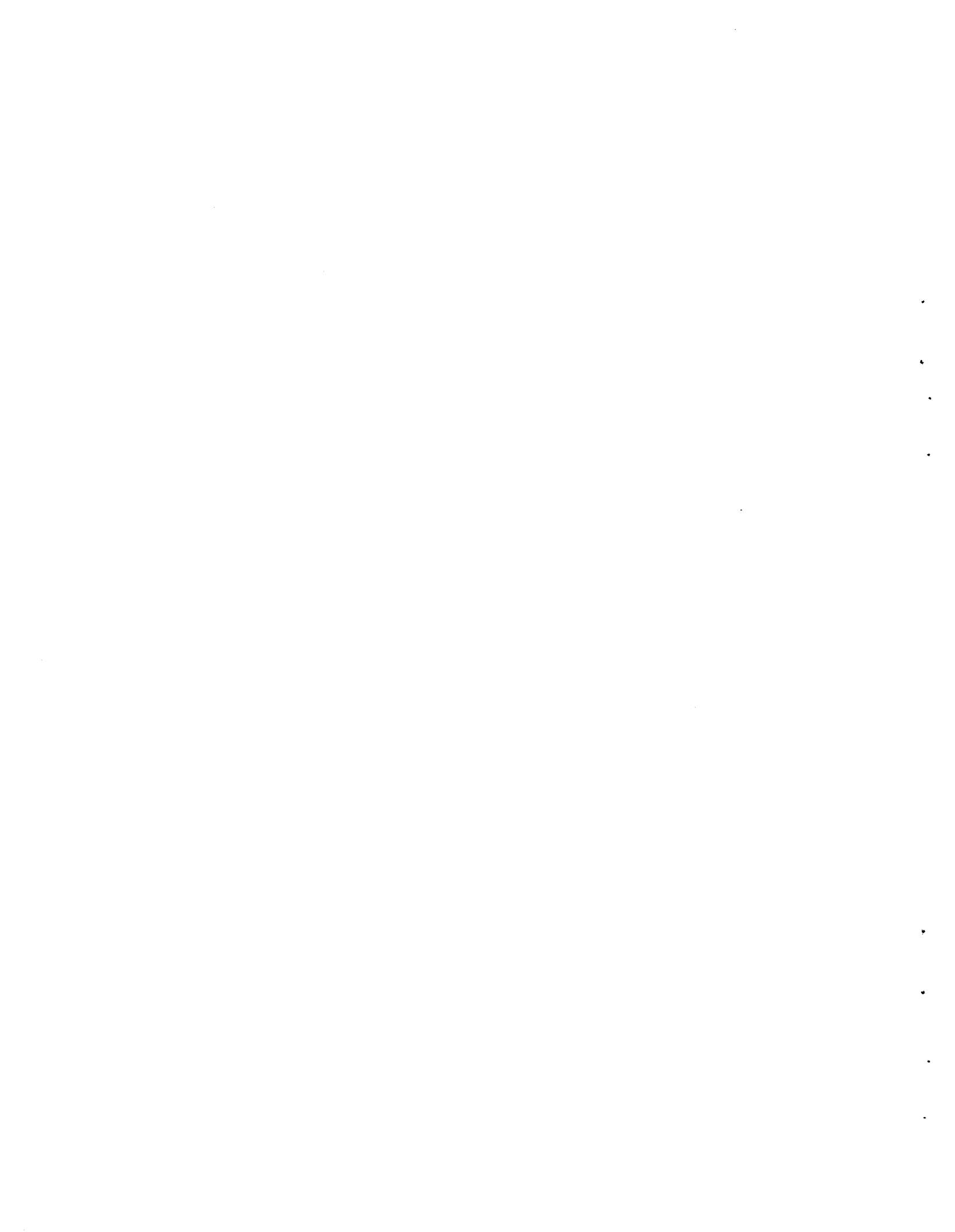
Carolyn S. DeVine
Senior Geologist



David K. Davies, Ph.D
President
Certified Professional
Geologist No. 4188

CONTENTS

FOREWORD.	iii
SUMMARY	v
FIGURES	xi
TABLES.	xv
INTRODUCTION.	1
SECTION I - CHARACTERISTICS OF CAPROCKS (JOACHIM AND PLATTIN FORMATIONS), THE JOACHIM-ST. PETER TRANSITION ZONE, AND THE UPPER ST. PETER SANDSTONE	I-1
CORE EXAMINATION	I-1
COMPOSITION AND TEXTURE.	I-13
SELECTED PHOTOMICROGRAPHS.	I-22
X-RAY DIFFRACTION ANALYSIS	I-50
SCANNING ELECTRON MICROSCOPY	I-56
COMPARATIVE CHARACTERISTICS OF THE GREEN, WHITE, AND MEDIUM TO DARK GRAY ST. PETER SANDSTONE.	I-78
SECTION II - POROSITY AND PERMEABILITY.	II-1
SECTION III - MECHANICAL STRENGTH	III-1
SECTION IV - THERMAL TESTING.	IV-1
SELECTED PHOTOMICROGRAPHS.	IV-17
SECTION V - GEOCHEMICAL EVALUATION.	V-1
POTENTIAL EFFECTS OF THE INJECTION OF WARM, HUMID AIR ON MINERAL PHASES PRESENT IN THE ST. PETER SANDSTONE.	V-15
CONCLUSIONS.	V-16
SECTION VI - SUGGESTIONS FOR POST-TEST ANALYSIS	VI-1
APPENDIX - MECHANICAL STRENGTH.	A-1



FIGURES

1	Location Map Illustrating Positions of Cored Wells Studied in the Yakley Field Near Pittsfield, Illinois.	2
2	Ternary Rock Classification Scheme.	11
I-1	Slabbed Core Specimen, Joachim Formation.	I-4
I-2	Slabbed Core Specimen, Joachim-St. Peter Transition.	I-8
I-3	Slabbed Core Specimen, St. Peter Sandstone (White)	I-10
I-4	Slabbed Core Specimen, St. Peter Sandstone (Gray).	I-11
I-5	Generalized Lithologic Column, Yakley Well Field	I-12
I-6	Joachim Dolomite Formation Features	I-22
I-7	Joachim-St. Peter Transition Formation Features.	I-24
I-8	Joachim-St. Peter Transition Formation Features.	I-26
I-9	Joachim-St. Peter Transition Formation Features.	I-28
I-10	Uppermost Greet St. Peter, Lowermost Transition Formation Features	I-30
I-11	Green St. Peter Sandstone Formation Features.	I-32
I-12	Green St. Peter Sandstone Formation Features.	I-34
I-13	Green St. Peter Sandstone Formation Features.	I-36
I-14	Green St. Peter Sandstone Formation Features.	I-38
I-15	White St. Peter Sandstone Formation Features.	I-40

I-16	White St. Peter Sandstone Formation Features.	I-42
I-17	White St. Peter Sandstone Formation Features.	I-44
I-18	White St. Peter Sandstone Formation Features.	I-46
I-19	Dark Gray St. Peter Sandstone Formation Features.	I-48
I-20	Joachim Dolomite Pore Fill Minerals and Microporosity	I-58
I-21	Joachim Dolomite Pore Fill Minerals and Microporosity	I-60
I-22	Joachim Dolomite Pore Fill Minerals and Microporosity	I-62
I-23	Joachim-St. Peter Transition Pore Fill Minerals and Microporosity.	I-64
I-24	Green St. Peter Sandstone Pore Fill Minerals and Microporosity.	I-66
I-25	Green St. Peter Sandstone Pore Fill Minerals and Microporosity.	I-68
I-26	Green St. Peter Sandstone Pore Fill Minerals and Microporosity.	I-70
I-27	Green St. Peter Sandstone Pore Fill Minerals and Microporosity.	I-72
I-28	White St. Peter Sandstone Pore Fill Minerals and Microporosity	I-74
I-29	Dark Gray St. Peter Sandstone Pore Fill Minerals and Microporosity.	I-76
II-1	Porosity-Permeability Cross-Plot, Caprock Samples	II-5
II-2	Caprock Permeabilities Plotted as a Function of Distance Above the Joachim-St. Peter Contact. .	II-6
II-3	Porosity-Permeability Cross-Plot of Measured Values for the Joachim-St. Peter Transition . .	II-8

II-4	Porosity-Permeability Cross-Plot of Measured Values for the Green St. Peter Sandstone. . . .	II-10
II-5	Porosity-Permeability Cross-Plot of Measured Values for the White St. Peter Sandstone. . . .	II-12
II-6	Porosity-Permeability Cross-Plot of Measured Values for the Gray St. Peter Sandstone	II-14
III-1	Caprock Specimens Subjected to Triaxial Compressive Strength Testing.	III-4
III-2	Triaxial Compressive Strength Test Arrangement	III-8
III-3	Caprock, Transition Zone and St. Peter Sandstone Samples Subjected to Uniaxial Compressive Strength Testing.	III-10
IV-1	Effect of Heating Joachim-St. Peter Transition Formation Sample.	IV-18
IV-2	Effect of Heating Green St. Peter Formation Sample.	IV-20
IV-3	Effect of Heating Green St. Peter Formation Sample.	IV-22
IV-4	Effect of Heating Green St. Peter Formation Sample.	IV-24
IV-5	Effect of Heating Green St. Peter Formation Sample.	IV-26
IV-6	Transition Zone Formation SEM Examination	IV-30
IV-7	Transition Zone Formation SEM Examination	IV-32
IV-8	Green St. Peter Sandstone SEM Examination	IV-34
IV-9	Green St. Peter Sandstone SEM Examination	IV-36
IV-10	Green St. Peter Sandstone SEM Examination	IV-38
IV-11	Green St. Peter Sandstone SEM Examination	IV-40
IV-12	Green St. Peter Sandstone SEM Examination	IV-42
IV-13	Green St. Peter Sandstone SEM Examination	IV-44
IV-14	White St. Peter Sandstone SEM Examination	IV-46

IV-15	White St. Peter Sandstone SEM Examination . . .	IV-48
IV-16	White St. Peter Sandstone SEM Examination . . .	IV-50
IV-17	White St. Peter Sandstone SEM Examination . . .	IV-52
IV-18	White St. Peter Sandstone SEM Examination . . .	IV-54
IV-19	White St. Peter Sandstone SEM Examination . . .	IV-56
IV-20	Green St. Peter Sandstone SEM Examination . . .	IV-58
IV-21	Green St. Peter Sandstone SEM Examination . . .	IV-60
IV-22	Green St. Peter Sandstone SEM Examination . . .	IV-62
VI-1	Location Map Illustrating Pre-Test Well Positions and Suggested Positions of Post- Test Wells.	VI-3

TABLES

1	List of Samples and Analyses.	5
2	Wentworth Size Scale.	10
I-1	Petrographic Analysis - Joachim Dolomite.	I-16
I-2	Petrographic Analysis - Joachim-St. Peter Transition.	I-17
I-3	Thin Section Analysis - Joachim-St. Peter Transition.	I-18
I-4	Thin Section Analysis - St. Peter (Green)	I-19
I-5	Thin Section Analysis - St. Peter (White)	I-20
I-6	Thin Section Analysis - St. Peter (Dark Gray)	I-21
I-7	Semiquantitative X-Ray Diffraction Analysis of the Fine (Less than 5-Micron) Size Fraction, Caprock Samples	I-51
I-8	Semiquantitative X-Ray Diffraction Analysis of the Fine (Less Than 5-Micron) Size Fraction, Joachim-St. Peter Transition Zone	I-52
I-9	Semiquantitative X-Ray Diffraction Analysis of the Fine (Less Than 5-Micron) Size Fraction, Green St. Peter Sandstone	I-53
I-10	Semiquantitative X-Ray Diffraction Analysis of the Fine (Less Than 5-Micron) Size Fraction, White St. Peter Sandstone	I-54
I-11	Semiquantitative X-Ray Diffraction Analysis of the Fine (Less Than 5-Micron) Size Fraction, Medium to Dark Gray St. Peter Sandstone	I-55
I-12	Comparative Petrographic Characteristics of the Green, White, and Medium to Dark Gray St. Peter Sandstone	I-79
I-13	Comparative Mineralogic Characteristics of the Green, White, and Dark Gray St. Peter Sandstone Based on Fine Fraction X-Ray Diffraction Analysis.	I-80
II-1	Porosity and Air Permeability of the Caprock, Yakley Wells.	II-4

II-2	Boyle's Law Porosities and Air Permeabilities of Transition Zone Samples, Yakley Wells	II-7
II-3	Boyle's Law Porosities and Air Permeability of Green St. Peter Sandstone Samples, Yakley Wells	II-9
II-4	Boyle's Law Porosity and Air Permeability of White St. Peter Sand Samples, Yakley Wells . . .	II-11
II-5	Boyle's Law Porosity and Air Permeability of Medium to Dark Gray St. Peter Sand Samples, Yakley Wells.	II-13
III-1	Results of Triaxial Compressive Strength Testing Under a Confining Pressure of 1000 psi, Yakley 7 Well.	III-3
III-2	Unconfined Uniaxial Test Specimens and Results, Yakley Wells.	III-9
IV-1	Samples Heated at 390 ^o F for 24 and 48 Hours . . .	IV-2
IV-2	Samples Heated at 350 ^o F and 1000 psi for 24 Hours	IV-3
IV-3	Thin Section Analysis, Yakley Well C, Joachim- St. Peter Transition, 643.0 Feet.	IV-4
IV-4	Thin Section Analysis, Yakley Well C, St. Peter (Green), 645.0 Feet	IV-5
IV-5	Thin Section Analysis, Yakley Well C, St. Peter (White), 652.0 and 654.4 Feet	IV-6
IV-6	Thin Section Analysis, Yakley Well D, St. Peter (Green), 638.0 and 640.5 Feet	IV-7
IV-7	Thin Section Analysis, Yakley IW Well, St. Peter (Green), 653 Feet	IV-8
IV-8	Thin Section Analysis, Yakley Well A, St. Peter (Green), 662.0 Feet	IV-9
IV-9	Thin Section Analysis, Yakley IW Well, St. Peter (Green), 652.0 and 655.0 Feet	IV-10
IV-10	Thin Section Analysis, Yakley Well A, St. Peter (White), 671.1 Feet	IV-11
IV-11	Thin Section Analysis, Yakley Well A, St. Peter (Dark Gray)	IV-12

IV-12	Thin Section Analysis, Yakley IW Well	IV-13
IV-13	Semiquantitative X-Ray Diffraction Analysis of the Fine (Less Than 5-Micron) Size Fraction From Thermal Testing.	IV-14
IV-14	Semiquantitative X-Ray Diffraction Analysis of the Fine (Less Than 5-Micron) Size Fraction From Thermal Testing.	IV-15
IV-15	Semiquantitative X-Ray Diffraction Analysis of the Fine (Less Than 5-Micron) Size Fraction From Thermal Testing.	IV-16
IV-16	Semiquantitative X-Ray Diffraction Analysis of the Fine (Less Than 5-Micron) Size Fraction From Yakley IW.	IV-17
V-1	Water Analysis, Galena Formation.	V-7
V-2	Water Analysis, St. Peter	V-8
V-3	Distribution of Aqueous Species and Activities, Galena Water.	V-9
V-4	Possible Mineral Phases Which May Precipitate From Galena Waters.	V-11
V-5	Distribution of Important Aqueous Species, St. Peter Formation Water	V-12
V-6	Potential for Mineral Phase Precipitation from St. Peter Formation Waters.	V-14



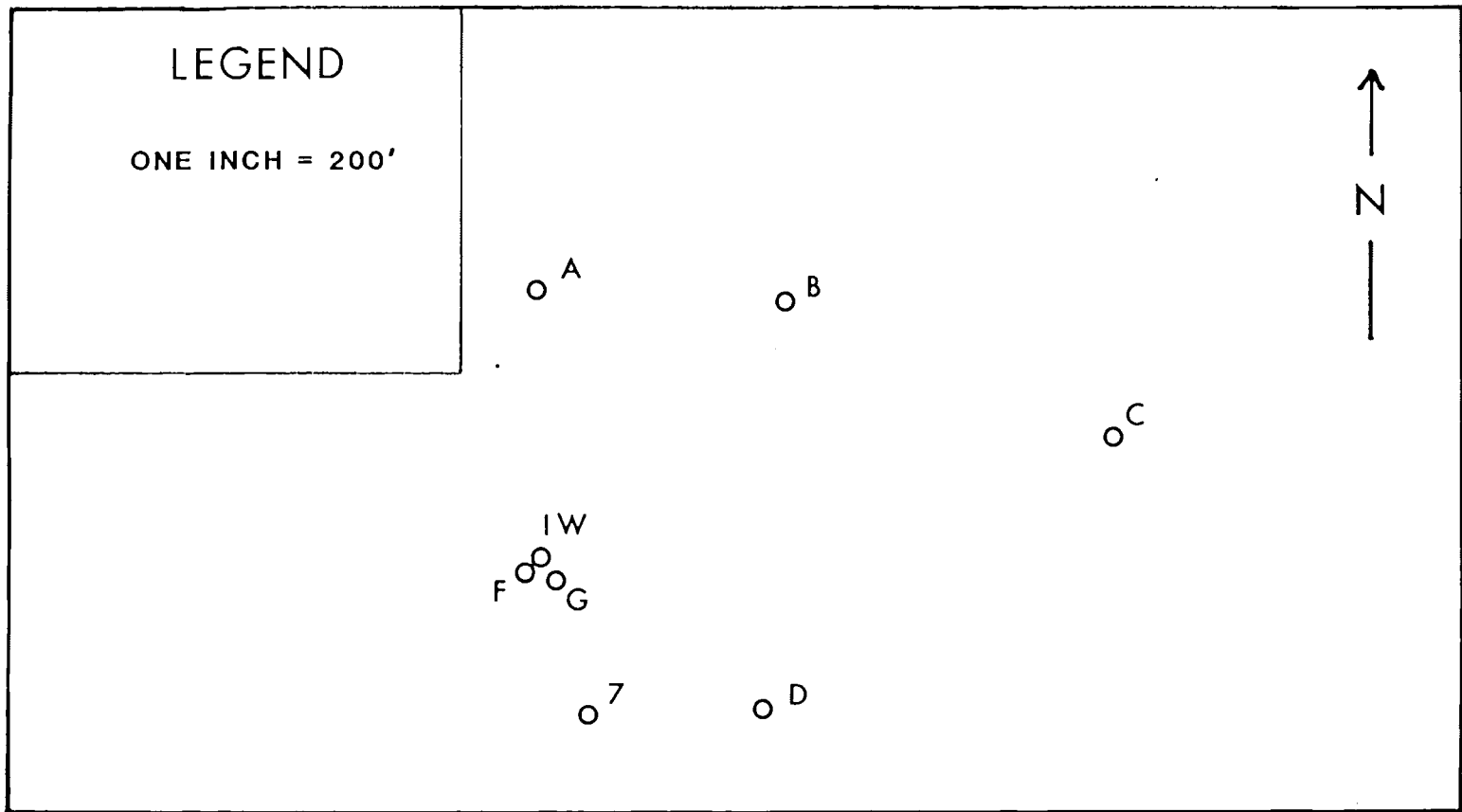
PRE-TEST GEOLOGICAL AND GEOCHEMICAL EVALUATION
OF THE CAPROCK, ST. PETER SANDSTONE
AND FORMATION FLUIDS
YAKLEY FIELD, PIKE COUNTY, ILLINOIS

INTRODUCTION

Results of the detailed study of cores taken from eight wells (A,B,C,D,F,G,IW, and 7, Figure 1) in the Yakley Field near Pittsfield, Illinois are presented in this report. A list of samples and analyses performed is given in Table 1. Porosities and either vertical or horizontal permeabilities were determined for 76 samples. Selected, representative samples were examined with the scanning electron microscope and the petrographic microscope, and selected samples were subjected to fine (less than five micron) X-ray diffraction analysis. The triaxial compressive strength under a confining pressure of 1000 p.s.i., was measured for eight samples from the Yakley No. 7 Well. Experiments were designed and conducted to determine the effect of heating on the St. Peter Sandstone. Unconfined uniaxial compressive strengths, including stress-strain relationships, were determined for 14 samples selected from Yakley Wells A,B,C,D, and IW. Water quality results, given in the Dames and Moore Report of March, 1981, were subjected to computer analysis using the WATEQF program.

This study was undertaken to satisfy the requirements of paragraph 2, topic 2 of the 23 October 1981 letter from Mr. Robert Allen of Battelle, Pacific Northwest Laboratories, entitled "Experimental Test Plan For Aquifer Evaluation". Specifically, to:

- 1) Determine compositional and textural characteristics of potential caprocks (Plattin and Joachim Formations), the Joachim-St. Peter transition zone, and the St. Peter Sandstone.
- 2) Measure and evaluate porosities and permeabilities of representative caprock and reservoir samples.
- 3) Determine mechanical strengths of caprock and reservoir samples.
- 4) Assess mineralogic variations within the upper St. Peter Sandstone.



2

FIGURE 1. Location Map Illustrating Positions of Cored Wells Studied in the Yakley Field Near Pittsfield, Illinois

- 5) Evaluate mineralogic changes which might occur due to the injection of hot air.
- 6) Assess geochemical reactions which might occur during air injection as the result of the reaction of air with either the rock or formation water.

Chemical formulas used throughout the text include the following:

CaCO_3	= Calcite, Aragonite
$\text{CaMg}(\text{CO}_3)_2$	= Dolomite
$\text{Ca}(\text{Mg, Fe})(\text{CO}_3)_2$	= Ankerite
SiO_2	= Quartz (Silica)
FeS_2	= Pyrite
FeS_2	= Marcasite
$\text{K}_{0-2}\text{Al}_4(\text{Si}_{8-6}\text{Al}_{0-2})\text{O}_{20}(\text{OH})_4$	= Illite
KAlSi_3O_8	= Potassium Feldspar
CaSO_4	= Anhydrite
$\text{CaSO}_4 \cdot 2\text{H}_2\text{O}$	= Gypsum
$\text{Al}_2\text{Si}_2\text{O}_5(\text{OH})_4$	= Kaolinite
$\text{Mg}_2(\text{CO}_3)(\text{OH})_2 \cdot 3\text{H}_2\text{O}$	= Artinite
BaSO_4	= Barite
$\text{Mg}(\text{OH})_2$	= Brucite
SrSO_4	= Celestite
SiO_2 (amorphous)	= Chalcedony
$\text{Ca}_5\text{F}(\text{PO}_4)_3$	= Fluorapatite
Fe_2O_3	= Hematite
$\text{CaMg}_3(\text{CO}_3)_4$	= Huntite
$\text{Mg}_4(\text{CO}_3)_3(\text{OH})_2 \cdot 3\text{H}_2\text{O}$	= Hydromagnesite
$\text{Ca}_5(\text{OH})(\text{PO}_4)_3$	= Hydroxyapatite
MgCO_3	= Magnesite
Fe_3O_4	= Magnetite
$\text{MnO}(\text{OH})$	= Manganite
MnO_2	= Pyrolusite

The report has been divided into six separate sections:

SECTION I	=	CHARACTERISTICS OF CAPROCKS (JOACHIM and PLATTIN FORMATIONS), JOACHIM - ST. PETER TRANSITION ZONES, AND THE UPPER ST. PETER SANDSTONE.
SECTION II	=	POROSITY AND PERMEABILITY.
SECTION III	=	MECHANICAL STRENGTH.

SECTION IV = THERMAL AND THERMAL-PRESSURED TESTING.
SECTION V = GEOCHEMICAL EVALUATION.
SECTION VI = SUGGESTIONS FOR POST-TEST ANALYSIS.

Five copies of this report have been forwarded to Mr. John Istvan of PB-KBB, Inc., Houston, Texas. David K. Davies and Associates retain one copy in their files for use in future conversations with authorized personnel of PB-KBB, Inc. regarding specific details of analytical results.

TABLE 1

LIST OF SAMPLES AND ANALYSES

Sample No.	Well	Depth, ¹ Ft.	Formation ²	Analysis						
				Porosity	Permeability ³	TS ⁴	XRD ⁵	SEM ⁶	Thermal ⁷	
D391-	Yakley-									
001	A	610.3	Plattin	X	X,v	-	-	-	-	-
002	A	611.5	Plattin- Joachim	X	X,v	-	-	-	-	-
003	A	613.3	Plattin- Joachim	X	X,v	-	X	-	-	-
004	A	625.9	Joachim	X	X,v	-	-	-	-	-
005	A	639.0	Joachim	X	X,v	-	-	-	-	-
006	A	641.0	Joachim	X	X,v	X	-	X	-	-
007	A	662.0	St.Peter (G)	X	X,h	X+H	X	X	X,H	X,H
008	A	671.1	St.Peter (W)	X	X,h	X,H	X	-	X,H	X,H
009	A	671.7	St.Peter (W)	X	X,h	X	-	-	X,H	X,H
010	A	677.0	St.Peter (Gy)	X	X,h	X,H	X	-	X,H	X,H
011	B	612.45	Plattin- Joachim	X	X,v	-	-	-	-	-
012	B	621.5	Joachim	X	X,v	-	-	-	-	-
013	B	628.0	Joachim	X	X,v	-	-	-	-	-
014	B	628.0	Joachim	X	X,v	-	-	-	-	-
015	B	634.0	Joachim	X	X,v	-	-	-	-	-
016	B	635.0	Joachim	X	X,v	-	-	-	-	-
017	B	635.0	Joachim	X	X,v	-	-	-	-	-
018	B	647.2	Joachim	X	X,v	-	-	-	-	-
019	B	651.0	Joachim	X	X,h	-	-	X	-	-
020	B	652.6	Joachim	X	X,v	X	X	X	-	-
021	C	625.7	Joachim	X	X,v	-	-	-	-	-
022	C	632.5	Joachim	X	X,v	-	-	-	-	-
023	C	637.0	Transition	X	X,v	X	-	-	-	-
024	C	637.0	Transition	X	X,v	-	-	-	-	-
025	C	639.0	Transition	X	X,v	-	-	-	-	-

TABLE 1, contd

Sample No.	Well	Depth, ¹ Ft.	Formation ²	Analysis						
				Porosity	Permeability ³	TS ⁴	XRD ⁵	SEM ⁶	Thermal ⁷	
D391-	Yakley-									
026	C	641.6	Transition	X	X,v	-	-	-	-	-
027	C	641.6	Transition	X	X,v	X	-	-	-	-
028	C	643.0	Transition	X	X,h	X	-	-	-	-
029	C	643.0	Transition	-	-	X+T	X	X(2)	X,T	-
030	C	644.0	Transition	X	X,h	X	-	-	-	-
031	C	644.0	Transition	X	X,v	-	-	-	-	-
032	C	644.6	St.Peter (G)	X	X,v	-	-	-	-	-
033	C	644.8	St.Peter (G)	X	X,h	-	-	-	-	-
034	C	645.0	St.Peter (G)	X	X,h	-	-	-	-	-
035	C	645.0	St.Peter (G)	-	-	X+T	X	X(2)	X,T	-
036	C	652.0	St.Peter (W)	X	X,h	-	-	-	-	-
037	C	652.0	St.Peter (W)	X	X,h	-	-	-	-	-
038	C	652.0	St.Peter (W)	-	-	X+T	X	X(3)	X,T	-
039	C	654.4	St.Peter (W)	-	-	X+T	X	X(3)	X,T	-
040	D	696.8	St.Peter (Gy)	X	X,v	-	-	-	-	-
041	D	697.0	St.Peter (Gy)	X	X,h	-	-	-	-	-
042	D	633.0	Transition	X	X,v	X	-	-	-	-
043	D	638.0	St.Peter (G)	-	-	X+T	X	X(2)	-	-
044	D	640.5	St.Peter (G)	X	X,h	-	-	-	-	-
046	D	640.5	St.Peter (G)	X	X,h	X+T	X	X	X,T	-
047	D	641.7	St.Peter (W)	X	X,v	X	-	-	-	-
048	D	641.9	St.Peter (W)	X	X,h	-	-	-	-	-
049	IW	640.1	Joachim	X	X,v	-	-	-	-	-
050	IW	645.1	Joachim	X	X,v	-	-	-	-	-
051	IW	645.45	Joachim	X	X,v	-	-	-	-	-
052	IW	645.8	Joachim	X	X,v	-	-	-	-	-

TABLE 1, contd

Sample No.	Well	Depth, ¹ Ft.	Formation ²	Analysis						
				Porosity	Permeability ³	TS ⁴	XRD ⁵	SEM ⁶	Thermal ⁷	
D391-	Yakley-									
053	IW	647.3	Joachim	X	X,v	-	-	-	-	-
054	IW	647.3	Joachim	X	X,v	X	-	-	-	-
055	IW	649	Joachim	X	X,v	X	X	-	-	-
056	IW	649.5	Transition	X	X,v	X+H	X	-	X,H	X,H
057	IW	651.5	Transition	X	X,v	-	X	X	-	-
058	IW	651.7	Transition	X	X,v	X	-	-	-	-
059	IW	652	St.Peter (G)	X	X,h	X+H	X	X	X,H	X,H
060	IW	652	St.Peter (G)	X	X,h	X	-	-	-	-
061	IW	653	St.Peter (G)	-	-	X+T	X	X(2)	X,T	X,T
062	IW	654	St.Peter (G)	X	X,h	X,H	X	-	X,H	X,H
063	IW	665.4	St.Peter (W)	X	X,h	X,H	X	X	X,H	X,H
064	IW	646	Joachim	X	X,v	-	-	-	-	-
065	IW	655	St.Peter (G)	X	X,h	X+H	X	X(2)	X,H	X,H
066	A	604.35	Plattin	X	X,v	-	-	-	-	-
067	C	707.8	St.Peter (Gy)	-	-	X	X	X	-	-
070	G	649.6	Transition	X	X,v	-	-	-	-	-
071	G	650.8	Transition	X	X,v	-	-	-	-	-
072	G	651.3	Transition	X	X,v	-	-	-	-	-
073	G	653.1	Transition	X	X,v	-	-	-	-	-
074	G	654.9	St.Peter (G)	X	X,v	-	-	-	-	-
075	G	656.5	St.Peter (G)	X	X,v	X	X	X	-	-
076	G	658.2	St.Peter (G)	X	X,v	X	-	-	-	-
077	G	668.0	St.Peter (W)	X	X,v	X	-	-	-	-
078	G	683.2	St.Peter (Gy)	X	X,v	-	-	-	-	-
079	G	694.2	St.Peter (Gy)	X	X,v	-	-	-	-	-
080	G	697.5	St.Peter (Gy)	X	X,v	-	-	-	-	-
081	F	650.4	Transition	X	X,v	-	-	-	-	-
082	F	648.6	Transition	X	X,v	-	-	-	-	-
083	F	657.0	St.Peter (G)	X	X,v	X	-	X	-	-

TABLE 1, contd

Sample No.	Well	Depth, ¹ Ft.	Formation ²	Analysis						
				Porosity	Permeability ³	TS ⁴	XRD ⁵	SEM ⁶	Thermal ⁷	
D391	Yakley-									
084	F	659.7	St. Peter (G)	X	X,v	X	-	-	-	-
085	F	659.9	St. Peter (W)	X	X,v	-	-	-	-	-
086	F	665.1	St. Peter (W)	X	X,v	-	-	-	-	-

¹Depths are core depths

²G = Green

W = White

Gy = Gray

Transition = Joachim-St. Peter Transition Zone

³v = Vertical

h = Horizontal

⁴TS = Petrographic analysis

H = Thermal, pressured

X+H = One normal thin section and one after heating

X+T = One normal thin section and one after heating

X,H = One thin section after heating

T = Thermal

⁵XRD = Fine Fraction X-Ray Diffraction

⁶SEM = Scanning electron microscope

(2) = One unheated sample and one heated sample

⁷H = Heated to 350°F at 1000 p.s.i.

T = Heated to 390°F

ANALYTICAL METHODS

General -

Techniques utilized in the analysis of samples from the Yakley Well Field are summarized below. All samples analyzed are representative of either specific formations or specific intervals.

Petrographic Analysis -

Thin sections of 48 samples from seven Yakley Wells were prepared and examined with the petrographic microscope (Table 1). To better define porosity, all samples were impregnated with blue epoxy resin prior to thin section preparation. The samples were then slabbed, mounted on a glass plate and ground to a thickness of approximately 30 microns. All thin sections were stained with Alizarin Red "S" dye to better distinguish between calcite and dolomite. Data which is obtained from petrographic examination include the following:

1) Grain Size -

The mean grain size is determined by measuring the long axis of 50 randomly selected quartz grains on the thin section. These measurements are summed and the average is taken. The mean grain size is then compared to the Wentworth scale (Table 2), and the size class is determined. The accuracy of this method is +1%.

2) Sorting -

The sorting is determined by two methods:

- a) Direct visual comparison of the thin section with standard charts prepared for various grain sizes (Beard and Weyl, AAPG Bulletin, 1973).
- b) The ratio of the long axis measurement of the largest grain to the mean grain size.

3) Bulk Composition -

Bulk compositions are determined by counting 100 points of an imaginary grid on the thin section. Incremental dimensions of the grid are set by the

TABLE 2
WENTWORTH SIZE SCALE

D_{mm}	Ø	SIZE CLASS	ROCK
4096	-12	BOULDER	CONGLOMERATE
256	-8	COBBLE	
64	-6	PEBBLE	
4	-2	GRANULE	
2	-1	VC SAND	
1	0	C SAND	SANDSTONE
1/2	1	M SAND	
1/4	2	F SAND	
1/8	3	VF SAND	
1/16	4	C SILT	
1/32	5	M SILT	SILTSTONE
1/64	6	F SILT	
1/128	7	VF SILT	
1/256	8	CLAY	CLAYSTONE
1/16384	14		

average grain size. The percentage by volume of constituents, such as detrital grains (quartz, feldspar, chert, etc.), cement (calcite, dolomite, authigenic clay, silica overgrowths, etc.), and depositional matrix, is determined with an accuracy of $\pm 1\%$. Compositions are then fitted to the sandstone classification scheme of Folk (Figure 2).

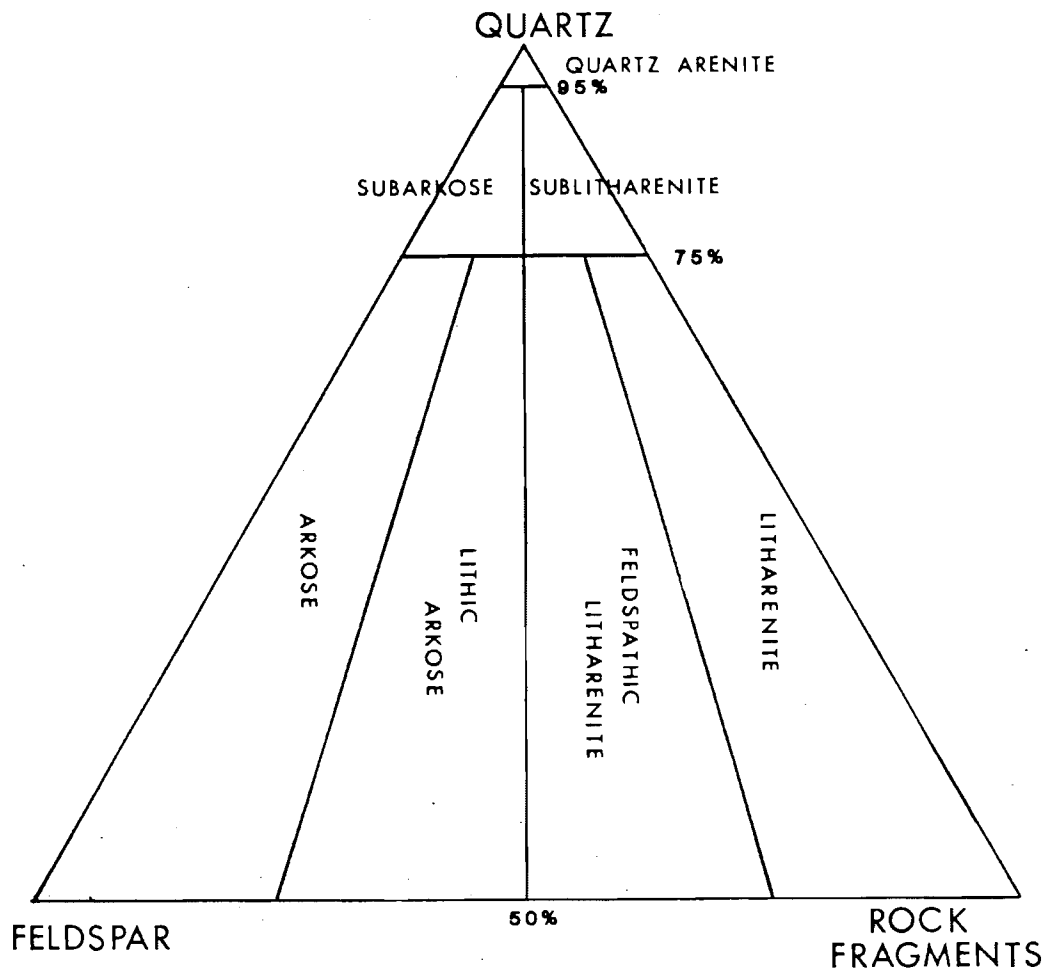


FIGURE 2. Ternary Rock Classification Scheme (after Folk 1968). Only monocrystalline quartz is included in the quartz pole. The feldspar pole includes those rock fragments which may contain feldspar (igneous and gneissic fragments). Polycrystalline quartz, chert, and micas are included in the rock fragment pole.

4) Porosity Origin -

From thin section examination, the type of porosity (primary or secondary) may be determined. Primary porosity is intergranular, and secondary porosity results from the partial or complete dissolution of unstable grains. The morphology of the pore system may also be examined. With adequate samples, qualitative estimates of porosity and permeability may be made.

5) Diagenetic History -

The porosity, permeability, and degree of alteration of a specimen, observed today, is the direct result of diagenetic alterations which have occurred throughout the history of the specimen. By careful observation the diagenetic history of a sample, and, hence, the interval it represents may be unraveled, particularly with regard to porosity reduction or enhancement and the emplacement of the late stage cements.

6) Percent Solubles -

The percentage of material soluble in hydrochloric acid, present as either discrete grains or as cement, may be estimated.

7) Fabric -

Grain to grain relations (the ways in which grains are put together to make an aggregate) are determined from thin section examination. Fabric characteristics include the type of grain to grain contact and the packing.

Results of the petrographic examination of Yakley Well field samples are presented in tabular form and as a series of color photographs in Sections I and IV.

X-Ray Diffraction Analysis -

Fine (less than five micron) size fraction X-ray diffraction analysis is utilized to elucidate the composition of, primarily, those minerals present in the pore system. Other phases present in this size fraction include dispersed detrital matrix, minerals cleaved during sample preparation, and loosely joined rock fragments. Samples for analysis are first

dispersed and, after an appropriate settling time (32 minutes), the less than five micron size fraction is separated and transferred to a glass plate. Samples are analyzed in the air dried and glycolated states.

Results of X-ray diffraction analysis are presented in tabular form in Sections I and IV.

Scanning Electron Microscopy (SEM) -

The scanning electron microscope is utilized to examine pore fill minerals, grains, and etched grain surfaces. The SEM is fitted with an energy dispersive X-ray unit which enables the analyst to simultaneously examine the morphology of pore fill minerals and determine their elemental (chemical) composition. Sodium (atomic number = 11) represents the lower limit of elements which can be detected with certainty. Results of the SEM examination are presented as a series of black and white photographs in Sections I and IV.

Porosity and Permeability -

Boyle's Law porosities and either vertical or horizontal air permeabilities were measured for 76 representative samples from seven wells. Results of these measurements are presented in tabular form in Section II.

Mechanical Strength -

Triaxial compressive strengths, with 1000 p.s.i. confining pressure, were measured for eight samples, and 14 samples were subjected to unconfined uniaxial compressive strength testing. A discussion of these tests and results are presented in Section III.

Thermal Testing -

Two separate sets of St. Peter Sandstone samples were heated to either 390°F or 350°F with a confining pressure of 1000 p.s.i. to evaluate potential mineralogic changes which might occur in the pore system. Results of these tests are presented in Section IV.



SECTION I

CHARACTERISTICS OF CAPROCKS (JOACHIM AND PLATTIN FORMATIONS), THE JOACHIM- ST. PETER TRANSITION ZONE, AND THE UPPER ST. PETER SANDSTONE

CORE EXAMINATION

General -

Seven wells were drilled and cored in the Yakley field (Figure 1). Cores taken have been described in detail, and a summary is presented. For convenience, the discussion is divided into five groups - Caprock (Joachim and Platteville Formations), Joachim-St. Peter Transition, Green St. Peter Sandstone, White St. Peter Sandstone, and Medium to Dark Gray St. Peter Sandstone. Representative features of each descriptive unit are presented in a series of color photographs (Figures I-1 through I-4). A generalized lithologic log is presented in Figure I-5.

Caprock -

The lowermost portion of the Platteville Formation and the entire Joachim Formation were cored in two boreholes. The Platteville is a very fine-grained light gray to buff limestone which becomes increasingly dolomitic toward the contact with the Joachim Formation. Undulose limy shale partings occur near the base of the Platteville.

The Joachim Formation is a buff to dark brown fine-grained dolomite. Upper portions of the Joachim dolomite are characterized by vertical to subvertical fractures which are infilled by calcite, sphalerite, and galena. Very thin (less than 1 cm) black shale partings occur throughout. Open vertical fractures and open or calcite-filled vugs occur to within five feet of the Joachim-St. Peter contact. Characteristic features of the Joachim Formation are illustrated in Figure I-1. The entire Joachim Formation was not cored in all wells.

Joachim-St. Peter Transition -

The Joachim-St. Peter Transition is defined by the first obvious appearance of detrital quartz grains in the dolomite. Rocks of the transition zone are generally vuggy and shale partings appear to be stylolitic. Sand content increases to

the contact with the green St. Peter Sandstone. Characteristic features of the transition zone are illustrated in Figure I-2. The transition zone varies in thickness from 2.8 to 7 feet.

St. Peter Sandstone -

The entire St. Peter Formation was not penetrated during coring or drilling. The upper portion has been divided into three units, based on color, for convenience of description.

Green -

The St. Peter green sand is medium-grained. Black horizontal or disrupted laminations are present. Grains are frequently coated with black iron sulfide. Clays and iron sulfide form the laminations. The green sand varies in thickness from 8.7 to 11.1 feet.

White -

The white St. Peter sand is generally finer grained than the green sand and more well-cemented. Open or filled vertical to subvertical fractures occur. Minor black pore fill (iron sulfide) is present. Characteristic features are illustrated in Figure I-3.

Medium to Dark Gray -

The medium to dark gray St. Peter sand contains abundant iron sulfide and exhibits vertical streaks resulting from differential ground water percolation. Distinct, sub-vertical fractures, generally marked as a black streak, occur. Characteristic features are illustrated in Figure I-4.

The following pages present selected photographs of slabbed core specimens representative of the caprock and St. Peter sandstone. Depths are marked on slabbed faces unless otherwise indicated.

FIGURE I-1

FORMATION: JOACHIM

PHOTOGRAPH

DESCRIPTION

- | | |
|---|---|
| A | The upper Joachim Dolomite is laminated and contains some evidence of soft sediment deformation. Vertical cracks are generally infilled with calcite, galena, and/or sphalerite. Discontinuous vertical and unoriented areas of the slabbed core are infilled by calcite. |
| B | Close-up view of A illustrates soft sediment deformation and a sphalerite filled vug. |
| C | Compact dolomite exhibits vertical to subvertical fractures. Black areas are infilled by very finely crystalline pyrite. Frequent dense laminations of shale occur at this depth. |
| D | Close-up view of C shows that the thick shale lamination is actually composed of many thin shale laminations. Pyrite has been partially oxidized (rust stain). |

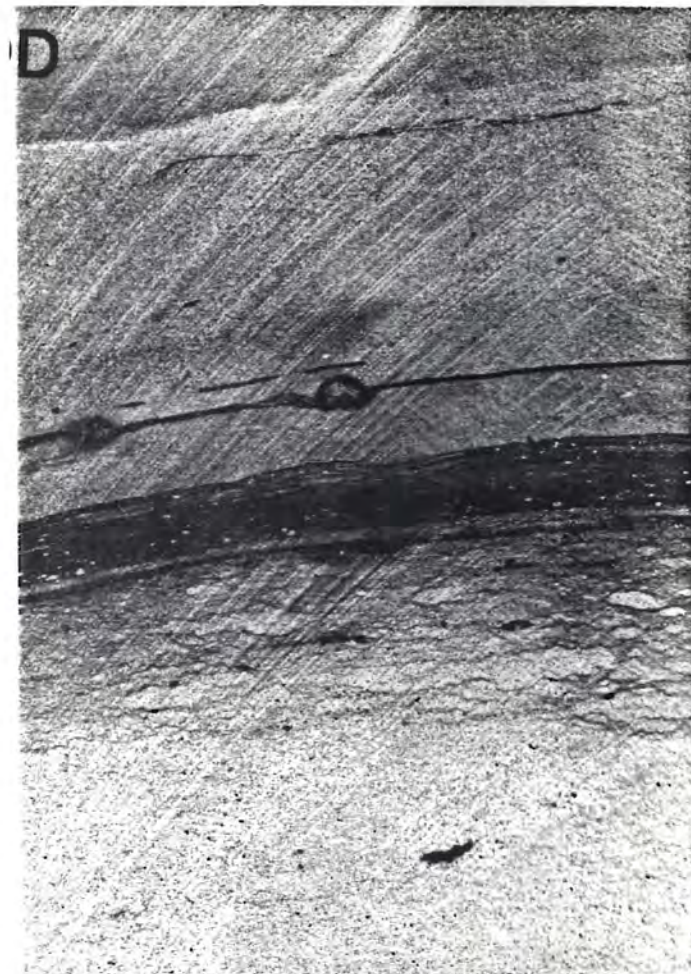
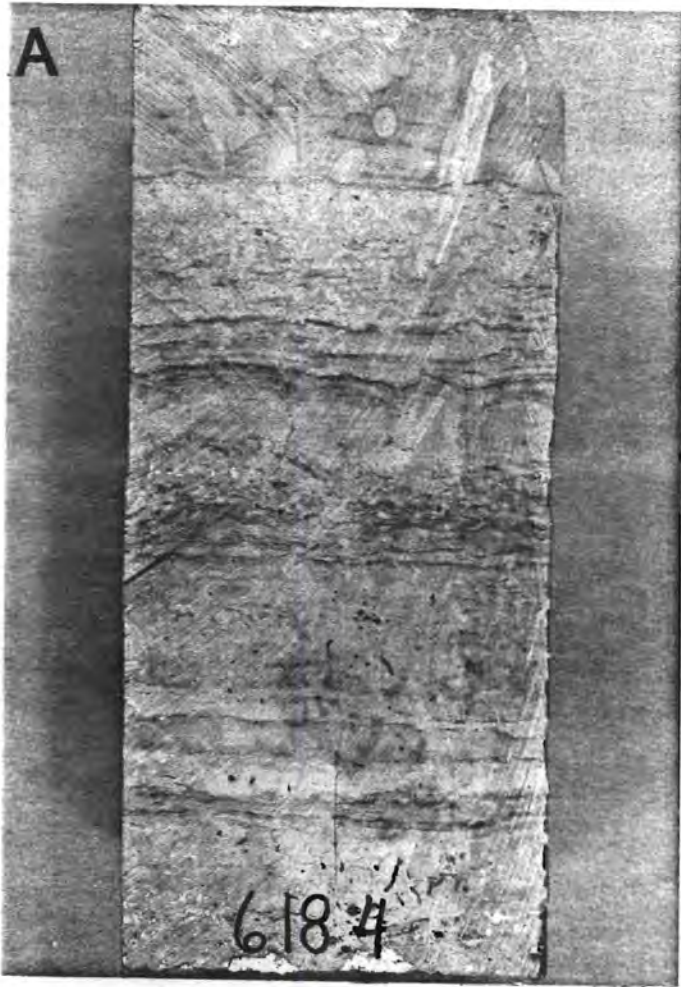


FIGURE I-1, continued

FORMATION: Joachim

PHOTOGRAPH

DESCRIPTION

E,F,G

These photographs of slabbed core specimens illustrate characteristic features of middle Joachim dolomite. The middle Joachim is frequently fractured, and fractures are commonly infilled by calcite. Disrupted to nearly horizontal shale partings (black) occur sparsely. Discontinuous subhorizontal to subvertical areas contain pyrite.

H

The basal Joachim dolomite frequently exhibits disrupted laminations which have been slightly deformed and may be algal in origin.

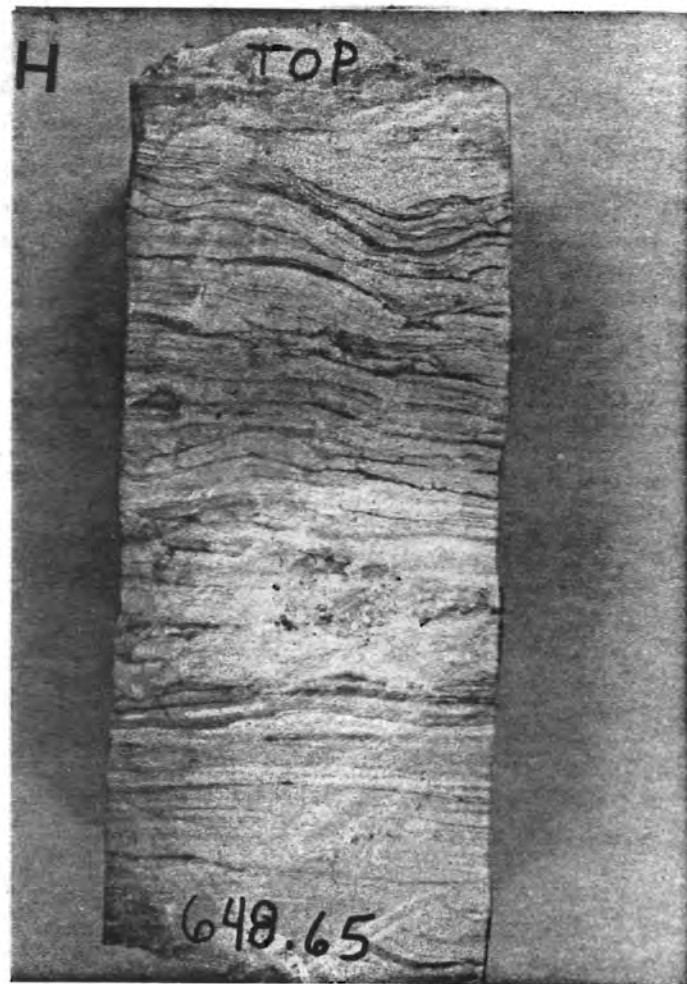
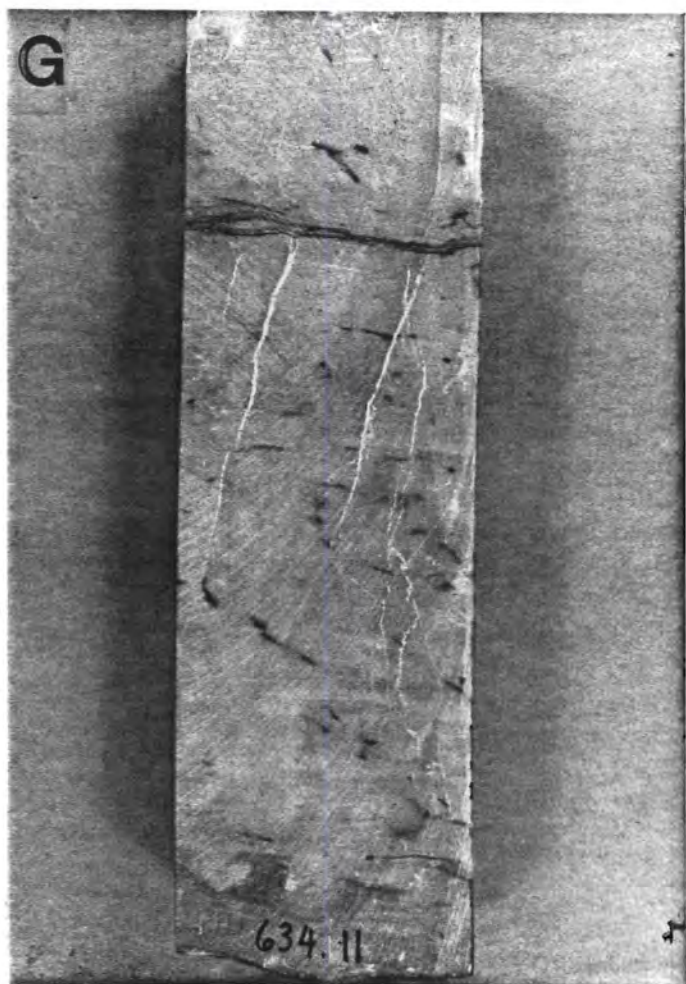
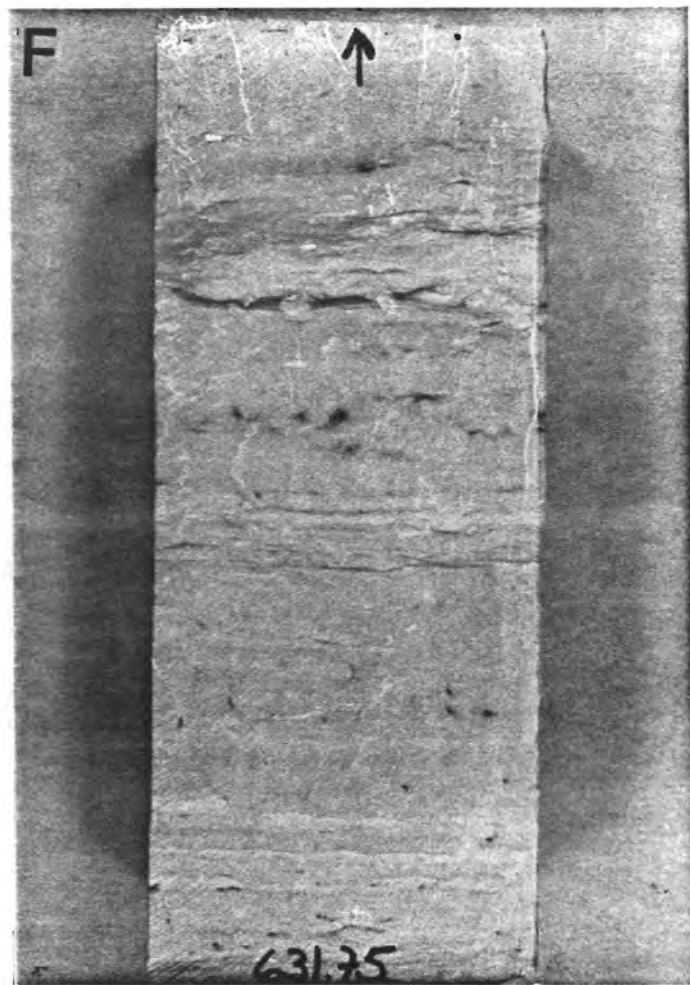
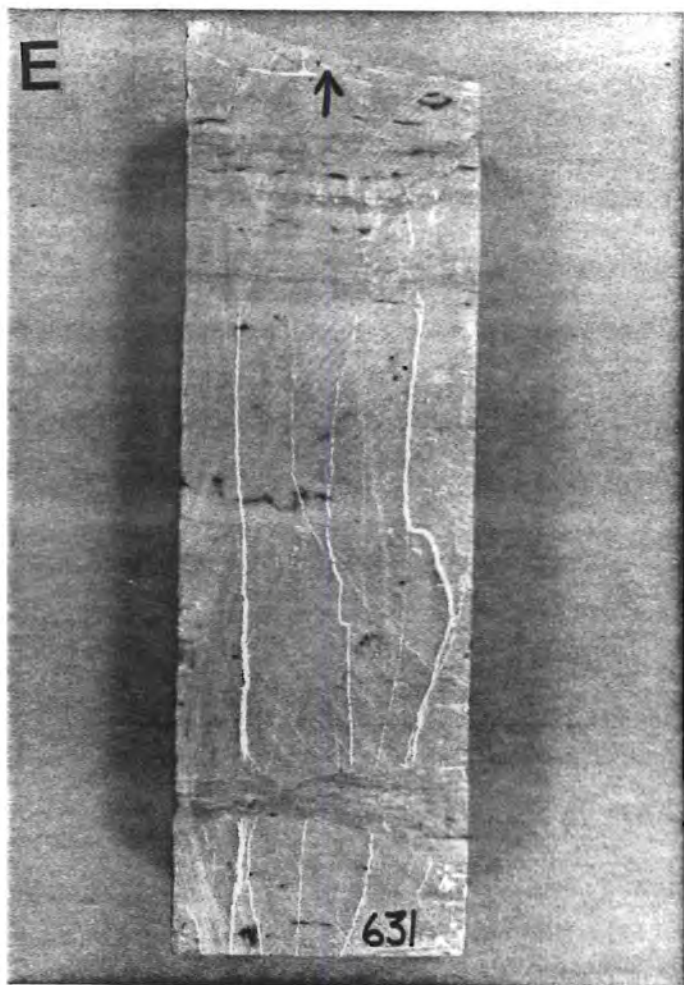


FIGURE I-2

FORMATION: Joachim-St. Peter Transition

PHOTOGRAPH

DESCRIPTION

- A Near the top, this specimen is almost totally dolomite, with few scattered quartz grains. Near the center, dolomite clasts are distributed throughout a quartz-rich layer. Quartz content increases to the base.
- B This specimen consists of tightly cemented quartz with some dolomite clasts.
- C Close-up view of B shows that some portions of the specimen are porous. However, the vugs are not well interconnected. Dolomite clasts (dark gray and buff) are well illustrated by this view.

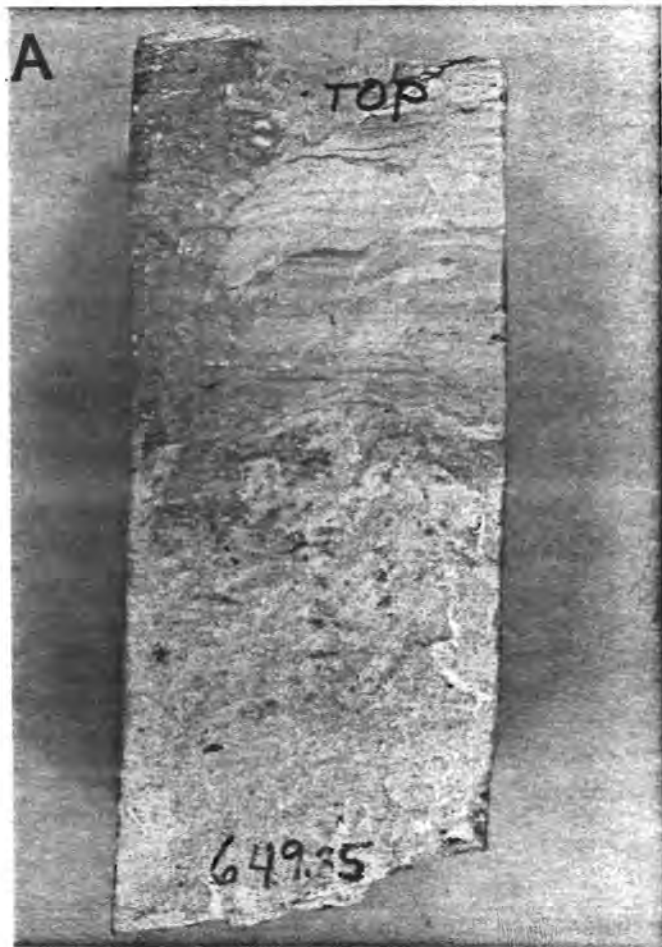


FIGURE I-3

FORMATION: St. Peter Sandstone (White)

PHOTOGRAPH

DESCRIPTION

A,B (665.6 feet)

At these depths, the St. Peter Sandstone is commonly fractured. The fractures are either open or infilled by calcite.

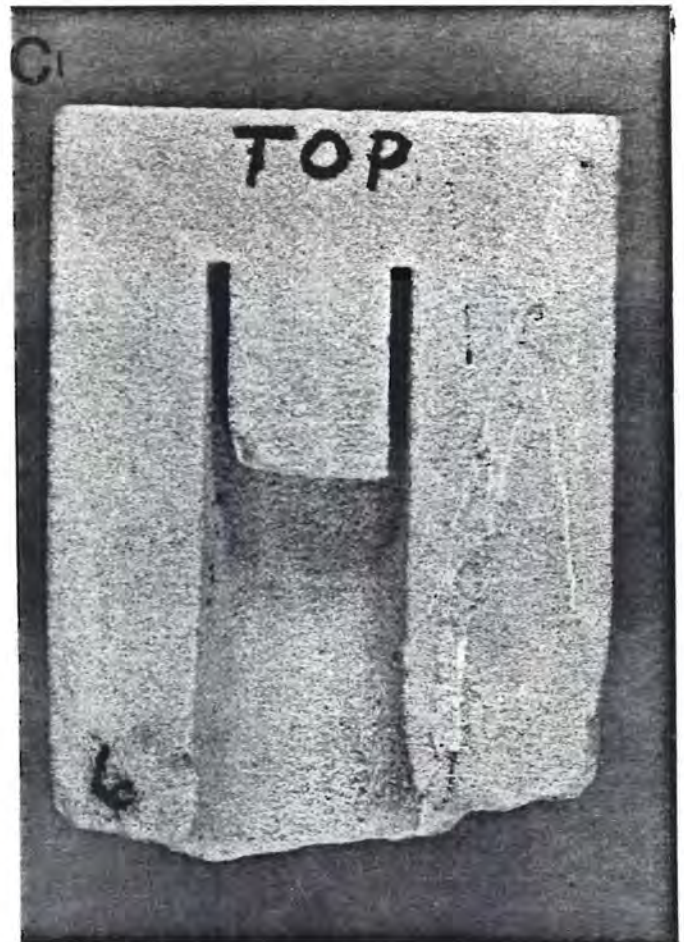
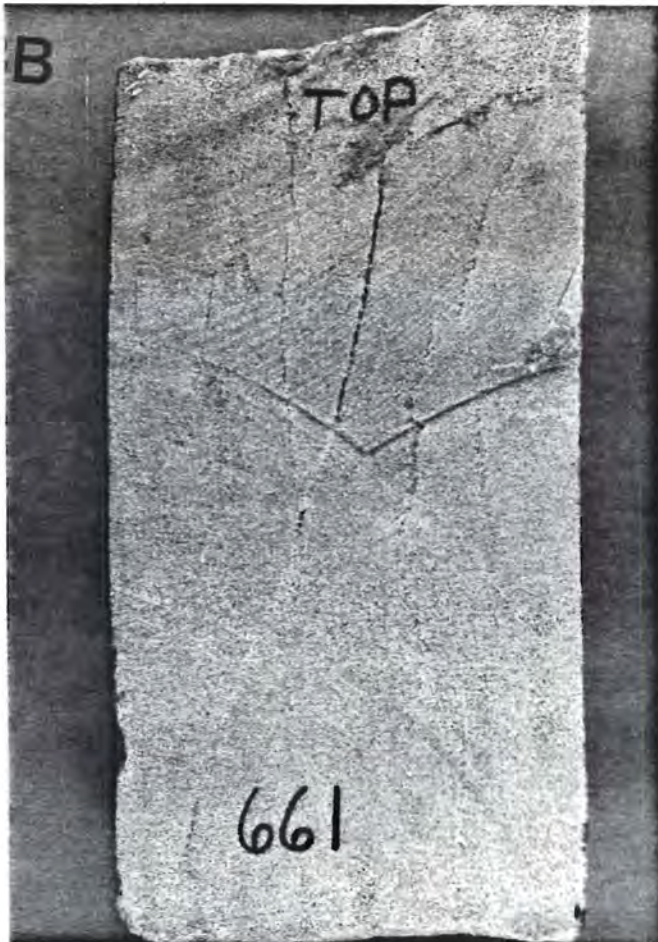


FIGURE I-4

FORMATION: St. Peter Sandstone (Gray)

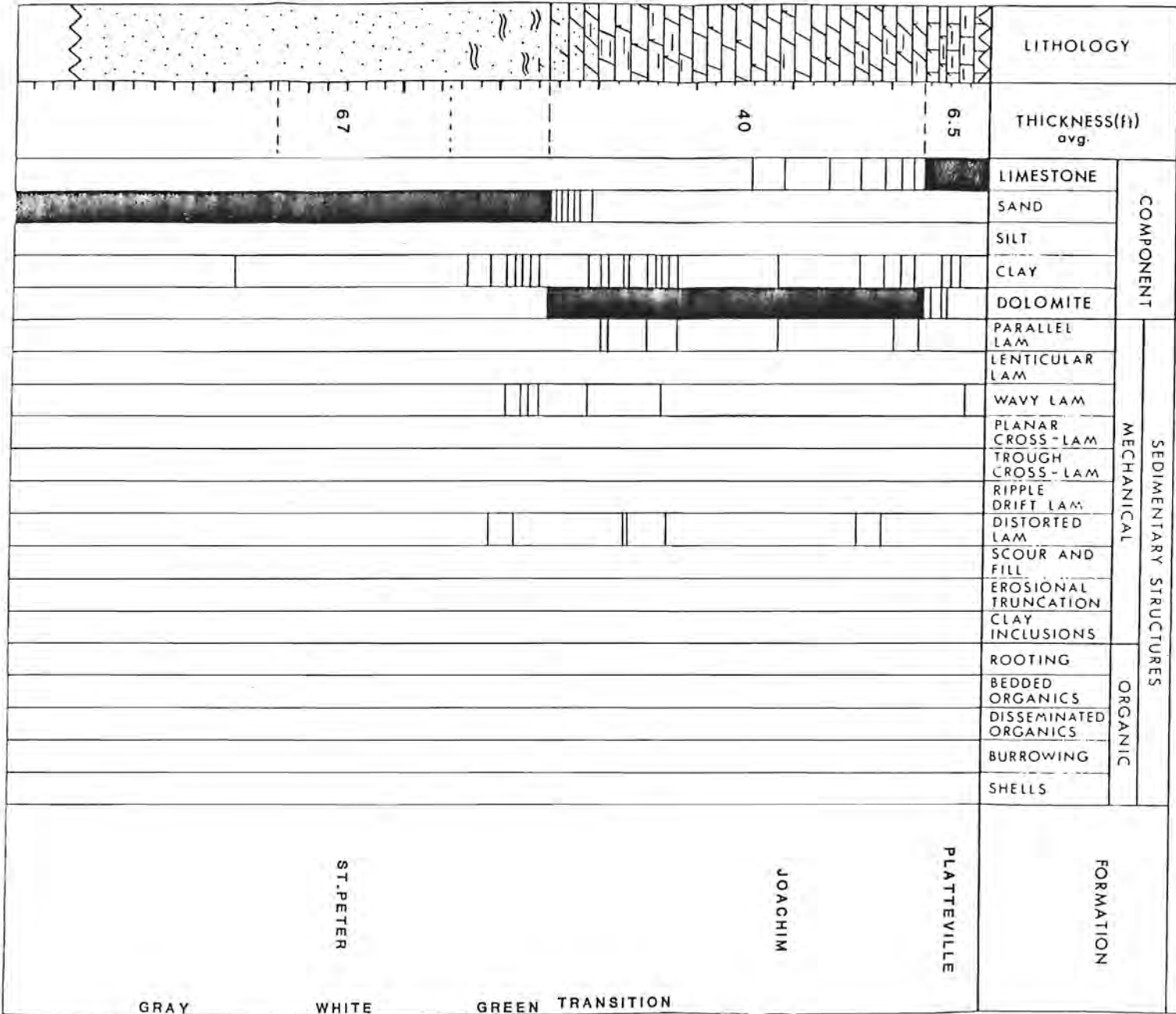
DESCRIPTION

The gray St. Peter Sandstone is characterized by the presence of abundant pyrite (black). Vertical streaks on the face most probably reflect the differential percolation of ground water. The black streak at high angle to the core is an area of concentration of pyrite and perhaps reflects subsurface movement along planes of weakness in the St. Peter.



FIGURE I-5

GENERALIZED LITHOLOGIC COLUMN YAKLEY WELL FIELD
 (Cored interval only)



COMPOSITION AND TEXTURE

General -

Thin sections of 48 core plugs from all wells were prepared and examined. The purpose of this examination was to determine compositional and textural characteristics of the Caprock, the Joachim-St. Peter Transition, and the St. Peter Sandstone. Results of this examination are presented in Tables I-1 to I-6 and in Figures I-6 to I-19. For convenience, the interval has been divided into five descriptive units.

Joachim Formation -

Four samples of the Joachim Formation were examined. The Joachim consists, dominantly, of finely crystalline dolomite (96-99%). Dolomite crystals are generally euhedral and are less than 0.06 mm in long dimension measurement. Minor calcite (0-3%), pyrite (0-1%) and clay (0-1%) are other chemical precipitates. Detrital quartz (Tr-2%) occurred in all samples examined. A trace (less than 1%) amount of anhydrite was present in one sample. The Joachim dolomite is texturally a very finely crystalline carbonate rock, with the dolomite crystallites formed as a recrystallization product, probably from lime mud. The detailed petrography is given in Table I-1. Figure I-6 is a color photomicrograph of a representative sample.

Joachim-St. Peter Transition -

Seven samples from the Joachim-St. Peter Transition zone were examined in detail. Of these, five samples are dominantly dolomite (54-94%). These samples contain quartz (3-43%), and some silica overgrowths occur on quartz grains. Calcite occurs in three samples. Intraclasts (clasts formed in the basin of deposition) occur in two samples. One sample contains detrital clay matrix. Details of the petrographic examination are presented in Tables I-2 and I-3.

Two Joachim-St. Peter Transition samples were selected from very sandy members of the zone. These samples contained no dolomite but are poorly sorted, medium grained sandstones, consisting of quartz (77-81%), detrital clay matrix (19-22%) with trace amounts of mica, heavy minerals and iron sulfide. Details of the petrographic examination are presented in Table I-3. One dolomite sample is listed in this Table (I-3) because it contains detrital clay matrix. Characteristic features of transition zone specimens are illustrated in Figures I-7 through I-10.

Green St. Peter Sandstone -

Five green St. Peter Sandstone samples were examined. Details of the petrography are presented in Table I-4. Characteristic features are illustrated in Figures I-11 through I-14. The green St. Peter is a medium to coarse grained (average grain diameter=0.44-0.63 mm) poorly to moderately well sorted sandstone. Monocrystalline quartz is the dominant detrital grain (69-86%). Detrital clay matrix (Tr-27%) occurs in all samples analyzed. Dominant cements include authigenic clay and silica. Although the framework grains are texturally and compositionally mature, the green St. Peter Sandstone is texturally immature, due to the presence of detrital matrix. The green St. Peter Sandstone is classified as a quartz arenite.

The fabric of the sand is variable. Grains may exhibit concavo-convex contacts, point contacts, or in some instances "float" in the detrital matrix.

White St. Peter Sandstone -

Three samples of white St. Peter Sandstone were examined. Results of the petrographic examination are presented in Table I-5, and characteristic features are illustrated in Figures I-15 through I-18. The petrography of sample -039 is given in Table IV-5 of Section IV.

White St. Peter Sand samples are generally moderately well to well sorted and are medium grained (average grain diameter = 0.37 to 0.45 mm). The sample from Yakley Well A, depth of 671.7 feet, is representative of the lowermost white St. Peter Sandstone and exhibits characteristics of both the white and medium to dark gray St. Peter. Monocrystalline quartz (85-87%) is the dominant detrital grain, and detrital grains are cemented by silica. Some authigenic clay also occurs as cement. Abundant authigenic iron sulfide and calcite cement occur in the lowermost sample.

The white St. Peter Sandstone is texturally mature, containing minor to no detrital clay matrix. Detrital grains are also classified as mature. The sandstone is classified as a quartz arenite.

Original grain contacts, where observed are concavo-convex or point.

Medium to Dark Gray St. Peter Sandstone -

One sample was examined. The detailed petrography is presented in Table I-6 and characteristic features are illustrated in Figure I-19.

The dark gray St. Peter Sandstone is moderately well sorted and medium grained (average grain diameter = 0.37 mm). The only mineral phases present are detrital quartz grains (87%), authigenic clay (5%), and authigenic iron sulfide (8%).

The sandstone is texturally mature relative to both grain composition and detrital clay matrix content. The sandstone is classified as a quartz arenite.

Grains generally exhibit concavo-convex contacts although some point contacts may be observed (Figure I-19).

TABLE I-2

PETROGRAPHIC ANALYSIS

FORMATION JOACHIM-ST. PETER TRANSITION

LI-I

Sample No.	Depth, Ft	Yakley Well	Al- lochens		Matrix		AUTHIGENIC PRECIPITATES ¹											DETRITAL GRAINS					TOTALS			
			Intraclasts	Coated Grains	Calcite Mud	Dolomite Mud	Calcite	Dolomite	Quartz	Anhydrite	Gypsum	Halite	Siderite	Pyrite	Celestite	Clay	Feldspar	Chert	Quartz	Mica	Feldspar	Rock Fragments	Mud Balls	Total Carbonate	Total Evaporite	Total Detrital
D391-023	637.0	C	18	-	-	-	7	72	-	-	-	-	-	-	-	-	-	3	-	-	-	-	-	97	-	3
027	641.6	C	Tr	-	-	-	3	59	3	-	-	-	-	-	-	-	-	35	-	-	-	-	-	62	-	35
042	633.0	D	-	-	-	-	-	54	3	-	-	-	-	-	-	-	-	43	-	-	-	-	-	54	-	43
056	649.5	IV	-	-	-	-	-	94	-	-	-	-	-	-	-	-	-	6	-	-	-	-	-	94	-	6

¹ Calcite has recrystallized from lime mud. Dolomite, with the addition of Mg²⁺ to formation waters, recrystallized from lime mud. Quartz is present as silica overgrowths.

TABLE I-3
THIN SECTION ANALYSIS

FORMATION: JOACHIM-ST. PETER TRANSITION

Depth (Ft)	Yakley Well	TEXTURE		GRAIN COMPOSITION														MX	CEMENT COMPOSITION							TOTALS			Sample ID Number			
		Mean Grain Size (mm) ¹	Overall Sorting	Monocrystalline Quartz	Polycrystalline Quartz	Mica	K-Feldspar	Plagioclase Feldspar	Chert	Igneous RF's	Metamorphic RF's	Sandstone Fragments	Clay Balls	Shale Fragments	Plant Remains	Carbonate Fragments	Shell Fragments		Glauconite	Heavy Minerals	Authigenic Feldspar	Detrital Clay Matrix	Authigenic Clay	Silica	Calcite	Dolomite	Siderite	Anhydrite		Pyrite	Total Quartz	Total Clay Minerals
643.0 C	0.42	PS	81	-	-	-	-	-	-	-	-	-	-	-	-	-	-	-	Tr	-	19	-	-	-	-	-	-	Tr	81	19	-	D391-028
644.0 C	0.50	PS	77	1	Tr	-	-	-	-	-	-	-	-	-	-	-	-	-	Tr	-	22	-	-	-	-	-	Tr	78	22	-	D391-030	
651.7TW	0.10	NA	32	-	-	1	-	-	-	-	-	-	-	-	-	-	-	-	-	1	8	1	-	2	55	-	-	-	32	9	57	D391-058

MX = Depositional matrix (fines deposited simultaneously with the sand grains). RF's = Rock Fragments.
1 = Bimodal grain size distribution, coarser mode reported.

TABLE I-4
THIN SECTION ANALYSIS

FORMATION: ST. PETER (GREEN)

Depth (Ft)	Yakley Well	TEXTURE		GRAIN COMPOSITION																MX	CEMENT COMPOSITION							TOTALS			Sample ID Number		
		Mean Grain Size (mm)	Overall Sorting	Monocrystalline Quartz	Polycrystalline Quartz	Nica	K-Feldspar	Plagioclase Feldspar	Chert	Igneous RF's	Metamorphic RF's	Sandstone Fragments	Clay Balls	Shale Fragments	Plant Remains	Carbonate Fragments	Shell Fragments	Glauconite	Heavy Minerals		Others	Detrital Clay Matrix	Authigenic Clay	Silica	Calcite	Dolomite	Siderite	Anhydrite	Pyrite	Total Quartz		Total Clay Minerals	Total Carbonates
652.0	IW	0.63	PS	69	-	-	-	-	-	-	-	-	-	-	-	-	-	-	Tr	-	14	3	14	-	-	-	-	-	Tr	83	17	-	060
657.0	F	0.48	MWS	79	2	-	-	-	-	-	-	-	-	-	-	-	-	-	Tr	-	18	Tr	-	-	-	-	-	1	81	18	-	083	
659.7	F	0.45	MWS	86	1	-	-	-	-	-	-	-	-	-	-	-	-	-	Tr	-	Tr	13	-	-	-	-	-	Tr	87	13	-	084	
656.5	G	0.55	PS	84	1	-	Tr	-	-	-	-	-	-	-	-	-	-	-	Tr	-	15	-	-	Tr	-	-	Tr	85	15	-	075		
658.2	G	0.44	PS	73	-	-	-	-	-	-	-	-	-	-	-	-	-	-	Tr	-	27	-	-	-	-	-	-	Tr	73	27	-	076	

MX = Depositional matrix (fines deposited simultaneously with the sand grains). RF's = Rock Fragments.
1 = Bimodal grain size distribution, coarse mode reported.

TABLE I-5
THIN SECTION ANALYSIS

FORMATION: ST. PETER (WHITE)

Depth (Ft)	Yakley Well	TEXTURE		GRAIN COMPOSITION														MX		CEMENT COMPOSITION							TOTALS			Sample ID Number					
		Mean Grain Size (mm)	Overall Sorting	Monocrystalline Quartz	Polycrystalline Quartz	Mica	K-Feldspar	Plagioclase Feldspar	Chert	Igneous RF's	Metamorphic RF's	Sandstone Fragments	Clay Balls	Shale Fragments	Plant Remains	Carbonate Fragments	Shell Fragments	Glauconite	Heavy Minerals	Others	Detrital Clay Matrix	Authigenic Clay	Silica	Calcite	Dolomite	Siderite	Anhydrite	Iron Sulfide*	Total Quartz		Total Clay Minerals	Total Carbonates			
641.7	D	0.45	WS	87	Tr	-	-	-	-	-	-	-	-	-	-	-	-	-	-	-	-	-	-	-	-	-	-	-	-	-	-	-	-	047	
668.0	G	0.38	MMS	85	-	-	Tr	-	-	-	-	-	-	-	-	-	-	-	Tr	-	-	Tr	15	-	-	-	-	-	-	-	Tr	100	-	-	077
671.7	A	0.37	MMS	87	-	-	-	-	-	-	-	-	-	-	-	-	-	-	Tr	-	4	-	3	-	-	-	-	-	-	6	90	4	-	009	

MX = Depositional matrix (lines deposited simultaneously with the sand grains). RF's = Rock Fragments.
* = Includes pyrite and marcasite.

SELECTED PHOTOMICROGRAPHS

Characteristic features of the caprock (Joachim dolomite), the Joachim-St. Peter Transition, and the green, white, and gray St. Peter sandstone are illustrated in Figures I-6 through I-19. All samples have been impregnated with blue epoxy resin and stained with Alizarin Red "S" dye.

FIGURE I-6

WELL: YAKLEY "A"

FORMATION: JOACHIM DOLOMITE

DEPTH: 641.0 Feet

SAMPLE NO.: D391-006

RED DOT = 0.03 mm

DESCRIPTION

Dolomite (flesh colored) is the dominant mineral present in the Joachim Formation at this depth in Well A. Minor quartz (colorless) occurs. Intercrystalline, unconnected small pores (blue) occupy about 12% of the rock volume. Black areas are sulfides. Dolomite crystals are euhedral indicating that they formed as a result of recrystallization of another carbonate phase, probably micrite (lime mud). Crossed nicols.

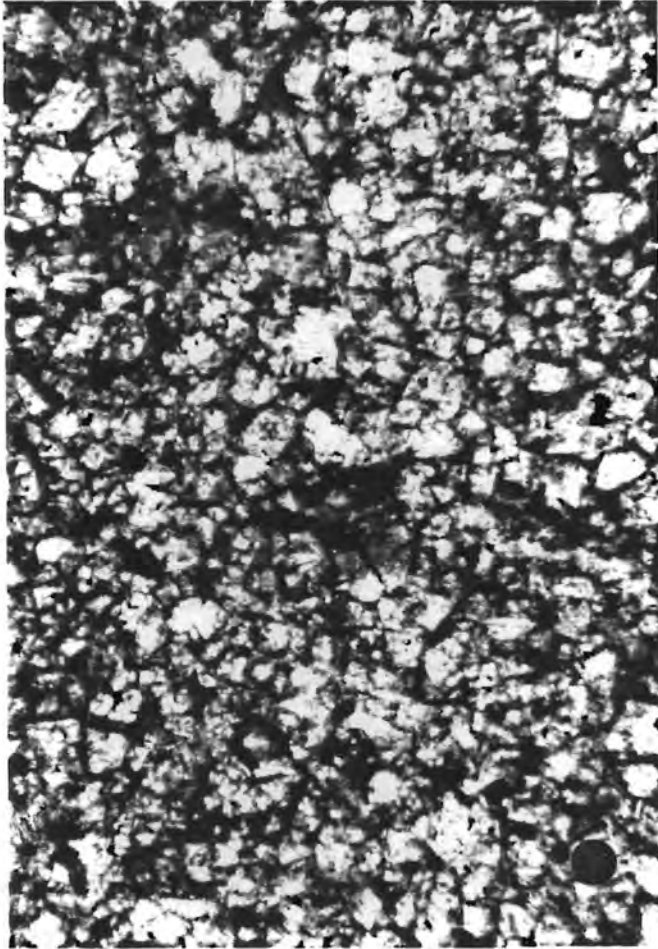


FIGURE I-7

WELL: YAKLEY "IW"

FORMATION: JOACHIM-ST. PETER TRANSITION

DEPTH: 651.7 Feet

SAMPLE NO.: D391-058

RED DOT = 0.12 mm

PHOTOGRAPH

DESCRIPTION

A

Finely crystalline dolomite (recrystallized from lime mud) occurs at this depth (medium to dark brown) and is interlayered with poorly sorted quartz (colorless). Dolomite (pale yellow) partially cements quartz grains. Black areas on the left of the photograph are iron sulfides. (Plane polarized light).

B

Crossed nicols view of A shows that some porosity (blue areas of A) is partially filled by dolomite. The black, rhombohedral shaped area in the finely crystalline dolomite is the result of the dissolution of a dolomite rhomb.

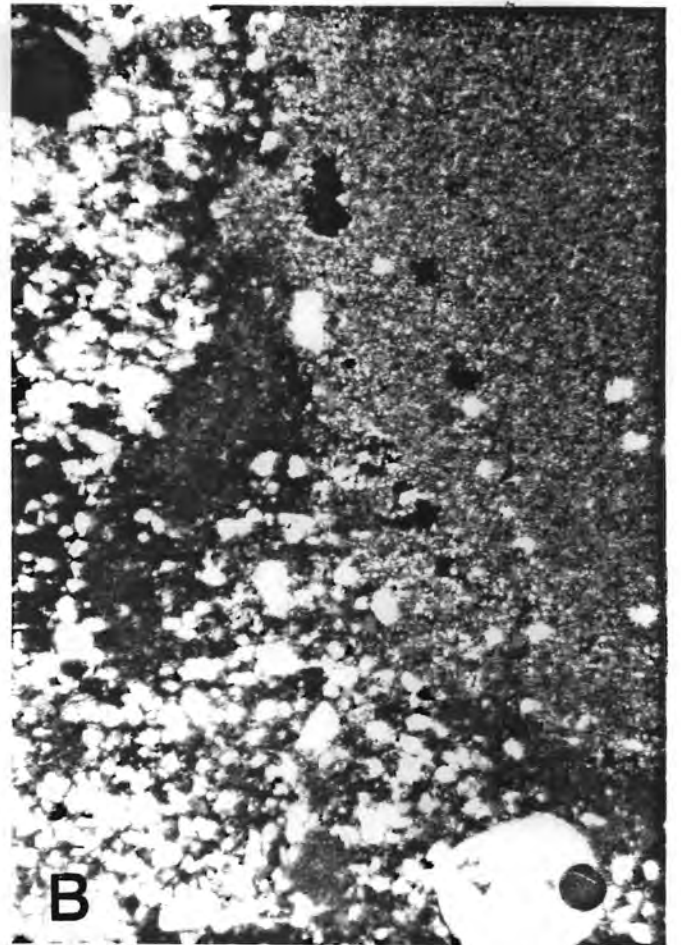


FIGURE I-8

WELL: YAKLEY "C"

FORMATION: JOACHIM-ST. PETER TRANSITION

DEPTH: Photo A = 637.0 Ft; Photo B = 641.6 Feet

SAMPLE NO.: A: D391-023; B: D391-027

RED DOT = 0.03 mm

PHOTOGRAPH

DESCRIPTION

A

Partially recrystallized dolomite intraclasts (dark brown with green) are set in a recrystallized dolomite matrix (colorless). Some very fine grained quartz (rounded, colorless) occurs. Pinkish areas are calcite. (Crossed nicols).

B

Minor silica overgrowths occur on quartz grains (colorless or gray). The quartz appears to nearly float in the fine grained dolomite (pale yellow) matrix. Very finely crystalline dolomite intraclasts (medium brown) have been partially recrystallized. (Crossed nicols). Black areas are open pores.

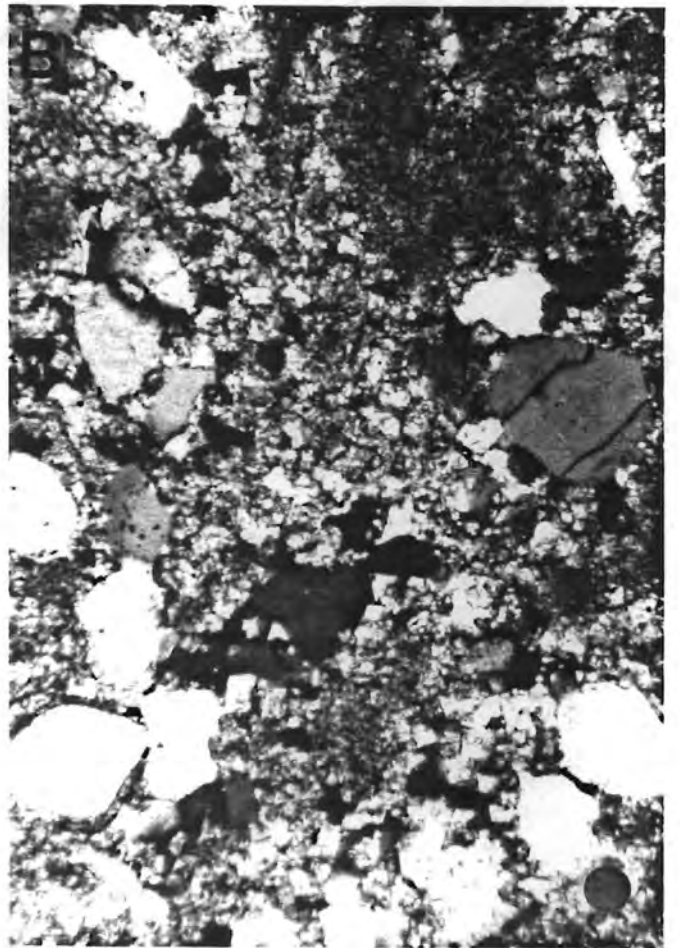


FIGURE I-9

WELL: YAKLEY "C"

FORMATION: JOACHIM-ST. PETER TRANSITION

DEPTH: Photos A & B: 643.0 Ft; Photo C: 644.0 Feet

SAMPLE NO.: A & B: D391-028; C: D391-030

<u>PHOTOGRAPH</u>	<u>MAGNIFICATION</u>	<u>DESCRIPTION</u>
A	Red Dot = 0.12 mm	Poorly sorted medium grained transitional sand composed dominantly of quartz (colorless). Iron sulfide (black) has crystallized in the pore system. Clay (blue-green) is abundant. (Plane polarized light). Note the bimodal grain size distribution.
B	Red Dot = 0.12 mm	Under crossed nicols, clays are seen to drape many of the quartz grains. The depositional matrix also appears to be moderately well crystallized. X-ray diffraction analysis confirms that some sericite is present.
C	Red Dot = 0.03 mm	This uppermost green, lower most transition sand contains carbonaceous (brown) laminations. Quartz (colorless) grain size distribution is bimodal. Minor iron sulfide is present (plane polarized light).

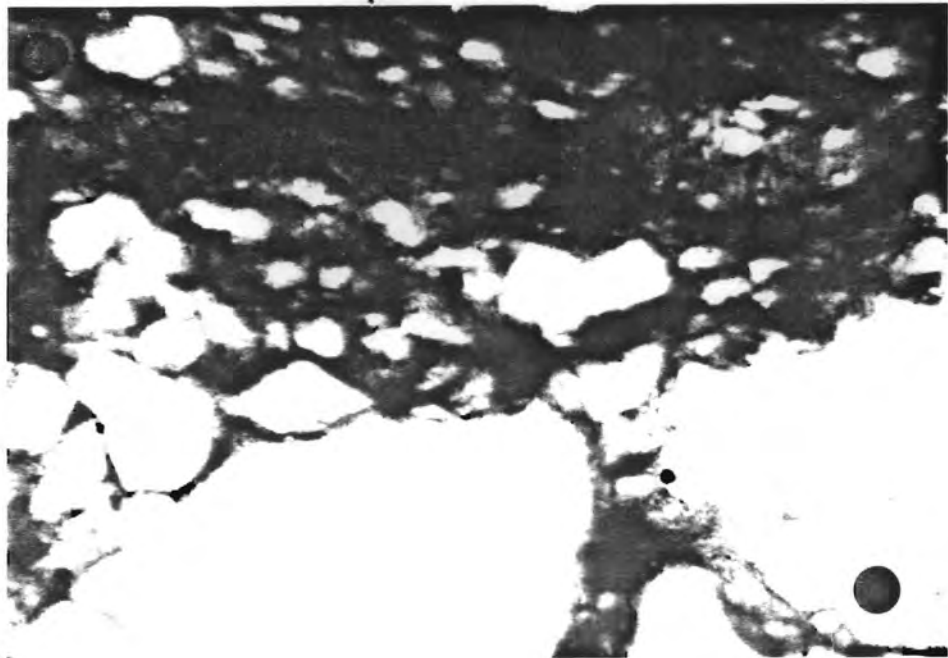
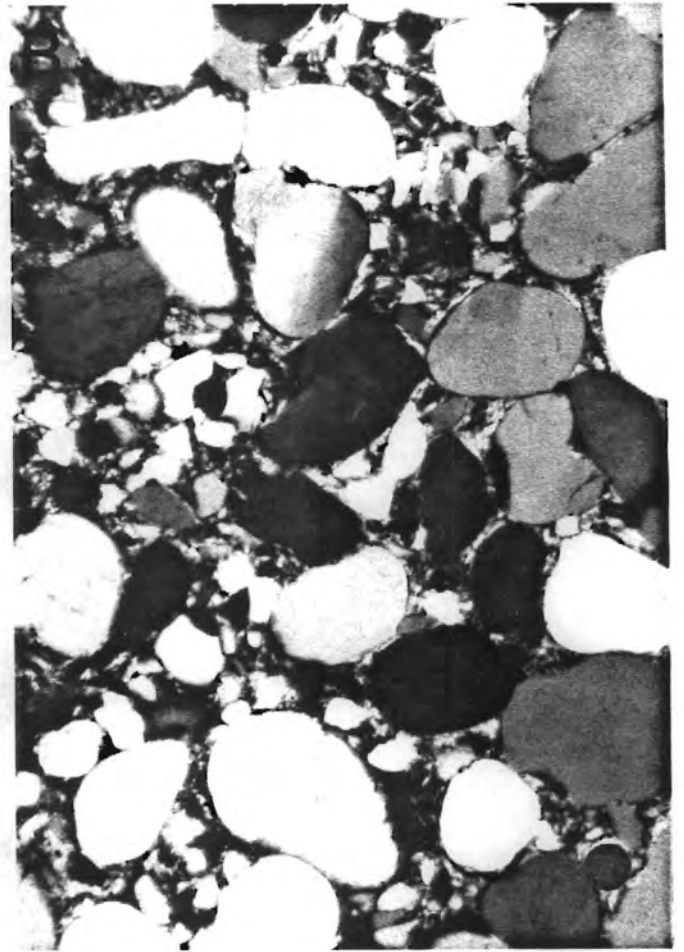
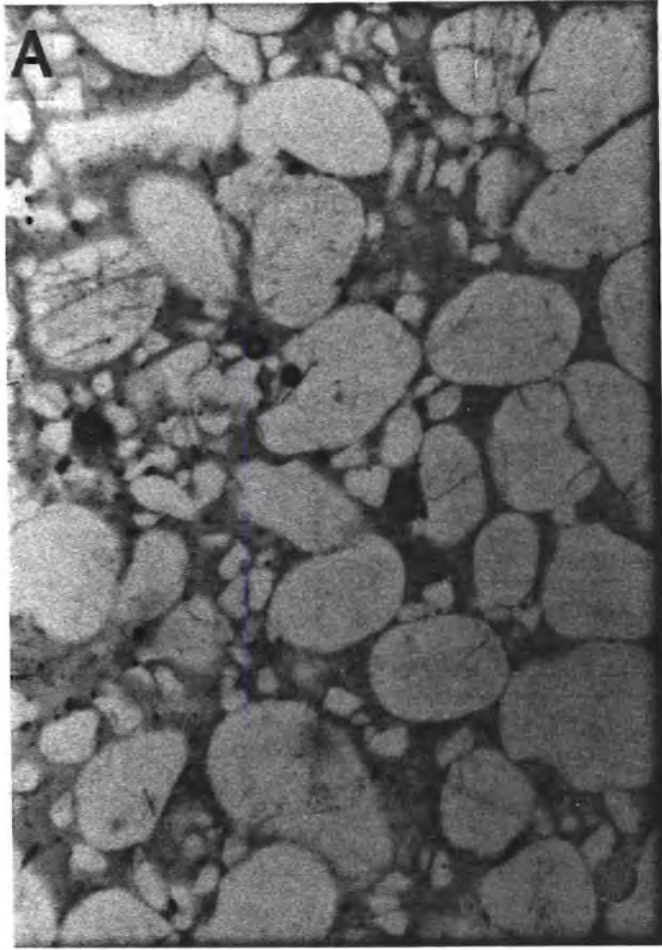


FIGURE I-10

WELL: YAKLEY "D"

FORMATION: UPPERMOST GREEN ST. PETER, LOWERMOST TRANSITION

DEPTH: 633.0 Feet

SAMPLE NO.: D391-042

RED DOT = 0.12 mm

PHOTOGRAPH

DESCRIPTION

A

Quartz grains (colorless) appear to float in the dark brown to black depositional matrix. Quartz grains are subrounded to well rounded, and the grain size distribution is bimodal. Dolomite crystallites (flesh colored, rhombs) occur sporadically throughout. (Plane polarized light).

B

A crossed nicols view reveals that most quartz grains (colorless to black) are rimmed by authigenic cement, which is dolomite.

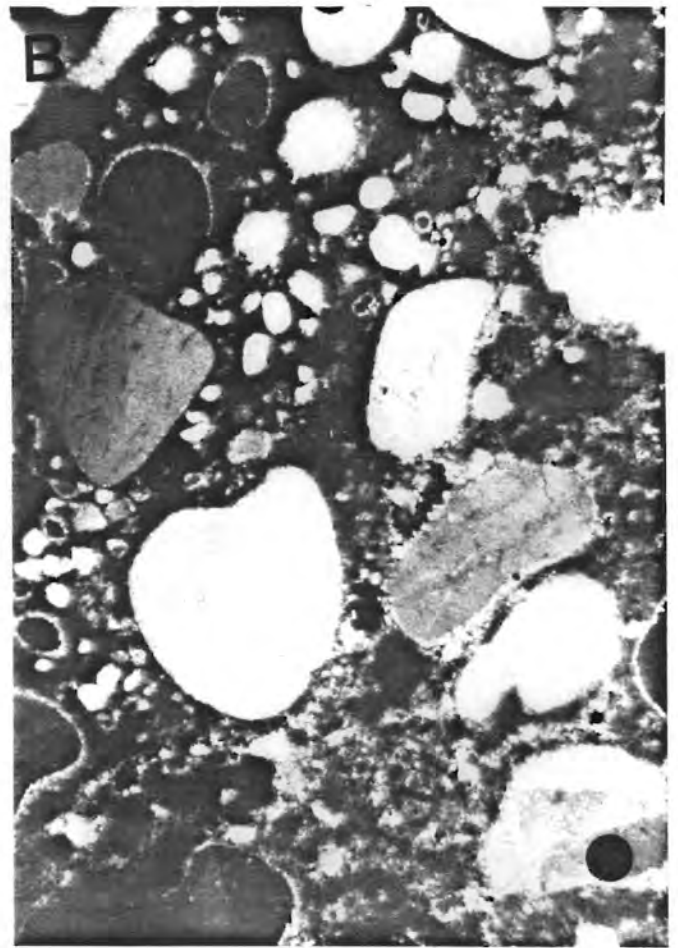
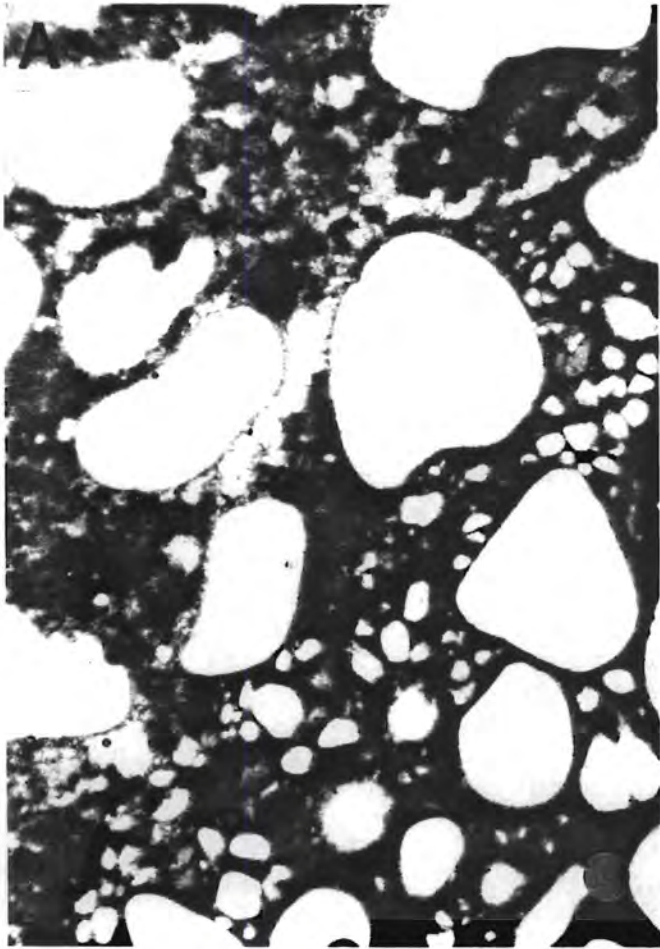


FIGURE I-11

WELL: YAKLEY "F"

FORMATION: ST. PETER SANDSTONE (GREEN)

DEPTH: 657.0 Feet

SAMPLE NO.: D391-083

<u>PHOTOGRAPH</u>	<u>MAGNIFICATION</u>	<u>DESCRIPTION</u>
A	Red Dot = 0.12 mm	Poorly sorted medium grained sandstone composed of quartz (colorless). Quartz grains are subrounded to well rounded. Depositional matrix (medium to dark brown) occludes much of the pore space. Minor calcite cement (pink) occurs in this sand: (Plane polarized light).
B,C	Red Dot = 0.03 mm	Higher magnification views illustrate that the matrix is fine grained and contains some dolomite. Both pyrite and marcasite (black) have crystallized in the pore system. Heavy minerals (dark brown, photo C) occur in trace (less than 1%) amounts throughout the interval. Quartz grains frequently contain inclusions (rutile?). (Plane polarized light).
D	Red Dot = 0.03 mm	Crossed nicols view of C illustrates that the matrix is finely crystalline.

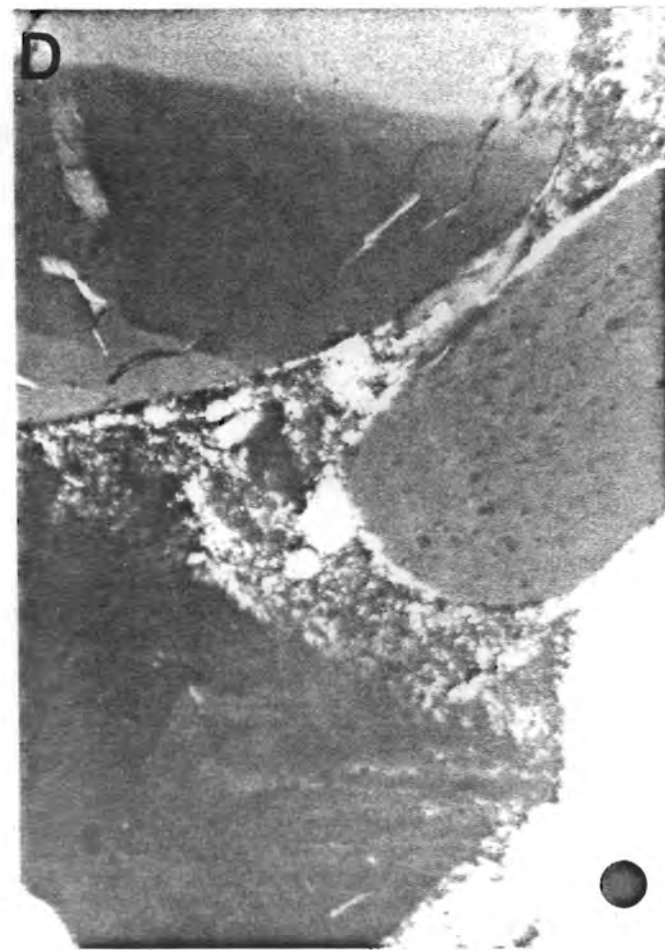
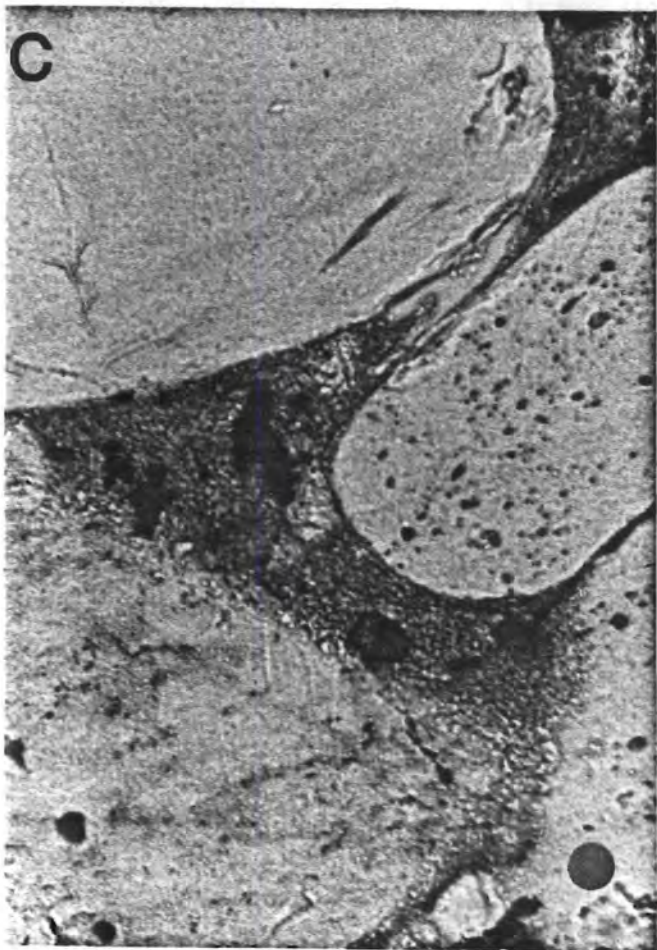
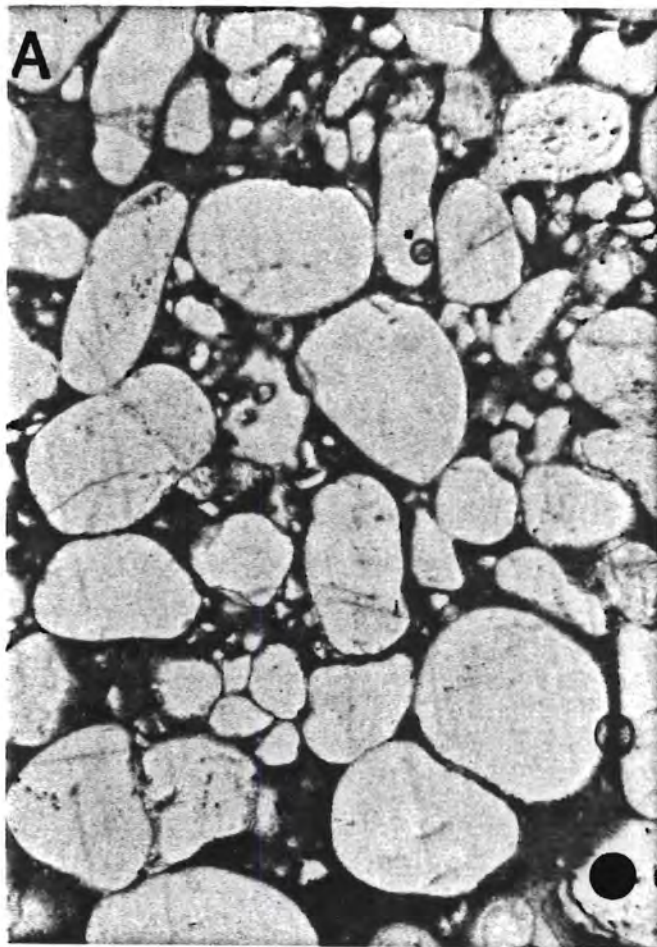


FIGURE I-12

WELL: YAKLEY "F"

FORMATION: ST. PETER SANDSTONE (GREEN)

DEPTH: 659.7 Feet

SAMPLE NO.: D391-084

<u>PHOTOGRAPH</u>	<u>MAGNIFICATION</u>	<u>DESCRIPTION</u>
A	Red Dot = 0.12 mm	Medium grained moderately well sorted sandstone consisting of quartz (colorless). Quartz grains are subangular to well rounded and are surrounded by clay rims (green). The green sand at this depth is more porous (blue) than at shallower depths. (Plane polarized light).
B	Red Dot = 0.012 mm	Very high magnification view illustrating a partial green clay rim and inclusions in quartz grains (pink). "Ghosts" of dolomite rhombs occur in the pore system. (Plane polarized light).
C,D	Red Dot = 0.03 mm	Photo C was taken in plane polarized light and photo D was taken with crossed nicols. This pair of photos illustrates the distribution and degree of crystallinity of the matrix. Green clay partially or completely rims quartz grains and is moderately well crystallized.

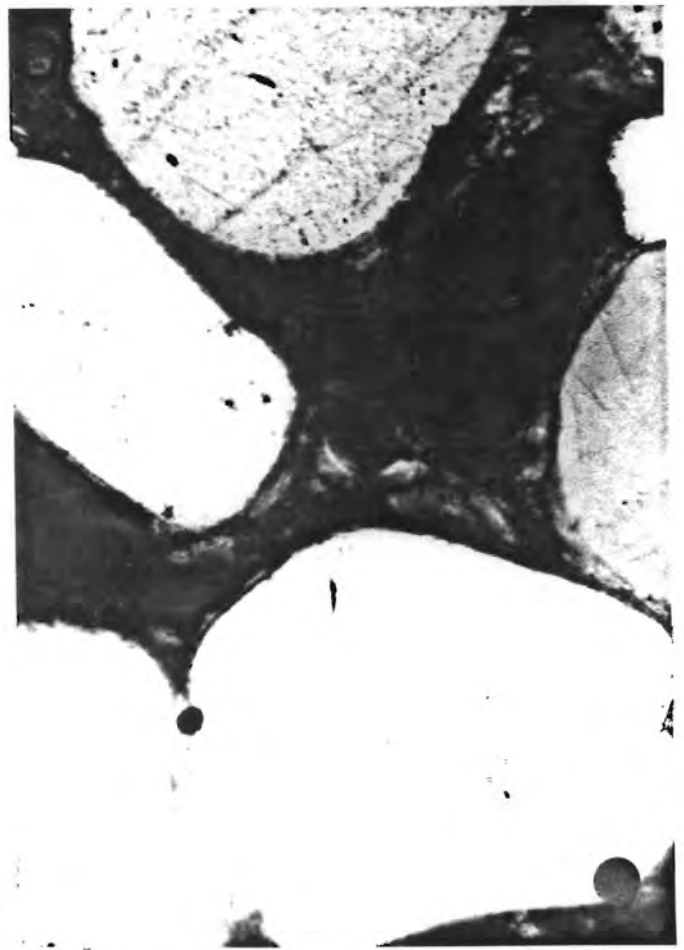
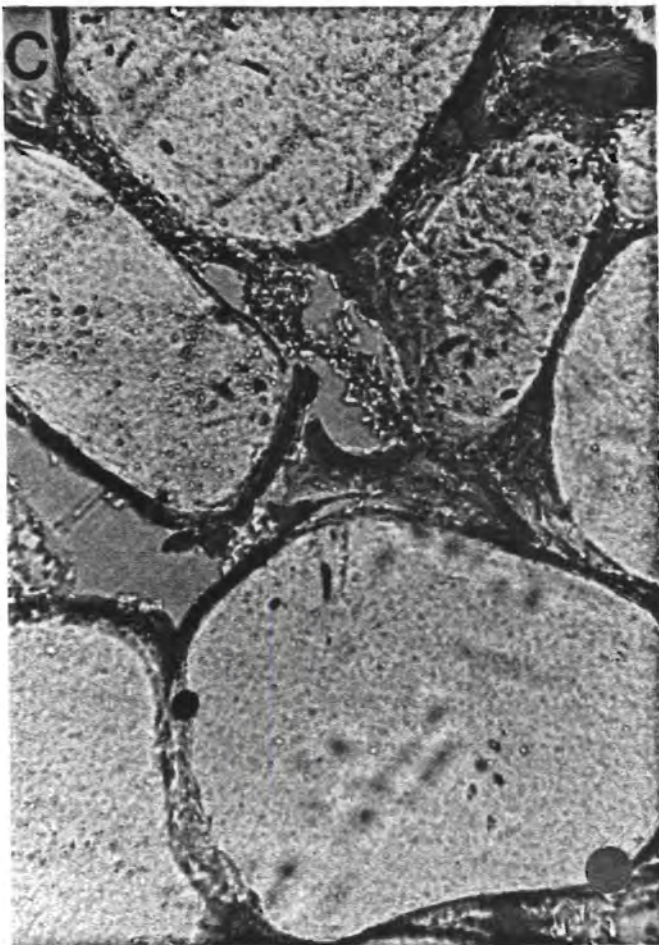
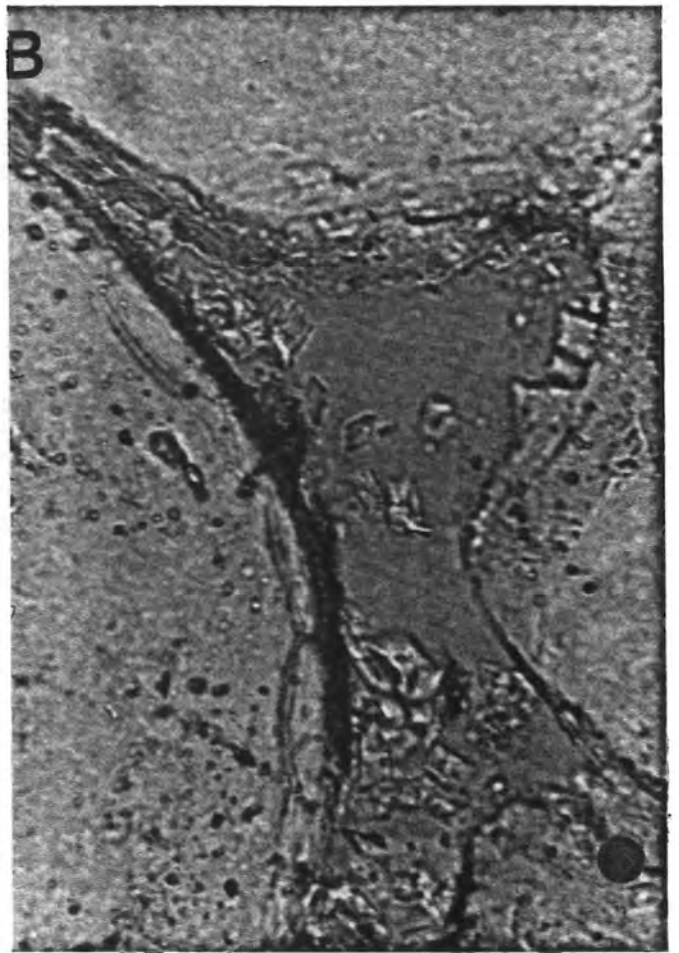
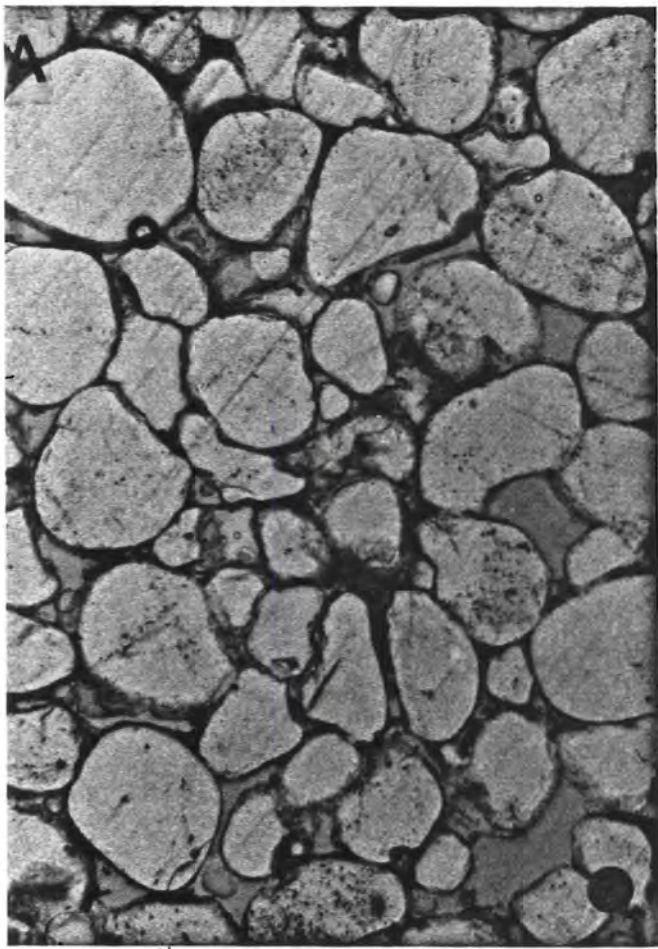


FIGURE I-13

WELL: YAKLEY "G"

FORMATION: ST. PETER SANDSTONE (GREEN)

DEPTH: 656.5 Feet

SAMPLE NO.: D391-075

<u>PHOTOGRAPH</u>	<u>MAGNIFICATION</u>	<u>DESCRIPTION</u>
A	Red Dot = 0.12 mm	Medium grained poorly sorted sandstone composed of quartz (colorless). Quartz grains are subrounded to well rounded, and the grain size distribution is bimodal. The finer mode is associated with depositional matrix (black). (Plane polarized light).
B	Red Dot = 0.03 mm	Higher magnification view of the depositional matrix illustrating that it is a mixture of clay and iron sulfide. (Plane polarized light).
C,D	Red Dot = 0.012 mm	These very high magnification views (C: plane polarized light; D: crossed nicols) illustrate another pore filled by depositional matrix. The small crystallites seen in photo C are authigenic feldspars and are mixed with depositional clay.

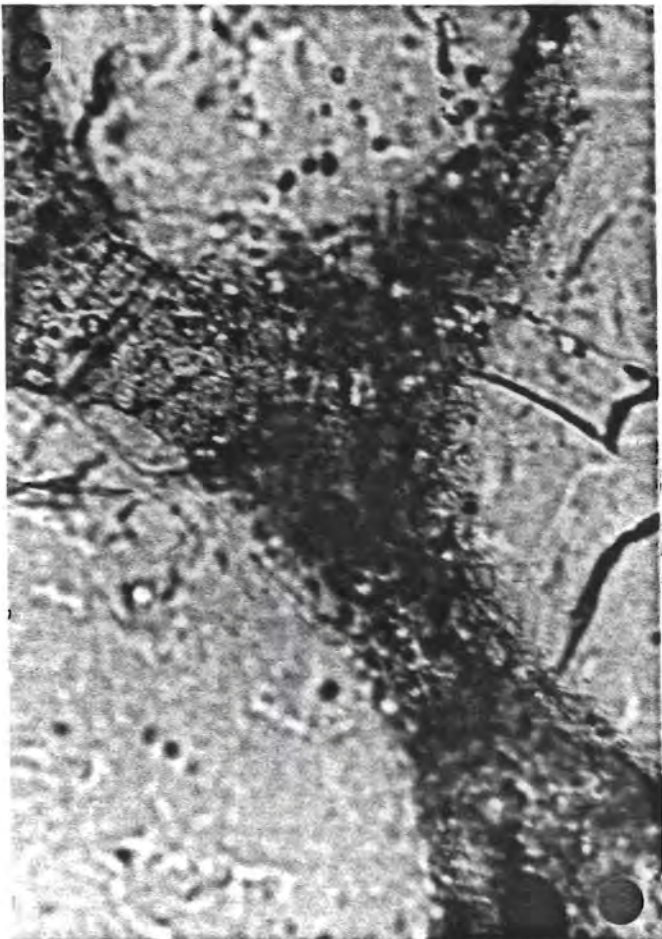
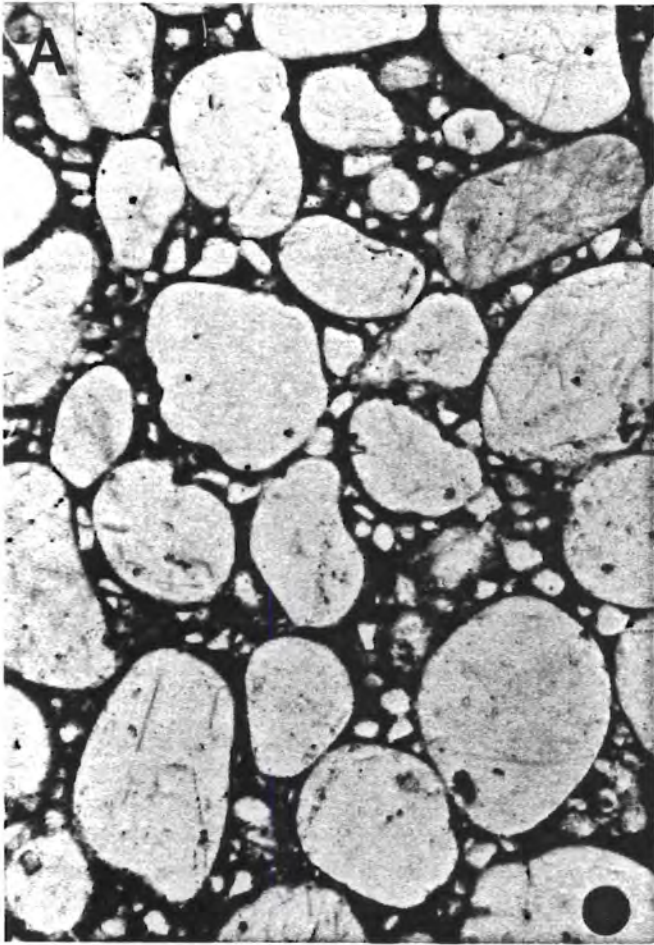


FIGURE I-14

WELL: YAKLEY "G"

FORMATION: ST. PETER SANDSTONE (GREEN)

DEPTH: 658.2 Feet

SAMPLE NO.: D391-076

<u>PHOTOGRAPH</u>	<u>MAGNIFICATION</u>	<u>DESCRIPTION</u>
A	Red Dot = 0.12 mm	Poorly sorted medium grained sandstone consisting of quartz (colorless). Quartz grains are subangular to well rounded. Depositional matrix (brown) is abundant. Iron sulfides (black) have crystallized in the pore system. (Plane polarized light).
B	Red Dot = 0.012 mm	High magnification view of a pore completely filled by depositional matrix. Iron sulfides (black) are also present in the pore system.
C,D	Red Dot = 0.03 mm	This pair of photos illustrate the distribution and crystallinity of the matrix (C: plane polarized light; D: crossed nicols). Some porosity (blue) is present. Iron sulfide (black) is abundant in this view and has crystallized at the expense of quartz. Quartz grains (colorless) contain rod-like inclusions. Depositional matrix rims quartz grains and has partially recrystallized.

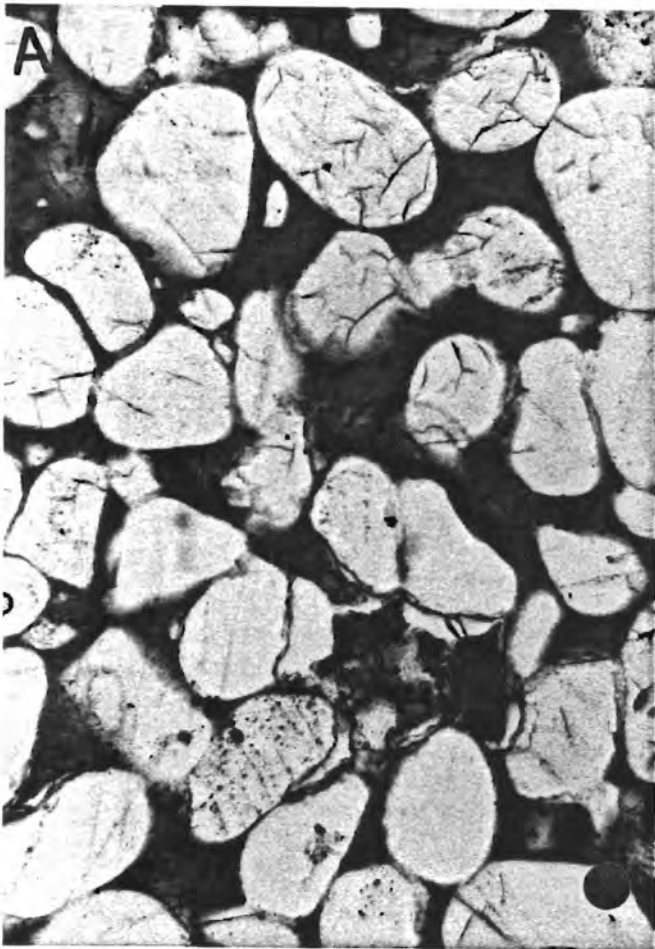


FIGURE I-15

WELL: YAKLEY "D"

FORMATION: ST. PETER (WHITE)

DEPTH: 641.7 Feet

SAMPLE NO.: D391-047

RED DOT = 0.12 mm

PHOTOGRAPH

DESCRIPTION

A

Well sorted medium grained sandstone consisting of quartz (colorless) and cemented by silica overgrowths (colorless). Original quartz grains were subrounded to well rounded, and their boundaries are marked by dust rims. Pyrite (black) and sparse authigenic clay cement (bluish-green) occur. Pink stained areas are calcite-rich. (Plane polarized light).

B

Crossed nicols view of A further illustrates the presence of silica overgrowths and shows their interpenetration. The presence of a large polycrystalline quartz grain (bottom, center) is revealed by crossed nicols examination. Some pore spaces are partially filled by authigenic clay (gray and black speckled).

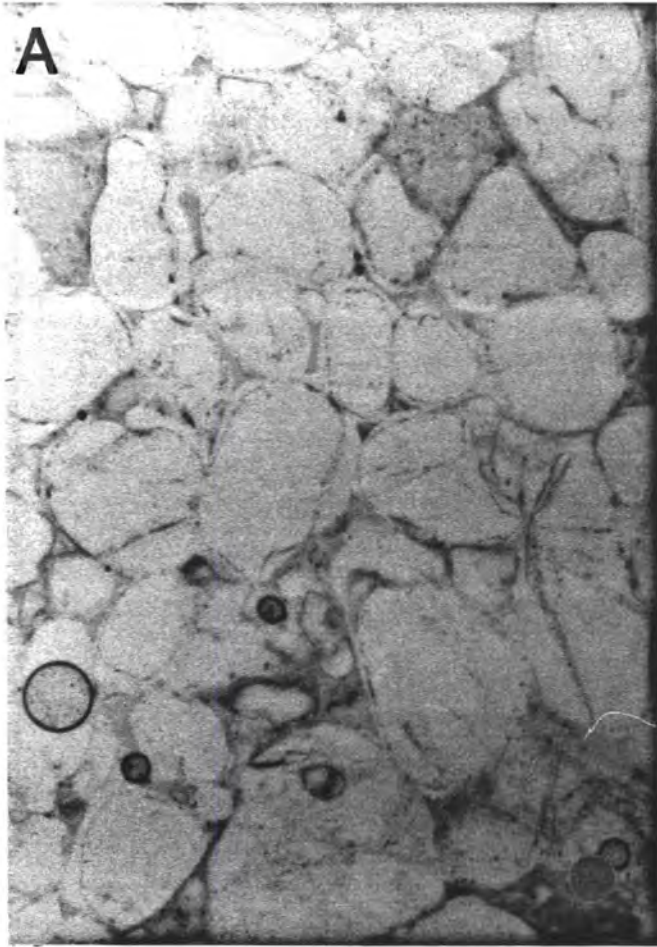


FIGURE I-16

WELL: YAKLEY "G"

FORMATION: ST. PETER SANDSTONE (WHITE)

DEPTH: 668.0 Feet

SAMPLE NO.: D391-077

<u>PHOTOGRAPH</u>	<u>MAGNIFICATION</u>	<u>DESCRIPTION</u>
A	Red Dot = 0.12 mm	Moderately well sorted medium grained sandstone consisting dominantly of quartz (colorless). Silica overgrowths loosely cement the rock. Some pyrite (black) occurs at this depth. (Plane polarized light).
B	Red Dot = 0.03 mm	Higher magnification view illustrates the euhedral nature of the silica overgrowths. The black circle is an air bubble, formed during thin section preparation. (Plane polarized light).
C,D	Red Dot = 0.03 mm	Crossed nicols. Silica overgrowths are generally cleaner than the quartz grains on which they nucleate. This is well illustrated in photo C. Silica overgrowths are not apparent in photo D.

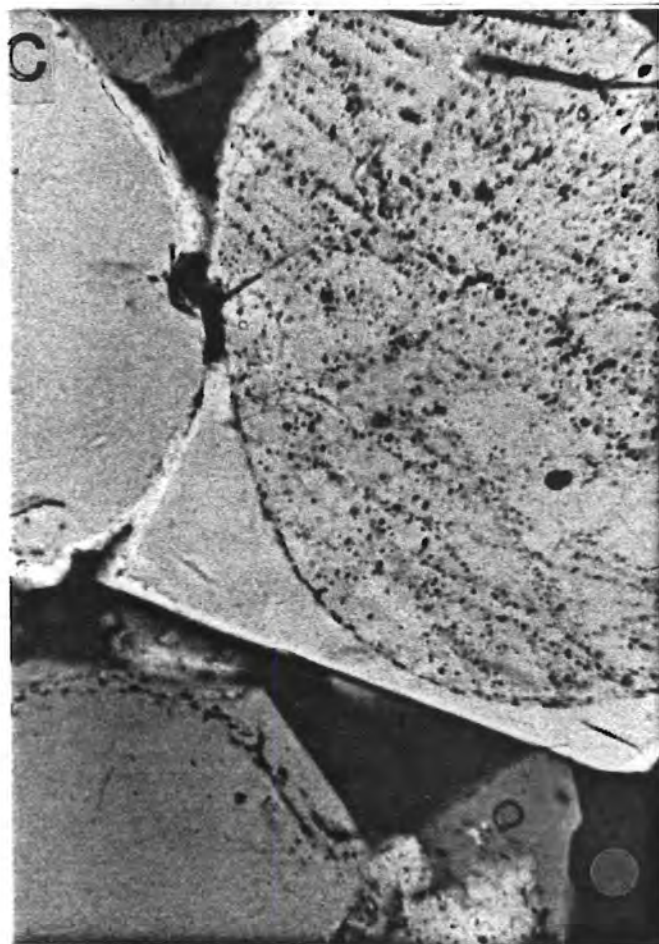
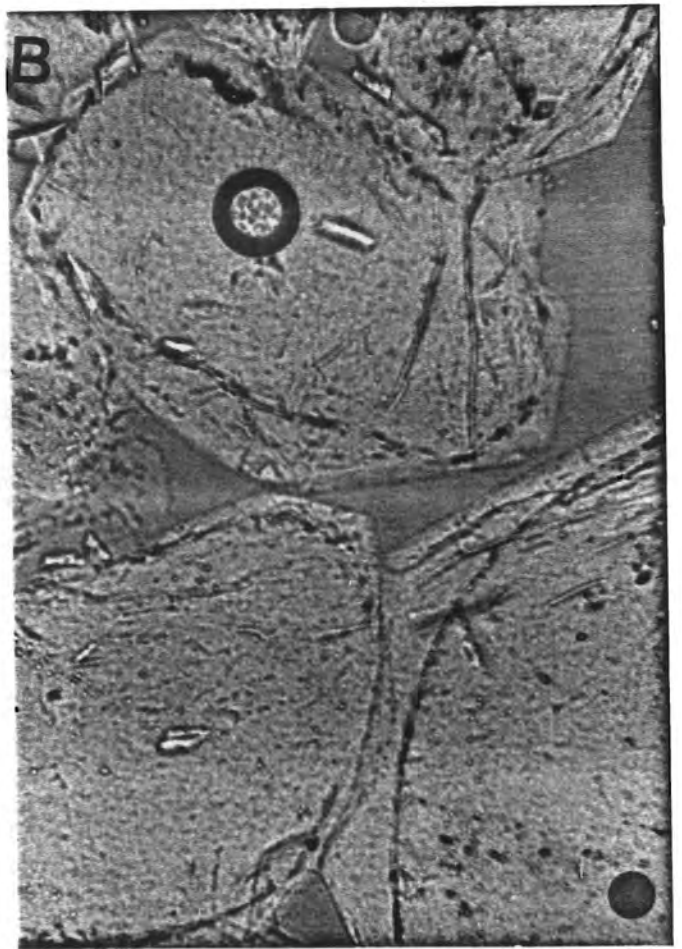
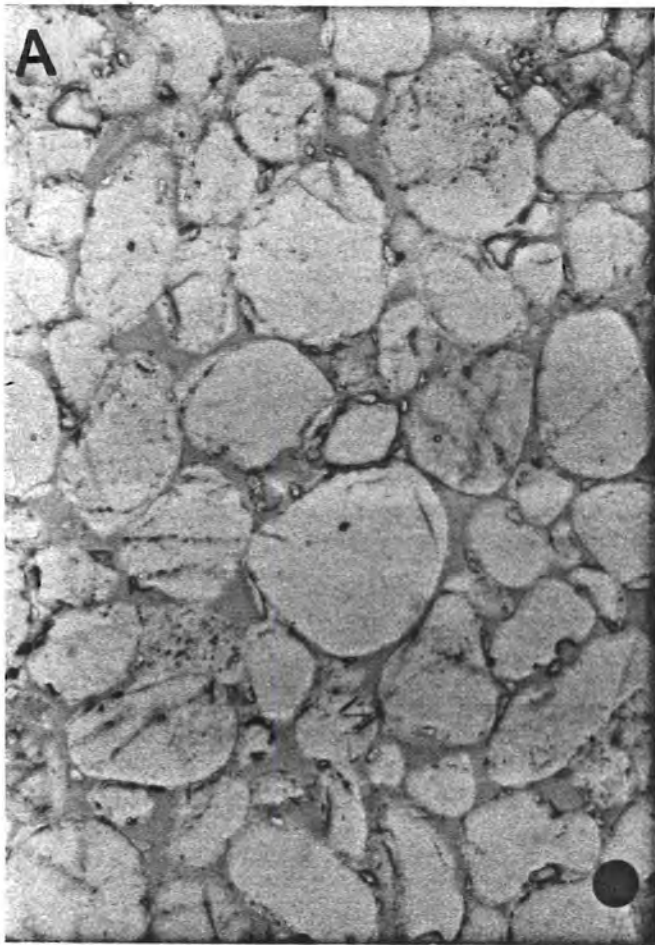


FIGURE I-17

WELL: YAKLEY "C"

FORMATION: ST. PETER (WHITE)

DEPTH: 654.4 Feet

SAMPLE NO.: D391-039

Red Dot = 0.12 mm

DESCRIPTION

Medium grained moderately well sorted sandstone consisting of quartz (colorless). The sand is partially cemented by silica overgrowths and authigenic clay (green). Calcite cement (pink) is dominant. Frequently, at this depth, the white St. Peter sandstone is fractured, and vertical fractures are infilled with calcite. The order of cementation, observed for this particular sample is:

- Oldest: 1) Minor pyrite (black) precipitation on original grains.
- 2) Precipitation of silica overgrowths.
- 3) Precipitation of minor authigenic clay.
- Youngest: 4) Precipitation of calcite.

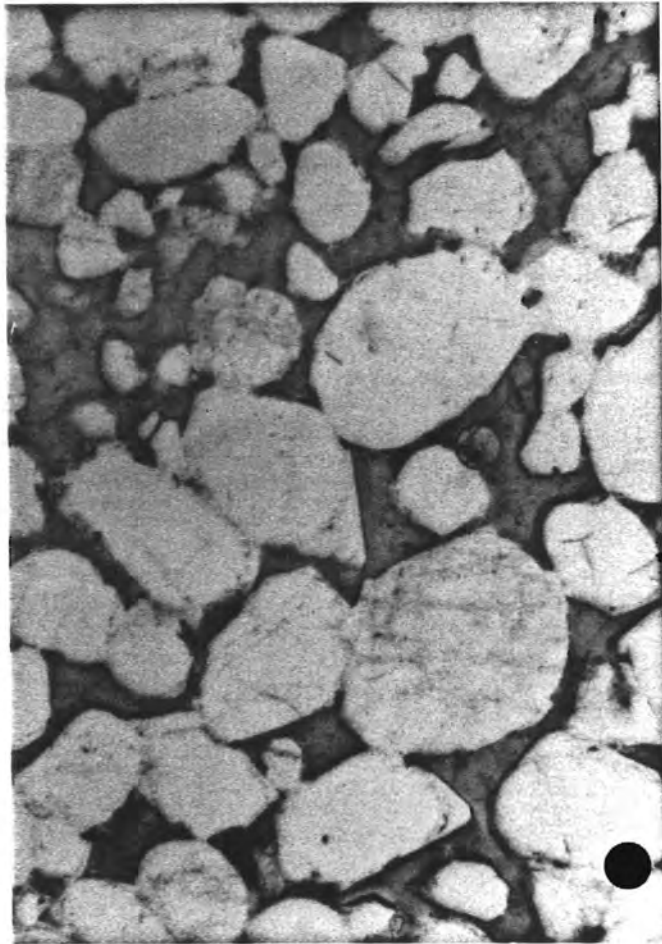


FIGURE I-18

WELL: YAKLEY "A"

FORMATION: ST. PETER (WHITE)

DEPTH: 671.7 Feet

SAMPLE NO.: D391-009

RED DOT = 0.12 mm

DESCRIPTION

Medium grained poorly sorted sandstone composed of quartz (colorless). Minor silica overgrowths appear to be sutured. Abundant iron sulfide (black) precipitation has occurred. Some detrital clay (dark brown) is present. This sample is representative of the lower white St. Peter Sandstone.

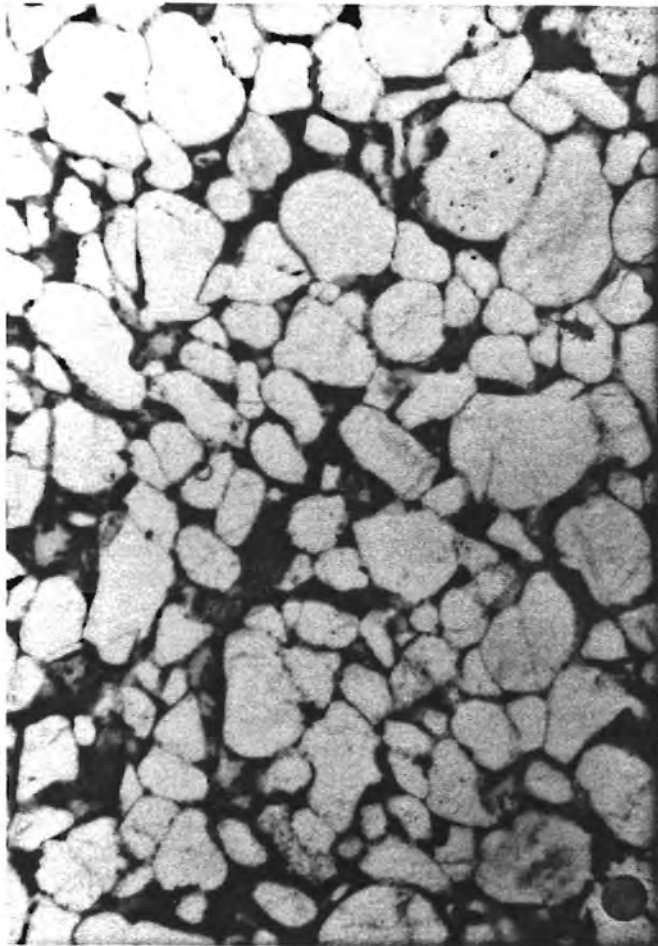


FIGURE I-19

WELL: YAKLEY "C"

FORMATION: ST. PETER SANDSTONE (DARK GRAY)

DEPTH: 707.8 Feet

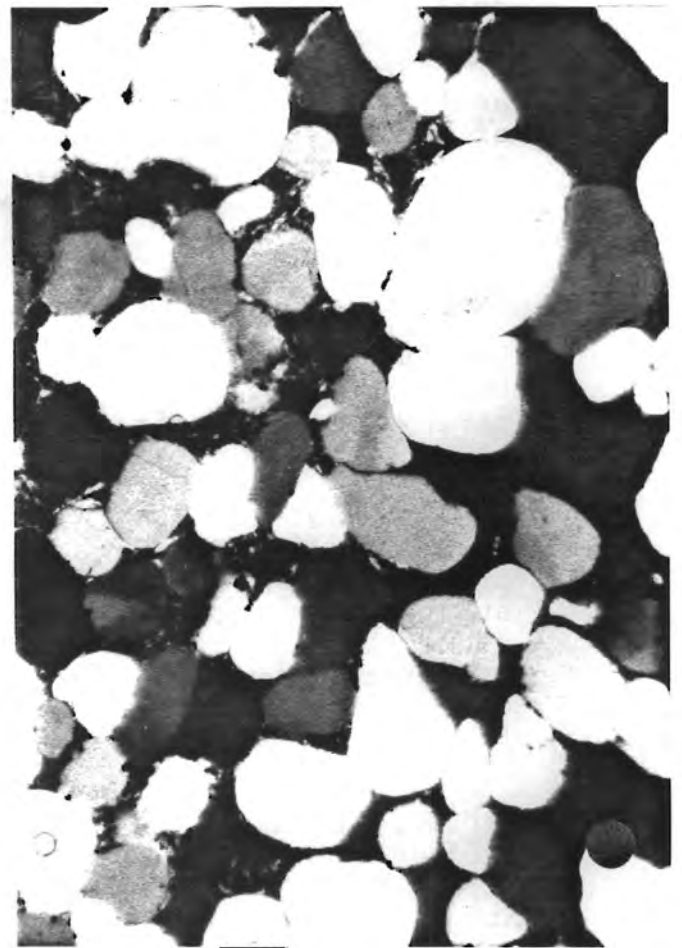
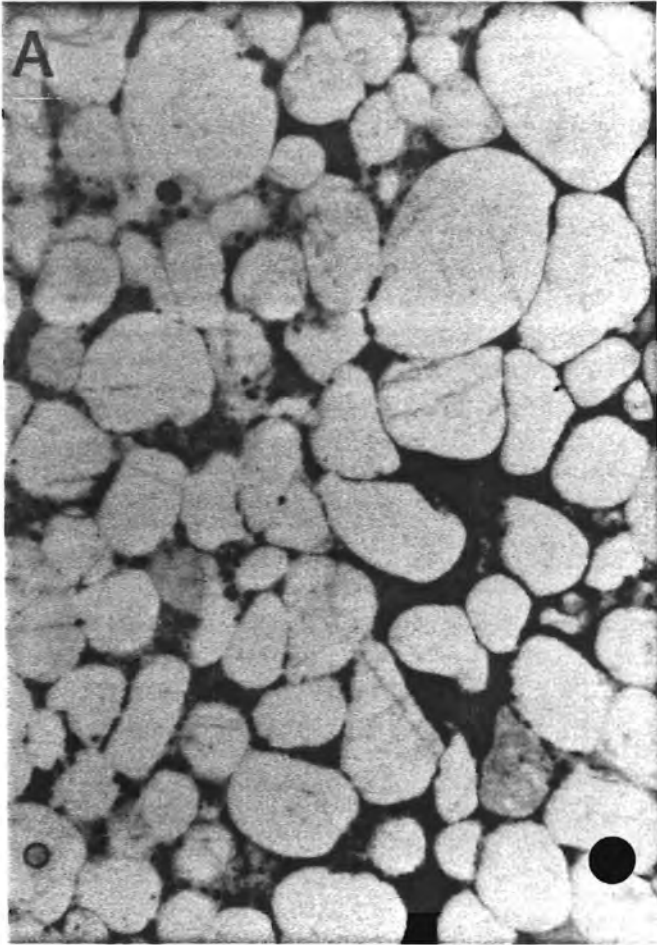
SAMPLE NO.: D391-067

RED DOT = 0.12 mm

PHOTOGRAPH

DESCRIPTION

- | | |
|---|---|
| A | Moderately well sorted medium grained sandstone composed dominantly of quartz (colorless). The sand is cemented by iron sulfide (black) and authigenic clay (greenish-blue). Minor silica overgrowths occur. (Plane polarized light). |
| B | This crossed nicols view shows that authigenic clay is distributed sporadically in the pore system. Quartz grains have been partially etched during iron sulfide precipitation. |



X-RAY DIFFRACTION ANALYSIS

General -

Representative samples of the Caprock, the Joachim-St. Peter Transition, and the various St. Peter Sandstones were subjected to fine (less than five micron) fraction X-ray diffraction analysis. Results of this analysis are presented in Tables I-7 through I-11.

Joachim Formation -

Three samples were subjected to analysis. The Joachim is composed of ferroan dolomite or ankerite (49-78%) and calcite (7-25%). Quartz (12-19%) is the only other constituent occurring in all samples. Other constituents include illite and potassium feldspar, detected in one sample, and anhydrite, detected in two samples. Results are given in Table I-7.

Joachim-St. Peter Transition -

The fine fraction of three transition zone samples was analyzed by X-ray diffraction. One sample was composed only of ankerite. Illite (9-19%) and quartz (26-69%) occurred as dominant mineral phases in the other samples. Dolomite, pyrite, and potassium feldspar were other phases detected. Results are presented in Table I-8.

Green St. Peter Sandstone -

Since air will most likely be injected into the green St. Peter and since the fine fraction analysis should yield, primarily, the composition of pore fill minerals, eight samples were analyzed. Detailed results are presented in Table I-9.

Quartz (20-85%) and illite (4-42%) occur in all samples. Kaolinite (4%) is the only other clay mineral detected and was present in only one sample. Potassium feldspar (5-27%) is another major constituent. Other mineral phases present include calcite, marcasite, sericite, pyrite, ankerite, and anhydrite.

White St. Peter Sandstone -

The fine fraction of the white St. Peter consists primarily, of quartz (31-67%), illite (17-59%), and potassium feldspar (3-17%). Other constituents occurring sporadically in the interval include calcite, marcasite, pyrite, and anhydrite. Results are presented in Table I-10.

Medium to Dark Gray St. Peter Sandstone -

Results of the X-ray diffraction analysis of two samples of the medium to dark gray St. Peter are presented in Table I-11. Quartz (14%), illite (25-28%) and trace (less than 1%) amounts of potassium feldspar were detected in both samples. Kaolinite (46%) was detected in both samples. Kaolinite (46%) was detected in one sample, and pyrite (41%) was detected in the other sample. Other constituents detected include calcite, dolomite, anhydrite, and sericite.

TABLE I-7

Semiquantitative X-Ray Diffraction Analysis of the Fine (Less Than 5 Micron) Size Fraction, Caprock Samples

Well	A	B	IW
Depth (Ft)	613.3	652.6	649.0
Sample No.	D391-003	D391-020	D391-055
Illite-Smectite	-	-	-
Illite	4	-	-
Kaolinite	-	-	-
Chlorite	-	-	-
Quartz	12	19	15
Potassium Feldspar	6	-	-
Plagioclase Feldspar	-	-	-
Calcite	27	25	7
Dolomite	-	50	-
Ankerite	49	-	78
Anhydrite	2	6	-

TABLE I-8

Semiquantitative X-Ray Diffraction Analysis of the
 Fine (Less Than 5 Micron) Size Fraction, Joachim-St. Peter
 Transition Zone

Well	C	IW	IW
Depth (Ft)	643.0	649.5	651.5
Sample No.	D391-029	D391-056	D391-057
Illite-Smectite	-	-	-
Illite	19	-	9
Kaolinite	-	-	-
Chlorite	-	-	-
Quartz	69	-	26
Potassium Feldspar	-	-	12
Plagioclase Feldspar	-	-	-
Calcite	-	-	2
Dolomite	-	-	51
Pyrite	12	-	-
Ankerite	-	100	-

TABLE I-9

Semi-quantitative X-Ray Diffraction Analysis of the
 Fine (Less Than 5 Micron) Size Fraction,
 Green St. Peter Sandstone

Well	A	C	D	D	IW	IW	IW	IW	G
Depth (Ft)	662.0	645.0	638.0	641.0	652.0	653.0	654.0	655.0	656.5
Sample No. D391	-007	-035	-043	-046	-059	-061	-062	-065	-075
Illite-Smectite	-	-	-	-	-	-	-	-	-
Illite	15	42	4	19	18	10	36	32	13
Kaolinite	-	-	-	-	4	-	-	-	-
Chlorite	-	-	-	-	-	-	-	-	-
Quartz	75	20	85	67	31	57	44	39	53
Potassium Feldspar	10	-	5	6	11	27	12	8	21
Plagioclase Feldspar	-	-	-	-	-	-	-	-	-
Calcite	-	1	4	3	-	3	5	3	4
Dolomite	-	-	-	-	-	-	Tr	-	-
Marcasite	-	9	-	-	5	-	-	5	-
Sericite	-	28	-	-	-	-	-	13	-
Pyrite	-	-	2	5	-	3	-	-	3
Ankerite	-	-	-	-	31	-	-	-	3
Anhydrite	-	-	-	-	-	-	3	-	-
Barite	-	-	-	-	-	-	-	-	3

TABLE I-10

Semiquantitative X-Ray Diffraction Analysis of the
Fine (Less Than 5 Micron) Size Fraction,
White St. Peter Sandstone

Well	A	C	C	IW
Depth (Ft)	671.1	652.0	654.4	665.4
Sample No.	D391-008	D391-038	D391-039	D391-063
Illite-Smectite	-	-	-	-
Illite	59	17	21	20
Kaolinite	-	-	-	-
Chlorite	-	-	-	-
Quartz	31	67	59	63
Potassium Feldspar	3	7	12	17
Plagioclase Feldspar	-	-	-	-
Calcite	-	4	-	-
Dolomite	-	-	-	-
Marcasite	7	-	5	-
Pyrite	-	5	-	-
Anhydrite	-	-	3	-

TABLE I-11

Semiquantitative X-Ray Diffraction Analysis of the
Fine (Less Than 5 Micron) Size Fraction, Medium to Dark
Gray St. Peter Sandstone

Well	A	C
Depth (Ft)	677.0	707.8
Sample No.	D391-010	D391-067
Illite-Smectite	-	-
Illite	25	28
Kaolinite	46	-
Chlorite	-	-
Quartz	14	14
Potassium Feldspar	Tr	Tr
Plagioclase Feldspar	-	-
Calcite	1	-
Dolomite	-	17
Anhydrite	1	-
Sericite	13	-
Pyrite	-	41

SCANNING ELECTRON MICROSCOPY (SEM)

The scanning electron microscope was utilized to observe the distribution of pore fill minerals in the St. Peter Sandstone and to detect microporosity in the caprock. Results are illustrated in a series of black and white photographs which accompany this report (Figures I-20 through I-29).

Joachim Dolomite -

Three Joachim dolomite samples were examined with the SEM (Figures I-20 through I-22). The Joachim is composed of well-crystallized dolomite rhombohedra. Micropores are abundant but are generally not connected. Anhydrite was detected in the pore system. Pyrite occurs as a late stage authigenic precipitate. Abundant fibrous authigenic illite precipitated after dolomitization. The Joachim most probably was originally deposited as lime mud (micrite). Subsequent recrystallization of lime mud to dolomite resulted in the formation of micropores.

Joachim - St. Peter Transition -

One sample from the transition zone was examined (Figure I-23). The examination indicates that quartz grains were deposited prior to dolomitization. Small dolomite crystals have nucleated on, and frequently encrust, quartz grains. Edges and corners of dolomite rhombohedra serve as nucleation sites for fibrous illite.

Green St. Peter Sandstone -

Four samples of the green St. Peter Sandstone were examined with the SEM (Figures I-24 through I-27). The sand is generally porous and permeable. Some silica overgrowths, dolomite and fibrous illite occur as cement. Marcasite and pyrite are common pore fill minerals in the green St. Peter Sandstone.

SEM examination reveals that the majority of illite, detected by X-ray diffraction analysis, is structural clay (detrital clay matrix). Potassium feldspar occurs in the green sand as an authigenic precipitate. Crystals are generally less than 10 microns in long dimension measurement.

White St. Peter Sandstone -

Characteristic features of the white St. Peter Sandstone are illustrated in Figure I-28. Silica overgrowths and fibrous illite occur in the pore system. Pore throats are frequently



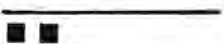


bridged by fibrous illite. By contrast with the green St. Peter, no structural clay is present, and silica overgrowths and fibrous illite are substantially more abundant.

Gray St. Peter Sandstone -

Characteristic features of the gray St. Peter Sandstone are illustrated in Figure I-29. Pore throats are bridged by fibrous illite. Pyrite is abundant and anhydrite occurs at this depth.

SCANNING ELECTRON MICROGRAPH SCALE

The micron marker indicates the photograph scale by displaying a system of bars and dots which correspond to the viewing and photographing magnification. The relative distance represented by the micron marker and the bar length for a set magnification is as follows:

Magnification	Marker display	Relative distance (μm)
100,000x		0.1 (1000 \AA)
10,000-70,000x		1.0
1,000- 7,000x		10.0
100 - 700x		100.0
15 - 70x		1000.0 (1 mm)

- Note 1: The above table can be read as follows:
The first dot is read as "1", and all other dots are read as "0". For instance, if two dots are displayed, it indicates that the length of the bar corresponds to "1", "0" μm (=10 μm). If no dots appear at all, it indicates that the relative distance is 0.1 μm .
- Note 2: The magnification of the image displayed on the viewing CRT is approx. 1.2 times that indicated on the magnification indicator. However, since the length of the micron bar corresponds to this ratio, the micron marker can be read as displayed.

FIGURE I-20

WELL: YAKLEY A

FORMATION: JOACHIM DOLOMITE

DEPTH: 641.0 Feet

D391-006

<u>PHOTOGRAPH NO.</u>	<u>MAGNIFICATION</u>	<u>DESCRIPTION</u>
0798	100x	Well crystallized dolomite rhombohedra (D) and micro intergranular porosity (P) are illustrated in this survey view. The porosity is probably secondary, generated during the recrystallization of lime mud to dolomite.
0800	700x	Closer inspection reveals that dolomite (D) occurs in a variety of sizes and that intergranular pores are abundant.
0799 0801	1000x 3000x	Higher magnification views illustrate that authigenic illite (I) is frequently intergrown with dolomite (D). Pyrite (P) occurs as a late stage precipitate.

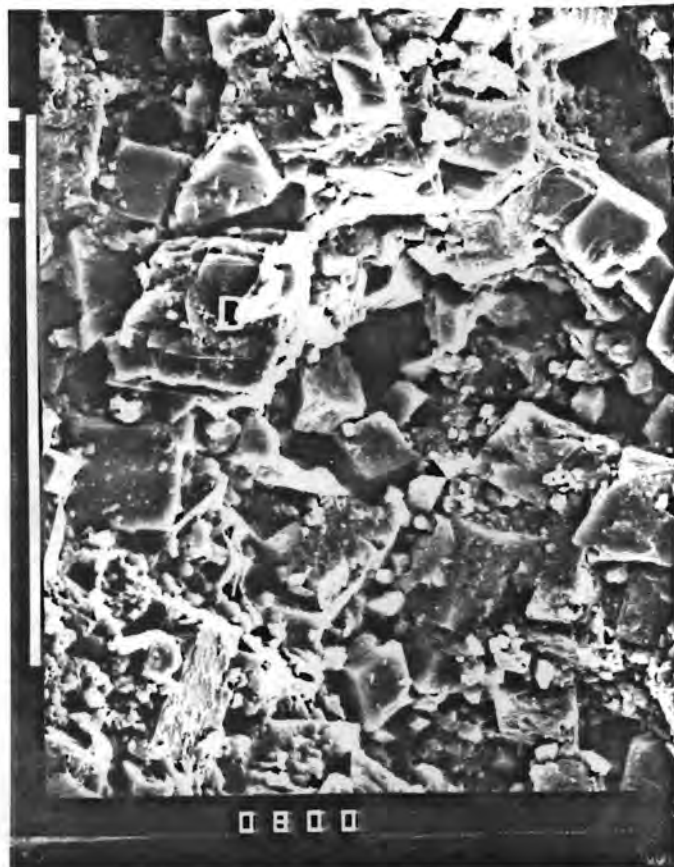
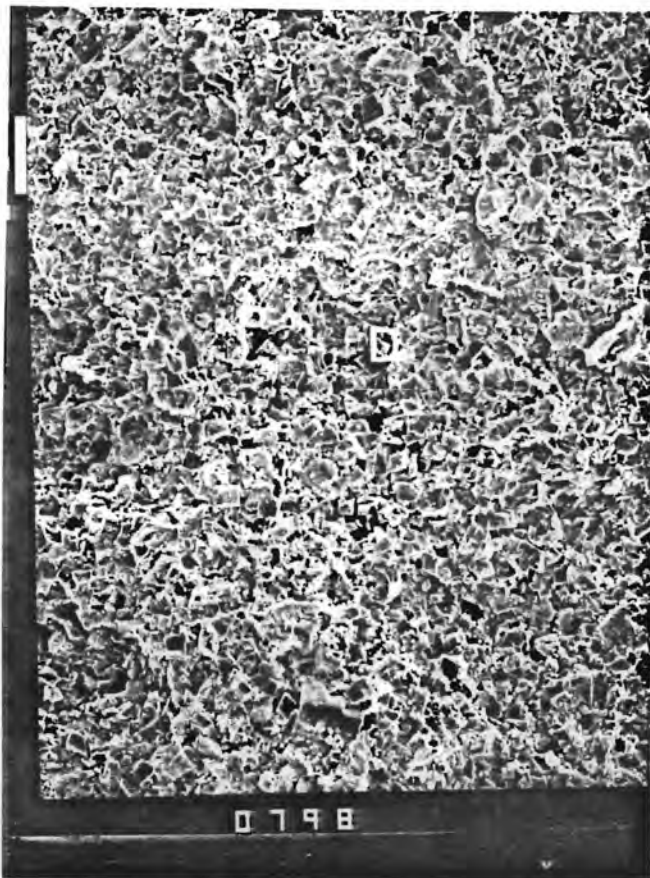


FIGURE I-21

WELL: YAKLEY "B"

FORMATION: JOACHIM DOLOMITE

DEPTH: 651 Feet

D391-019

<u>PHOTOGRAPH NO.</u>	<u>MAGNIFICATION</u>	<u>DESCRIPTION</u>
9227	20x	General view of finely textured dolomite.
9230	300x	Higher magnification view reveals that this sample consists of finely crystalline dolomite and detrital clay matrix.
9228	1500x	Anhydrite (A) is common at this depth.
9229	2000x	Authigenic dolomite (D) crystallites commonly serve as nucleation sites for illite (I).

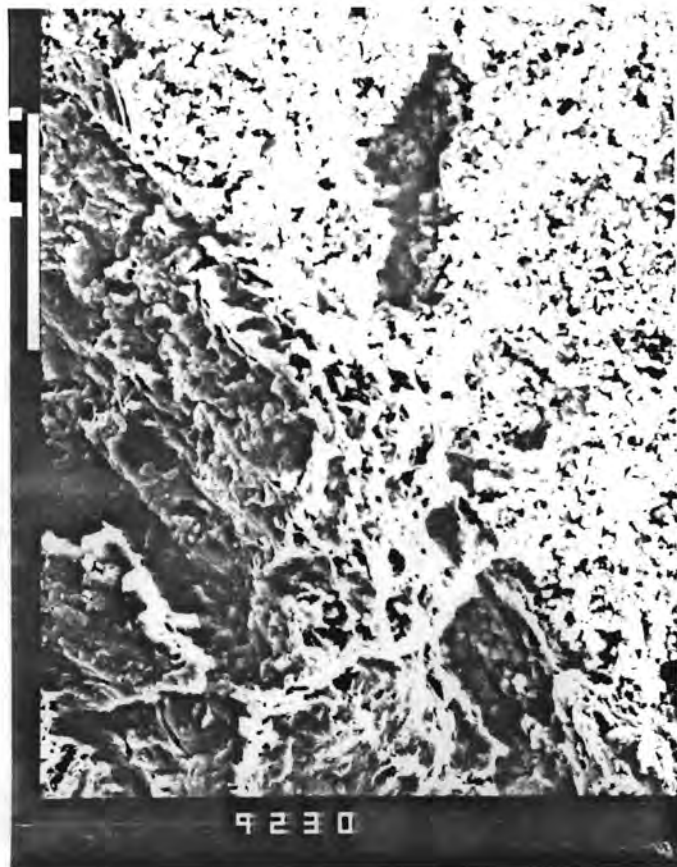


FIGURE I-22

WELL: YAKLEY "B"

FORMATION: JOACHIM DOLOMITE

DEPTH: 652.6 Feet

D391-020

<u>PHOTOGRAPH NO.</u>	<u>MAGNIFICATION</u>	<u>DESCRIPTION</u>
0698	100x	Minor dolomite crystals (D) are set in a very fine grained matrix (M). Small pores (P) are not connected.
0699	400x	Close inspection reveals that the matrix (M) is composed dominantly of dolomite (D).
0700	1500x	Very well crystallized, fresh dolomite (D) and some fibrous illite (I) occur in this sample.
0702	2000x	This high magnification view demonstrates that dolomite (D) serves as a nucleation site for fibrous illite (I). Pyrite (P) is a late stage precipitate.

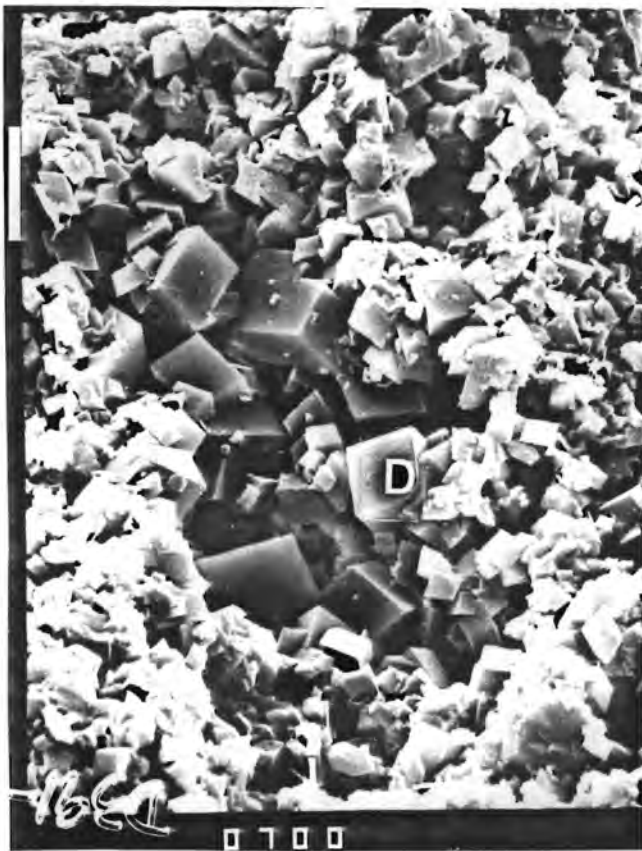
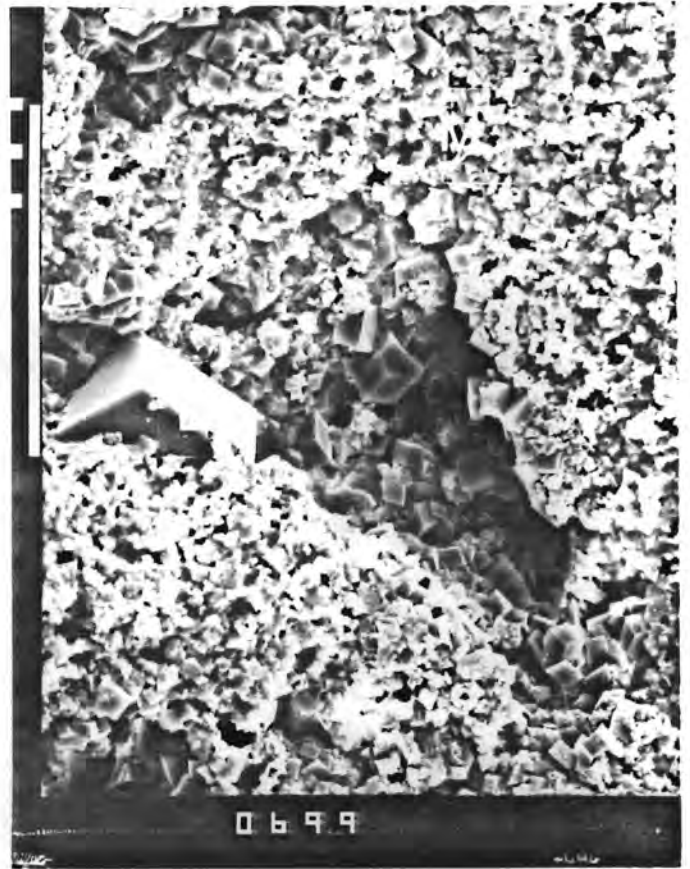
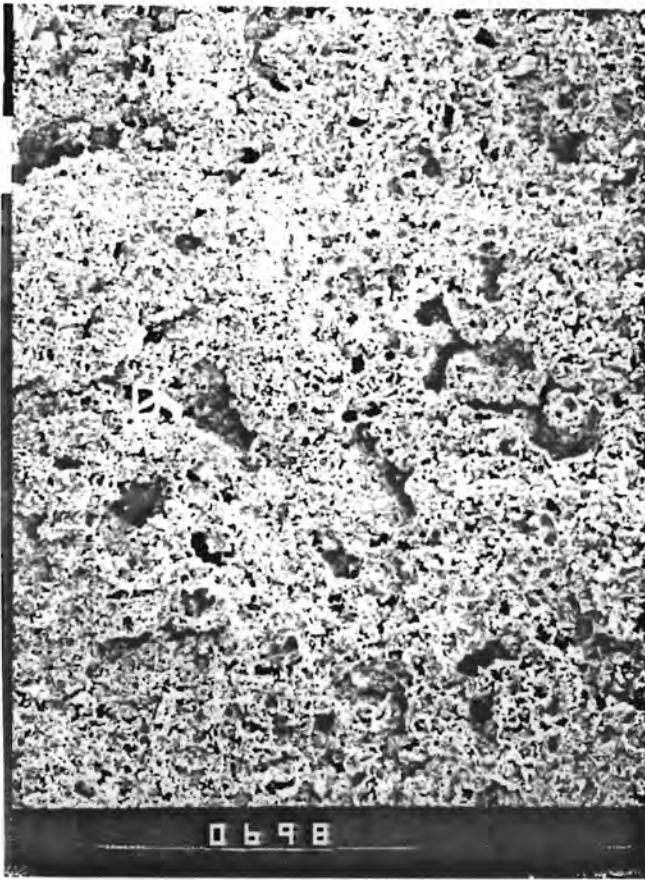


FIGURE I-23

WELL: YAKLEY INJECTION WELL

FORMATION: JOACHIM ST. PETER TRANSITION

DEPTH: 651.5 Feet

D391-057

<u>PHOTOGRAPH NO.</u>	<u>MAGNIFICATION</u>	<u>DESCRIPTION</u>
9219	30x	Some grains (G) are visible in this low magnification view.
9222	700x	Finely crystalline dolomite (D) is abundant as a grain coating.
9220	1000x	Fibrous illite (I) has nucleated along edges and at corners of dolomite (D) crystallites. Many of the dolomite crystals are partially leached.

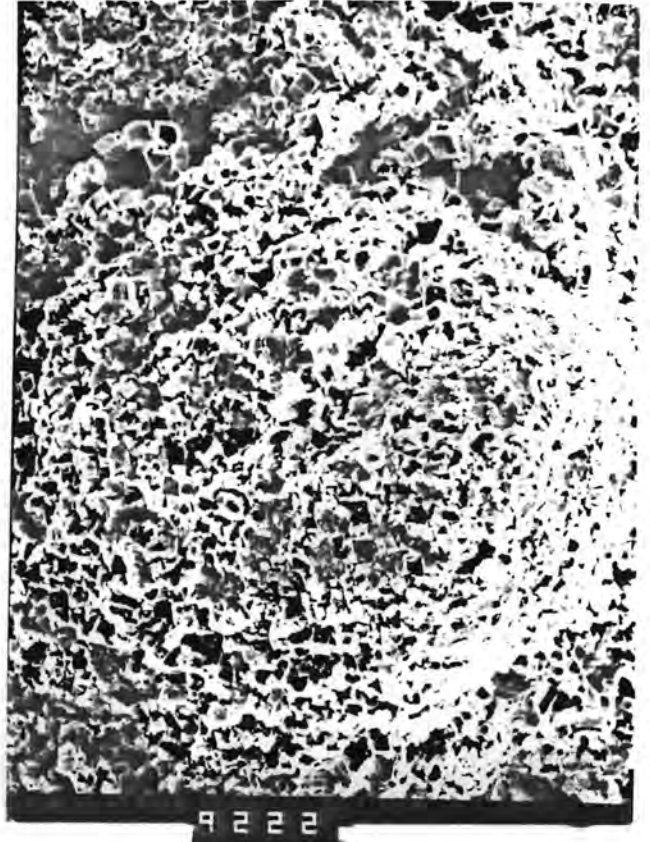


FIGURE I-24

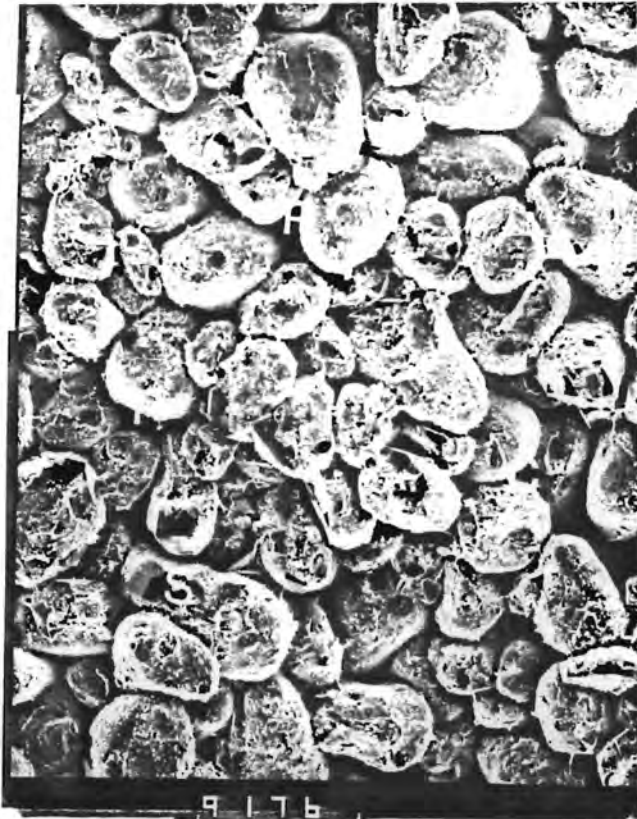
WELL: YAKLEY A

FORMATION: ST. PETER SANDSTONE (GREEN)

DEPTH: 662 Feet

D391-007

<u>PHOTOGRAPH NO.</u>	<u>MAGNIFICATION</u>	<u>DESCRIPTION</u>
9176	30x	Low magnification view of loosely cemented St. Peter sandstone. Abundant interconnected porosity (P) is partially occluded by silica overgrowths (S) and authigenic clay (C).
9178	300x	Microquartz crystallites, euhedral silica overgrowths (S) and minor dolomite are present in this pore.
9179	450x	Abundant silica overgrowths (S) and microdolomite crystals (D) are dominant cements at this depth.



9 1 7 6



9 1 7 8



9 1 7 9

FIGURE I-25

WELL: YAKLEY INJECTION WELL

FORMATION: ST. PETER SANDSTONE (GREEN)

DEPTH: 652 Feet

D391-059

<u>PHOTOGRAPH NO.</u>	<u>MAGNIFICATION</u>	<u>DESCRIPTION</u>
9231	30x	Quartz grains (Q) are surrounded by detrital clay matrix.
9233	700x	Higher magnification views illustrate common pore fill minerals at this depth. Marcasite (M) silica overgrowths (S) and fibrous illite (I) commonly occur. Kaolinite (K) occurs only rarely.
9232	1000x	

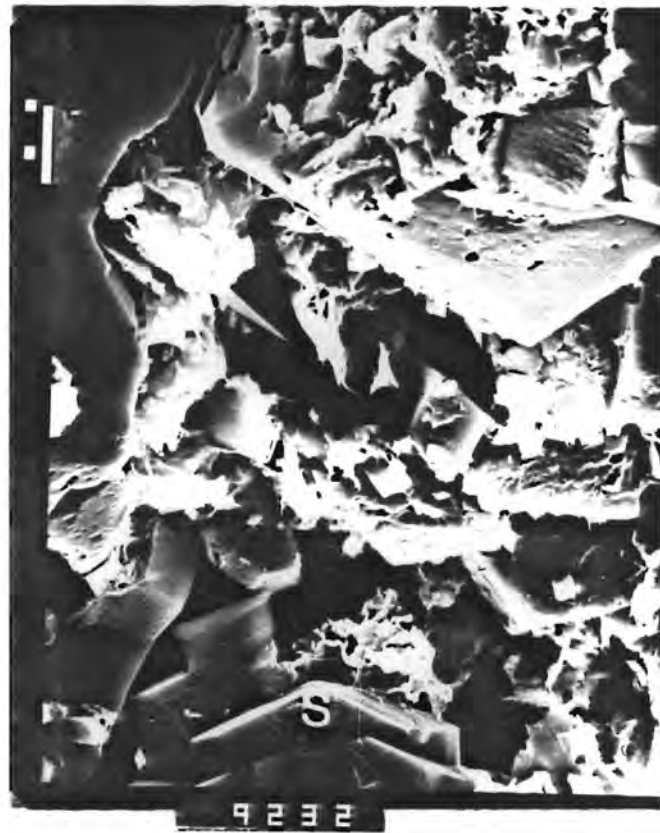
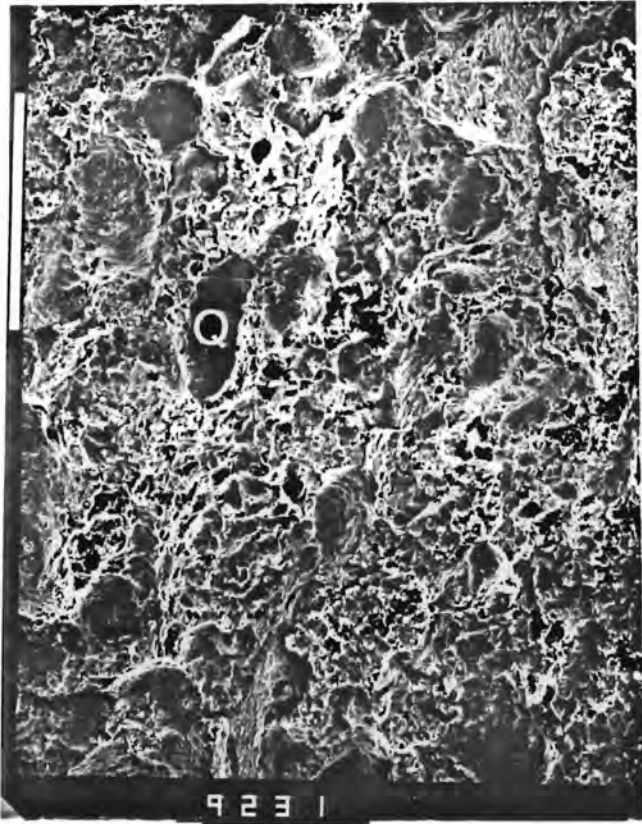


FIGURE I-26

WELL: YAKLEY G

FORMATION: ST. PETER SANDSTONE (GREEN)

DEPTH: 656.5 Feet

D391-075

<u>PHOTOGRAPH NO.</u>	<u>MAGNIFICATION</u>	<u>DESCRIPTION</u>
1182	30x	Quartz grains (G) are engulfed by depositional matrix (M).
1185	200x	Silica overgrowths (S) partially occlude porosity. Depositional matrix (M) is abundant.
1183	700x	Silica overgrowths (S) and a partially leached feldspar (F) partially occupy pore space.
1184	1000x	Authigenic feldspar (F), silica overgrowths (S) and authigenic fibrous illite (I) occlude porosity in this view.

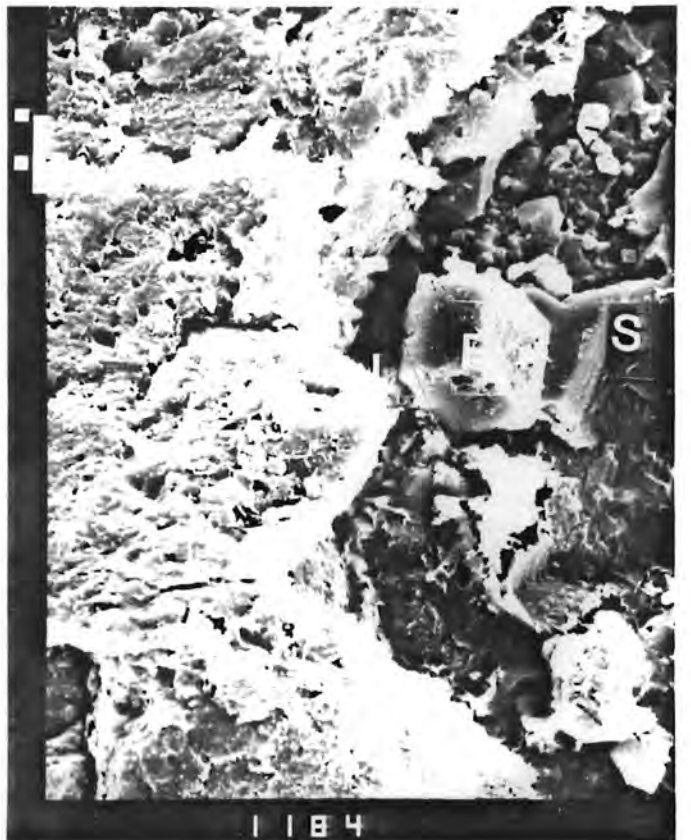
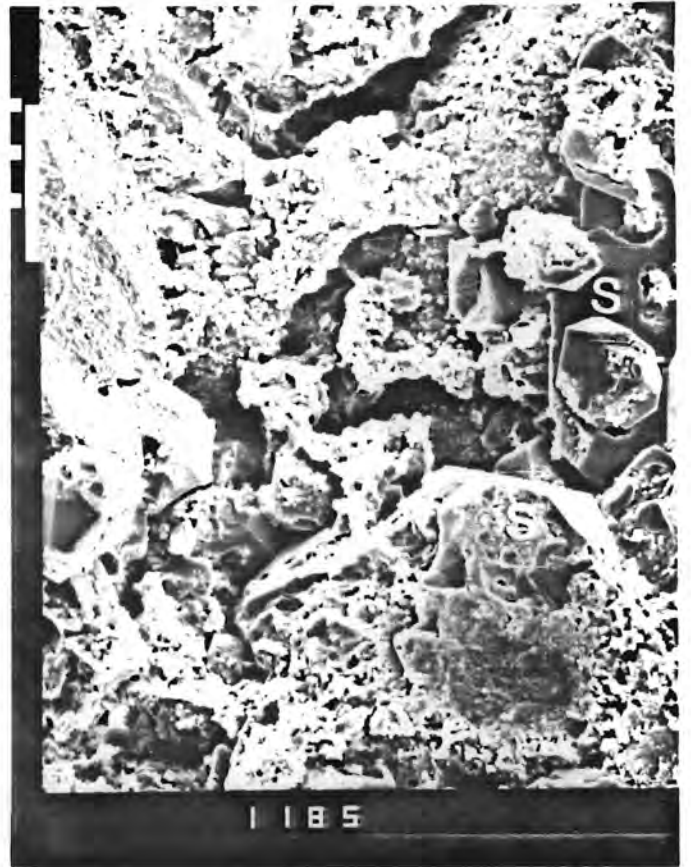


FIGURE I-27

WELL: YAKLEY F

FORMATION: ST. PETER SANDSTONE (GREEN)

DEPTH: 657.0 Feet

D391-083

<u>PHOTOGRAPH NO.</u>	<u>MAGNIFICATION</u>	<u>DESCRIPTION</u>
1178	45x	Depositional matrix (M) partially occludes porosity between grains (G).
1181	300x	Minor silica overgrowths (S) occur at this depth. Grains rimmed by thick coatings of depositional matrix (M) have no overgrowths.
1180	1000x	Framboidal pyrite (P) occurs commonly at this depth. Authigenic illite (I) has partially coated some grains. The matrix (M) appears to be composed of illite.
1179	1000x	Authigenic illite (I) partially coats grains.

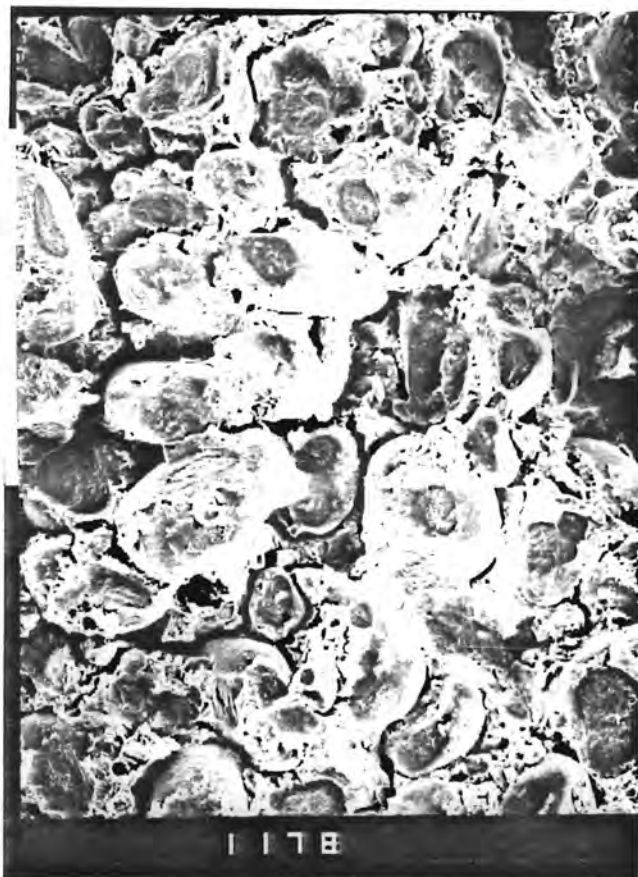


FIGURE I-28

WELL: YAKLEY IW

FORMATION: ST. PETER SANDSTONE (WHITE)

DEPTH: 665.4 Feet

D391-063

<u>PHOTOGRAPH NO.</u>	<u>MAGNIFICATION</u>	<u>DESCRIPTION</u>
6787 6784 6788	700x	These three views illustrate characteristic features of the white St. Peter. Very little depositional matrix occurs. The sand grains are loosely cemented by fibrous illite (I) and silica overgrowths (S). Pore throats are frequently bridged by illite (I).

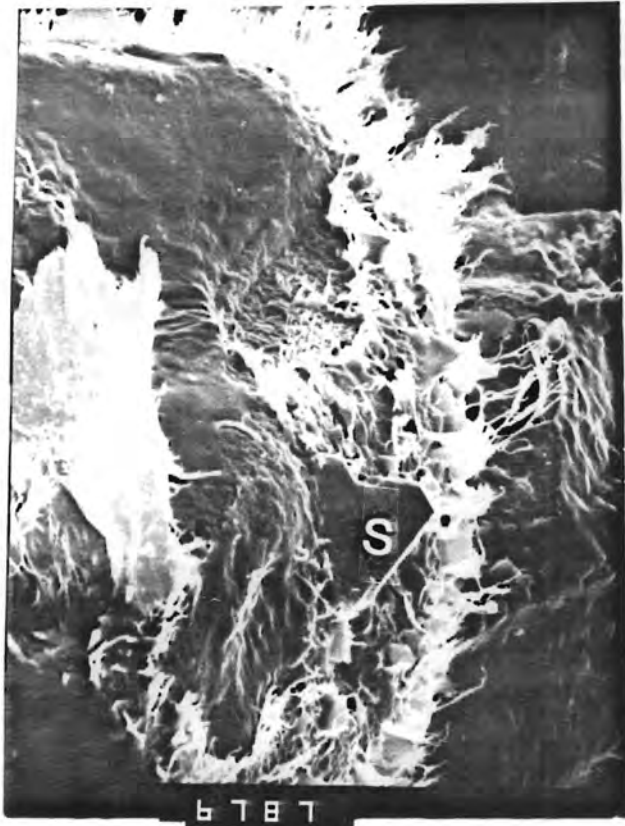


FIGURE I-29

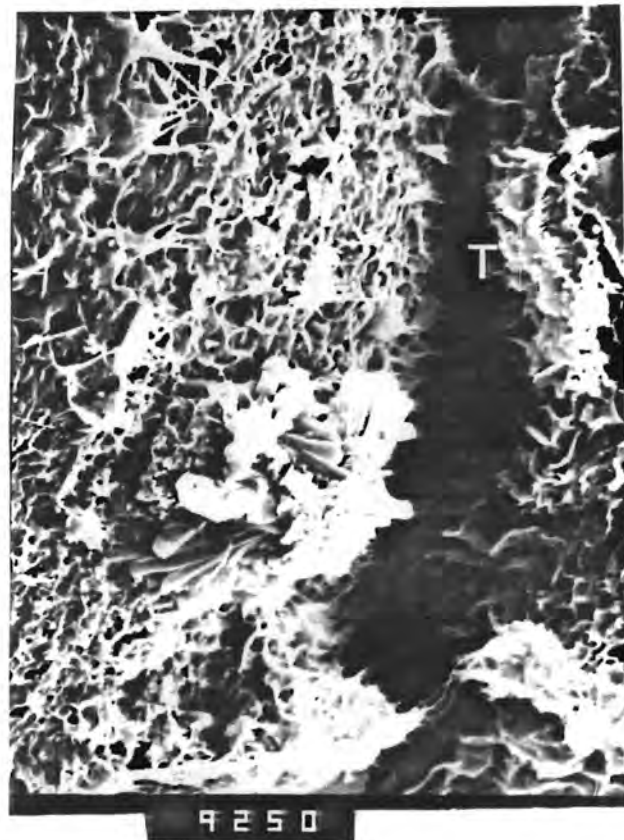
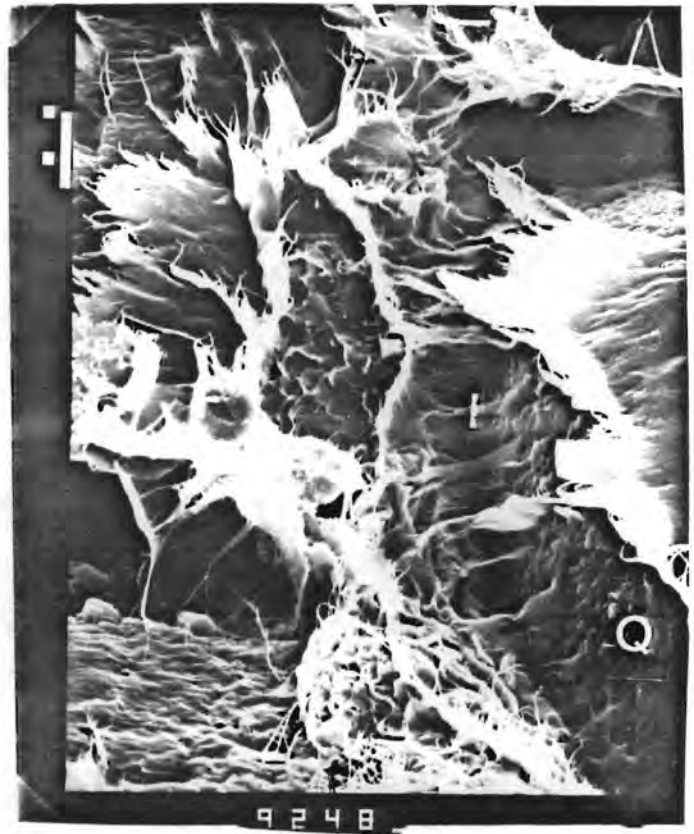
WELL: YAKLEY "C"

FORMATION: ST. PETER SANDSTONE (DARK GRAY)

DEPTH: 707.8 Feet

D391-067

<u>PHOTOGRAPH NO.</u>	<u>MAGNIFICATION</u>	<u>DESCRIPTION</u>
9247	45x	Abundant intergranular porosity exists between quartz grains (Q). Detrital and authigenic clay (C) partially occlude some pore space.
9248	1000x	These higher magnification views illustrate common pore fill minerals at this depth. Fibrous illite (I) is a common grain coating and bridges pore throats (T) between adjacent quartz grains (Q). Pyrite microcrystals (P) and anhydrite (A) are other common minerals in the pore system.
9250	1500x	



COMPARATIVE CHARACTERISTICS OF THE GREEN,
WHITE, AND MEDIUM TO DARK GRAY ST. PETER SANDSTONE

General -

Compositional and textural characteristics of the three sand varieties are summarized in Table I-12. Mineral phases detected by fine fraction X-ray diffraction, with the exception of quartz, are summarized in Table I-13.

Composition and Texture -

The green St. Peter Sandstone is coarser grained than either the white or the gray St. Peter. Grain sizes are distributed bimodally in the green St. Peter, and the sand is texturally immature. By contrast, the white and gray sands generally do not exhibit a bimodal grain size distribution and are texturally mature. White and gray sandstones are generally better sorted than the green sandstone. Quartz grains of the white and gray St. Peter Sandstone exhibit concavo-convex or point contacts. The fabric of the green sandstone is highly variable. Detrital clay matrix content decreases with depth, and the relative quartz content increases. Authigenic clay is the dominant cement in the green and gray St. Peter, but silica is the dominant cement in the white St. Peter.

Fine Fraction Mineralogy -

Illite occurs throughout the interval but is more abundant in the green and white St. Peter samples analyzed than in the gray St. Peter. Authigenic potassium feldspar decreases in abundance with depth. Pyrite is far more abundant in the gray sand than in either the green or white sand. Further comparisons are inconclusive.

TABLE I-12

COMPARATIVE PETROGRAPHIC CHARACTERISTICS OF THE GREEN,
WHITE, AND MEDIUM TO DARK GRAY ST. PETER SANDSTONE.

CHARACTERISTIC	GREEN	WHITE	GRAY
GRAIN SIZE, mm	0.44-0.63 Medium to Coarse Generally Bimodal	0.37-0.45 Medium	0.37 Medium
SORTING	Poorly to Moderately Well Sorted	Moderately to Well Sorted	Moderately Well Sorted
TEXTURAL MATURITY	Immature	Mature	Mature
FABRIC	Variable	Concavo-Convex or Point Grain Contacts	Concavo-Convex Contacts, Minor Point Contacts.
QUARTZ (%)	73-86	85-87	87
DETRITAL CLAY MATRIX (%)	Tr-27	0-4	0
CEMENT	Authigenic Clay Silica	Silica	Authigenic Clay

TABLE I-13

COMPARATIVE MINERALOGIC CHARACTERISTICS OF THE GREEN,
WHITE, AND DARK GRAY ST. PETER SANDSTONE BASED ON
FINE FRACTION X-RAY DIFFRACTION ANALYSIS. QUARTZ IS
NOT INCLUDED.

MINERAL PHASE	GREEN	WHITE	DARK GRAY
Illite	4-42%	17-59%	25-28%
Potassium Feldspar	10-27%	7-17%	Tr
Calcite	1-5%	3-4%	0-1%
Marcasite	3-9%	5-7%	-
Pyrite	2-5%	0-5%	0-41%
Sericite	0-28%	-	0-13%
Dolomite	0-3%	-	0-17%
Anhydrite	0-3%	0-3%	0-1%
Kaolinite	-	-	0-46%

SECTION II

POROSITY AND PERMEABILITY

General -

Boyle's Law porosities and either vertical or horizontal air permeabilities were measured for 76 samples from seven Yakley Wells. Samples selected for analysis are representative of the caprock, the Joachim - St. Peter transition, and the upper St. Peter Sandstone. Results are discussed for each grouping and are presented in tabular form.

Caprock -

Thirty vertical and one horizontal permeability measurements were made. Porosities were measured for all samples. These results are presented in Table II-1. Generally, caprock permeability increases with depth. Vertical permeability varies from 0.03 to 71.0 md. Porosity varies from 0.8 to 38.6%. A porosity/permeability cross-plot is presented in Figure II-1, and permeability variations relative to distance from the St. Peter contact are given in Figure II-2.

With the exception of one sample, porosity and permeability vary logarithmically with one another.

Joachim - St. Peter Transition -

Either vertical or horizontal air permeability measurements were made for 12 transition zone samples. Porosities were measured and all data is recorded in Table II-2. Porosities in this zone vary from 9.6 to 35.7%. Vertical permeabilities range from 0.06 to 26.0 md. Horizontal permeabilities measured for two samples were 0.24 and 390 md. The greater permeability value represents a green sandstone layer within the transition zone. A porosity/permeability cross-plot is given in Figure II-3. Porosities and permeabilities do not appear to depend on one another.

St. Peter Sandstone -

Porosities and either horizontal or vertical permeabilities were measured for 34 St. Peter Sandstone samples, including

green sand, white sand and dark or light gray sand samples. For convenience, the discussion of measurements is divided by color.

Green Sand -

Porosities vary from 10.0 to 23.0%. Vertical permeabilities range from 0.93 to 3890 md, and horizontal permeabilities range from 2.08 to 6098 md. Porosity/permeability cross-plots are presented in Figure II-4. Results are presented in Table II-3. In a very general way, as the porosity increases, the permeability increases.

White Sand -

Porosities of white sand samples vary from 9.7 to 20.9%. Horizontal permeabilities range from 13 to 5248 md, and vertical permeabilities range from 78 to 2866 md. Permeability of the white St. Peter sandstone appears to be controlled by cementation patterns rather than by spatial orientation. A porosity/permeability cross-plot is presented in Figure II-5. A crude correlation between porosity and permeability exists. Results are presented in Table II-4.

Medium to Dark Gray Sand -

Four vertical and one horizontal air permeability measurements indicate that vertical permeability is greater than horizontal permeability. Vertical permeability ranged from 78 to 417 md. Porosities varied from 14.2 to 17.7%. Results are presented in Table II-5. A porosity/permeability cross-plot demonstrates that porosity and permeability are independent variables (Figure II-6).

Conclusions -

1. Caprock permeability increases with depth. As the Joachim-St. Peter transition zone is neared, the permeability of the Joachim dolomite increases, in general.
2. Green sand samples are generally more permeable than either white or medium to dark gray St. Peter Sand samples.

3. Based on a comparison of vertical and horizontal permeability determinations, all St. Peter sands appear to be anisotropic.
 - a. In general, vertical green sand permeabilities are less than horizontal permeabilities. This is due to the presence of horizontal laminations of detrital clay matrix which occur throughout the green sand interval.
 - b. Although white sand porosities and permeabilities appear to be independent, a crude correlation may exist. Permeability appears to depend more on cementation than on vertical or horizontal orientations.
 - c. Generally, vertical permeabilities of medium to dark gray sands are greater than horizontal permeabilities. This is probably due to the fact that selective flow paths have been developed in this direction.

TABLE II-1

POROSITY AND AIR PERMEABILITY OF THE CAPROCK, YAKLEY WELLS

<u>Well</u>	<u>Depth, Ft</u>	<u>Rock Type</u>	<u>k_v, md</u>	<u>k_h, md</u>	<u>Ø, %</u>
IW	640.1	Dolomite	0.62		18.2
IW	645.1	Dolomite	0.59		18.2
IW	645.45	Dolomite	0.08		10.2
IW	645.8	Dolomite	0.13		4.7
IW	646.0	Dolomite	0.14		21.7
IW	647.3	Dolomite	9.63		34.2
IW	647.3	Dolomite	21.0		36.2
IW	649.0	Dolomite	20.0		36.0
A	604.3	Dolomitic Limestone	0.04		0.8
A	610.3	Limestone	0.03		0.8
A	611.5	Dolomite	0.03		1.6
A	613.3	Dolomite	0.04		8.0
A	625.9	Dolomite	0.76		12.4
A	639.0	Dolomite	4.66		19.9
A	641.0	Dolomite	0.84		14.9
B	612.45	Dolomite	0.13		27.2
B	621.5	Dolomite	5.10		15.6
B	628.0	Dolomite	71.0		25.9
B	628.0	Dolomite	7.46		22.4
B	634.0	Dolomite	0.76		19.5
B	635.0	Dolomite	0.15		13.0
B	635.0	Dolomite	0.19		14.8
B	647.2	Dolomite	1.28		19.4
B	651.0	Dolomite		5.8	32.0
B	652.6	Dolomite	7.2		32.0
C	625.7	Dolomite	1.82		16.9
C	632.5	Dolomite	0.22		15.3
C	637.0	Dolomite	0.08		14.6
C	637.0	Dolomite	0.03		1.8
C	639.0	Dolomite	24.0		38.6

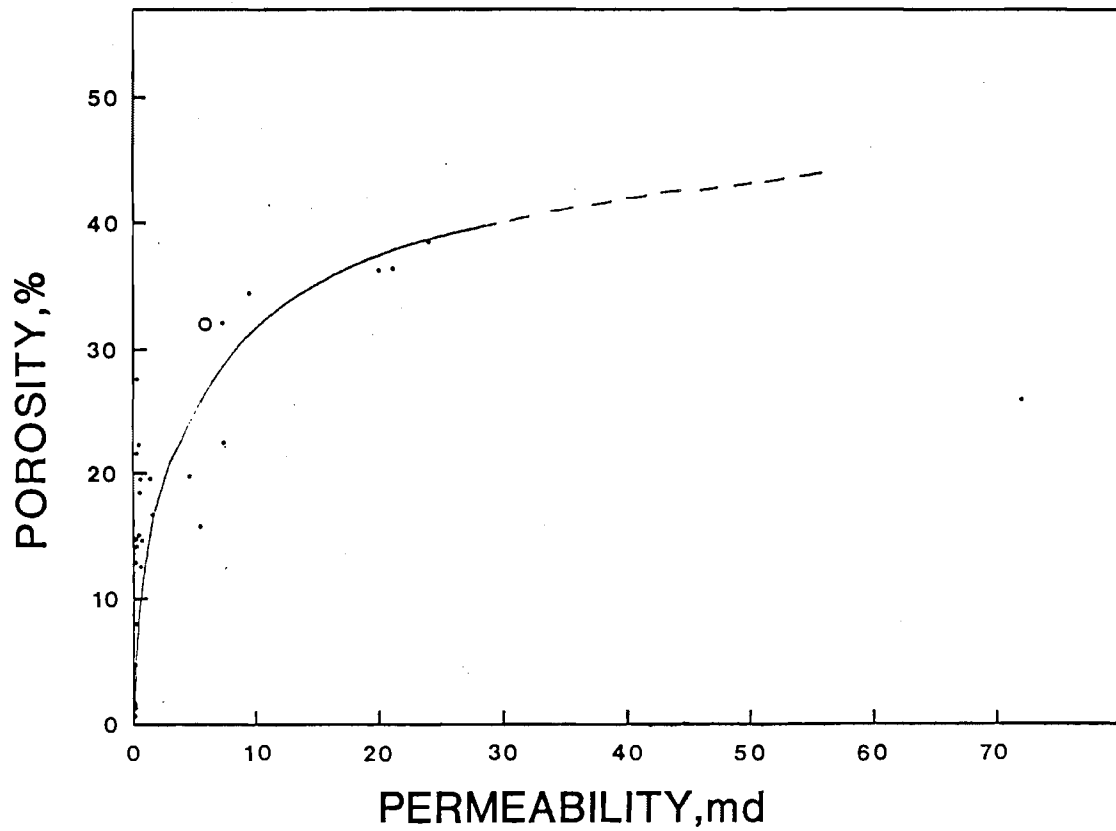


FIGURE II-1. Porosity-permeability cross-plot, caprock samples. Horizontal permeability measurement indicated by a circle (o); vertical permeability measurements indicated by dots (·).

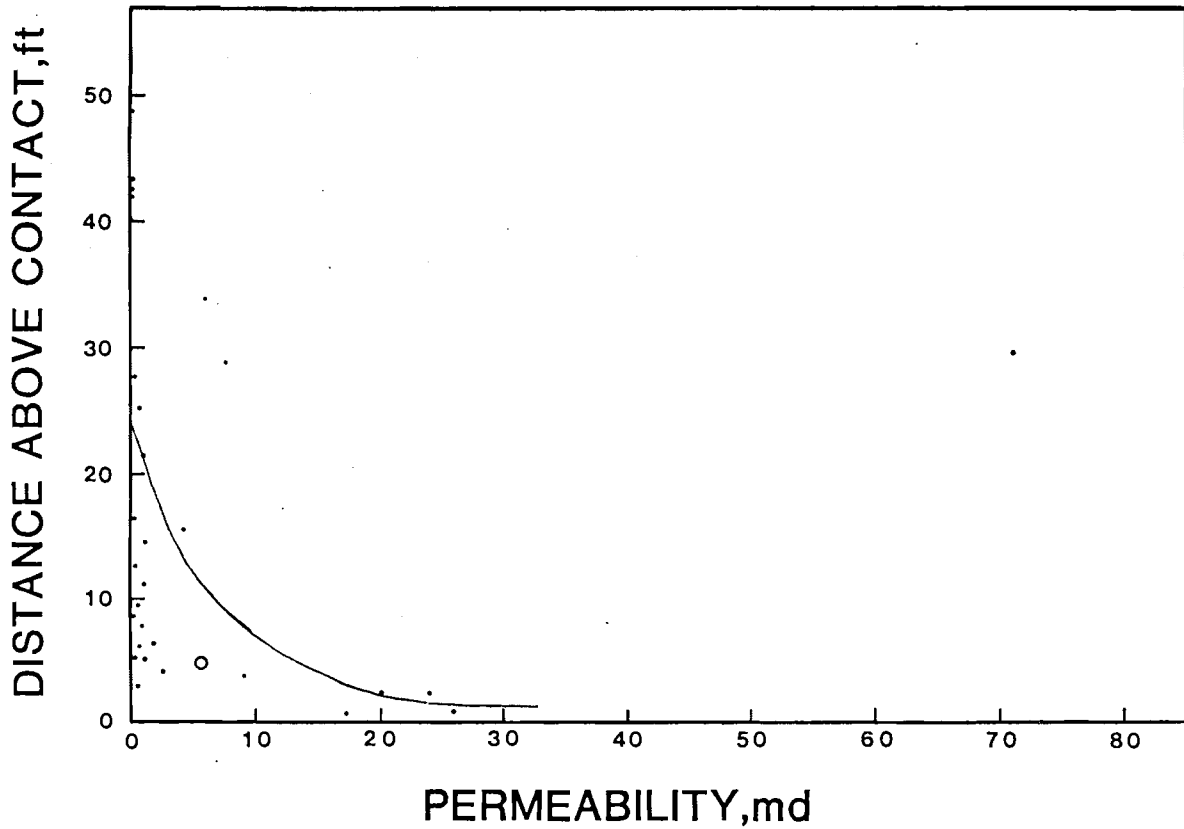


FIGURE II-2. Caprock permeabilities are plotted as a function of distance above the Joachim-St. Peter contact. Very crudely, the permeability increases as the contact is approached. Dots (·) represent vertical permeability measurements. The circle (o) is a horizontal permeability measurement.

TABLE II-2

BOYLE'S LAW POROSITIES AND AIR PERMEABILITIES
OF TRANSITION ZONE SAMPLES, YAKLEY WELLS

<u>WELL</u>	<u>Depth, Ft.</u>	<u>Rock Type</u>	<u>k_v, md</u>	<u>k_h, md</u>	<u>$\phi, \%$</u>
IW	649.5	Sandy Dolomite	26.0		35.7
C	641.6	Sandy Dolomite	0.71		29.2
C	641.6	Sandy Dolomite	9.92		16.9
C	643.0	Green Sandstone		390	19.0
C	644.0	Sandstone w/Dolomite	3.12		15.1
C	644.0	Sandstone w/Dolomite		0.24	9.6
D	633	Sandy Dolomite	17.0		16.1
F	648.6	Sandy Dolomite	12		10.6
F	650.4	Sandy Dolomite	14		19.0
G	649.6	Punky Sandy Dolomite	5.47		20.9
G	650.8	Sandy Dolomite	6.03		16.1
G	651.3	Sandy Dolomite	0.06		15.6

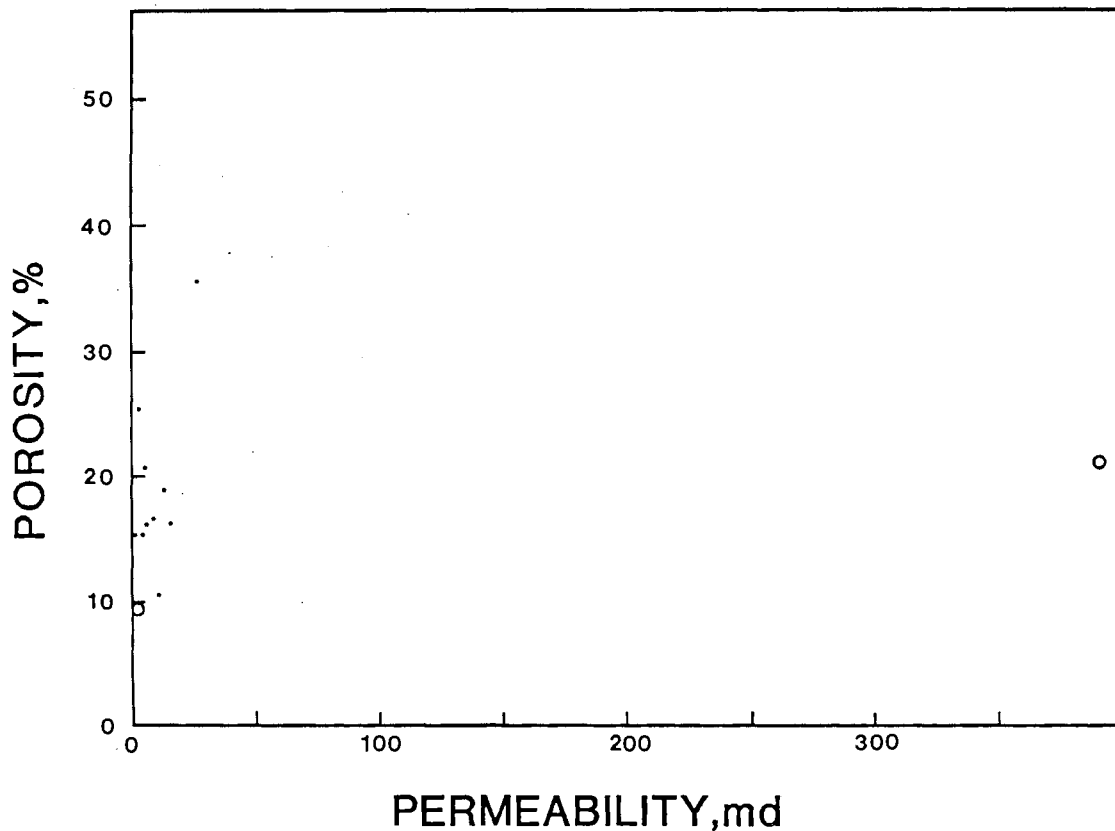


FIGURE II-3. Porosity-permeability cross-plot of measured values for the Joachim-St. Peter Transition. Circles (o) represent horizontal permeability measurements. Dots (·) represent vertical permeability measurements. With the exception of one horizontal measurement, all permeabilities are less than 50 md.

TABLE II-3

BOYLE'S LAW POROSITY AND AIR PERMEABILITY OF GREEN
ST. PETER SANDSTONE SAMPLES, YAKLEY WELLS

<u>Well</u>	<u>Depth, Ft.</u>	<u>k_v, md</u>	<u>k_h, md</u>	<u>ϕ, %</u>
IW	652.0		2.08	11.6
IW	652.0		141	16.6
IW	654.0		556	17.4
IW	655.0		1262	19.0
A	662.0		6098	23.0
C	644.6	3.83		18.3
C	644.8		245	16.4
C	645.0		3.37	10.1
D	633.0	17.0		16.1
F	657.0	11		14.7
F	659.7	3890		21.2
G	653.1	509		16.7
G	654.9	372		17.2
G	656.5	0.93		10.0
G	658.2	61		16.5

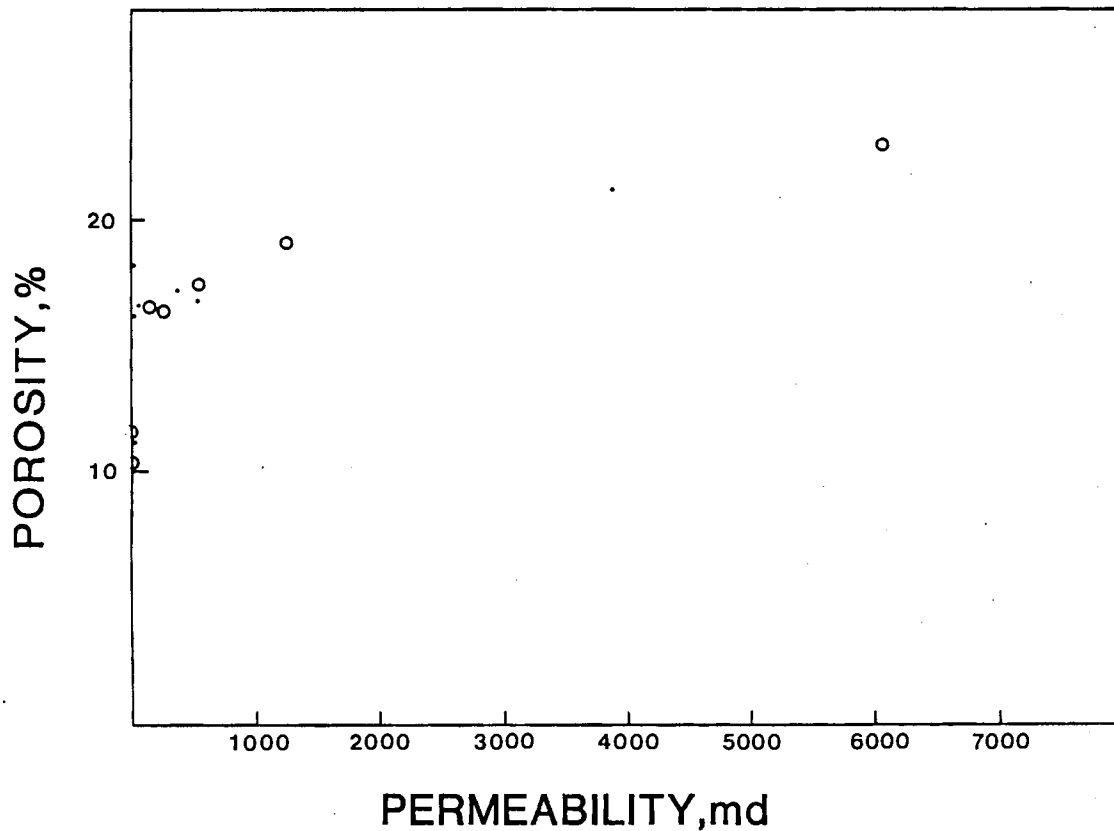


FIGURE II-4. Porosity-permeability cross-plot of measured values for the green St. Peter Sandstone. Horizontal permeabilities are indicated by circles (o), and vertical permeabilities are indicated by dots (·). Horizontal permeabilities generally tend to be greater than vertical permeabilities. A crude linear correlation (with a porosity intercept of about 17%) may exist between porosity and permeability.

TABLE II-4

BOYLE'S LAW POROSITY AND AIR PERMEABILITY
OF WHITE ST. PETER SAND SAMPLES, YAKLEY WELLS

<u>Well</u>	<u>Depth, Ft.</u>	<u>k_v, md</u>	<u>k_h, md</u>	<u>ϕ, %</u>
IW	665.4		823	16.6
A	671.1		13	9.7
A	671.7		42	10.6
A	677.0		631	16.8
C	652.0		599	19.4
C	652.0		684	20.1
D	641.0		5248	20.9
D	641.7	605		13.0
D	641.9		544	12.5
F	659.9	2866		15.8
F	665.1	936		17.7
G	668	78		15.3

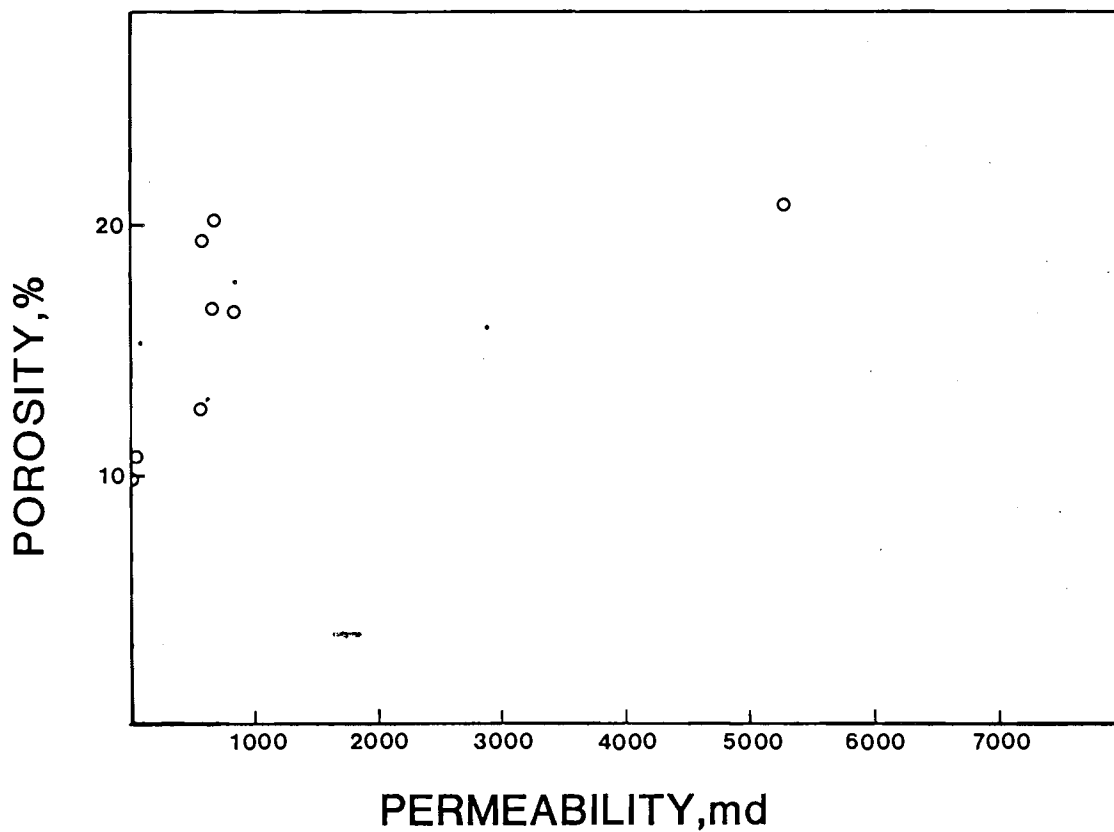


FIGURE II-5. Porosity-permeability cross-plot of measured values for the white St. Peter Sandstone. Circles (o) represent horizontal permeability measurements, and dots (·) represent vertical permeability measurements. Generally, horizontal permeabilities are greater than vertical permeabilities. Porosity and permeability appear to be independent variables, although a crude linear correlation may exist between them.

TABLE II-5

BOYLE'S LAW POROSITY AND AIR PERMEABILITY OF
MEDIUM TO DARK GRAY ST. PETER SAND SAMPLES, YAKLEY WELLS

<u>Well</u>	<u>Depth, Ft.</u>	<u>k_v, md</u>	<u>k_h, md</u>	<u>ϕ, %</u>
D	696.8	79		17.7
D	697.0		31	15.3
G	683.2	78		15.3
G	694.2	199		14.2
G	697.5	417		15.2

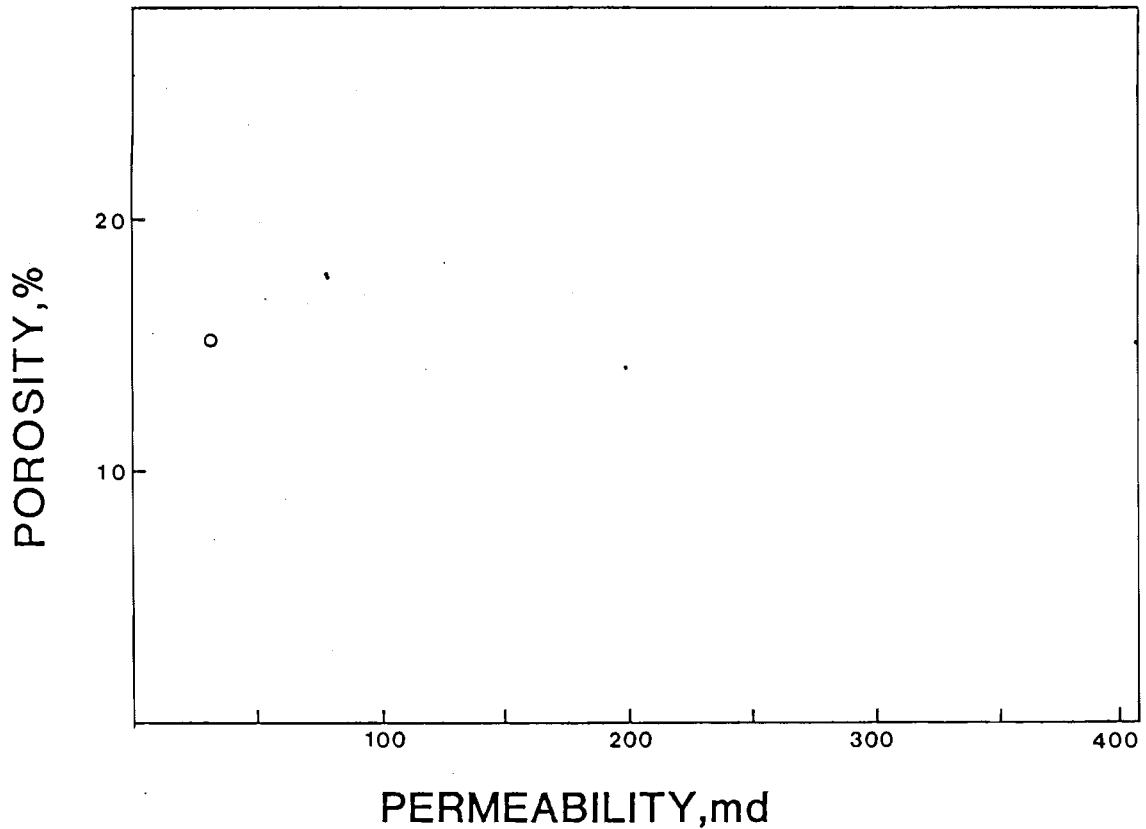


FIGURE II-6. Porosity-permeability cross-plot of measured values for the gray St. Peter Sandstone. Circles (o) represent horizontal permeability measurements, and dots (·) represent vertical permeability measurements. Porosity and permeability appear to be independent variables. Vertical permeabilities are greater than the one horizontal measurement, but, before the conclusion that vertical permeabilities are generally greater than horizontal permeabilities may be reached, more data are required.

SECTION III

MECHANICAL STRENGTH

General -

Confined triaxial and unconfined uniaxial compressive strengths were determined for 8 samples from the Yakley 7 Well and 14 samples from Yakley Wells A,B,C,D, and IW, respectively. Test procedures and results are discussed and interpreted.

Triaxial Compressive Strengths

Eight 1 7/8 - inch core samples from the caprock of the Yakley 7 well were failed at a confining pressure of 1000 p.s.i. Results are presented in Table III-1. Black and white photographs of samples before testing are presented in Figure III-1.

Samples were prepared according to standards outlined in the ASTM publication "Standard Test Method for Triaxial Compressive Strength of Undrained Rock Core Specimens Without Pore Pressure Measurements." Samples were trimmed, and core ends were planed. Samples were then tested by applying a constant hydraulic pressure (1000 p.s.i.) to the curved surface of the cylindrical specimen while simultaneously applying a compressive axial load, continuously increased, until the specimen failed. Components of force are illustrated in Figure III-2.

Uniaxial Compressive Strength -

Fourteen 3 1/2 - inch diameter core specimens were failed under a uniaxial compressive load. A constant loading pressure of 150 p.s.i. per second was applied. Results are presented in Table III-2. Samples tested from the Yakley Injection Well are shown in Figure III-3 in the pre-test condition. Post-test samples are not available for examination. The compressive strength, C_o , is given by:

$$C_o = \frac{F_c}{A}$$

Where:

F_c = Applied compressive load at failure
 A = Cross-sectional area

Stress-strain relationships were also determined for each specimen during uniaxial testing. These results are graphically displayed in Figures A-1 through A-29 and are tabulated in Tables A-3 through A-16 in the Appendix, which accompanies this report.

Results -

Triaxial compressive strengths of caprock samples from Yakley well 7, with a confining pressure of 1000 p.s.i., vary from 2813 p.s.i. to 17803 p.s.i. As anticipated, those samples with open vugs and open vertical fractures failed under lower loading forces than did compact or laminated caprock samples.

Unconfined uniaxial compressive strengths of all samples tested varied from 1170 p.s.i. to 10880 p.s.i. Sandy and vuggy dolomites and the green sand sample generally failed under lower loads than did massive dolomites and limestones or white St. Peter Sandstone.

Stress-strain plots (Appendix, Figures A-1 through A-29) indicate that most samples tested behave as Maxwell elastico-viscous, Bingham plasticoviscous, or Hookian elastic solids.

Conclusions -

1. The triaxial compressive strength, under 1000 p.s.i. confining pressure, of all caprock samples exceeds those reported in the Dames and Moore report of March 1981. However, fewer samples were subjected to failure in the current study.
2. Unconfined uniaxial compressive strengths represent minimum failure strengths; however, the minimum strength was 1170 p.s.i.
3. Of the samples tested, none will fail under anticipated test pressures.

TABLE III-1

RESULTS OF TRIAXIAL COMPRESSIVE STRENGTH TESTING
UNDER A CONFINING PRESSURE OF 1000 psi, YAKLEY 7 WELL

SAMPLE	DEPTH (FT)	DENSITY (g/cm ³)	DESCRIPTION	STRENGTH (lb/in ²)
A	609.3-609.85	2.485	Dolomite, open vugs, convolute laminations	11625
B	612.8-613.55	2.485	Dolomite, open vugs, open vertical fracture	5555
C	617.7-618.2	2.341	Dolomite, compact	15340
D	620.2-620.50	2.389	Dolomite, horizontal shale laminations	17083
E	621.35-621.95	2.308	Dolomite with shale partings and stylolite	11972
F	632.65-633.45	2.277	Dolomite, pyritic, compact	13861
G	633.5-634.20	2.308	Dolomite, pyritic, convolute laminations	15028
H	638.5-639.00	1.892	Dolomite, "punky" vuggy	2813

The photographs in Figure III-1 illustrate specimens subjected to triaxial compressive strength testing with a confining pressure of 1000 psi. All test specimens are from Yakley Well No. 7.

FIGURE III-1

Caprock specimens subjected to triaxial
compressive strength testing.

PHOTOGRAPH

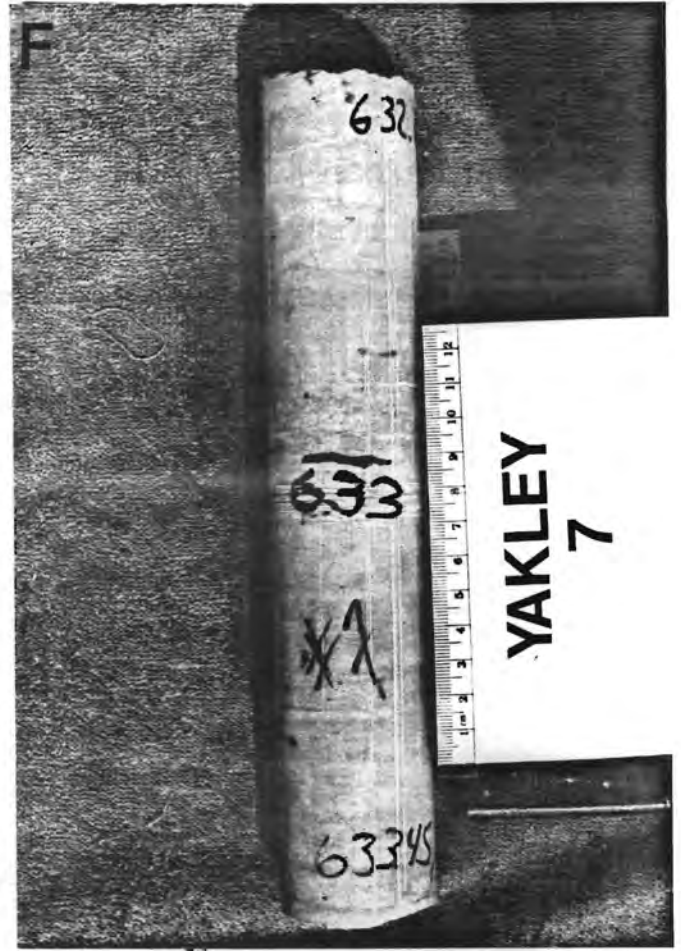
DESCRIPTION

- | | |
|---|--|
| A | Vuggy dolomite from a depth of 609.3-609.85 feet. Note convolute laminations near top of core specimen. Strength=11625 lb/in ² |
| B | Vuggy dolomite, with open vertical fracture nearly transecting the full core length, from a depth of 612.8-613.55 feet. Strength=5555 lb/in ² |
| C | Compact dolomite from a depth of 617.7-618.2 feet. Some convolute laminations occur near the middle of the core. Strength=15340 lb/in ² |
| D | Compact dolomite with shale laminations from a depth of 620.2-620.5 feet. Strength=17083 lb/in ² |



FIGURE III-1, Continued

<u>PHOTOGRAPH</u>	<u>DESCRIPTION</u>
E	Compact dolomite from a depth of 621.35-621.95 feet, with closed vertical fractures. Black areas are pyritic. Strength=11972 lb/in ²
F	Compact dolomite from a depth of 632.65-633.45 feet. Strength=13861 lb/in ²
G	Compact dolomite, pyritic, with convolute laminations. Strength=15028 lb/in ²
H	Vuggy dolomite from near the St. Peter contact (depth=638.5-639 feet). Vugs are open. Strength=2813 lb/in ²



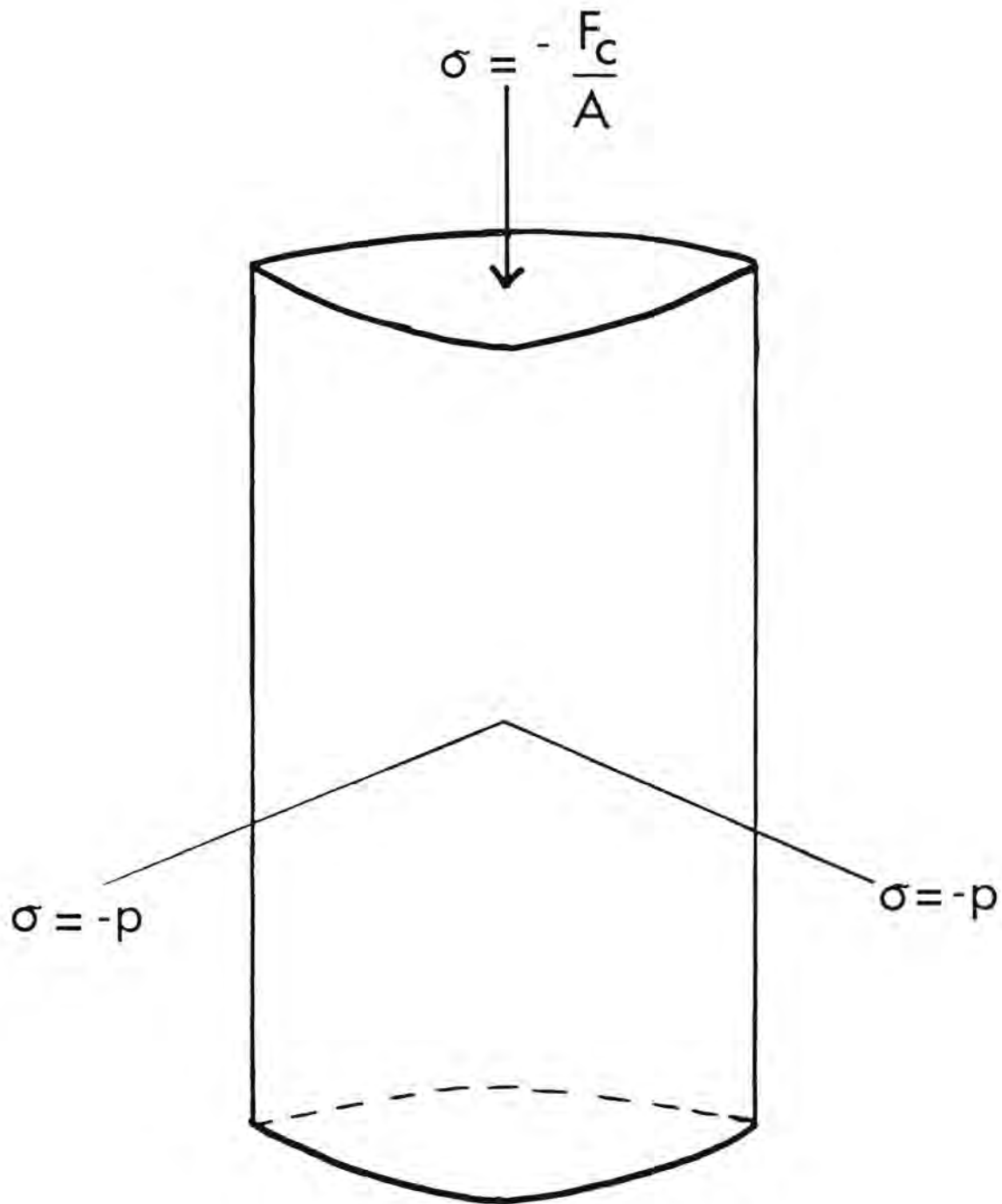


FIGURE III-2. Triaxial compressive strength test arrangement.

F_c = Compressive load at failure

A = Cross-sectional area

P = Confining pressure

$\sigma, \sigma_2, \sigma_3$ = Principal stresses

TABLE III-2

UNCONFINED UNIAXIAL TEST SPECIMENS AND RESULTS, YAKLEY WELLS

WELL	DEPTH (FT)	DENSITY (g/cm ³)	DESCRIPTION	STRENGTH (lb/in ²)
A	628.2-629.1	2.405	Dolomite, open fractures	6060
A	642.6-643.3	2.341	Dolomite, shaly, open vertical fractures	3215
B	604.6-605.2	2.694	Limestone, massive	7090
B	609.4-610.5	2.613	Dolomite, calcite-filled vugs	10880
B	611.5-612.35	2.357	Dolomite, shaly	7460
B	636-636.7	2.309	Dolomite, large (3mm-1cm) open vugs, vertical calcite-filled fractures	5090
C	627.8-628.7	2.325	Dolomite, vertical calcite veins	5150
D	619.9-620.6	2.405	Dolomite, irregular calcite veins	5720
D	629.3-630.1	2.116	Sandy dolomite, vuggy, open vertical veins	2790
D	648.8-649.6	2.341	Sandstone, white subvertical fracture	5820
IW	644.45-645.17	2.261	Dolomite, open vugs (~2mm)	2930
IW	649.8-650.4	2.100	Sandy dolomite, open pin point vugs	2140
IW	651.5-652.2	2.309	Sandstone, green, convolute laminations	1170
IW	665.25-666.2	2.245	Sandstone, white, hard	5880

Figure III-3 shows the Yakley injection well samples selected for uniaxial compressive strength testing.

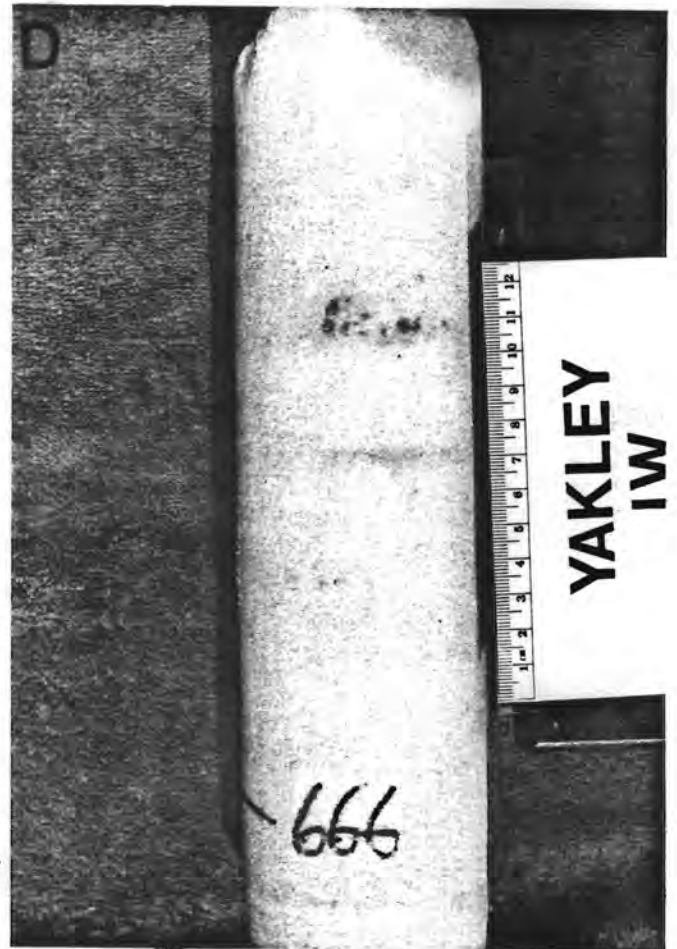
FIGURE III-3

Caprock, transition zone and St. Peter Sandstone samples subjected to uniaxial compressive strength testing.

PHOTOGRAPH

DESCRIPTION

- | | |
|---|---|
| A | Vuggy dolomite, somewhat compact, with convolute laminations near middle from a depth of 644.45-645.17 feet. Strength=2930 lb/in ² |
| B | Sandy dolomite, Joachim-St. Peter transition, from a depth of 649.8-650.4 feet. Pin point sized grains are quartz grains. The dolomite becomes sandier near the base. Strength=2140 lb/in ² |
| C | Sandy dolomite from a depth of 651.5-652.2 feet. Dolomite occurs at the top and bottom of this core specimen and is present, as clasts, within the green sand in the middle of the specimen. Strength=1170 lb/in ² |
| D | White St. Peter Sandstone from a depth of 665.25-666.2 feet. Strength=5880 lb/in ² |



SECTION IV
THERMAL TESTING

General

Seven core plugs from the green and white St. Peter Sandstone were heated 24-48 hours at 390°F to assess potential changes in the reservoir during hot air injection. Samples tested are given in Table IV-1.

An additional 14 core plugs from the Yakley Field were heated for 24 hours at 350°F with a confining pressure of 1000 p.s.i. Samples analyzed are given in Table IV-2.

Procedure -

Selected core plugs were heated for 24 hours at 390°F. After heating, the samples were dried in a dessicator for one hour and sampled. Some plugs were returned to the oven for an additional 24 hour heating period.

Additional plugs were heated at 350°F and 1000 p.s.i. for 24 hours. Eight of these plugs were selected for further analysis.

Thin sections of all plugs heated at 390°F for 24 or 48 hours and examined. Changes in pore system morphology and mineralogy were noted.

X-ray diffraction analysis of the fine fraction was utilized to detect sub-microscopic changes in mineralogy.

Pores of selected samples were examined with the scanning electron microscope.

Results -

Results of the petrographic examination are presented in Tables IV-3 through IV-12 and in a series of color photographs (Figures IV-1 through IV-5). Very generally, as time of heating is increased, a relative decrease in detrital matrix occurs in those samples which contain matrix. For those samples which were heated under pressure, total clay minerals appear to decrease with heating. The most notable effect of heating, as observed in nearly all samples, is the tendency of depositional matrix to "spall" from quartz grain surfaces.

Fine fraction X-ray diffraction results (Tables IV-13 through IV-16) are inconclusive. No significant changes or trends, with heating, are observed.

Spalling of detrital clay matrix is more clearly illustrated through the SEM examination (Figures IV-5 through IV-21). Pore fill minerals are generally unaffected by heating and grain surfaces are cleaner. In some instances, the matrix exhibits a "latticework" appearance.

Pyrite of two specimens of white sand which were heated at 350°F under 1000 p.s.i. was oxidized to hematite and free sulfur.

TABLE IV-1

SAMPLES HEATED AT 390°F FOR 24 AND 48 HOURS

Sample No.	Depth, Ft.	Yakley Well	Time of Heating	
			24hr	48hr
D391-029	643.0	C	X	-
D391-035	645.0	C	X	X
D391-038	652.0	C	X	X
D391-039	654.4	C	X	X
D391-043	638.0	D	X	-
D391-046	640.5	D	X	-
D391-061	653.0	IW	X	-

TABLE IV-2

SAMPLES HEATED AT 350°F AND 1000 P.S.I. FOR 24 HOURS
(ONLY THOSE SAMPLES SELECTED FOR ANALYSES ARE TABULATED)

Sample No.	Depth, Ft.	Yakley Well	Description
D391-007	662.0	A	Green St. Peter Sandstone no laminations
D391-008	671.1	A	White St. Peter
D391-010	677.0	A	Light Gray St. Peter
D391-056	649.5	IW	Sandy dolomite
D391-059	652.0	IW	Green St. Peter Sandstone, horizontal laminations
D391-062	654.0	IW	Green St. Peter Sandstone, discontinuous laminations
D391-065	655.0	IW	Green St. Peter Sandstone
D391-063	665.4	IW	White St. Peter Sandstone

TABLE IV-3

THIN SECTION ANALYSIS

		WELL	YAKLEY "C"		FORMATION	JOACHIM-ST. PETER TRANSITION		DEPTH	643.0 FEET																									
Depth (Ft)	TEXTURE		GRAIN COMPOSITION										CEMENT COMPOSITION		TOTALS		Sample ID Number																	
			Mean Grain Size (mm)	Overall Sorting	Monocrystalline Quartz	Polycrystalline Quartz	Mica	K-Feldspar	Plagioclase Feldspar	Chert	Igneous RF's	Metamorphic RF's	Sandstone Fragments	Clay Balls	Shale Fragments	Plant Remains		Carbonate Fragments	Shell Fragments	Glaucanite	Heavy Minerals	Others	Detrital Clay Matrix	Authigenic Clay	Silica	Calcite	Dolomite	Siderite	Anhydrite	Pyrite	Total Quartz	Total Clay Minerals	Total Carbonates	
643.0	0.44	PS	PS	79	-	-	-	-	-	-	-	-	-	-	-	-	-	-	-	Tr	-	21	-	-	-	-	-	-	-	79	21	-	0291 ¹	
643.0	0.42	PS	PS	85	-	-	-	-	-	-	-	-	-	-	-	-	-	-	-	Tr	-	14	-	1	-	-	-	-	-	86	14	-	029a ²	

MX = Depositional matrix (fines deposited simultaneously with the sand grains). RF's = Rock Fragments.
 1 = Unheated
 2 = Heated at 390°F for 24 hours.

S-ΔI

TABLE IV-4

THIN SECTION ANALYSIS

WELL YAKLEY "C" FORMATION ST. PETER (GREEN) DEPTH 645.0 Feet

Depth (Ft)	TEXTURE		GRAIN COMPOSITION																MX	CEMENT COMPOSITION						TOTALS			Sample ID Number ²				
	Mean Grain Size (mm) ¹	Overall Sorting	Monocrystalline Quartz	Polycrystalline Quartz	Mica	K-Feldspar	Plagioclase Feldspar	Chert	Igneous RF's	Metamorphic RF's	Sandstone Fragments	Clay Balls	Shale Fragments	Plant Remains	Carbonate Fragments	Shell Fragments	Glauconite	Heavy Minerals		Others	Detrital Clay Matrix	Authigenic Clay	Silica	Calcite	Dolomite	Siderite	Anhydrite	Pyrite		Total Quartz	Total Clay Minerals	Total Carbonates	
645.0	0.51	PS	75	-	-	-	-	-	-	-	-	-	-	-	-	-	-	Tr	-	25	Tr	-	-	-	-	-	Tr	75	25	-	035		
645.0	0.47	PS	79	-	-	-	-	-	-	-	-	-	-	-	-	-	-	Tr	-	21	Tr	-	-	-	-	-	Tr	79	21	-	035a		
645.0	0.55	PS	85	Tr	-	-	-	-	-	-	-	-	-	-	-	-	-	Tr	-	14	Tr	-	-	-	-	-	1	85	14	-	035b		

MX = Depositional matrix (fines deposited simultaneously with the sand grains). RF's = Rock Fragments.
 2 = Sample 035-unheated; 035a-heated 24 hrs. at 390F; 035b-heated 48 hrs. at 390°F.
 1 = Grain size distribution is bimodal. The coarse mode is reported here.

TABLE IV-5
THIN SECTION ANALYSIS

WELL YAKLEY "C" FORMATION ST. PETER (WHITE) DEPTH 652.0 and 654.4 Feet

Depth (Ft)	TEXTURE		GRAIN COMPOSITION														MX	CEMENT COMPOSITION						TOTALS			Sample ID Number ²					
	Mean Grain Size (mm) ¹	Overall Sorting	Monocrystalline Quartz	Polycrystalline Quartz	Mica	K-Feldspar	Plagioclase Feldspar	Chert	Igneous RF's	Metamorphic RF's	Sandstone Fragments	Clay Balls	Shale Fragments	Plant Remains	Carbonate Fragments	Shell Fragments		Glauconite	Heavy Minerals	Others	Detrital Clay Matrix	Authigenic Clay	Silica	Calcite	Dolomite	Siderite		Anhydrite	Pyrite	Total Quartz	Total Clay Minerals	Total Carbonates
652.0	0.42	PS	82	-	-	-	-	-	-	-	-	-	-	-	-	-	-	Tr	-	17	Tr	1	-	-	-	-	Tr	83	17	-	038	
652.0	0.44	PS	78	-	-	-	-	-	-	-	-	-	-	-	-	-	-	Tr	-	21	Tr	1	-	-	-	-	Tr	79	21	-	038a	
652.0	0.41	MWS	89	2	-	-	-	-	-	-	-	-	-	-	-	-	-	Tr	-	8	Tr	1	-	-	-	-	Tr	92	8	-	038b	
654.4	0.52	WS	81	-	-	-	-	-	-	-	-	-	-	-	-	-	-	Tr	-	Tr	3	14	2	-	-	-	Tr	95	3	2	039	
654.4	0.48	WS	82	Tr	-	-	-	-	-	-	-	-	-	-	-	-	-	Tr	-	Tr	7	7	4	-	-	-	Tr	89	7	4	039a	
654.4	0.52	WS	85	1	-	-	-	-	-	-	-	-	-	-	-	-	-	Tr	-	Tr	6	8	-	-	-	-	Tr	94	6	-	039b	

MX = Depositional matrix (fines deposited simultaneously with the sand grains). RF's = Rock Fragments.

1 = Grain size distribution is bimodal. The coarse mode is reported.

2 = Unheated samples: -038 and -039; heated for 24 hours at 390°F: -038a and -038b; heated for 48 hours at 390°F: 038b and 039b.

TABLE IV-6

THIN SECTION ANALYSIS

WELL YAKLEY "D"

FORMATION ST. PETER (GREEN)

DEPTH 638 and 640.5 Feet

L-VI

Depth (Ft)	TEXTURE		GRAIN COMPOSITION																	MX	CEMENT COMPOSITION							TOTALS			Sample ID Number..		
	Mean Grain Size (mm)	Overall Sorting	Monocrystalline Quartz	Polycrystalline Quartz	Mica	K-Feldspar	Plagioclase Feldspar	Chert	Igneous RF's	Metamorphic RF's	Sandstone Fragments	Clay Balls	Shale Fragments	Plant Remains	Carbonate Fragments	Shell Fragments	Glauconite	Heavy Minerals	Others		Detrital Clay Matrix	Authigenic Clay	Silica	Calcite	Dolomite	Siderite	Anhydrite	Pyrite	Total Quartz	Total Clay Minerals		Total Carbonates	
638	0.54	PS	85	Tr	-	-	-	-	-	-	-	-	-	-	-	-	-	Tr	-	13	2	-	-	-	-	-	Tr	85	15	-	043		
638	0.51	PS	77	Tr	-	-	-	-	-	-	-	-	-	-	-	-	-	Tr	-	22	Tr	1	-	-	-	-	Tr	78	22	-	043a		
640.5	0.46	PS	75	Tr	-	-	-	-	-	-	-	-	-	-	-	-	-	Tr	-	25	Tr	-	-	-	-	-	Tr	75	25	-	046		
640.5	0.36	PS	78	-	-	-	-	-	-	-	-	-	-	-	-	-	-	Tr	-	22	-	-	-	-	-	-	Tr	78	22	-	046a		

MX = Depositional matrix (fines deposited simultaneously with the sand grains). RF's = Rock Fragments.

1 = Grain size distribution is bimodal. The coarse mode is reported.

2 = Samples -043 and -046 unheated; Samples -043a and -046a heated for 24 hours at 390°F.

TABLE IV-7
THIN SECTION ANALYSIS

WELL		FORMATION										DEPTH																				
YARLEY "TW"		ST. PETER (GREEN)										653 Feet																				
Depth (Ft)	TEXTURE	GRAIN COMPOSITION										MX	CEMENT COMPOSITION					TOTALS	Sample ID Number													
		Mean Grain Size (mm)	Overall Sorting	Monocrystalline Quartz	Polycrystalline Quartz	Mica	K-Feldspar	Plagioclase Feldspar	Chert	Igneous RF's	Metamorphic RF's		Sandstone Fragments	Clay Balls	Shale Fragments	Plant Remains	Carbonate Fragments			Shell Fragments	Glauconite	Heavy Minerals	Others	Detrital Clay Matrix	Authigenic Clay	Silica	Calcite	Dolomite	Siderite	Anhydrite	Pyrite	Total Quartz
653		0.50 PS	92	-	-	-	-	-	-	-	-	-	-	-	-	-	-	-	-	-	4	-	4	-	-	-	-	-	-	-	-	D391
653		0.49 PS	81	-	-	-	-	-	-	-	-	-	-	-	-	-	-	-	-	-	19	-	-	-	-	-	-	-	-	-	-	061 2 061a

MX = Depositional matrix (fines deposited simultaneously with the sand grains). RF's = Rock Fragments.
 1 = Unheated
 2 = Heated at 390°F for 24 hours.

TABLE IV-8
THIN SECTION ANALYSIS

WELL	YAKLEY "A"		FORMATION	ST. PETER (GREEN)		DEPTH	662.0 Feet									
	TEXTURE		GRAIN COMPOSITION						MX	CEMENT COMPOSITION			TOTALS			
	Depth (Ft)	662.0	662.0	Mean Grain Size (mm)	0.41	MMS	90	1	-	-	-	-	-	-	-	-
			Overall Sorting	0.46	MMS	91	-	-	-	-	-	-	-	-	-	007H 2
			Monocrystalline Quartz													
			Polycrystalline Quartz													
			Mica													
			K-Feldspar													
			Plagioclase Feldspar													
			Chert													
			Igneous RF's													
			Metamorphic RF's													
			Sandstone Fragments													
			Clay Balls													
			Shale Fragments													
			Plant Remains													
			Carbonate Fragments													
			Shell Fragments													
			Glauconite													
			Heavy Minerals				Tr	Tr	-							
			Authigenic Feldspar				-	Tr								
			Detrital Clay Matrix						4							
			Authigenic Clay						3							
			Silica						2							
			Calcite													
			Dolomite													
			Siderite													
			Anhydrite													
			Pyrite							Tr						
			Total Quartz							93						
			Total Clay Minerals							7						
			Total Carbonates							-						
			Sample ID Number													

MX = Depositional matrix (fines deposited simultaneously with the sand grains). RF's = Rock Fragments.
 1 = Unheated.
 2 = Heated at 350°F and 1000 p.s.i. for 24 hours.

TABLE IV-9
THIN SECTION ANALYSIS

WELL	YAKLEY "TW"	FORMATION	ST. PETER (GREEN)	DEPTH	652.0 and 655.0 Feet																										
TEXTURE	Mean Grain Size (mm) ¹	GRAIN COMPOSITION				MX	CEMENT COMPOSITION				TOTALS	Sample ID Number ²																			
	Overall Sorting	Monocrystalline Quartz	Polycrystalline Quartz	Mica	K-Feldspar		Plagioclase Feldspar	Chert	Igneous RF's	Metamorphic RF's			Sandstone Fragments	Clay Balls	Shale Fragments	Plant Remains	Carbonate Fragments	Shell Fragments	Glauconite	Heavy Minerals	Authigenic Clay	Detrital Clay Matrix	Authigenic Clay	Silica	Calcite	Dolomite	Siderite	Anhydrite	Pyrite	Total Quartz	Total Clay Minerals
Depth (Ft)	652.0	0.64 PS	73	-	Tr	-	-	-	-	-	-	-	-	-	-	-	-	Tr	23	2	2	-	-	-	-	-	Tr	75	25	-	059
	652.0	0.56 PS	79	1	Tr	-	-	-	-	-	-	-	-	-	-	-	-	Tr	18	2	-	-	-	-	-	Tr	80	20	-	059H	
	655.0	0.46 PS	75	-	Tr	-	-	-	-	-	-	-	-	-	-	-	-	Tr	25	Tr	Tr	-	-	-	-	Tr	75	25	-	065	
	655.0	0.53 PS	76	Tr	-	-	-	-	-	-	-	-	-	-	-	-	-	Tr	21	-	3	-	-	-	-	Tr	79	21	-	065H	

MX = Depositional matrix (fines deposited simultaneously with the sand grains). RF's = Rock Fragments.
 1 = Grain size distribution is bimodal. Coarse mode is reported.
 2 = Unlettered samples not heated. Samples with "H" heated for 24 hours at 350°F and 1000 p.s.i.

TABLE IV-10

THIN SECTION ANALYSIS

WELL YAKLEY "A"		FORMATION ST. PETER (WHITE)		DEPTH 671.1	
TEXTURE	GRAIN COMPOSITION	MX	CEMENT COMPOSITION	TOTALS	
671.1	Depth (Ft)				
0.31	Mean Grain Size (mm)				
MMS	Overall Sorting				
93	Monocrystalline Quartz				
1	Polycrystalline Quartz				
-	Mica				
-	K-Feldspar				
-	Plagioclase Feldspar				
-	Chert				
-	Igneous RF's				
-	Metamorphic RF's				
-	Sandstone Fragments				
-	Clay Balls				
-	Shale Fragments				
-	Plant Remains				
-	Carbonate Fragments				
-	Shell Fragments				
-	Glauconite				
Tr	Heavy Minerals				
-	Others				
2	Detrital Clay Matrix				
1	Authigenic Clay				
3	Silica				
-	Calcite				
-	Dolomite				
-	Siderite				
-	Anhydrite				
Tr	Pyrite				
97	Total Quartz				
3	Total Clay Minerals				
-	Total Carbonates				
008H *	D391 - Sample ID Number				

MX = Depositional matrix (fines deposited simultaneously with the sand grains). RF's = Rock Fragments.
 * = Sample heated for 24 hours at 1000 p.s.i. and 350°F.

TABLE IV-11
THIN SECTION ANALYSIS

WELL YAKLEY "A"		FORMATION ST. PETER (DARK GRAY)		DEPTH 677.0 Feet	
TEXTURE	GRAIN COMPOSITION	MX	CEMENT COMPOSITION	TOTALS	
				Total Quartz	Total Clay Minerals
Depth (Ft)					
Mean Grain Size (mm)					
Overall Sorting					
Monocrystalline Quartz					
Polycrystalline Quartz					
Mica					
K-Feldspar					
Plagioclase Feldspar					
Chert					
Igneous RF's					
Metamorphic RF's					
Sandstone Fragments					
Clay Balls					
Shale Fragments					
Plant Remains					
Carbonate Fragments					
Shell Fragments					
Glauconite					
Heavy Minerals					
Others					
Detrital Clay Matrix					
Authigenic Clay					
Silica					
Calcite					
Dolomite					
Siderite					
Anhydrite					
Pyrite					
Total Quartz					
Total Clay Minerals					
Total Carbonates					
Sample ID Number					

MX = Depositional matrix (fines deposited simultaneously with the sand grains). RF's = Rock Fragments.
 * = Sample heated for 24 hours at 1000 p.s.i. and 350°F.

TABLE IV-12

THIN SECTION ANALYSIS

DEPTH	WELL	YAKLEY "IW"	FORMATION	SEE BELOW	GRAIN COMPOSITION										MX	CEMENT COMPOSITION							TOTALS	Sample ID Number												
					Monocrystalline Quartz	Polycrystalline Quartz	Mica	K-Feldspar	Plagioclase Feldspar	Chert	Igneous RF's	Metamorphic RF's	Sandstone Fragments	Clay Balls		Shale Fragments	Plant Remains	Carbonate Fragments	Shell Fragments	Glauconite	Heavy Minerals	Others			Detrital Clay Matrix	Authigenic Clay	Silica	Calcite	Dolomite	Siderite	Anhydrite	Pyrite	Total Quartz	Total Clay Minerals	Total Carbonates	
649.5					-	-	7	-	-	-	-	-	-	-	-	-	-	-	-	-	-	-	-	-	-	-	-	-	-	-	-	-	-	-	056H*	
654.0					0.55	PS	87	-	-	-	-	-	-	-	-	-	-	-	-	-	-	-	-	-	-	-	-	-	-	-	-	-	-	- 062H		
665.4					0.29	WS	87	-	-	-	-	-	-	-	-	-	-	-	-	-	-	-	-	-	-	-	-	-	-	-	-	-	- 063H			

MX = Depositional matrix (fines deposited simultaneously with the sand grains). RF's = Rock Fragments.
 * = All samples heated at 350°F and 1000 p.s.i. for 24 hours.

TABLE IV-13

SEMIQUANTITATIVE X-RAY DIFFRACTION ANALYSIS OF THE
FINE (LESS THAN 5 MICRON) SIZE FRACTION FROM
THERMAL TESTING
Sample a = 24 hr at 390°F; Sample b = 48 hr at 390°F;
unlettered samples are unheated

Depth(ft):	<u>WELL:</u>					<u>YAKLEY C</u>					
	643 (Transition)	645 (Green St. Peter)		652.0 (White St. Peter)		654.4 (White St. Peter)					
Sample No.	D391-029	-029a	-035	-035a	-035b	-038	-038a	-038b	-039	-039a	-039b
Illite-Smectite	-	-	-	-	-	-	-	-	-	-	-
Illite	19	26	42	9	8	22	34	15	21	59	27
Kaolinite	-	-	-	-	-	-	-	-	-	-	-
Chlorite	-	-	-	-	-	-	-	-	-	-	-
Quartz	69	57	20	86	78	78	59	80	59	9	63
Potassium Feldspar	-	5	-	5	8	-	7	-	12	6	6
Plagioclase Feldspar	-	-	-	-	-	-	-	-	-	-	-
Calcite	-	-	1	Tr	4	-	-	-	-	-	-
Dolomite	-	-	-	-	-	-	-	-	-	-	-
Marcasite	-	-	9	-	2	-	-	-	5	-	-
Pyrite	12	12	-	-	-	-	-	3	-	-	4
Sericite	-	-	28	-	-	-	-	2	-	15	-
Anhydrite	-	-	-	-	-	-	-	-	3	11	-

IV-14

TABLE IV-14

SEMIQUANTITATIVE X-RAY DIFFRACTION ANALYSIS OF THE
FINE (LESS THAN 5 MICRON SIZE FRACTION FROM
THERMAL TESTING

	<u>WELL:</u>		<u>YAKLEY D (GREEN ST. PETER)</u>		
Depth(ft):	638.0		640.5		
Sample No.	D391-	043	043a	046	046a
Illite-Smectite	-	-	-	-	-
Illite	4	5	19	17	
Kaolinite	-	-	-	-	-
Chlorite	-	-	-	-	-
Quartz	85	79	67	76	
Potassium Feldspar	5	8	6	7	
Plagioclase Feldspar	-	-	-	-	-
Calcite	4	4	3	-	
Dolomite	-	-	-	-	-
Pyrite	2	4	5	-	

TABLE IV-15

SEMIQUANTITATIVE X-RAY DIFFRACTION
ANALYSIS OF THE FINE (LESS THAN FIVE MICRON)
SIZE FRACTION FROM THERMAL TESTING; SAMPLE a =
HEATING FOR 24 HOURS AT 390°F

WELL	YAKLEY	IW
Depth (Ft)		
Sample No.	061	061a
Illite-Smectite	-	-
Illite	10	12
Kaolinite	-	-
Chlorite	-	-
Quartz	57	50
Potassium Feldspar	27	31
Plagioclase Feldspar	-	-
Calcite	3	4
Dolomite	-	-
Marcasite	-	3
Pyrite	3	-

TABLE IV-16

SEMIQUANTITATIVE X-RAY DIFFRACTION
ANALYSIS OF THE FINE (LESS THAN FIVE MICRON)
SIZE FRACTION FROM YAKLEY "IW". UNHEATED SAMPLE
AND SAMPLE HEATED TO 350° F at 1000 p.s.i.

Depth (Ft)		D391-065	D391-065H
Sample No.			
Illite-Smectite		-	-
Illite		32	37
Kaolinite		-	-
Chlorite		-	-
Quartz		39	49
Potassium Feldspar		8	14
Plagioclase Feldspar		-	-
Calcite		3	-
Dolomite		-	-
Marcasite		5	-
Sericite		13	-

SELECTED PHOTOMICROGRAPHS

Figures IV-1 through IV-5 illustrate the effect of heating selected St. Peter samples. Sample numbers with no letter are unheated. Samples designated by "a" were heated for 24 hours at 390°F. Samples designated by "b" were heated for 48 hours at 390°F. Samples designated by "H" were heated for 24 hours at 350°F and 1000 psi. All samples were impregnated with blue epoxy resin prior to thin section preparation and stained with Alizarin Red S dye.

FIGURE IV-1

WELL: YAKLEY C

FORMATION: JOACHIM-ST. PETER TRANSITION

DEPTH: 643.0 FEET

SAMPLE NO. D391-029,-029a

RED DOT = 0.12 mm

PHOTOGRAPH

DESCRIPTION

- A Medium grained, moderately well sorted sandstone consisting of quartz (colorless). Iron sulfide (black) occurs sporadically in the pore system as does depositional matrix (brown) in this unheated sample. (Plane polarized light).
- B Crossed nicols view of A. The depositional matrix (gold) is well crystallized and exhibits parallel extinction.
- C After heating for 24 hours at 390°F, the pore system appears to be significantly cleaner. Some spalling of depositional matrix from the surface of quartz grains has occurred.
- D Crossed nicols view of C shows that the crystallinity of the depositional matrix (gold) has changed slightly. By comparison with Photo B, the matrix appears to be more finely crystalline.

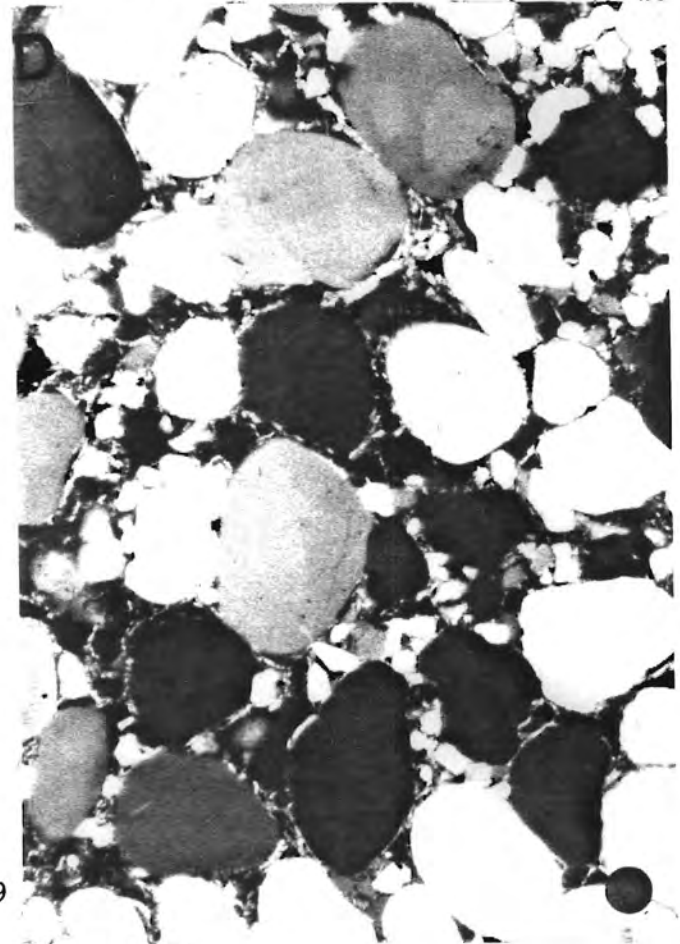
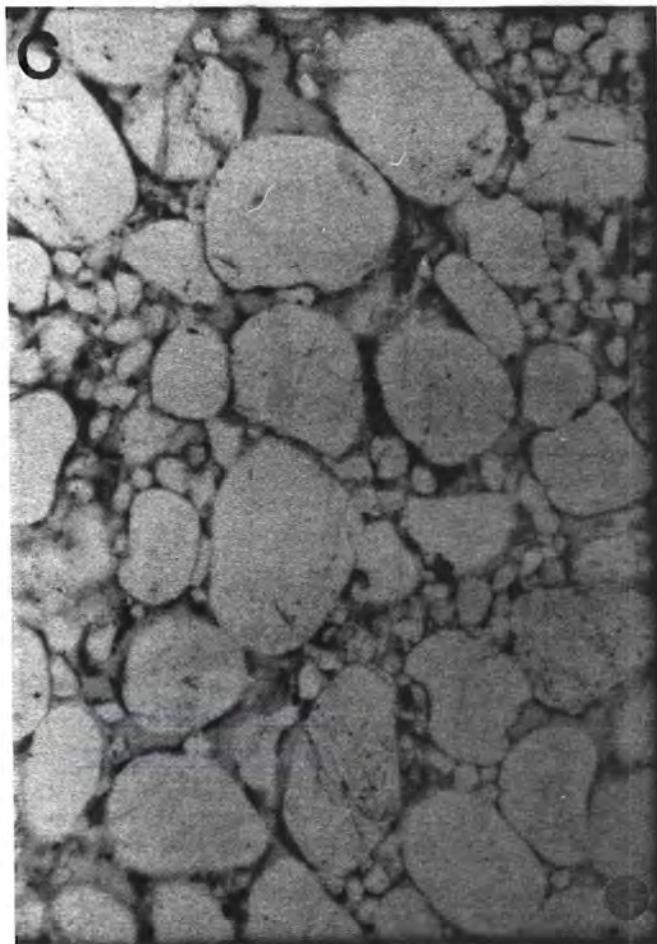
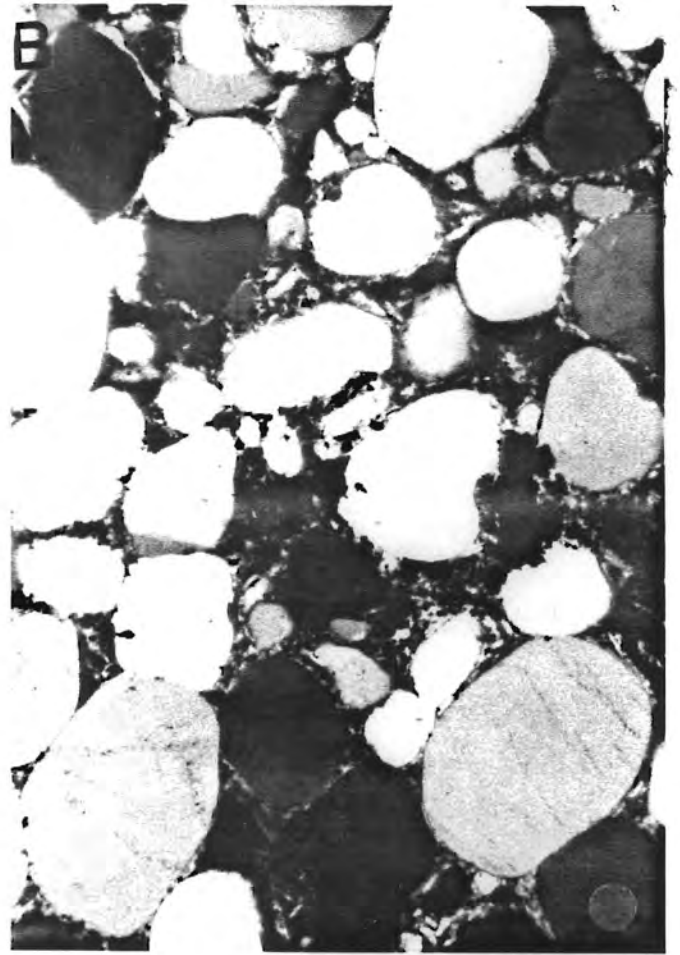
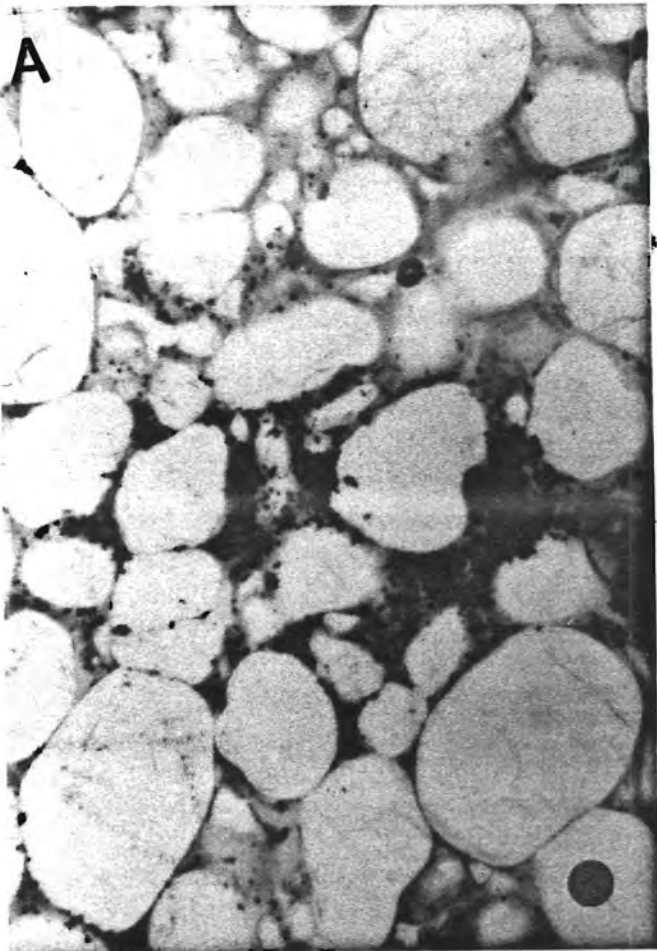


FIGURE IV-2

WELL: YAKLEY C

FORMATION: ST. PETER (GREEN)

DEPTH: 645.0 FEET

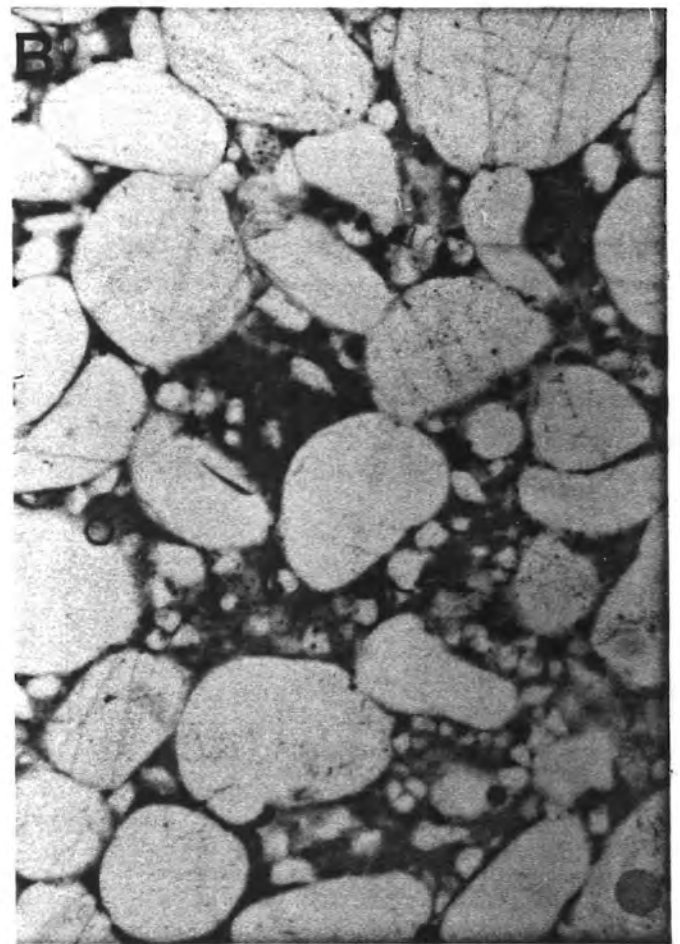
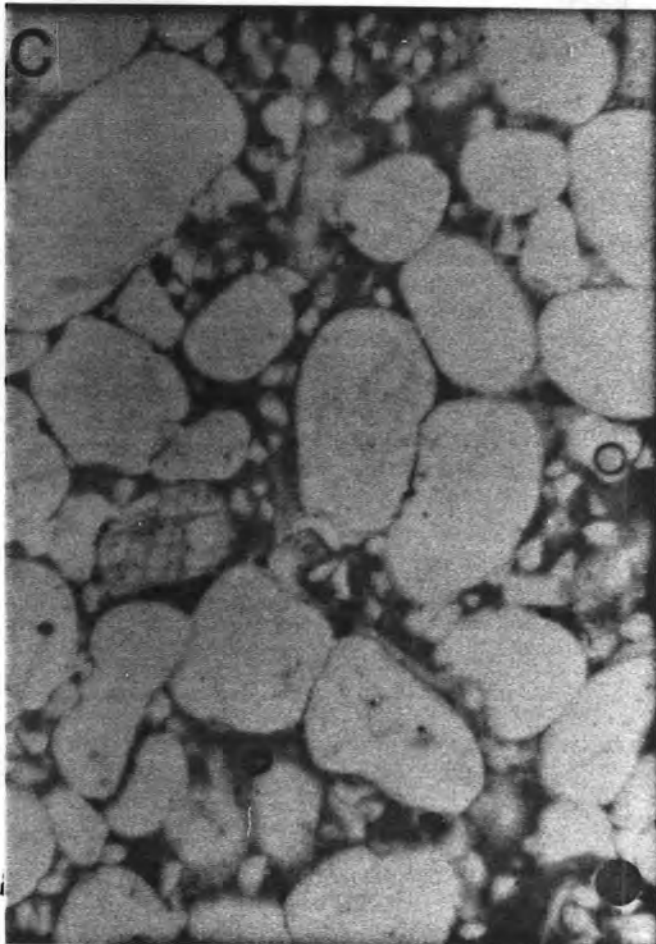
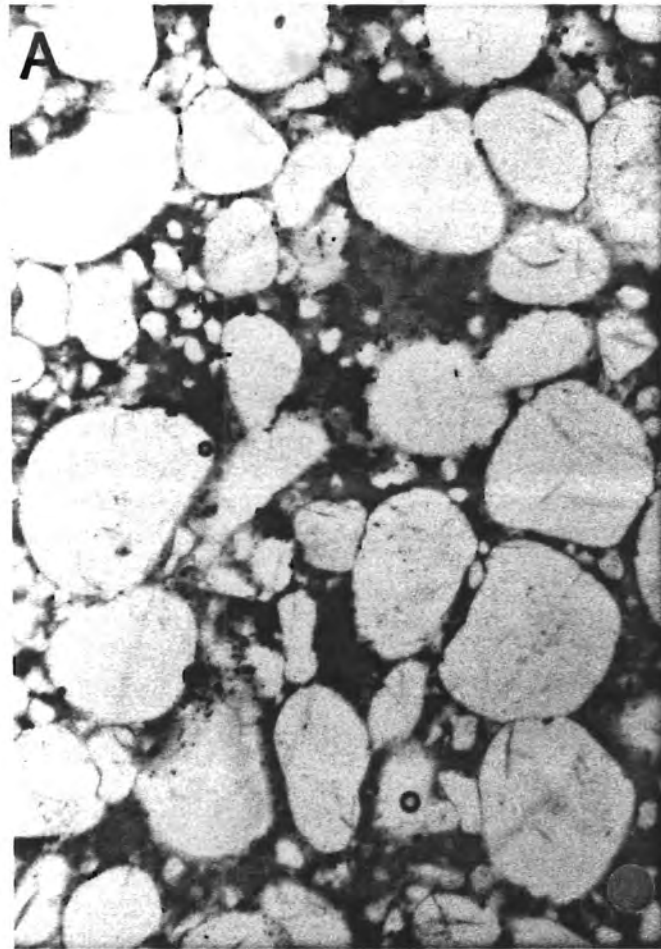
SAMPLE NO. D391-035,-035a,-035b

RED DOT = 0.12 mm
Plane Polarized Light

PHOTOGRAPH

DESCRIPTION

- A Medium grained poorly sorted, unheated sandstone. Quartz grains (colorless) are surrounded by detrital clay matrix (brown) and authigenic iron sulfide (black). Quartz grain size distribution is bimodal. The sample exhibits poor to moderate porosity.
- B This photo illustrates the effect of heating for 24 hours at 390°F. Porosity (blue) appears to have increased. Depositional matrix has spalled from quartz grain surfaces. Iron sulfide (black) appears to be less abundant, but this may be due to a natural uneven distribution of the phase.
- C After heating for 48 hours at 390°F, porosity has increased significantly. Depositional matrix is still in contact with quartz grains only in sheltered pores.



IV-21

FIGURE IV-3

WELL: YAKLEY IW

FORMATION: ST. PETER (GREEN)

DEPTH: 655 FEET

SAMPLE NO. D391-065H,-065

RED DOT = 0.12 mm

PHOTOGRAPH

DESCRIPTION

- A, B Photo A taken in plane polarized light; Photo B taken with crossed nicols. Sample heated for 24 hours at 350°F and 1000 p.s.i. Depositional matrix has spalled from quartz grains and is stained light pink by hematite generated during the heating process. With crossed nicols, the matrix has been recrystallized (compare with Photo D).
- C, D Photo C taken with plane polarized light; Photo D taken with crossed nicols. Unheated sample. Iron sulfides (black) are more abundant in the unheated sample than in the heated sample. (Compare Photos A and C). The matrix, under crossed nicols, appears to be more finely crystalline than that of the heated sample.

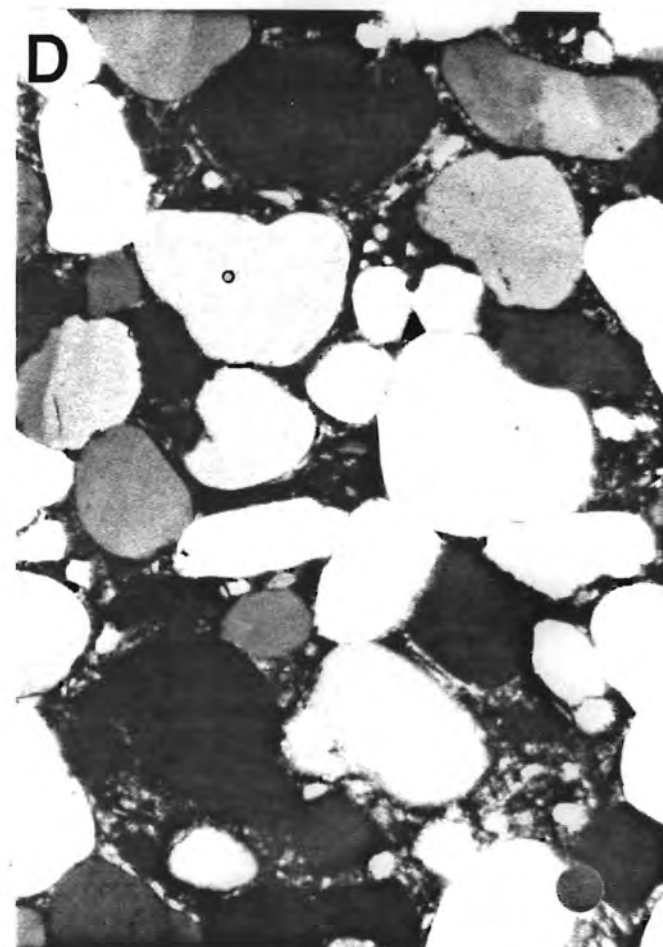
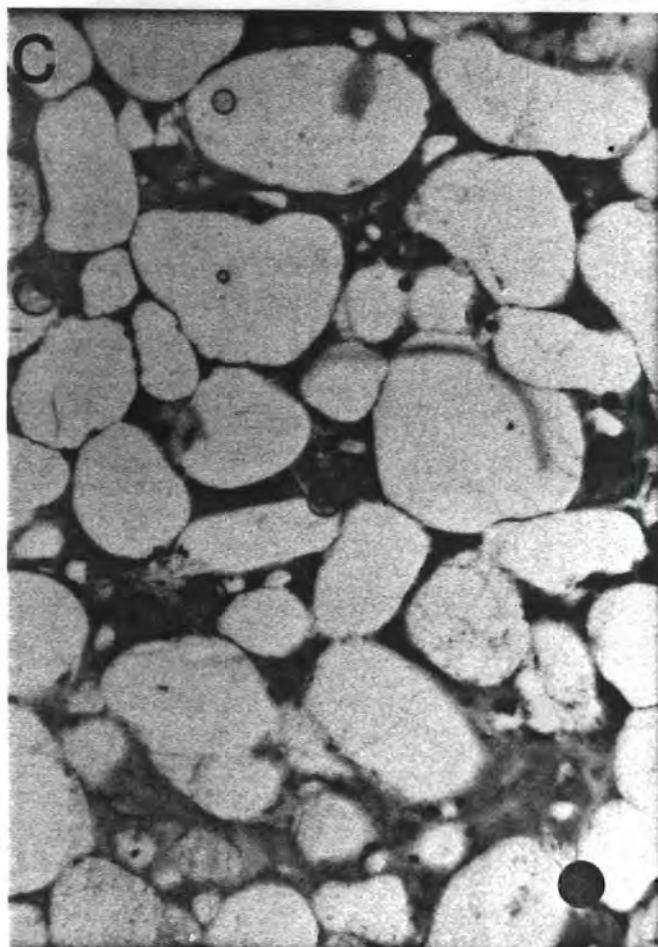
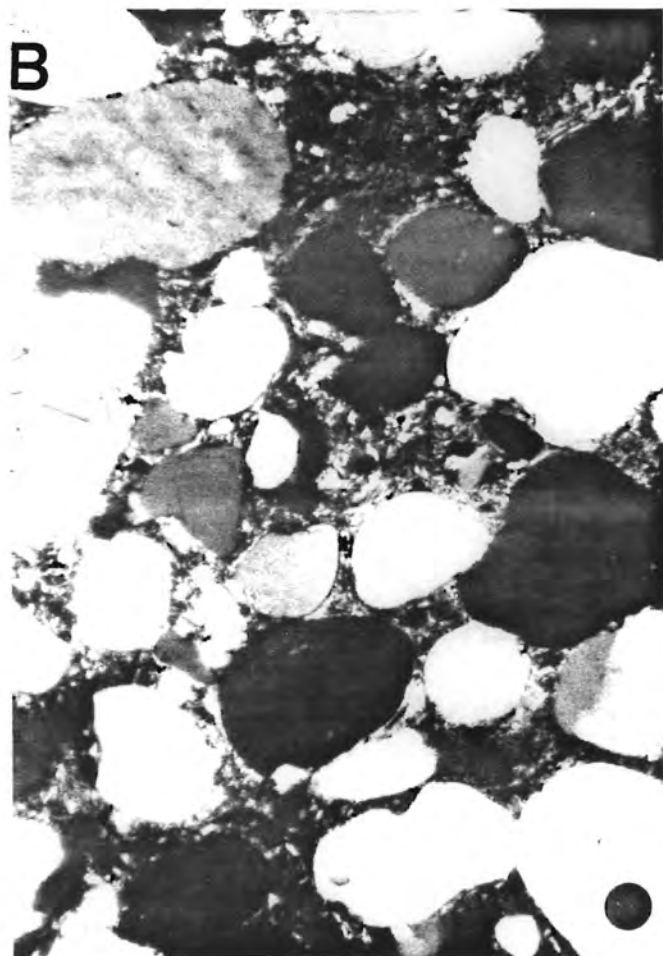
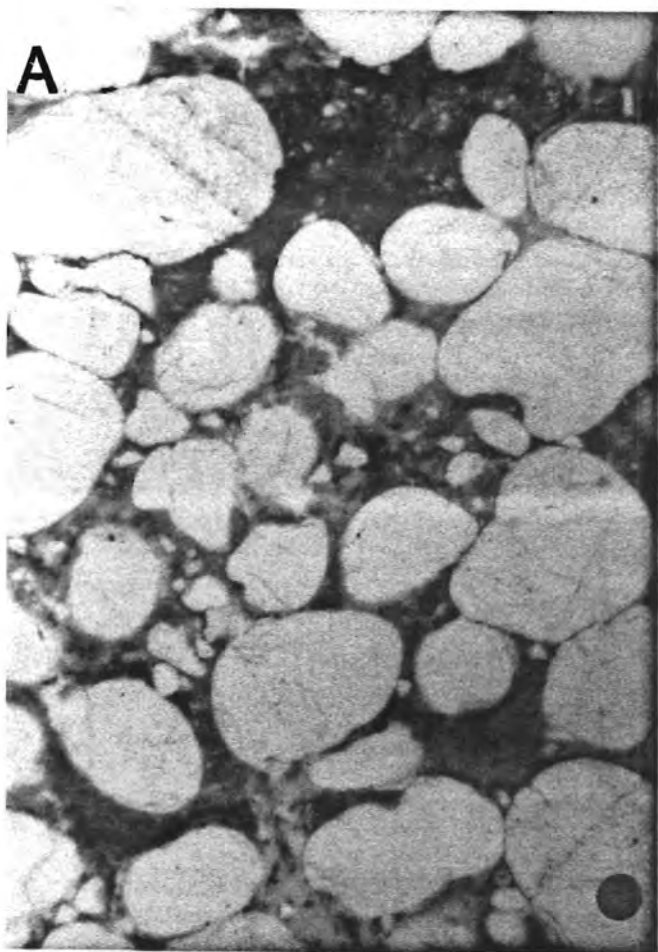


FIGURE IV-4

WELL: YAKLEY A

FORMATION: ST. PETER (GREEN)

DEPTH: 662.0 FEET

SAMPLE NO. D391-007H

Plane Polarized Light

Sample heated for 24 hours at 350°F and 1000 p.s.i.

<u>PHOTOGRAPH</u>	<u>MAGNIFICATION</u>	<u>DESCRIPTION</u>
A	Red dot=0.12 mm	Typically, the green St. Peter, at this depth contains abundant clay matrix. Detrital clay matrix is present but sparsely distributed. Iron sulfide (black) is also sparsely distributed.
B	Red dot=0.03 mm	This higher magnification view illustrates that iron minerals, codeposited with the matrix have been oxidized, giving rise to the reddish color. In addition, some pyrite, which forms the initial authigenic cement, at this depth, has been oxidized, leaving porosity between a quartz grain and an incomplete silica overgrowth.

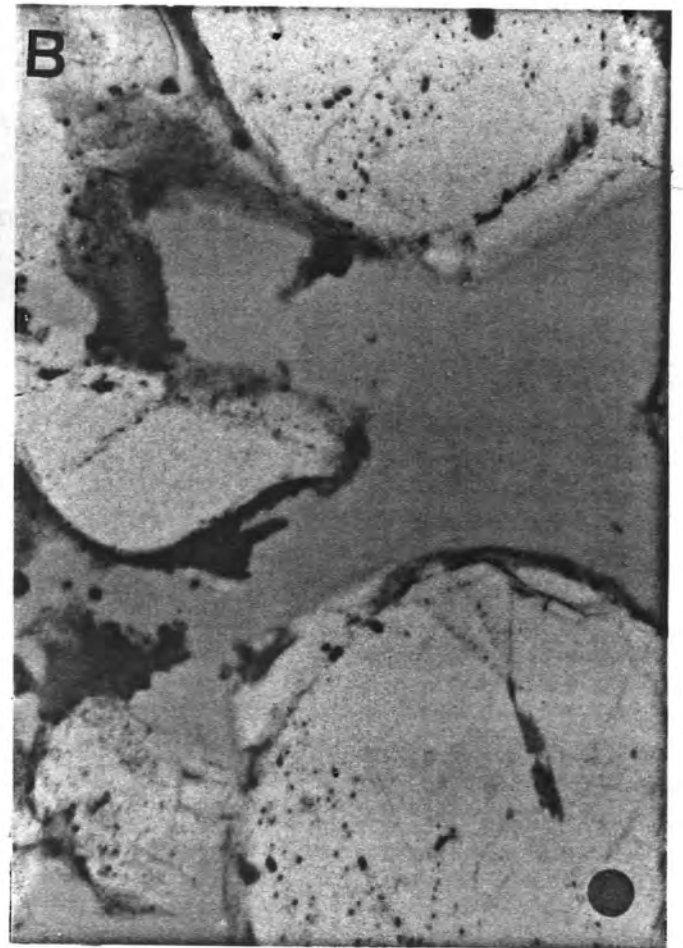
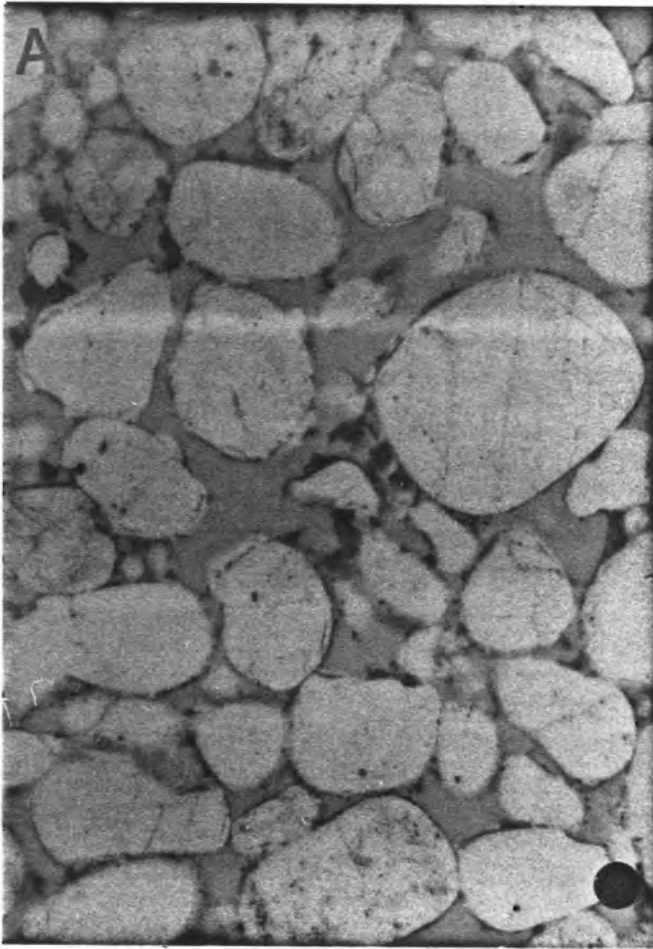


FIGURE IV-5

WELL: YAKLEY IW

FORMATION: ST. PETER (GREEN)

DEPTH: 652.0 FEET

SAMPLE NO. D391-059H

RED DOT = 0.12 mm

Photo A: Plane Polarized Light

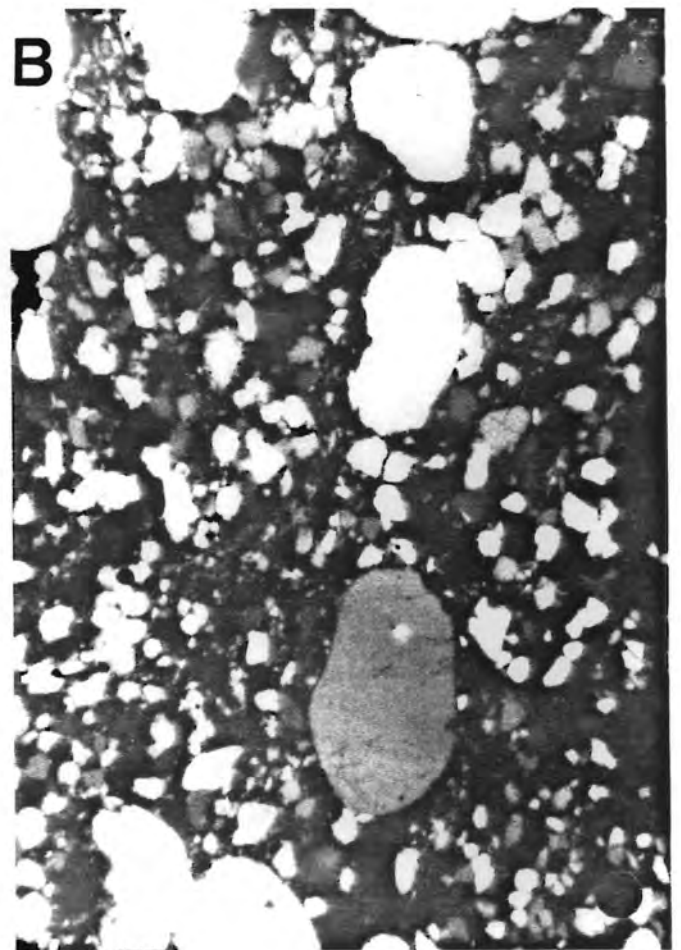
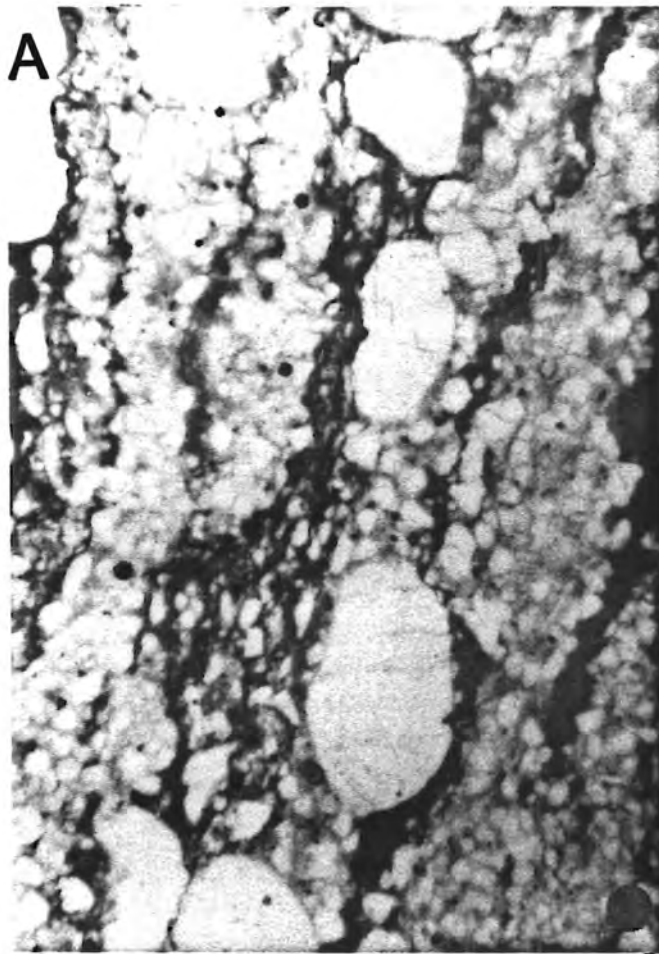
Photo B: Crossed Nicols

Sample heated for 24 hours at 350°F and 1000 p.s.i.

PHOTOGRAPH






DESCRIPTION

- A Green sands at this depth are composed primarily of quartz (colorless) and contain carbonaceous laminations and laminations of clay. Quartz grain size distribution is typically bimodal. The porosity (blue) of this sample is greater than that of unheated samples of a similar composition.
- B This view of A shows that the depositional matrix is very poorly crystalline. This could be an effect of heating.



SCANNING ELECTRON MICROGRAPH SCALE

The micron marker indicates the photograph scale by displaying a system of bars and dots which correspond to the viewing and photographing magnification. The relative distance represented by the micron marker and the bar length for a set magnification is as follows:

Magnification	Marker display	Relative distance (μm)
100,000x		0.1 (1000 \AA)
10,000-70,000x		1.0
1,000- 7,000x		10.0
100 - 700x		100.0
15 - 70x		1000.0 (1 mm)

Note 1: The above table can be read as follows:
The first dot is read as "1", and all other dots are read as "0". For instance, if two dots are displayed, it indicates that the length of the bar corresponds to "1", "0" μm (=10 μm). If no dots appear at all, it indicates that the relative distance is 0.1 μm .

Note 2: The magnification of the image displayed on the viewing CRT is approx. 1.2 times that indicated on the magnification indicator. However, since the length of the micron bar corresponds to this ratio, the micron marker can be read as displayed.

FIGURE IV-6

WELL: YAKLEY "C"

FORMATION: TRANSITION

DEPTH: 643.0 Feet

D391-029

<u>PHOTOGRAPH NO.</u>	<u>MAGNIFICATION</u>	<u>DESCRIPTION</u>
0810	30x	Grains (G) of the transition zone are surrounded by a clay matrix (M) which contains dolomite crystals. Quartz grain size distribution is bimodal.
0811	300x	Quartz grains (Q) are coated with minor authigenic illite (I) and partial silica overgrowths (S). A partially leached feldspar (F) and some matrix (M) also occur in this view.
0812	450x	These higher magnification views demonstrate the sparse occurrence of silica overgrowths (S) and very finely crystalline authigenic feldspar (F) associated with matrix (M).

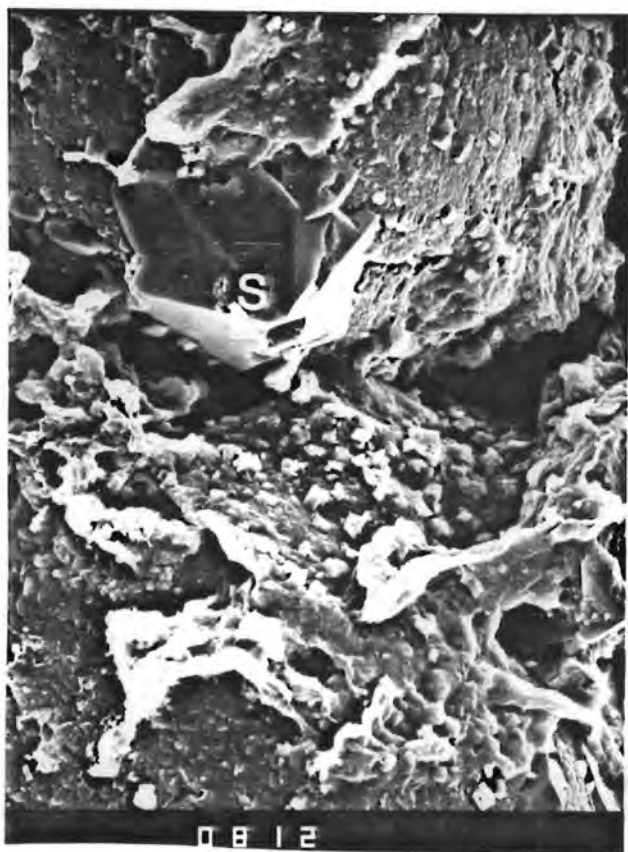
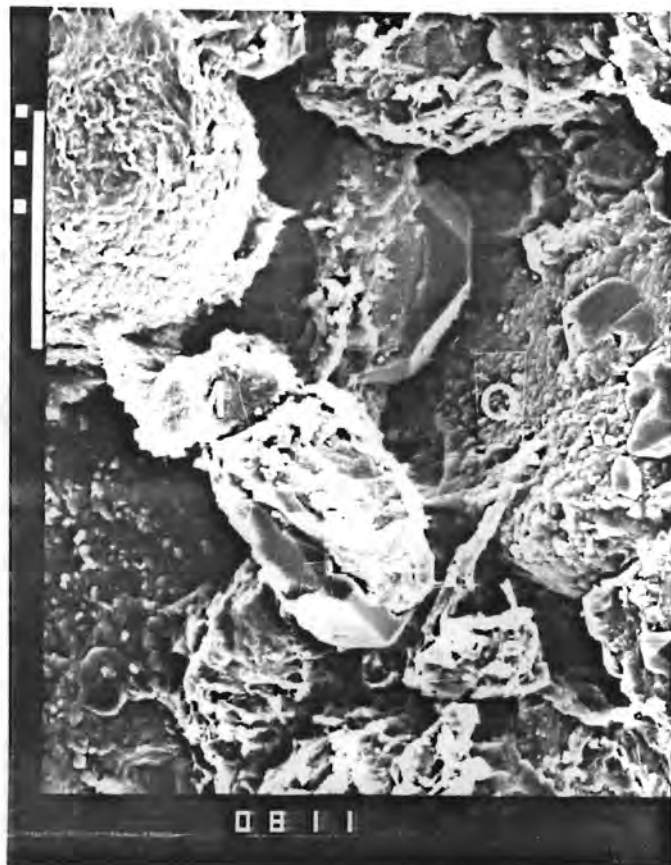
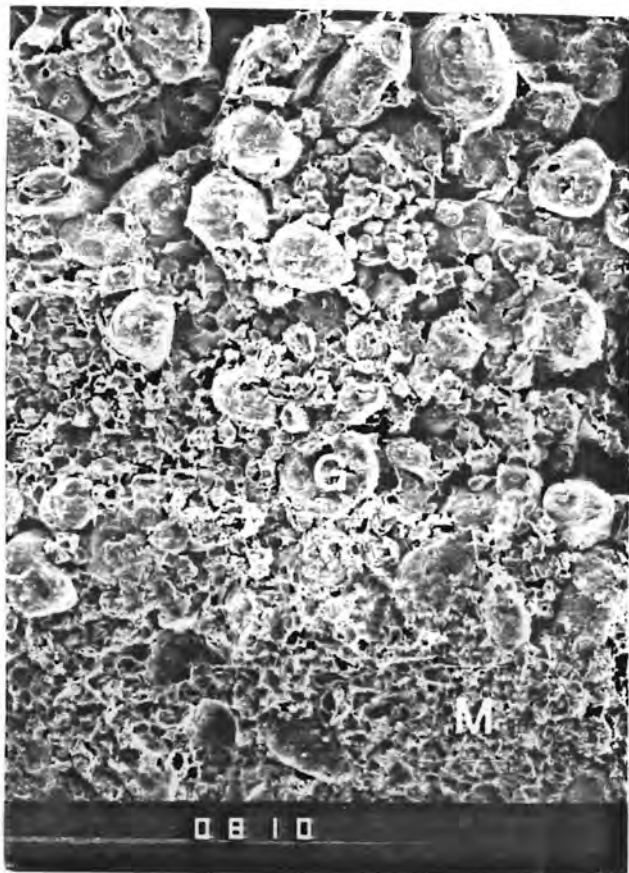


FIGURE IV-7

WELL: YAKLEY "C"

FORMATION: TRANSITION

DEPTH: 643.0 Feet

D391-029a

<u>PHOTOGRAPH NO.</u>	<u>MAGNIFICATION</u>	<u>DESCRIPTION</u>
0703	30x	The effect of heating a transition zone sample for 24 hours at 390°F is illustrated. Matrix (M) has been lifted from grain (G) surfaces. Illite (I) and microquartz crystals (Q) have been unaffected. Authigenic feldspar grains (F) occur sparsely and are unaffected.
0706	200x	
0705	1500x	
0704	3000x	

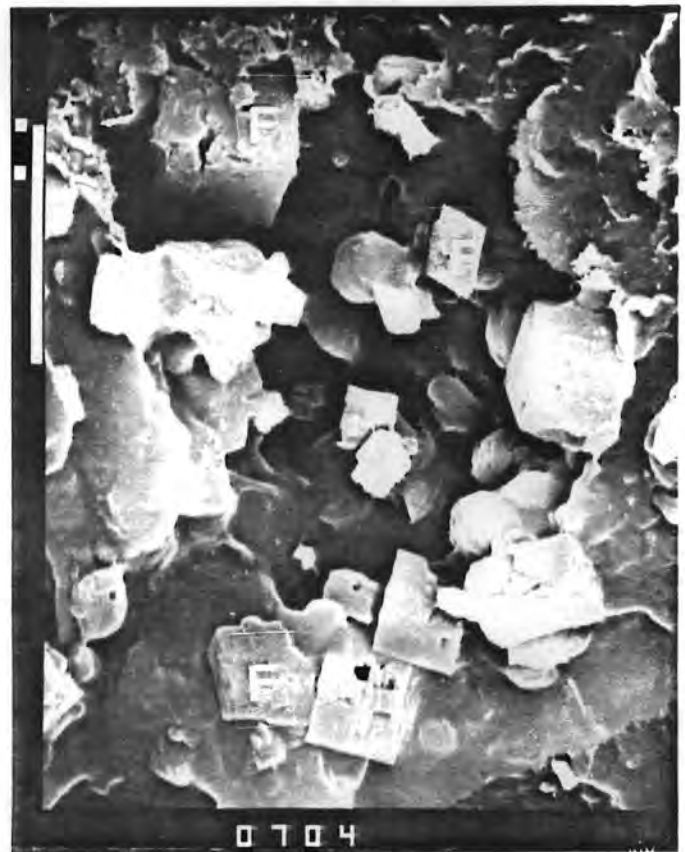
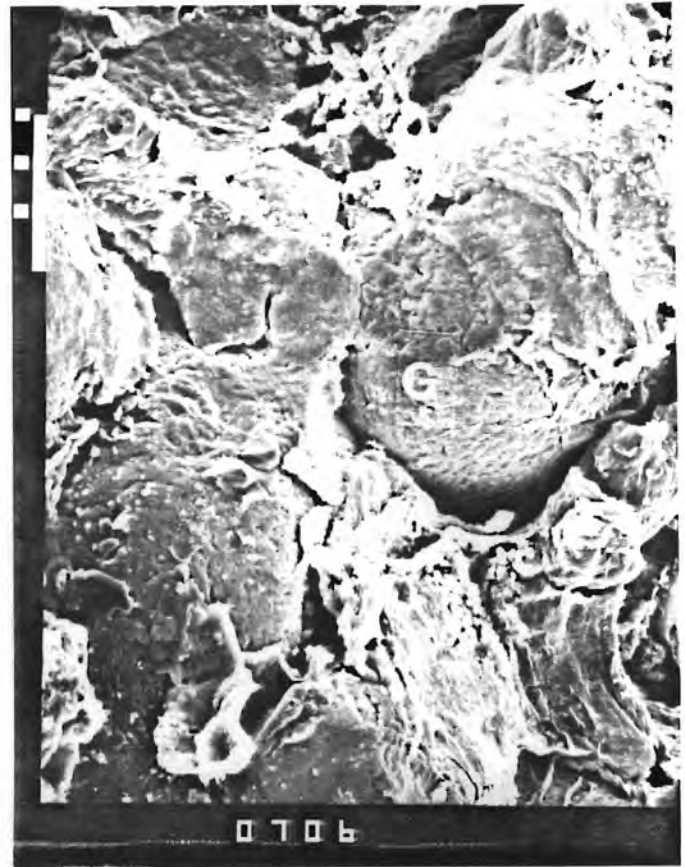
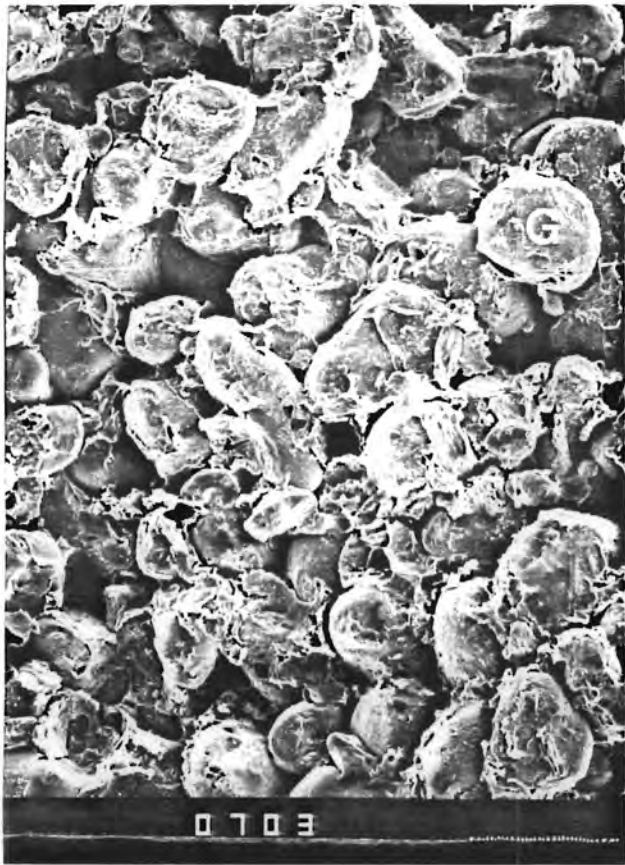


FIGURE IV-8

WELL: YAKLEY "D"

FORMATION: ST. PETER (GREEN)

DEPTH: 638.0 Feet

D391-043

<u>PHOTOGRAPH NO.</u>	<u>MAGNIFICATION</u>	<u>DESCRIPTION</u>
0819	30x	Grains (G) are completely surrounded by detrital clay matrix (M).
0820	300x	These higher magnification views illustrate the distribution and composition of matrix (M) at this depth. The matrix is composed, dominantly of illite. Some authigenic feldspar (F) and marcasite (MA) occurs. Authigenic illite (I) has nucleated on feldspar grains.
0821	700x	
0822	1500x	

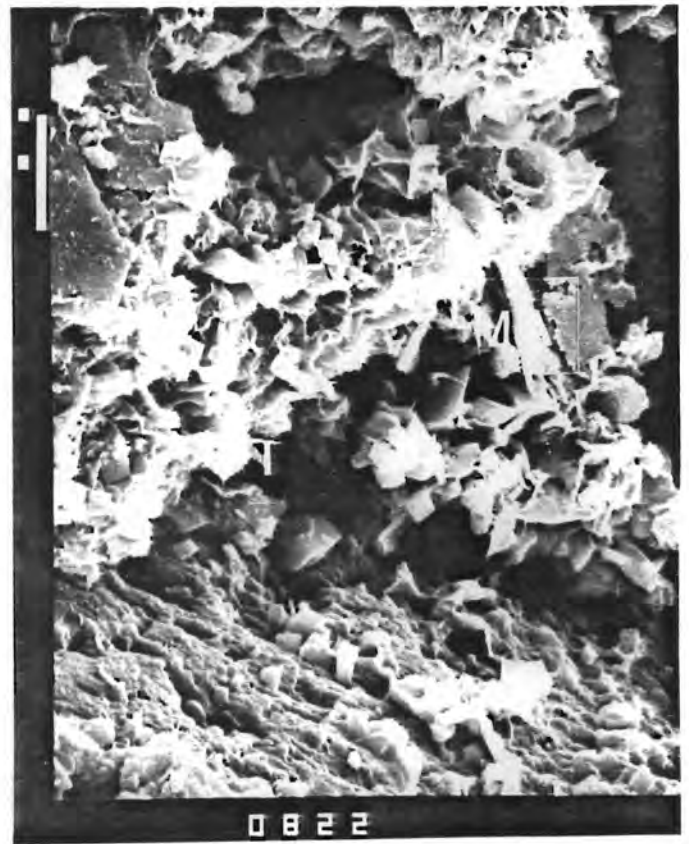
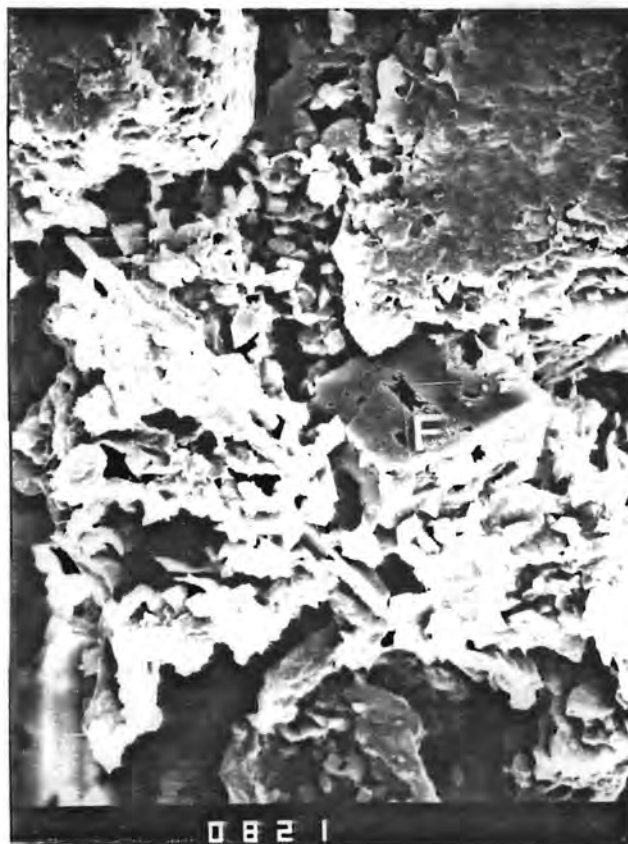
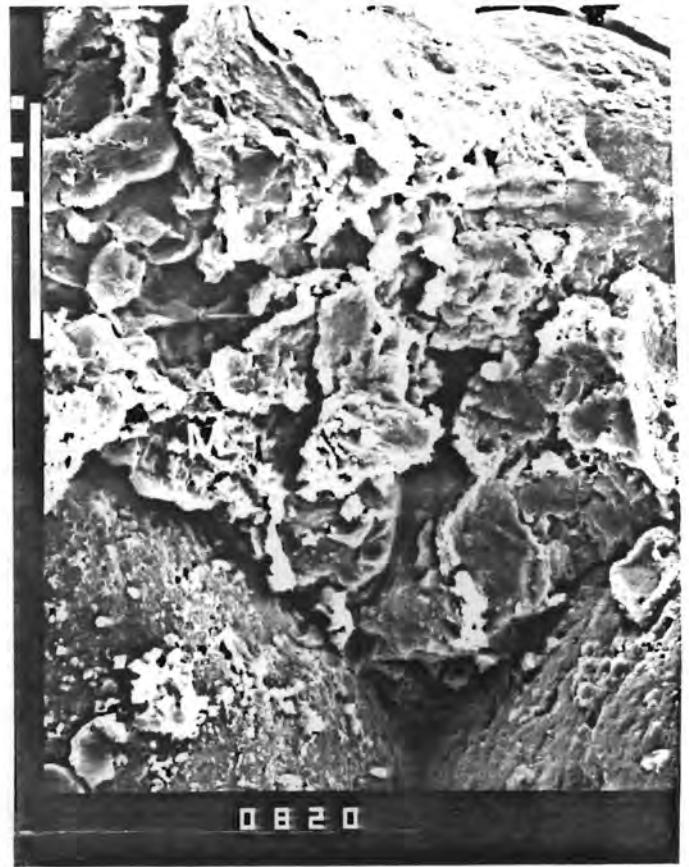
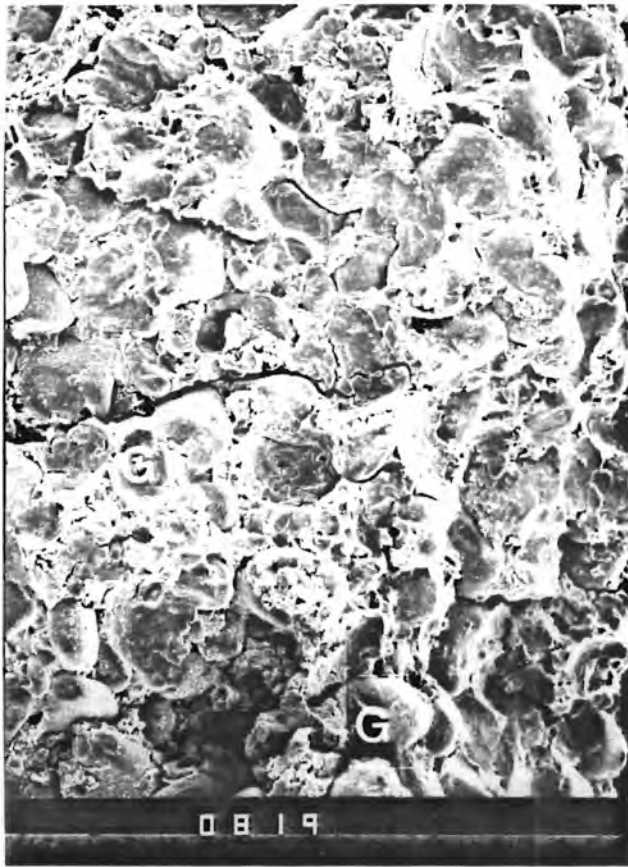


FIGURE IV-9

WELL: YAKLEY "D"

FORMATION: ST. PETER (GREEN)

DEPTH: 638.0 Feet

D391-043a

<u>PHOTOGRAPH NO.</u>	<u>MAGNIFICATION</u>	<u>DESCRIPTION</u>
0790	30x	After heating for 24 hours at 390°F, the matrix (M) has been lifted from grains (G).
0793	700x	These higher magnification views illustrate the effect of heating. The matrix (M) has been lifted from the surface of quartz grains (Q) and appears to have partially recrystallized. Quartz (Q) and authigenic feldspar (F) have been unaffected by heating.
0792	700x	
0791	1500x	

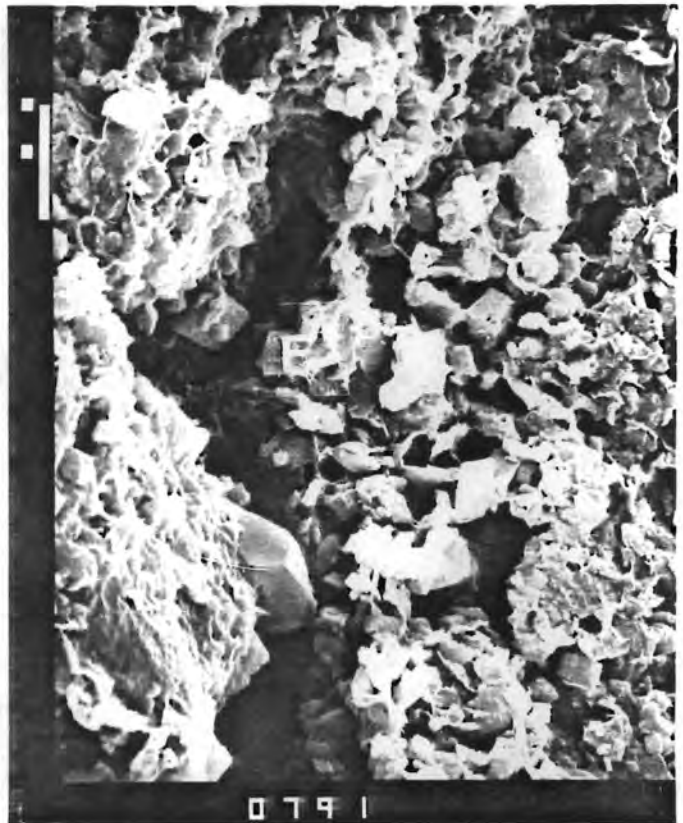
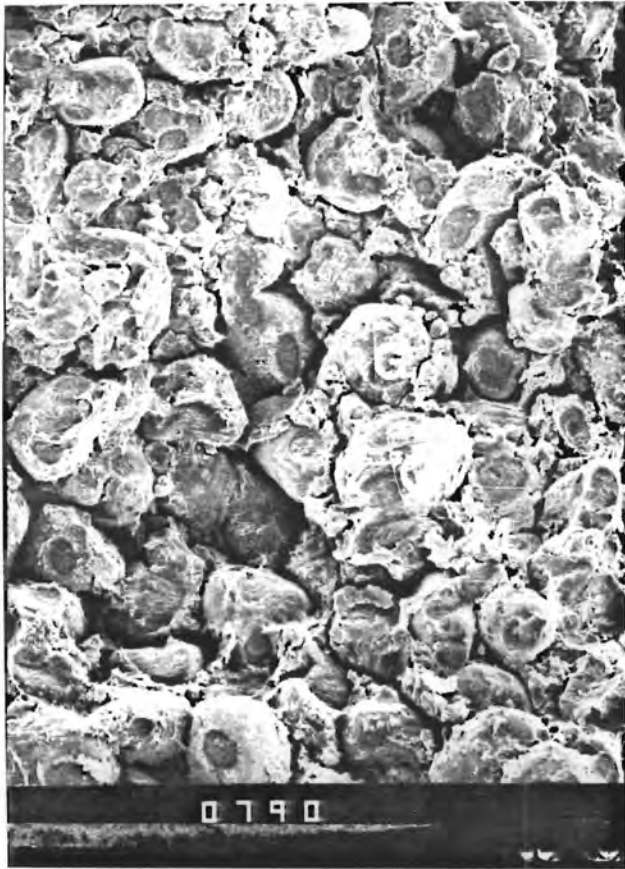


FIGURE IV-10

WELL: YAKLEY "C"

FORMATION: ST. PETER (GREEN)

DEPTH: 645 Feet

D391-035a

<u>PHOTOGRAPH NO.</u>	<u>MAGNIFICATION</u>	<u>DESCRIPTION</u>
0806	30x	After 24 hours of heating of 390 ^o F, the matrix (M) in this sample has assumed a "lattice work" appearance. Grains (G) are dominantly quartz.
0807	300x	Silica overgrowths (S) on quartz grains (Q) have been unaffected by heating.
0808	700x	Minor silica overgrowths (S) occur on a quartz grain (Q). The matrix is composed primarily of illite but some authigenic feldspar (F) also occurs. The matrix exhibits a "lattice work" appearance.
0809	3000x	Authigenic illite (I) has nucleated on authigenic feldspar (F) and is unaffected by heating.

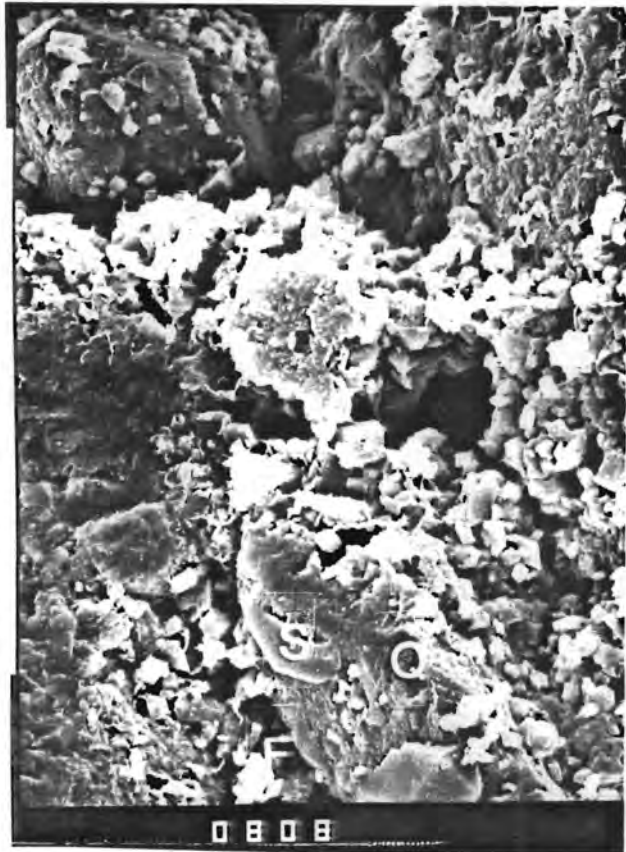
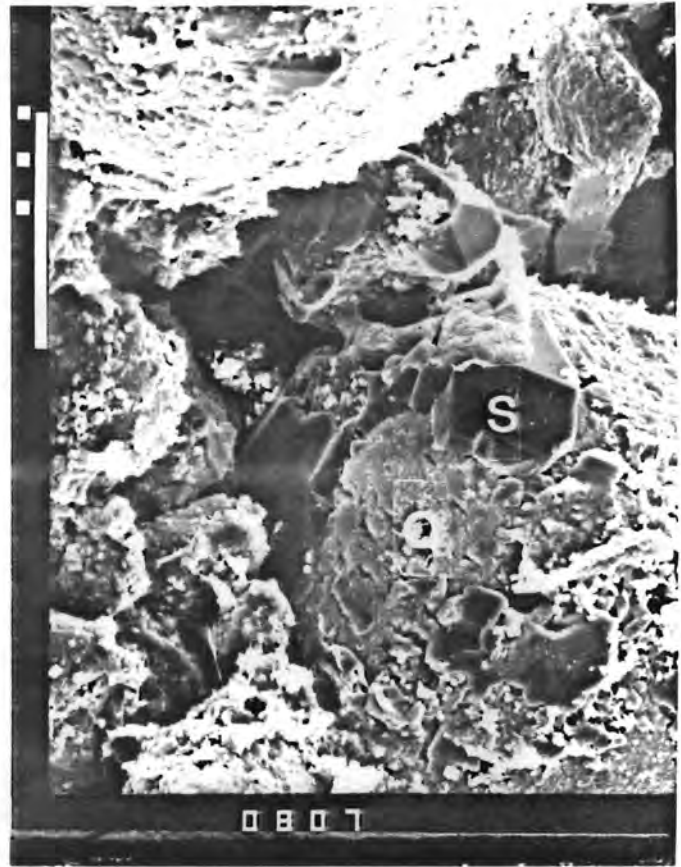
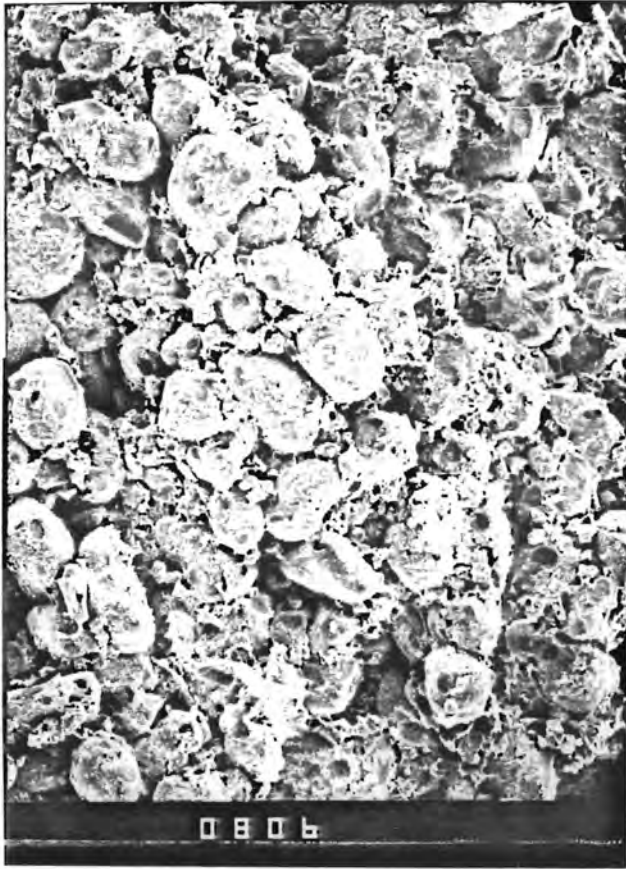


FIGURE IV-11

WELL: YAKLEY "C"

FORMATION: ST. PETER (GREEN)

DEPTH: 645 Feet

D391-035b

<u>PHOTOGRAPH NO.</u>	<u>MAGNIFICATION</u>	<u>DESCRIPTION</u>
0732	30x	The matrix (M) has been further disrupted by additional heating at 390°F and has been lifted from detrital grains (G).
0734	450x	These higher magnification photos illustrate the sparse presence of silica overgrowths (S) and the relationship of matrix (M) to quartz grains (Q).
0733	450x	
0735	700x	



FIGURE IV-12

WELL: YAKLEY "IW"

FORMATION: ST. PETER (GREEN)

DEPTH: 653.0 Feet

D391-061

<u>PHOTOGRAPH NO.</u>	<u>MAGNIFICATION</u>	<u>DESCRIPTION</u>
0728	20x	The green St. Peter Sandstone typically exhibits a bimodal grain size distribution. Large grains (G) are surrounded by matrix (M) which contains very much smaller quartz grains.
0729	450x	Higher magnification views illustrate common pore fill minerals. Marcasite (MA), silica overgrowths (S) on quartz grains, microquartz crystals (Q), authigenic feldspar (F), and illite (I) are very common at this depth.
0731	700x	
0730	2000x	

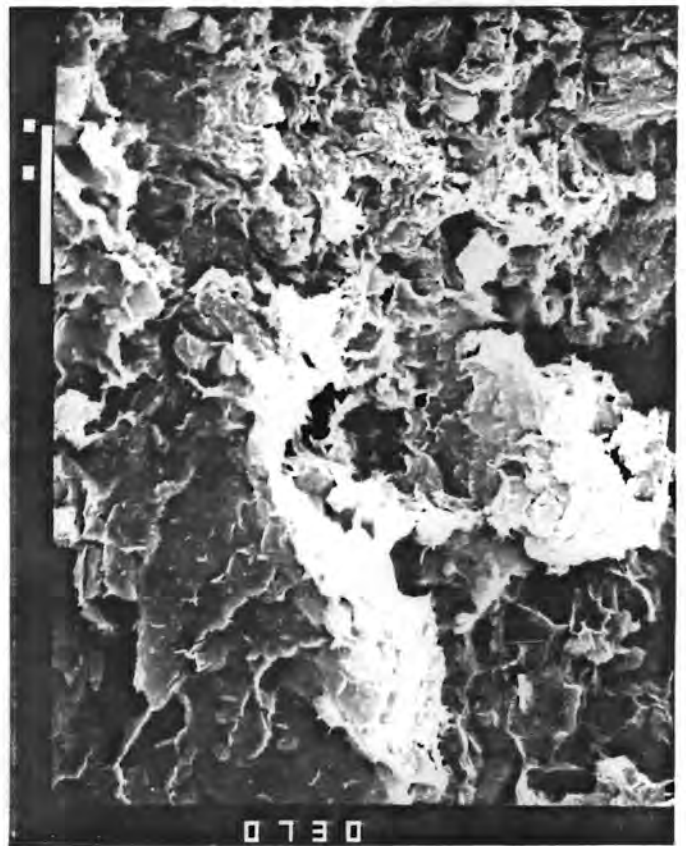
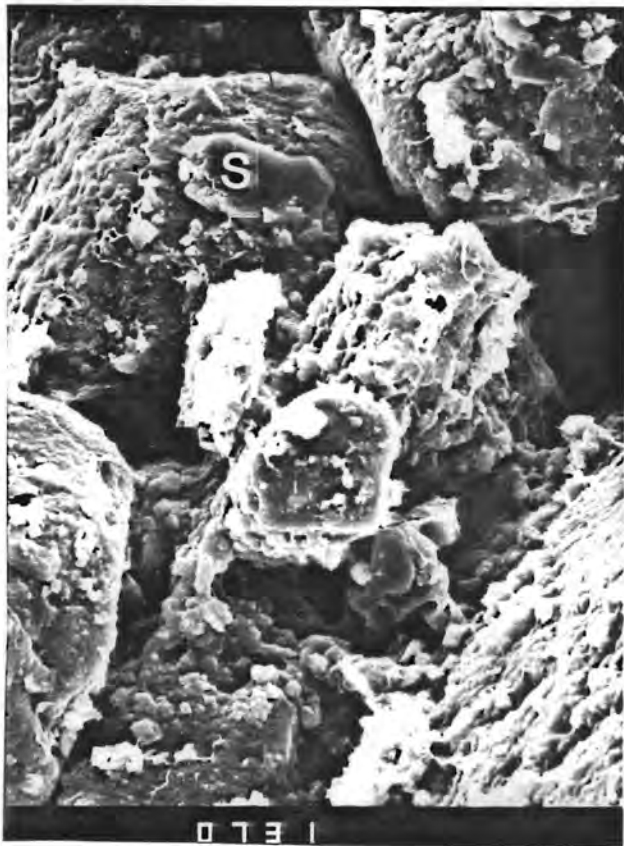


FIGURE IV-13

WELL: YAKLEY "IW"

FORMATION: ST. PETER (GREEN)

DEPTH: 653.0 Feet

D391-061a

<u>PHOTOGRAPH NO.</u>	<u>MAGNIFICATION</u>	<u>DESCRIPTION</u>
0794	20x	The bimodal grain size distribution is evident in this sample heated at 390°F for 24 hours. The matrix (M) is seen to be composed of small grains which surround large grains (G).
0795	450x	Abundant silica overgrowths (S) occur on quartz grains (Q). some marcasite (MA) and authigenic feldspar (F) occur in the pore system.
0796	700x	
0797	3000x	

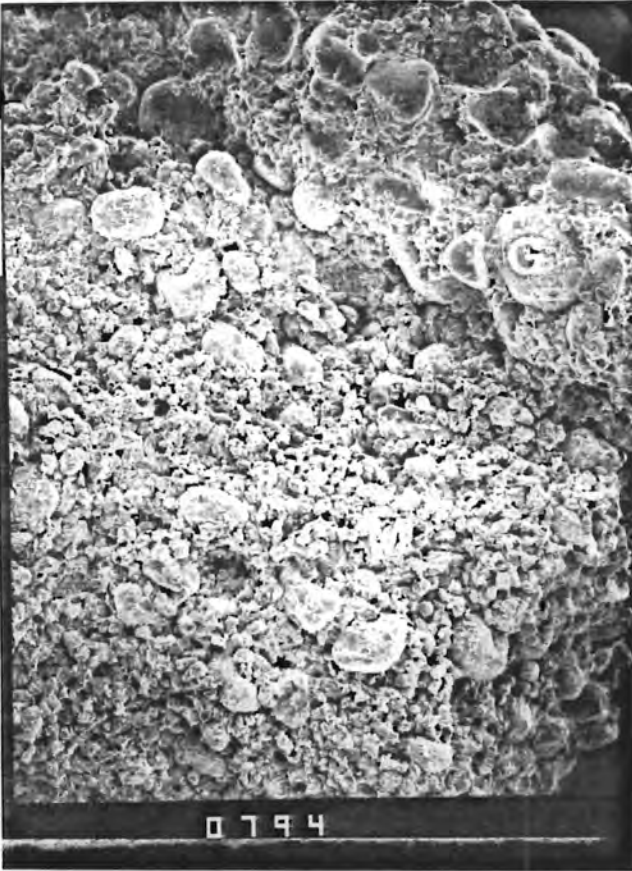


FIGURE IV-14

WELL: YAKLEY "C"

FORMATION: ST. PETER (WHITE)

DEPTH: 652.0 Feet

D391-038

<u>PHOTOGRAPH NO.</u>	<u>MAGNIFICATION</u>	<u>DESCRIPTION</u>
0802	45x	Quartz grains (G) are surrounded by a "fuzz" of authigenic clay and are loosely cemented by silica overgrowths.
0803	450x	This higher magnification view demonstrates that illite (I) is the dominant authigenic clay on quartz grains (Q), and authigenic feldspar (F) has precipitated on quartz surfaces. Framboidal pyrite (P) occurs in the pore system.
0804	700x	Abundant authigenic feldspar (F) is illustrated in this higher magnification view.
0805	2000x	Authigenic feldspar (F), illite (I), and marcasite (MA) have precipitated on this pitted quartz grain (Q).

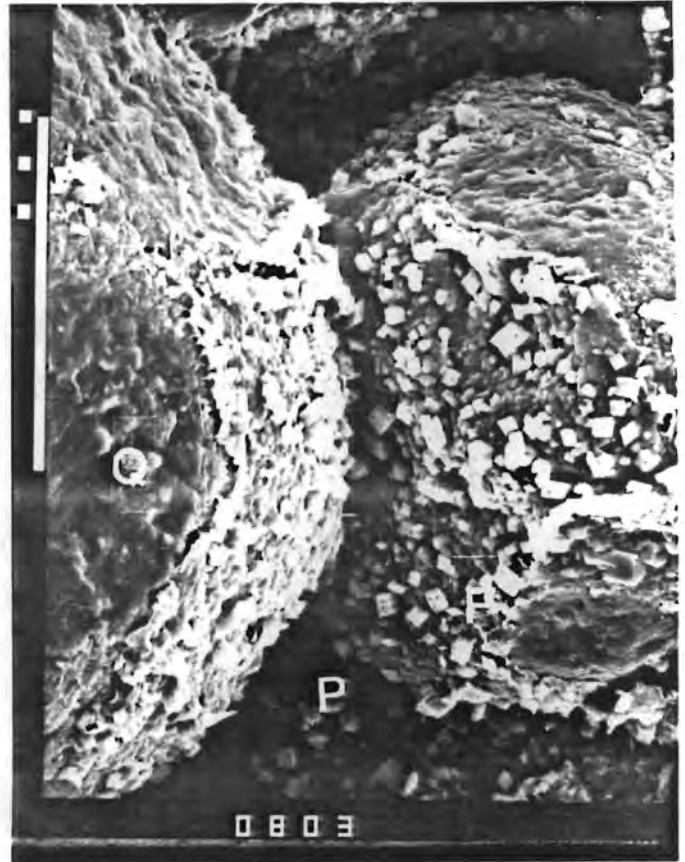
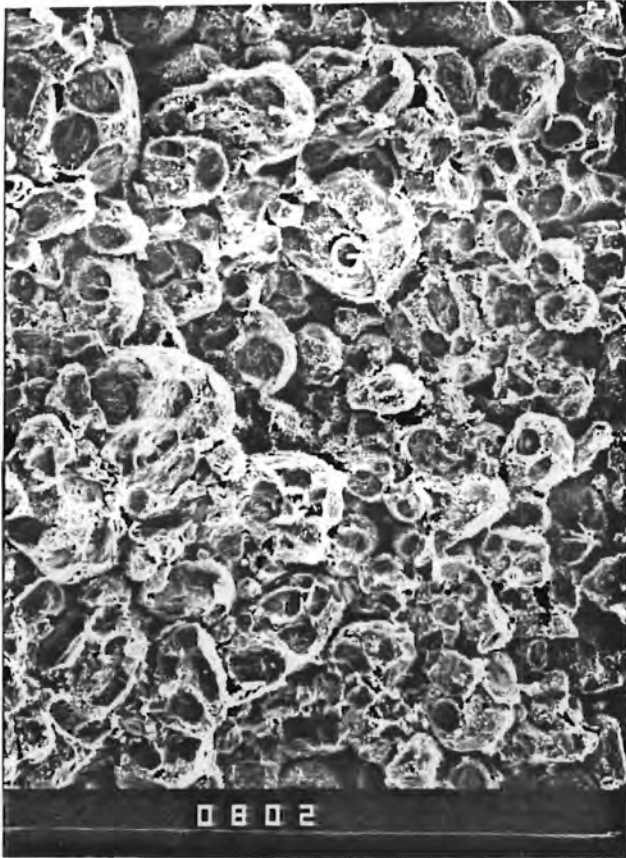


FIGURE IV-15

WELL" YAKLEY "C"

FORMATION: ST. PETER (WHITE)

DEPTH: 652.0 Feet

D391-038a

<u>PHOTOGRAPH NO.</u>	<u>MAGNIFICATION</u>	<u>DESCRIPTION</u>
0707	30x	Heating of the sample for 24 hours at 390 ^o F appears to have reduced porosity between grains (G). Clay fuzz is not as evident as in the unheated sample.
0709	450x	Some scaling of matrix has occurred. Illite (I) and feldspar (F) appear to be unaffected by heating. Other pore fill minerals include silica overgrowths (S), framboidal pyrite (P) and marcasite (MA).
0710	1500x	
0708	2000x	

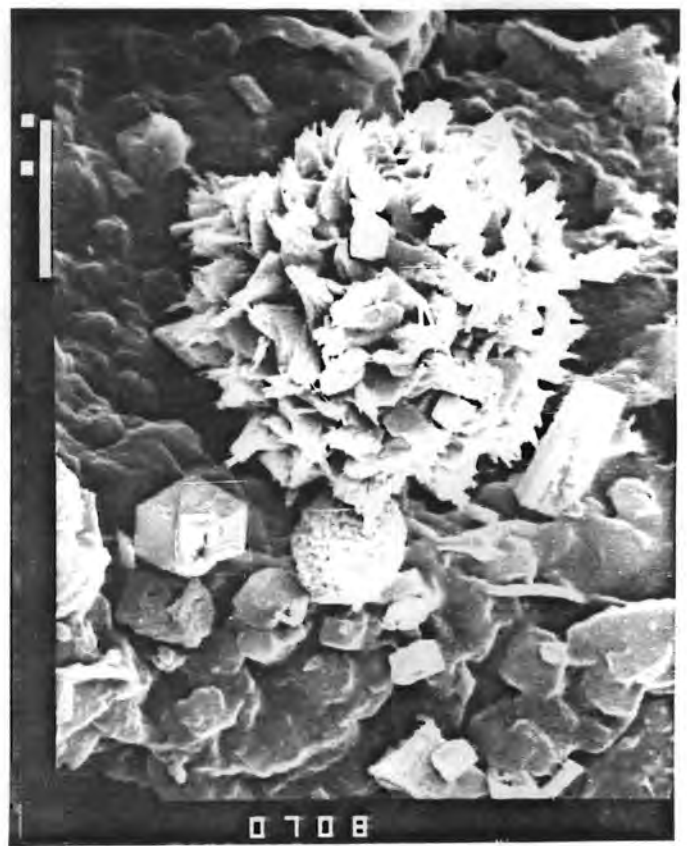
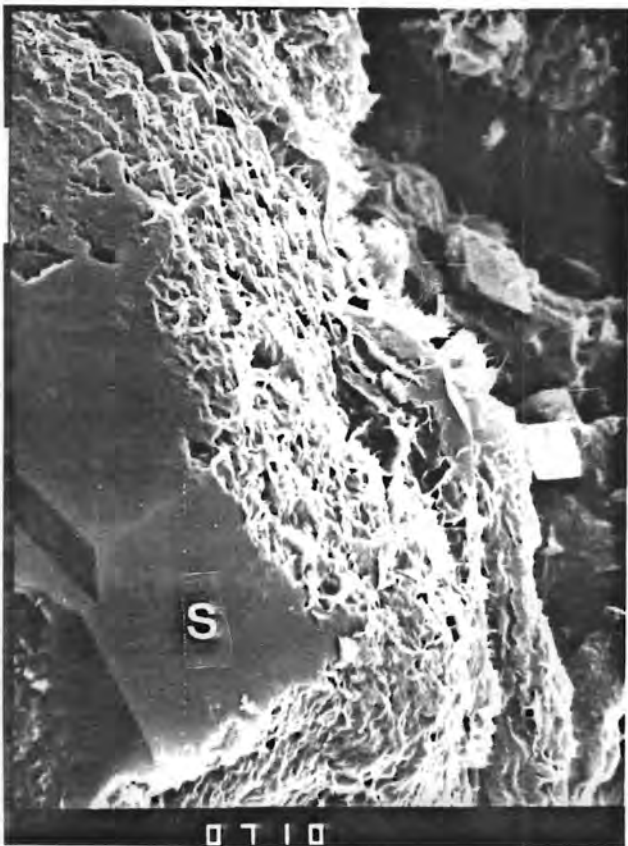


FIGURE IV-16

WELL: YAKLEY "C"

FORMATION: ST. PETER (WHITE)

DEPTH: 652.0 Feet

D391-038b

<u>PHOTOGRAPH NO.</u>	<u>MAGNIFICATION</u>	<u>DESCRIPTION</u>
0711	30x	After 48 hours of heating at 390°F more intergranular porosity appears to have been generated. Dominant grains (G) are quartz.
0713	450x	Closer examination of the pore system demonstrates that authigenic feldspar (F) is abundant. Framboidal pyrite (P) occurs occasionally. In instances where matrix (M) is present, it has spalled from the surface of quartz grains (Q), and the illite component (I) appears to be re-oriented.
0714	700x	
0712	1000x	

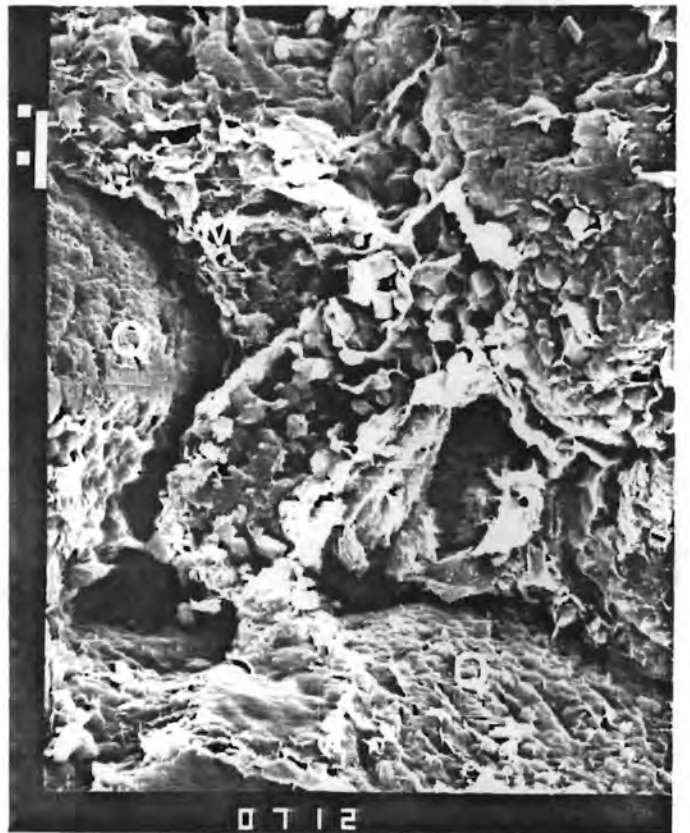
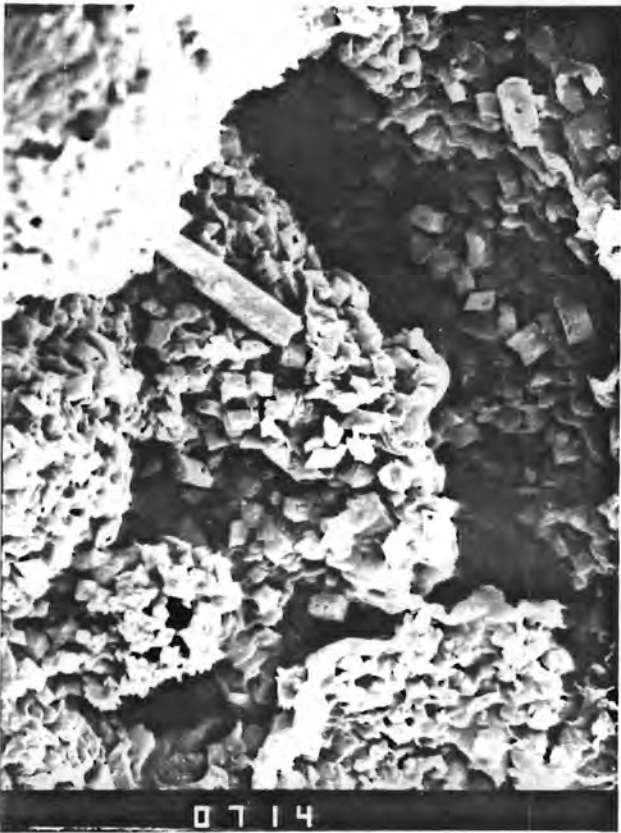
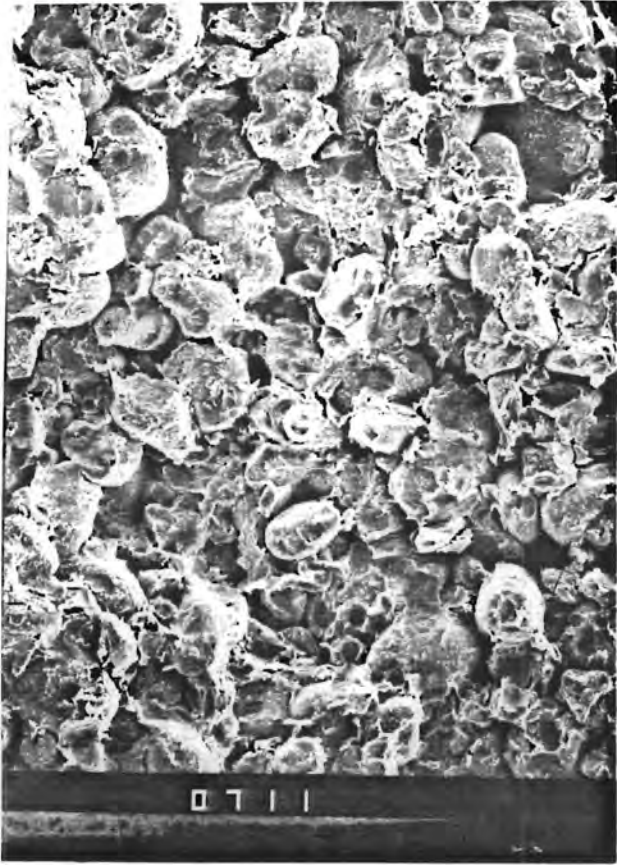


FIGURE IV-17

WELL: YAKLEY "C"

FORMATION: ST. PETER (WHITE)

DEPTH: 654.4 Feet

D391-039

<u>PHOTOGRAPH NO.</u>	<u>MAGNIFICATION</u>	<u>DESCRIPTION</u>
0715	30x	Good open porosity exists in this silica cemented sandstone. Grains (G) are partially coated with clay.
0716	150x	These higher magnification views show dominant pore fill minerals. Silica overgrowths (S) are common. Authigenic feldspar (F) frequently occludes porosity, and, occasionally, illite (I) has nucleated on feldspar grains.
0717	700x	
0718	2000x	

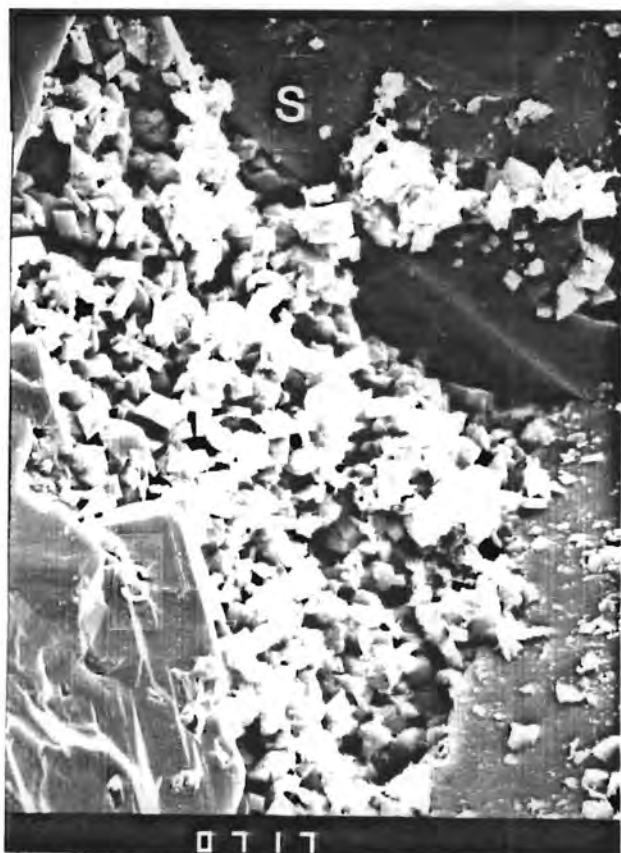
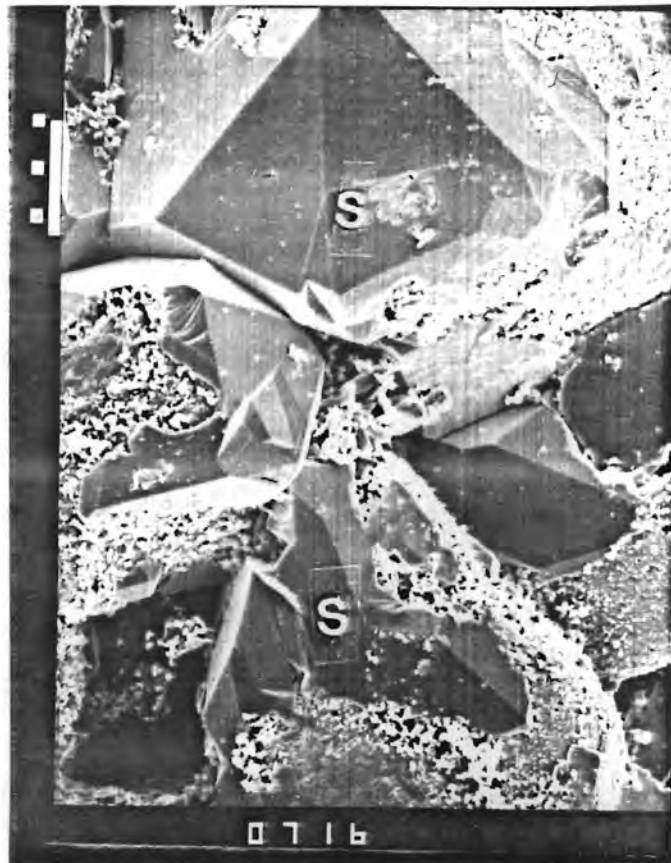
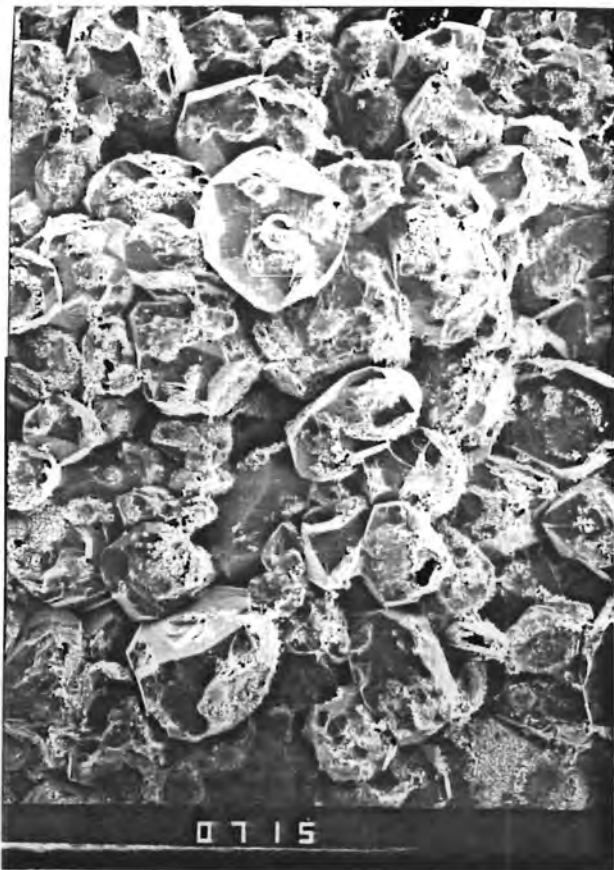


FIGURE IV-18

WELL: YAKLEY "C"

FORMATION: ST. PETER (WHITE)

DEPTH: 654.4 Feet

D391-039a

<u>PHOTOGRAPH NO.</u>	<u>MAGNIFICATION</u>	<u>DESCRIPTION</u>
0719	30x	After heating for 24 hours at 390°F, pore spaces (P) appear to be cleaner than in the unheated sample.
0720	450x	Framboidal pyrite (P) occurs sporadically in the pore system. Some pores are totally occluded by silica overgrowths (S), micro-quartz crystals (Q) and authigenic feldspar (F). Although illite (I) still coats some feldspar grains, its morphology is different. (Compare SEM 0722 with 0718).
0721	1500x	
0722	2000x	

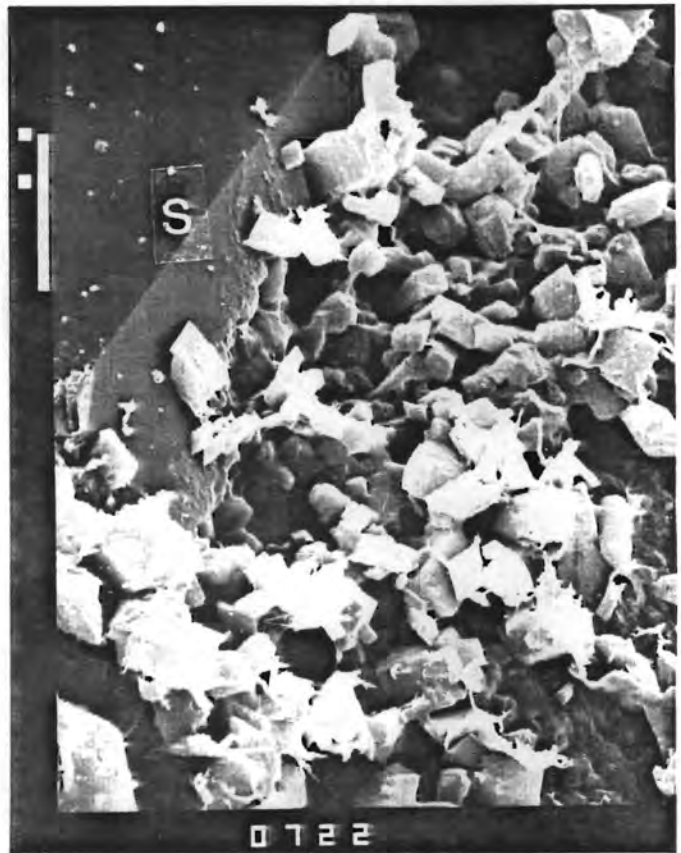
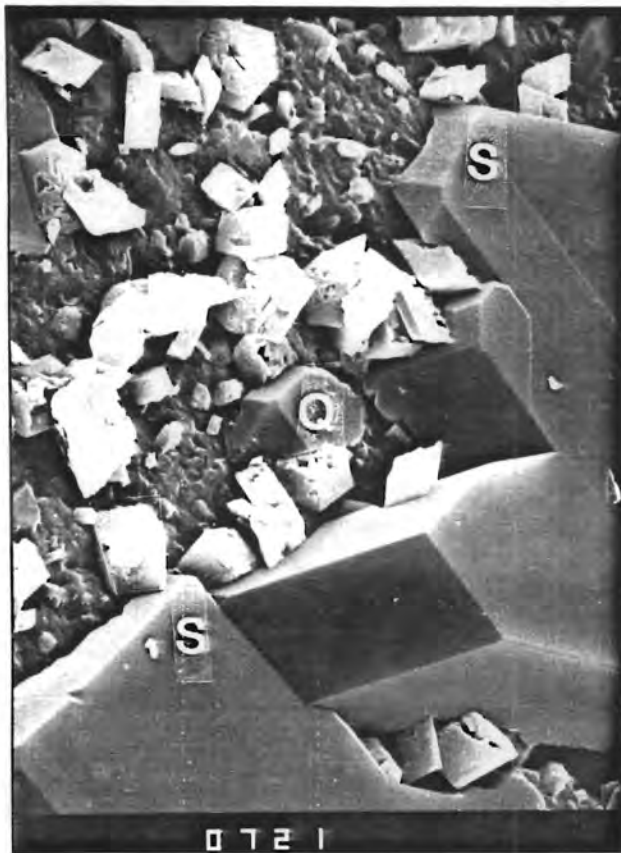
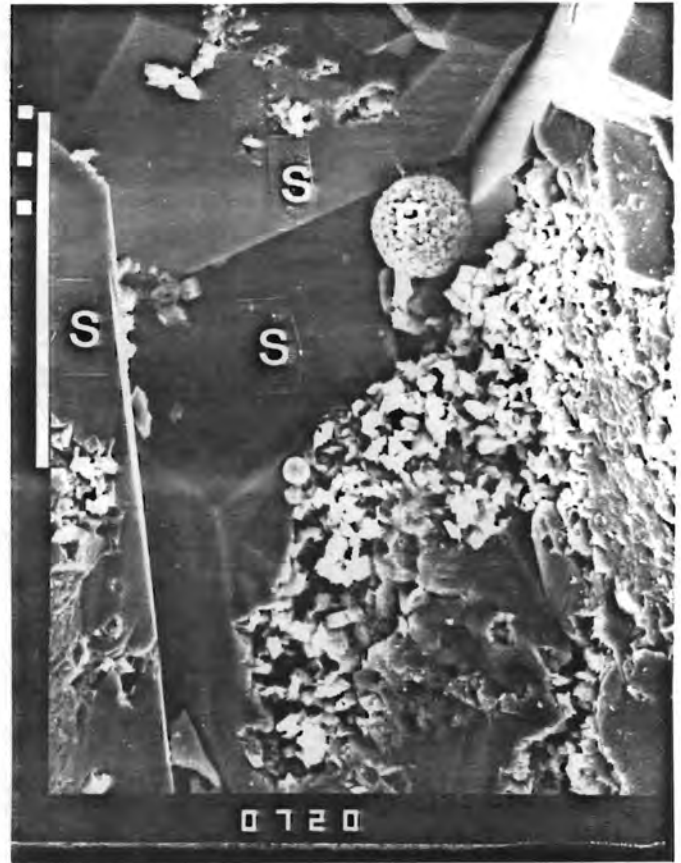


FIGURE IV-19

WELL: YAKLEY "C"

FORMATION: ST. PETER (WHITE)

DEPTH: 654.4 Feet

D391-039b

<u>PHOTOGRAPH NO.</u>	<u>MAGNIFICATION</u>	<u>DESCRIPTION</u>
0723	30x	Heating for 48 hours at 390°F appears to have decreased intergranular porosity.
0727	150x	Silica overgrowths (S) on quartz grains (Q) are fresh, but very finely crystalline material coats some grains. Closer inspection reveals that illite is absent and microfeldspar (F) crystals are abundant. The matrix (M) is composed of very finely crystalline feldspar.
0724	300x	
0725	450x	

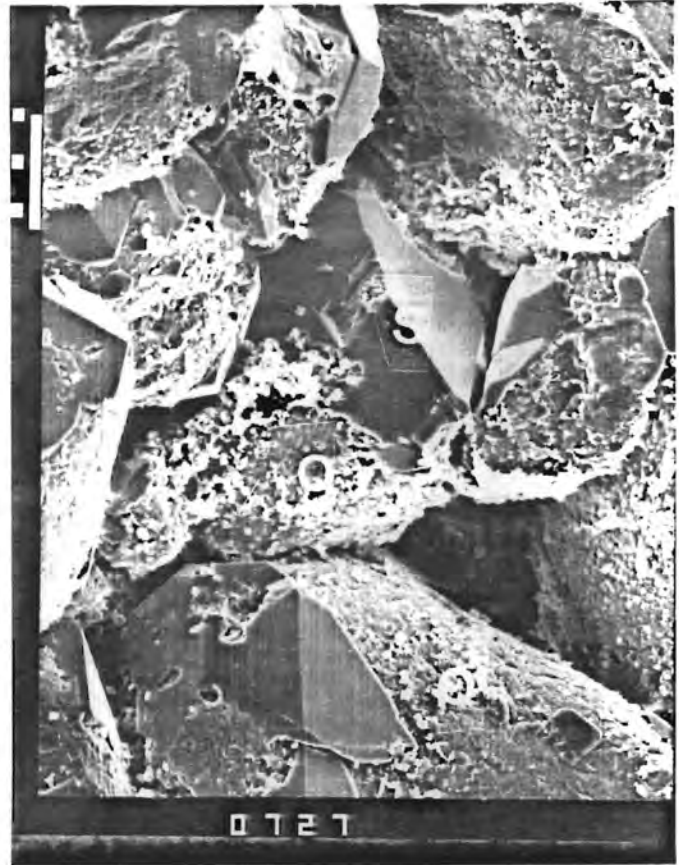
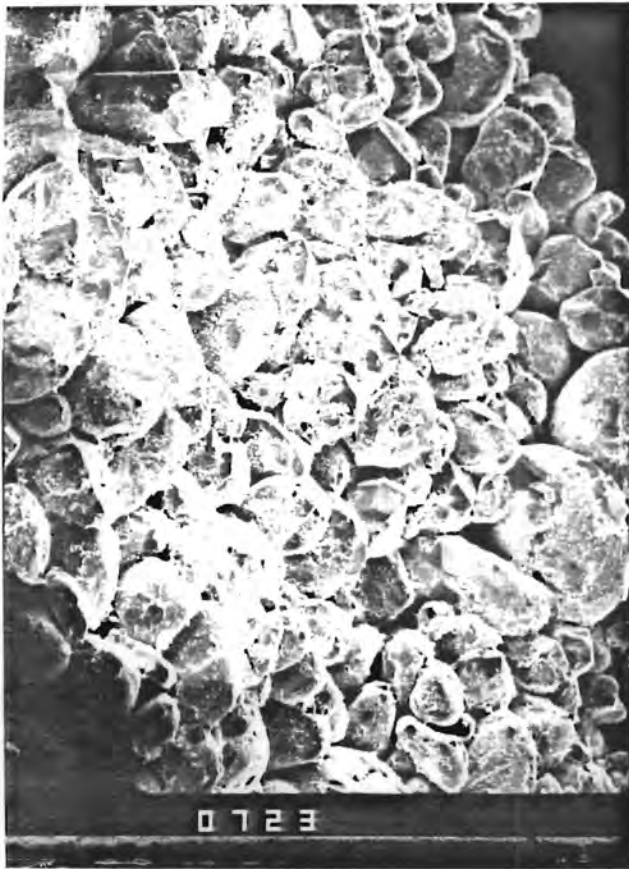


FIGURE IV-20

WELL: YAKLEY "D"

FORMATION: ST. PETER (GREEN)

DEPTH: 640.5 Feet

D391-046a

<u>PHOTOGRAPH NO.</u>	<u>MAGNIFICATION</u>	<u>DESCRIPTION</u>
0815	30x	These photographs illustrate the effect of heating the green St. Peter Sandstone at 390°F for 24 hours. The depositional matrix (M) has been lifted from grain surfaces (G). Framboidal pyrite (P), marcasite (MA) and authigenic feldspar (F) appear to be unaffected, although, in hand specimens, these minerals have partially rusted. The surface of this quartz grain (Q) has been cleaned of depositional matrix. Illite (I) appears to be unaffected.
0818	300x	
0817	1500x	
0816	1500x	

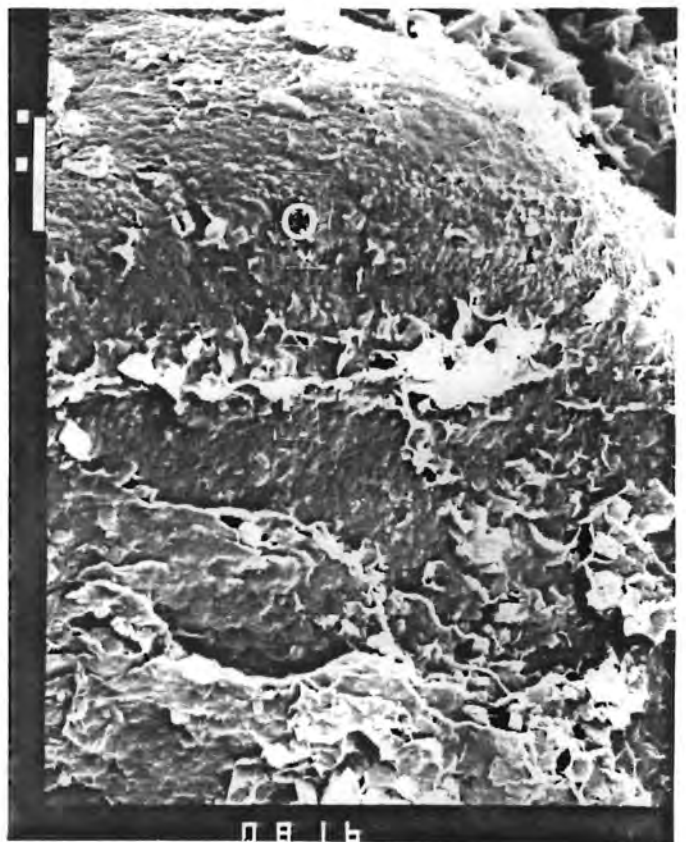
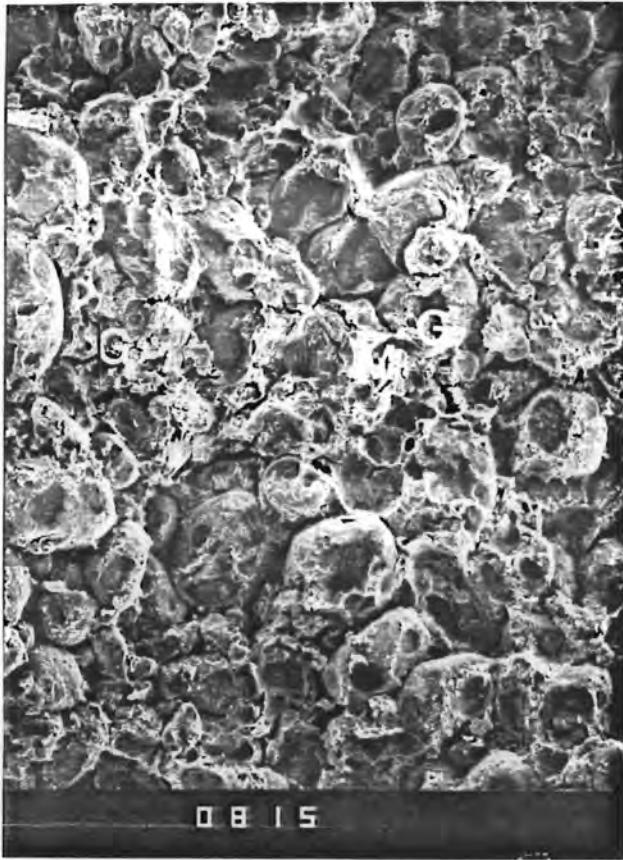


FIGURE IV-21

WELL: YAKLEY "IW"

FORMATION: ST. PETER SANDSTONE (GREEN)

DEPTH: 655.0 Feet

D391-065

<u>PHOTOGRAPH NO.</u>	<u>MAGNIFICATION</u>	<u>DESCRIPTION</u>
9193	30x	General view of a less porous sample. Clay (C) grain coating and silica overgrowths (S) on quartz grains (Q) are common.
9195	100x	Higher magnification views illustrating common pore fill minerals at this depth. Calcite (C), silica overgrowths (S) and illite (I) tightly cement quartz grains (Q).
9196	1000x	



FIGURE IV-22

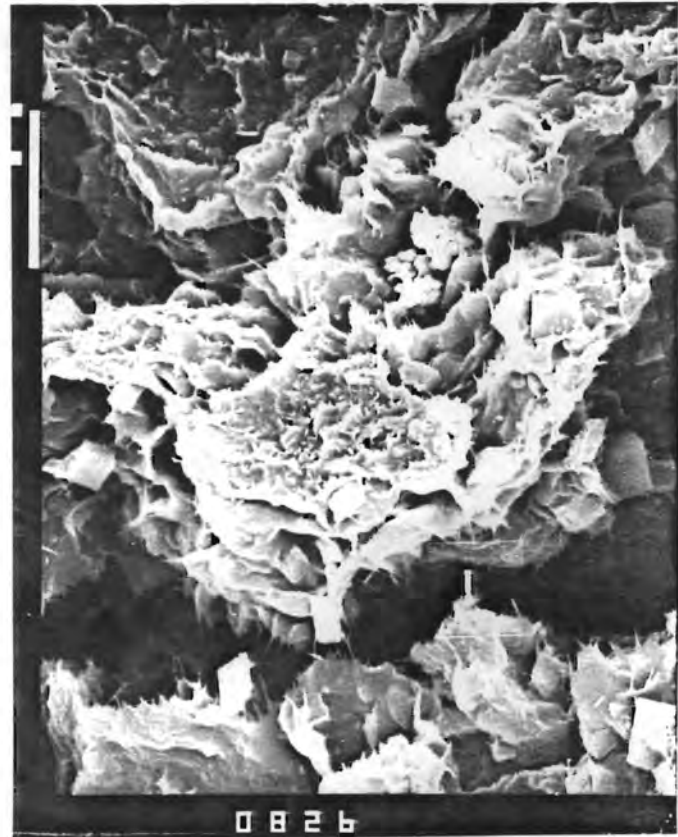
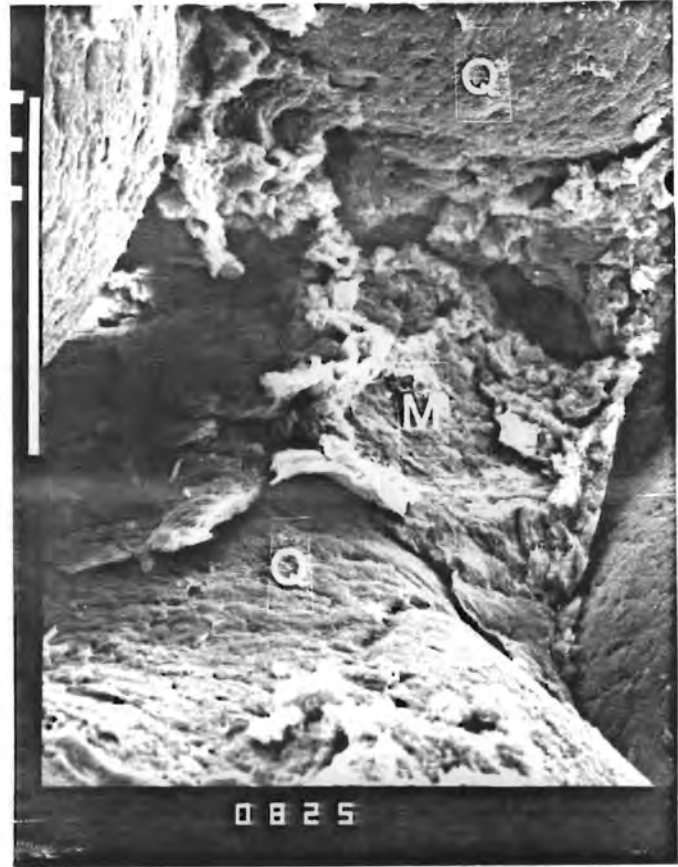
WELL: YAKLEY "IW"

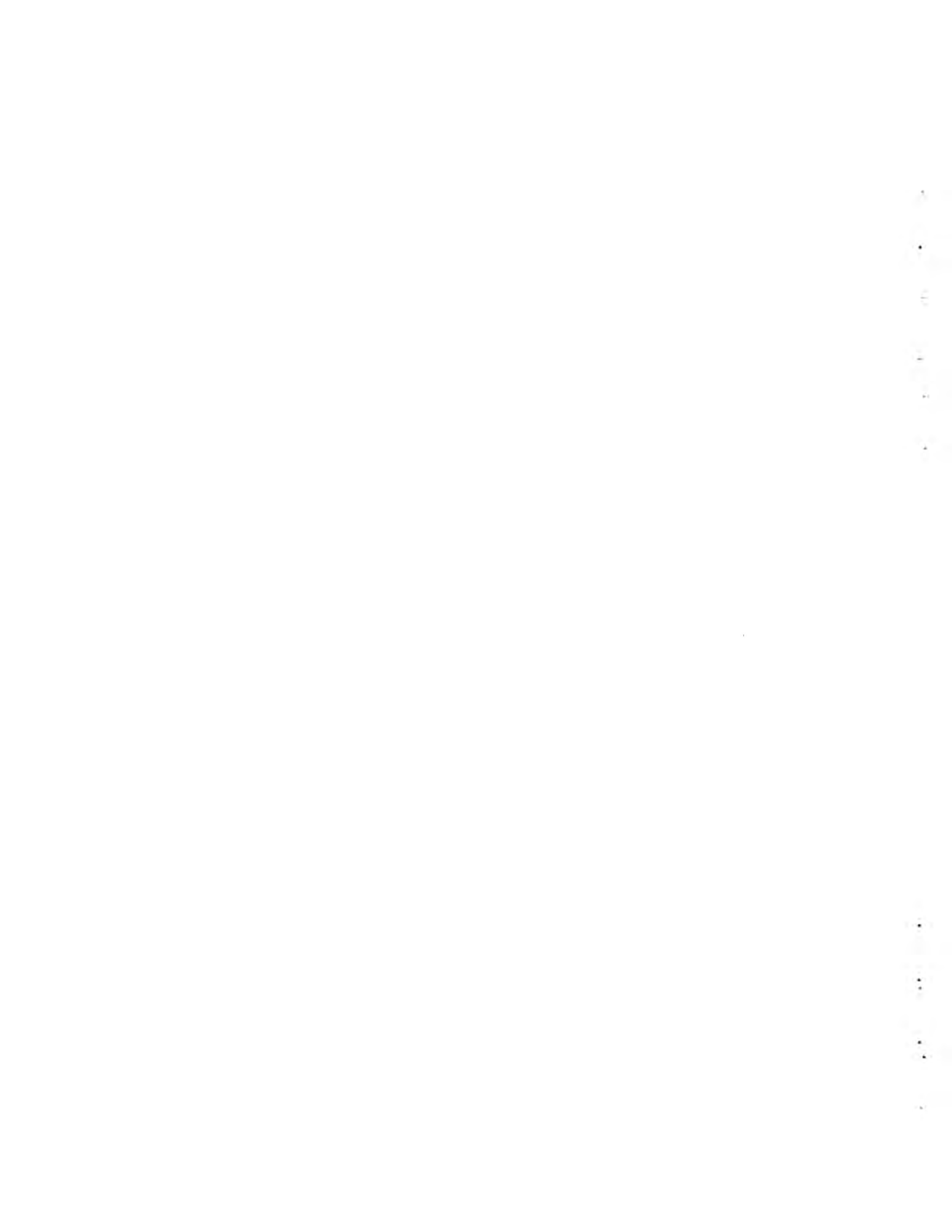
FORMATION: ST. PETER SANDSTONE (GREEN)

DEPTH: 655.0 Feet

D391-065H

<u>PHOTOGRAPH NO.</u>	<u>MAGNIFICATION</u>	<u>DESCRIPTION</u>
0823	30x	These four views illustrate the effects of heating the green St. Peter to 350°F at 1000 p.s.i. Grains (G) appear to be frosted. Depositional matrix (M) has been lifted from quartz grains (Q). Silica overgrowths (S) are unaffected. Fibrous illite (I) also appears to be unaffected.
0825	450x	
0827	450x	
0826	2000x	





SECTION V

GEOCHEMICAL EVALUATION

General -

The geochemical evaluation is divided into two parts. Water quality is discussed first. Included in this discussion are those mineralogic phases which may precipitate from formation fluids. The second part of this section includes a discussion of potential geochemical reactions which may occur as a result of air injection and cycling.

Theoretical Considerations -

Water analyses, expressed in mg/l for each component, are of value in the assessment of the potability of water from a given aquifer. Little information is gained concerning the precipitation of mineral phases relative to which the water may be saturated. These mineral phases may be identified by either hand-calculation using the analytical data or by feeding the analytical data into one of several computer programs, written specifically for this purpose. Because hand-calculation is tedious and time-consuming, the data were analyzed using the WATEQF computer program. Steps involved in the calculation are as follows:

1. Convert mg/l to molality

The concentration unit, molality, is defined as the number of moles of solute per liter (kilogram) of solvent. The number of moles of each component is determined by dividing the analytical concentration by the atomic weight, expressed in milligrams (mg).

As an example, assume a solution contains 232 mg/l of calcium (Ca^{2+}). The number of moles of calcium is:

$$\text{moles} = \frac{\text{mg/l}}{\text{atomic weight, mg}} = \frac{232 \text{ mg/l}}{40080 \text{ mg}}$$
$$\text{moles} = \underline{5.79 \times 10^{-3}}$$

This value is then divided by the density of the solution to obtain the total concentration (molality) of the species.

2. Compute the ionic strength of the solution from the molalities.

After the molalities have been computed for each aqueous species, the ionic strength of the solution is calculated.

$$I = 1/2 \sum m_i z_i^2$$

Where:

I = ionic strength
 m_i = molality of species
 z_i = oxidation state of species

Clearly, neutral aqueous species do not affect the ionic strength. Consider, as an example, the following analysis:

<u>Species</u>	<u>m_i</u>	<u>z_i</u>
Ca	3.2×10^{-4}	+2
Na	1.3×10^{-1}	+1
Cl ⁻	1.31×10^{-1}	-1
H ₄ SiO ₄	1.4×10^{-4}	0

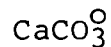
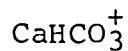
$$I = 1/2 \sum m_i z_i^2$$

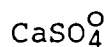
$$= 1/2 [(3.2 \times 10^{-4} (2)^2 + 1.3 \times 10^{-1} (1)^2 + 1.31 \times 10^{-1} (1)^2 + 1.4 \times 10^{-4} (0)^2]$$

$$I = 1.311 \times 10^{-1}$$

3. Determine the distribution of species and compute individual concentrations

In solutions of very low ionic strength (very dilute solutions), computations involving the formation of complex ions and species are not necessary. In natural water systems, however, the ionic strength is generally greater than 1×10^{-3} , and the formation of complex species must be considered. Suppose, for example, that the following species are present in an analyzed water: Ca²⁺, Mg²⁺, HCO₃⁻, CO₃²⁻, SO₄²⁻, Na⁺, H⁺, and OH⁻. Considering only the cation calcium, the following complex aqueous species may exist:





The total analytical molality of calcium will, therefore, be distributed among these species. In addition free calcium will remain in solution.

$$m_{\text{Ca}_T^{2+}} = m_{\text{Ca}^{2+}} + m_{\text{CaHCO}_3^+} + m_{\text{CaCO}_3^{\circ}} + m_{\text{CaSO}_4^{\circ}} + m_{\text{CaOH}^+}$$

Similar equations may be written for all complex species in solution, and individual concentrations may be calculated.

These calculations are carried out automatically by the WATEQF program.

4. Calculate the activity coefficient and activity

Activity coefficients (γ) of individual ionic species are calculated using the extended Debye-Huckel equation.

$$\log \gamma_i = \frac{-A \sqrt{I} z_i^2}{1 + B a^{\circ} \sqrt{I}}$$

Where:

γ_i = Activity coefficient of ion

z_i = Oxidation number of ion

a° = Distance of closest approach of ions

A, B = Constants, depend on the temperature of the solvent

at 15°C, A = 0.5000; B = 0.3262x10⁺⁸

After calculating γ_i for each species, the activity is calculated for each species.

$$a_i = \gamma_i m_i$$

Where a_i = Activity

5. Determine the ion activity product and degree of saturation for each potential mineral precipitate.

The ability to form precipitates from aqueous solution for aqueous species is evaluated. The degree of saturation is a measure of the tendency of precipitation of mineral phases. The degree of saturation (S) is determined by comparing the ion activity product (IAP) with the equilibrium constant (K) at a given temperature.

$$S = \frac{IAP}{K}$$

If

- S > 1, The solution is supersaturated with respect to the mineral phase.
- S = 1, The solution is saturated with respect to the mineral phase.
- S < 1, The solution is undersaturated with respect to the mineral phase.
- S > 1, Precipitation of the mineral phase is likely.
- S = 1, Precipitation of the mineral phase is possible.
- S < 1, Precipitation of the mineral phase is unlikely.

Consider calcite, CaCO_3 , as an example, and assume that the activity of the calcium ion is 4×10^{-3} and the activity of the carbonate ion is 1.4×10^{-5} .

$$\begin{aligned} IAP &= a_{\text{Ca}^{2+}} a_{\text{CO}_3^{2-}} \\ &= (4.3 \times 10^{-3}) (1.4 \times 10^{-5}) \end{aligned}$$

$$IAP = 6.02 \times 10^{-8}$$

$$\text{At } 15^\circ\text{C, } K_{\text{CaCO}_3} = 3.77 \times 10^{-9}$$

$$\begin{aligned} S &= \frac{IAP}{K} \\ &= \frac{6.02 \times 10^{-8}}{3.77 \times 10^{-9}} \end{aligned}$$

$$S = 15.97$$

Therefore, the hypothetical solution is supersaturated with respect to calcite, and the precipitation of calcite is likely.

Water Quality -

This discussion is based upon data presented in the Dames and Moore Report of March, 1981. Water samples from the St. Peter and Galena aquifers have not been analyzed from the Pittsfield site since this report was presented. Data utilized in the discussion are given in Tables V-1 and V-2. Only major aqueous species are considered in the evaluation.

Galena Formation Waters -

Galena formation water is slightly alkaline (pH=7.98) and is rich in calcium, magnesium, chloride, and bicarbonate (Table 1). The ionic strength of the water is 0.00817. WATEQF computer analysis of the raw data is presented in Tables 3 and 4.

Those mineral phases likely to precipitate from Galena waters include calcite, dolomite, pyrolusite, and manganese hydroxides.

St. Peter Formation Waters -

Water taken from the St. Peter Formation is slightly alkaline (pH=8.07) and is rich in calcium, magnesium, sodium, chloride, sulfate, and bicarbonate (Table 2). The ionic strength of the water is 0.061, and total dissolved solids equal 3345 mg/l. St. Peter formation water is therefore classified as brackish, and the analytical concentrations of species present generally exceed mandatory concentration limits of the U.S. Public Health Service for drinking purposes.

WATEQF computer analysis of the raw data is presented in Tables 5 and 6.

Mineral phases likely to precipitate from St. Peter waters include aragonite, barite, calcite, dolomite, iron hydroxides, fluorapatite, hematite, magnesite, magnetite, manganese hydroxides, pyrolusite, and quartz. Mineral phases which may precipitate from solution include celestite, chalcedony, gypsum, and hydroxyapatite.

Potential Effects of Air Injection on St. Peter Formation Water -

Air injection may affect the St. Peter Formation water in two ways:

- 1) Aqueous species may be oxidized
- 2) CO₂ may be liberated from the water, resulting in the precipitation of carbonates.

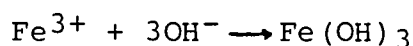
Each possibility is discussed briefly below.

1) The oxidation of species

Those species in the water which are subject to oxidation include:

Iron (II)
Manganese (II,III)

Iron (II) is readily oxidized to iron (III) in the presence of air. If the pH of the formation water is less than 2, Fe^{3+} presents no problem. However, if the pH of the solution rises above 2, the following reaction will occur:



Iron (III) hydroxide is a gelatinous, nearly colloidal, precipitate when first formed. It, potentially, will migrate at the interface between the air and water front. If enough Fe^{2+} is present in the solution, ferric (iron (III)) hydroxide may reduce permeability.

Manganese in either the 2+ or 3+ oxidation state will behave in a fashion similar to iron (II). Manganese (II) may be oxidized to manganese (III) and precipitate as $\text{Mn}(\text{OH})_3$, or Mn^{2+} may be oxidized to Mn^{4+} and precipitate as pyrolusite (MnO_2). Manganese (III), when oxidized to Mn^{4+} will form pyrolusite.

2) Carbonate precipitation through CO_2 evolution

Aqueous solutions containing the bicarbonate ion will evolve CO_2 upon contact with air, provided that the $p\text{CO}_2$ of the solution is greater than $10^{-3.5}$ (3.16×10^{-4}). St. Peter waters would be in equilibrium with an atmosphere of $p\text{CO}_2 = 10^{-2.83}$ (1.474×10^{-3}). Carbon dioxide gas, therefore, will be evolved from St. Peter Formation water until the water is at equilibrium with injected air. Concomitant with CO_2 evolution is an increase in the pH of the water. As the pH increases, the tendency for carbonate (aragonite, calcite, dolomite, etc.) precipitation also increases, because the water will shift to the carbonate ion stability field.

The precipitation of carbonate phases in the pore system will reduce permeability.

TABLE V-1

WATER ANALYSIS, GALENA FORMATION

Temperature = 15°C

pH = 7.98

<u>SPECIES</u>	<u>mg/l, analyzed</u>	<u>molality, analyzed (TOTAL)</u>
Ca ²⁺	60.2	1.488 x 10 ⁻³
Mg ²⁺	27.6	1.124 x 10 ⁻³
Cl ⁻	142.0	3.967 x 10 ⁻³
SO ₄ ²⁻	1.658	1.710 x 10 ⁻⁵
HCO ₃ ⁻	126.648	2.056 x 10 ⁻³
NH ₄ ⁺	0.55	3.02 x 10 ⁻⁵
Boron (Total)	1.72	1.576 x 10 ⁻⁴
Ba ²⁺	0.07	5.048 x 10 ⁻⁷
Mn ⁴⁺	0.073	1.316 x 10 ⁻⁶

TABLE V-2

WATER ANALYSIS, ST. PETER

Temperature = 15°C

pH = 8.07

SPECIES	mg/l (analyzed)	molality (calculated from analysis)
Ca ²⁺	138	3.42 x 10 ⁻³
Mg ²⁺	63	2.57 x 10 ⁻³
Na ⁺	853	3.69 x 10 ⁻²
K ⁺	37.9	9.63 x 10 ⁻⁴
Cl ⁻	1260	3.53 x 10 ⁻²
SO ₄ ²⁻	731	7.56 x 10 ⁻³
HCO ₃ ⁻	242	3.94 x 10 ⁻³
H ₄ SiO ₄ ^o	785	1.3 x 10 ⁻⁴
Fe ²⁺	9 x 10 ⁻³	1.6 x 10 ⁻⁷
PO ₄ ³⁻	6 x 10 ⁻²	6.28 x 10 ⁻⁷
Sr ²⁺	4.06	4.6 x 10 ⁻⁵
F ⁻	2.01	1.05 x 10 ⁻⁴
NH ₄ ⁺	2.58	1.42 x 10 ⁻⁴
Li ⁺	0.586	8.39 x 10 ⁻⁵
NO ₃ ⁻	0.11	1.76 x 10 ⁻⁶
H ₃ BO ₃ ^o	2.54	2.33 x 10 ⁻⁴
Ba ²⁺	0.03	2.17 x 10 ⁻⁷
Mn ²⁺	0.085	1.54 x 10 ⁻⁶

TABLE V-3

DISTRIBUTION OF AQUEOUS SPECIES AND ACTIVITIES, GALENA WATER

SPECIES	PPM ¹	m, calc ²	γ^3	a ⁴
Ca ²⁺	58.6	1.46x10 ⁻³	6.97x10 ⁻¹	1.02x10 ⁻³
Mg ²⁺	26.8	1.1x10 ⁻³	7.00x10 ⁻¹	7.72x10 ⁻⁴
H ⁺	1.16x10 ⁻⁵	1.15x10 ⁻⁸	9.11x10 ⁻¹	1.05x10 ⁻⁸
Cl ⁻	141	3.97x10 ⁻³	9.10x10 ⁻¹	3.61x10 ⁻³
SO ₄ ²⁻	1.365	1.42x10 ⁻⁵	6.94x10 ⁻¹	9.86x10 ⁻⁶
HCO ₃ ⁻	120.4	1.97x10 ⁻³	9.14x10 ⁻¹	1.8x10 ⁻³
CO ₃ ²⁻	5.5x10 ⁻¹	9.19x10 ⁻⁶	6.97x10 ⁻¹	6.41x10 ⁻⁶
H ₂ CO ₃ ⁰	3.07	4.95x10 ⁻⁵	1.00	4.96x10 ⁻⁵
OH ⁻	8.19x10 ⁻³	4.82x10 ⁻⁷	9.11x10 ⁻¹	4.39x10 ⁻⁷
MgOH ⁺	2.23x10 ⁻³	5.4x10 ⁻³	9.11x10 ⁻¹	4.92x10 ⁻⁸
MgSO ₄ ⁰	1.21x10 ⁻¹	1.01x10 ⁻⁶	1.00	1.01x10 ⁻⁶
MgHCO ₃ ⁺	1.43	1.68x10 ⁻⁵	9.11x10 ⁻¹	1.53x10 ⁻⁵
MgCO ₃ ⁰	3.41x10 ⁻¹	4.05x10 ⁻⁶	1.00	4.05x10 ⁻⁶
CaOH ⁺	6.56x10 ⁻⁴	1.15x10 ⁻⁸	9.11x10 ⁻¹	1.05x10 ⁻⁸
CaSO ₄ ⁰	2.55x10 ⁻¹	1.87x10 ⁻⁶	1.00	1.88x10 ⁻⁶
CaHCO ₃ ⁺	1.56	1.54x10 ⁻⁵	9.11x10 ⁻¹	1.4x10 ⁻⁵
CaCO ₃ ⁰	7.66x10 ⁻¹	7.65x10 ⁻⁶	1.00	7.67x10 ⁻⁶
HSO ₄ ⁻	8.13x10 ⁻⁷	8.38x10 ⁻¹²	9.11x10 ⁻¹	7.63x10 ⁻¹²
H ₂ SO ₄ ⁰	1.06x10 ⁻⁴⁶	1.08x10 ⁻⁵¹	1.00	1.08x10 ⁻⁵¹
HCl ⁰	1.37x10 ⁻³⁶	3.78x10 ⁻⁴¹	1.00	3.78x10 ⁻⁴¹
Mn ²⁺	6.59x10 ⁻⁶	1.20x10 ⁻¹⁰	6.89x10 ⁻¹	8.27x10 ⁻¹¹
Mn ³⁺	7.23x10 ⁻²	1.32x10 ⁻⁶	4.33x10 ⁻¹	5.69x10 ⁻⁷

¹Parts Per Million

²Calculated from density of solution and distribution of species

³Activity coefficient

⁴Activity

TABLE V-3, contd

SPECIES	PPM ¹	m, calc ²	γ^3	a ⁴
MnOH ⁺	8.05x10 ⁻⁹	1.12x10 ⁻¹³	9.11x10 ⁻¹	1.02x10 ⁻¹³
Mn(OH) ₃ ⁻	4.93x10 ⁻¹⁷	4.66x10 ⁻²²	9.11x10 ⁻¹	4.24x10 ⁻²²
MnHCO ₃ ⁺	9.87x10 ⁻⁷	8.51x10 ⁻¹²	9.11x10 ⁻¹	7.76x10 ⁻¹²
MnSO ₄ ⁰	5.05x10 ⁻⁹	3.35x10 ⁻¹⁴	1.00	3.35x10 ⁻¹⁴
MnCl ⁺	1.2x10 ⁻⁷	1.33x10 ⁻¹²	9.11x10 ⁻¹	1.21x10 ⁻¹²
MnCl ₂ ⁰	1.49x10 ⁻¹⁰	1.18x10 ⁻¹⁵	1.00	1.18x10 ⁻¹⁵
MnCl ₃ ⁻	3.41x10 ⁻¹³	2.11x10 ⁻¹⁸	9.11x10 ⁻¹	1.92x10 ⁻¹⁸
HMnO ₂ ⁻	2.53x10 ⁻¹⁶	2.87x10 ⁻²¹	9.11x10 ⁻¹	2.61x10 ⁻²¹
H ₃ BO ₃ ⁰	9.28	1.5x10 ⁻⁴	1.00	1.5x10 ⁻⁴
H ₂ BO ₃ ⁻	4.56x10 ⁻¹	7.5x10 ⁻⁶	9.11x10 ⁻¹	6.84x10 ⁻⁶
NH ₃ ⁰	1.2x10 ⁻²	7.03x10 ⁻⁷	1.00	7.04x10 ⁻⁷
NH ₄ ⁺	5.32x10 ⁻¹	2.95x10 ⁻⁵	9.11x10 ⁻¹	2.69x10 ⁻⁵
NH ₄ SO ₄ ⁻	4.27x10 ⁻⁴	3.75x10 ⁻⁹	9.11x10 ⁻¹	3.41x10 ⁻⁹
Ba ²⁺	6.93x10 ⁻²	5.05x10 ⁻⁷	6.89x10 ⁻¹	3.47x10 ⁻⁷
BaOH ⁺	1.02x10 ⁻⁷	6.6x10 ⁻¹³	9.11x10 ⁻¹	6.02x10 ⁻¹³

¹Parts Per Million

²Calculated from density of solution and distribution of species

³Activity coefficient

⁴Activity

TABLE V-4

POSSIBLE MINERAL PHASES WHICH MAY PRECIPITATE
FROM GALENA WATERS

Phase	IAP ¹	KT ²	$S^3 = \frac{IAP}{KT}$	POTENTIAL TO PRECIPITATE
Aragonite	6.52×10^{-9}	7.25×10^{-9}	9.06×10^{-1}	Possible
Barite	3.43×10^{-12}	7.34×10^{-11}	4.67×10^{-2}	Unlikely
Calcite	6.52×10^{-9}	3.77×10^{-9}	1.73	Likely
Dolomite	3.23×10^{-17}	1.55×10^{-17}	2.08	Likely
Magnesite	4.95×10^{-9}	8.26×10^{-9}	5.99×10^{-1}	Possible
Witherite	2.23×10^{-12}	1.73×10^{-9}	1.29×10^{-3}	Unlikely
Pyrolusite	$4.73 \times 10^{+25}$	$4.01 \times 10^{+16}$	$1.18 \times 10^{+9}$	Likely
Mn(OH) ₃	4.82×10^{-26}	6.99×10^{-37}	$6.88 \times 10^{+10}$	Likely
Manganite	4.96×10^{-17}	5.78×10^{-1}	$8.57 \times 10^{+17}$	Likely

¹Ion activity product

²Equilibrium constant at 15°C

³Degree of saturation

S > 1, Supersaturated, precipitation likely.

S = 1, Saturated, precipitation possible.

S < 1, Undersaturated, precipitation possible to unlikely.

TABLE V-5

DISTRIBUTION OF IMPORTANT AQUEOUS SPECIES, ST. PETER
FORMATION WATER¹

SPECIES	PPM ¹	m, calc ²	γ^3	a ⁴
Ca ²⁺	1.1x10 ²	2.74x10 ⁻³	4.53x10 ⁻¹	1.24x10 ⁻³
Mg ²⁺	5.24x10 ¹	2.16x10 ⁻³	4.66x10 ⁻¹	1.00x10 ⁻³
Na ⁺	8.32x10 ²	3.63x10 ⁻²	8.14x10 ⁻¹	2.95x10 ⁻²
K ⁺	3.69x10 ¹	9.48x10 ⁻⁴	8.02x10 ⁻¹	7.60x10 ⁻⁴
H ⁺	1.05x10 ⁻⁵	1.04x10 ⁻⁸	8.12x10 ⁻¹	8.51x10 ⁻⁹
Cl ⁻	1.25x10 ³	3.53x10 ⁻²	8.02x10 ⁻¹	2.83x10 ⁻²
SO ₄ ²⁻	5.83x10 ²	6.08x10 ³	4.40x10 ⁻¹	2.68x10 ⁻³
HCO ₃ ⁻	2.23x10 ²	3.66x10 ⁻³	8.19x10 ⁻¹	3.00x10 ⁻³
CO ₃ ²⁻	1.74	2.81x10 ⁻⁵	4.51x10 ⁻¹	1.31x10 ⁻⁵
H ₂ CO ₃ ⁰	4.09	6.62x10 ⁻⁵	1.01	6.72x10 ⁻⁵
OH ⁻	1.13x10 ⁻²	6.63x10 ⁻⁷	8.12x10 ⁻¹	5.39x10 ⁻⁷
F ⁻	1.88	9.92x10 ⁻⁵	8.12x10 ⁻¹	8.06x10 ⁻⁵
MgOH ⁺	4.01x10 ⁻³	9.73x10 ⁻⁸	8.12x10 ⁻¹	7.90x10 ⁻⁸
MgSO ₄ ⁰	4.24x10 ¹	3.53x10 ⁻⁴	1.01	3.58x10 ⁻⁴
MgHCO ₃ ⁺	3.49	4.11x10 ⁻⁵	8.12x10 ⁻¹	3.33x10 ⁻⁵
MgCO ₃ ⁰	9.00x10 ⁻¹	1.07x10 ⁻⁵	1.01	1.08x10 ⁻⁵
MgF ⁺	2.17x10 ⁻¹	5.03x10 ⁻⁶	8.12x10 ⁻¹	4.08x10 ⁻⁶
CaOH ⁺	1.10x10 ⁻³	1.94x10 ⁻⁸	8.12x10 ⁻¹	1.57x10 ⁻⁸
CaSO ₄ ⁰	8.36x10 ¹	6.16x10 ⁻⁴	1.01	6.24x10 ⁻⁴
CaHCO ₃ ⁺	3.55	3.52x10 ⁻⁵	8.12x10 ⁻¹	2.86x10 ⁻⁵
CaCO ₃ ⁰	1.89	1.89x10 ⁻⁵	1.01	1.92x10 ⁻⁵
CaF ⁺	4.98x10 ⁻²	8.46x10 ⁻⁷	8.12x10 ⁻¹	6.87x10 ⁻⁷
NaSO ₄ ⁻	5.70x10 ¹	4.80x10 ⁻⁴	8.12x10 ⁻¹	3.90x10 ⁻⁴
NaHCO ₃ ⁰	4.13	4.93x10 ⁻⁵	1.01	5.00x10 ⁻⁵
NaCO ₃ ⁻	4.35x10 ⁻¹	5.26x10 ⁻⁶	8.12x10 ⁻¹	4.27x10 ⁻⁶
H ₄ SiO ₄ ⁰	1.23x10 ¹	1.28x10 ⁻⁴	1.01	1.30x10 ⁻⁴
H ₃ SiO ₄	1.23x10 ⁻¹	1.29x10 ⁻¹	8.12x10 ⁻¹	1.05x10 ⁻⁶

TABLE V-5, contd

SPECIES	PPM ¹	m, calc ²	γ^3	a ⁴
H ₂ SiO ₄ ²⁻	1.56x10 ⁻⁵	1.66x10 ⁻¹⁰	4.35x10 ⁻¹	7.23x10 ⁻¹¹
Fe ²⁺	1.66x10 ⁻³⁰	2.97x10 ⁻³⁵	4.35x10 ⁻¹	1.29x10 ⁻³⁵
Fe ³⁺	2.43x10 ⁻¹³	4.36x10 ⁻¹⁸	1.54x10 ⁻¹	6.73x10 ⁻¹⁹
Mn ²⁺	4.33x10 ⁻⁶	7.90x10 ⁻¹¹	4.35x10 ⁻¹	3.44x10 ⁻¹¹
Mn ³⁺	8.42x10 ⁻²	1.53x10 ⁻⁶	1.54x10 ⁻¹	2.36x10 ⁻⁷
MnOH ⁺	4.60x10 ⁻⁹	6.42x10 ⁻¹⁴	8.12x10 ⁻¹	5.22x10 ⁻¹⁴
PO ₄ ³⁻	4.09x10 ⁻⁶	4.32x10 ⁻¹¹	1.54x10 ⁻¹	6.66x10 ⁻¹²
HPO ₄ ²⁻	3.40x10 ⁻²	3.55x10 ⁻⁷	4.35x10 ⁻¹	1.54x10 ⁻⁷
H ₃ BO ₃ ⁰	1.34x10 ¹	2.18x10 ⁻⁴	1.01	2.21x10 ⁻⁴
H ₂ BO ₃ ⁻	9.23x10 ⁻¹	1.52x10 ⁻⁵	8.12x10 ⁻¹	1.23x10 ⁻⁵
NO ₃ ⁻	1.09x10 ⁻¹	1.76x10 ⁻⁶	8.12x10 ⁻¹	1.43x10 ⁻⁶
NH ₃ ⁰	5.87x10 ⁻²	3.45x10 ⁻⁶	1.01	3.50x10 ⁻⁶
NH ₄ ⁺	2.41	1.33x10 ⁻⁴	8.12x10 ⁻¹	1.08x10 ⁻⁴
NH ₄ SO ₄ ⁻	5.27x10 ⁻¹	4.63x10 ⁻⁶	8.12x10 ⁻¹	3.76x10 ⁻⁶
Li ⁺	5.73x10 ⁻¹	8.29x10 ⁻⁵	8.12x10 ⁻¹	6.73x10 ⁻⁵
LiOH ⁰	1.02x10 ⁻⁶	4.27x10 ⁻¹¹	1.01	4.33x10 ⁻¹¹
LiSO ₄ ⁻	9.97x10 ⁻²	9.71x10 ⁻⁷	8.12x10 ⁻¹	7.89x10 ⁻⁷
Sr ²⁺	4.01	4.60x10 ⁻⁵	4.35x10 ⁻¹	2.00x10 ⁻⁵
SrOH ⁺	8.57x10 ⁻⁶	8.22x10 ⁻¹¹	8.12x10 ⁻¹	6.68x10 ⁻¹¹
Ba ²⁺	2.97x10 ⁻²	2.16x10 ⁻⁷	4.35x10 ⁻¹	9.45x10 ⁻⁸
BaOH ⁺	3.80x10 ⁻⁸	2.47x10 ⁻¹³	8.12x10 ⁻¹	2.00x10 ⁻¹³

¹Parts Per Million

²Calculated from density of solution and distribution of species

³Activity coefficient

⁴Activity

TABLE V-6

POTENTIAL FOR MINERAL PHASE PRECIPITATION
FROM ST. PETER FORMATION WATERS

PHASE	IAP ¹	KT ²	S ³ =IAP/KT	POTENTIAL FOR PRECIPITATION
Anhydrite	3.3494x10 ⁻⁶	3.5308x10 ⁻⁵	9.4864x10 ⁻²	Unlikely
Aragonite	1.6395x10 ⁻⁸	7.2488x10 ⁻⁹	2.2618	Likely
Artinite	5.9223x10 ⁻²⁴	4.4346x10 ⁻¹⁹	1.3355x10 ⁻⁵	Unlikely
Barite	2.5382x10 ⁻¹⁰	7.3416x10 ⁻¹¹	3.4573	Likely
Brucite	2.9366x10 ⁻¹⁶	3.7015x10 ⁻¹²	7.9336x10 ⁻⁵	Unlikely
Calcite	1.6395x10 ⁻⁸	3.7749x10 ⁻⁹	4.3432	Likely
Celestite	5.3843x10 ⁻⁸	3.6376x10 ⁻⁷	1.4802x10 ⁻¹	Possible
Chalcedony	1.3069x10 ⁻⁴	2.2888x10 ⁻⁴	5.7101x10 ⁻¹	Possible
Dolomite	2.1752x10 ⁻¹⁶	1.5519x10 ⁻¹⁷	1.4016x10 ¹	Likely
Fe(OH) ₃	1.0866x10 ⁶	7.6736x10 ⁴	1.4160x10 ¹	Likely
Fluorapatite	1.4246x10 ⁻⁵⁸	5.1171x10 ⁻⁶⁸	2.7841x10 ⁹	Likely
Fluorite	8.1049x10 ⁻¹²	8.3213x10 ⁻¹²	9.7400x10 ⁻¹	Possible
Gypsum	3.3392x10 ⁻⁶	1.7154x10 ⁻⁵	1.9466x10 ⁻¹	Possible
Hematite	1.1861x10 ¹²	5.9923x10 ⁻⁴	1.9794x10 ¹⁵	Likely
Huntite	3.8291x10 ⁻³²	1.3972x10 ⁻³⁰	2.7406x10 ⁻²	Unlikely
Hydromagnesite	6.8272x10 ⁻⁴⁰	6.7476x10 ⁻³⁸	1.0118x10 ⁻²	Unlikely
Hydroxyapatite	9.5326x10 ⁻⁶¹	1.6287x10 ⁻⁶⁰	5.8527x10 ⁻¹	Possible
Magnesite	1.3268x10 ⁻⁸	8.2588x10 ⁻⁹	1.6065	Likely
Magnetite	1.1004x10 ¹⁰	2.9462x10 ⁻⁹	3.7349x10 ¹⁸	Likely
Mn(OH) ₃	3.7177x10 ⁻²⁶	6.9980x10 ⁻³⁷	5.3126x10 ¹⁰	Likely
Manganite	3.8309x10 ¹⁷	5.7810x10 ⁻¹	6.6268x10 ¹⁷	Likely
Pyrolusite	4.5009x10 ²⁵	4.0109x10 ¹⁶	1.1222x10 ⁹	Likely
Quartz	1.3069x10 ⁻⁴	6.8673x10 ⁻⁵	1.9031	Likely

¹Ion Activity Product

²Equilibrium Constant at 15°C

³Degree of Saturation

S > 1, Supersaturated, Precipitation Likely

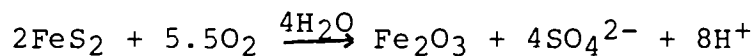
S = 1, Saturated, Precipitation Possible

S < 1, Undersaturated, Precipitation Possible to Unlikely

POTENTIAL EFFECTS OF THE INJECTION OF WARM, HUMID
AIR ON MINERAL PHASES PRESENT IN THE ST. PETER SANDSTONE

The St. Peter Sandstone is composed primarily of quartz (SiO₂, 69-92%). Quartz should be relatively unaffected by air injection unless the pH of residual waters rises above 9. Quartz is more soluble in warm water than in waters at formation temperatures and is more soluble in waters of pH greater than 9 than in waters of lower pH. However, the dissolution of quartz should be only minimal during air injection and cycling.

Iron sulfides (pyrite and marcasite) are distributed in the pore system of the St. Peter Sandstone. These sulfides are more abundant in the green and dark gray sand than in the white sand. Morphologically, the pyrite occurs in either framboidal masses with crystallites being generally less than 1 micron in size or in finely disseminated masses. Marcasite occurs as bladed crystals generally 5-100 microns in length and 1-18 microns in width. Some marcasite aggregates exhibit the characteristic "cock's comb" external morphology. Both minerals will be susceptible to oxidation when contacted by warm, humid air. Pyrite will probably be more susceptible than marcasite because of its finely crystalline nature which gives rise to a high surface area to volume ratio. In either case, the following reaction will occur:



The hematite (Fe₂O₃) formed in this fashion should be finely divided and capable of migration through the pore system with the moving water-air interface. In addition, the sulfate (SO₄²⁻) ions produced may precipitate with calcium to form gypsum or barium to form barite.

As was noted in the previous section of this report (Section IV), under thermal-pressured conditions (350°F, 1000 p.s.i.) illite present in the pore system as either detrital clay matrix or as an authigenic cement appeared to recrystallize slightly.

CONCLUSIONS

The following conclusions may be drawn from the geochemical evaluation:

1. Water Quality

- a. Galena Formation water is slightly alkaline and is saturated with respect to calcite, dolomite, pyrolusite, and manganese hydroxide.
- b. St. Peter Formation water is slightly alkaline.
- c. The level of total dissolved solids, sulfate, and chloride found in the St. Peter Formation water exceeds maximum mandatory concentration limits set by the U.S. Public Health Service for drinking water.
- d. St. Peter Formation waters are saturated with respect to aragonite, barite, calcite, dolomite, iron hydroxides, fluorapatite, hematite, magnesite, magnetite, manganese hydroxides, pyrolusite, and quartz. These phases are likely to precipitate from the water.

2. Effect of Air Injection on St. Peter Water

- a. Species in a reduced or partially reduced state (Fe^{2+} , Mn^{2+} and Mn^{3+}) will be oxidized and will form insoluble residues (hydroxides or oxides).
- b. Carbon dioxide gas (CO_2) will be evolved from the formation water, and the pH will rise, shifting the water into the carbonate (CO_3^{2-}) stability field. The probability for the precipitation of carbonate mineral phases will be enhanced.

3. Effect of Air Injection on St. Peter Minerals

- a. Quartz (SiO_2) will not chemically react with air; however, in the presence of warm, humid air and if the pH of residual formation water rises above 9, some dissolution of quartz may occur. This effect should be greatest at the air-water interface but should be relatively insignificant.

- b. Pyrite and marcasite (FeS_2) will be oxidized. Sulfate ions and either hematite, iron (III) hydroxide ($\text{Fe}(\text{OH})_3$), or iron hydroxy oxide ($\text{FeO}(\text{OH})$) will be produced.
- c. Detrital and authigenic illite may be recrystallized.

Recommendations -

Extensive air drilling has taken place in the Yakley field since the St. Peter water samples were analyzed. It is imperative that the St. Peter water be analyzed prior to air injection and cycling. In addition several thousands of gallons of water have been adsorbed into the St. Peter formation during drilling and logging. The water quality may now be significantly different.

X-ray diffraction analysis of green St. Peter sand from Well G revealed the presence of a previously undetected mineral phase, barite (BaSO_4). The precipitation of this phase may be the direct result of drilling the injection well.

.

.

.

.

.

.

.

.

.

.

.

Results of all post-test analyses must be compared with pre-test analyses for meaningful relationships to be obtained. The purpose of, and information to be gained from, each test is discussed, briefly, below.

1) Porosity and Permeability

Measurements of porosity and horizontal or vertical permeability should be restricted to those samples which are visually very similar to samples previously tested; otherwise, results can not be compared. Because porosity and permeability are highly variable with regard to cementation and horizontal clay laminations, results may be invalid unless comparisons are made on a 1 to 1 basis.

2) Petrographic Examination

Thin section examination of critical samples may yield information regarding the migration of pore fill minerals and the generation of new minerals in the pore system. Thin section examination permits the analyst to select specific samples for scanning electron microscopy and X-ray diffraction analysis.

3) Scanning Electron Microscopy -

The scanning electron microscope should be used to examine selected pores in detail. Because of high magnifications possible with the SEM, newly formed mineral phases in the pore system may be detected, and their elemental compositions may be determined with the EDS.

4) X-ray Diffraction Analysis -

Depending on the duration of testing, newly formed mineral phases will, most probably be less than five microns in size. Pre-existing minerals (such as authigenic feldspar) may be dislodged and transported away from the injection well. X-ray diffraction analysis of the fine fraction will enable the determination of new crystalline mineral phases or the absence of pre-test mineral phases.

SECTION VI

SUGGESTIONS FOR POST-TEST ANALYSIS

General -

To determine the effect of air injection into the St. Peter Sandstone, suggestions are presented for post-test coring and core analyses. Changes in the St. Peter Sandstone and Joachim dolomite, induced by the injection, cycling, and exposure to warm humid air may be readily detected.

Coring -

Suggested coring locations are presented in Figure VI-1. Locations 1 and 2 are new bore holes and will serve to monitor changes in the aquifer with respect to distance from the injection well. Fifty to sixty feet of core should be taken from boring location 1, and 30 to 40 feet of core should be taken from boring location 2. Boring location 3 is the most critical site. Once again, 50 to 60 feet of core should be taken.

Of the total cored interval for each boring, 10-15 feet of Joachim dolomite should be taken. The entire cored interval should be carefully examined, marked, and preserved, in the field, prior to shipment.

Water Quality -

After coring, water samples should be taken from the St. Peter Sandstone and analyzed. These analyses may then be compared with pre-test analyses to determine the effect, if any, on the water quality.

Core Analyses -

The effects of air injection and cycling may be quantified and examined by the following techniques:

- 1) Porosity and permeability measurements
- 2) Petrographic examination
- 3) Examination of the pore system with the scanning electron microscope
- 4) Fine fraction X-ray diffraction analysis

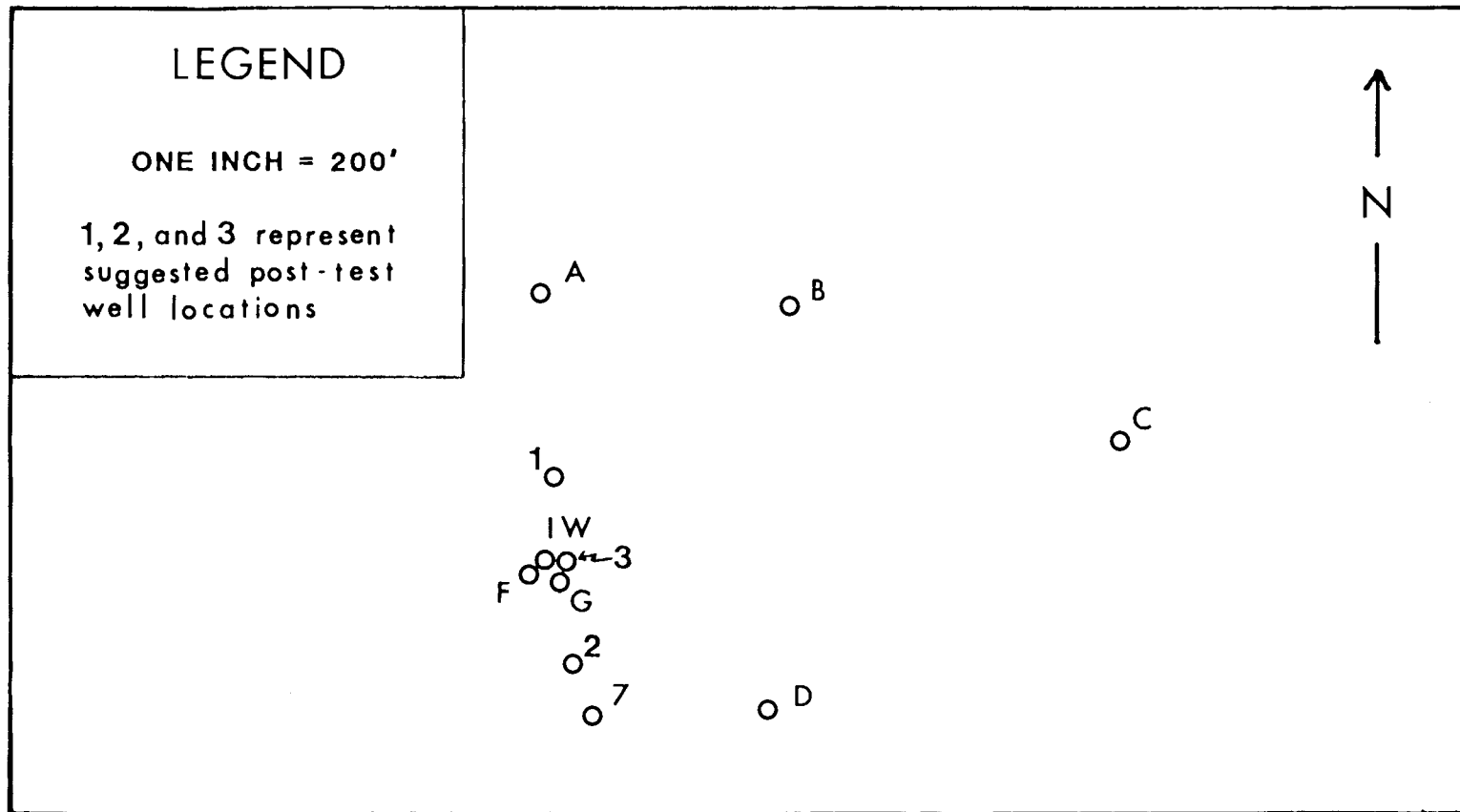


FIGURE VI-1. Location map illustrating pre-test (A,B,C,D,F,G,IW and 7) well positions and suggested positions of post-test wells (1,2,3).

APPENDIX

MECHANICAL STRENGTH



McClelland engineers, inc./geotechnical consultants

P. O. Box 37321, Houston, Texas 77036, Tel 713/772-3701, Telex 762-447

October 30, 1981

PB-KBB Inc.
11999 Katy Freeway
Suite #600
Houston, TX 77079

Attention: Mr. John Istvan

Gentlemen:

Enclosed are laboratory test results on samples supplied to our Houston laboratory by Ms. Kathy Duchac. A summary of strength results is presented on Attachments 1 and 2.

The triaxial compression test results are reported only on Attachment 1. The original request was to perform triaxial compression on all the samples, but because of the samples of large diameter, it was not possible. Ms. Duchac changed the testing request, for the larger diameter samples, to unconfined compression tests with strain gages to monitor lateral and axial strain.

The unconfined compression tests are presented in summary form (Attachment 2) as well as plots of stress versus strain and lateral strain versus axial strain. I have also included a plot of all stress-strain curves for the unconfined compression tests combined into one plot.

We appreciate the opportunity to be of service to you on this project. Please call us if you have any further questions.

Very truly yours,

McCLELLAND ENGINEERS, INC.

Willard L. DeGroff

Willard L. DeGroff, P.E.
Laboratory Manager

WLD/jd
Enclosures

TABLE A-1
TRIAXIAL TESTING RESULTS

Boring 7

Penetration (ft)	Sample	Density (pcf)	Confining Pressure (psi)	Ultimate Strength (ksf)
609.85	A	155	1000	1674
613.55	B	155	1000	800
618.21	C	146	1000	2209
620.50	D	149	1000	2460
621.35	E	144	1000	1724
633.45	F	142	1000	1996
634.20	G	144	1000	2164
639.00	H	118	1000	405

TABLE A-2

Attachment 2

UNCONFINED COMPRESSION TEST RESULTS

Penetration (ft)	Sample	Density (pcf)	Confining Pressure (psi)	Ultimate Strength (ksf)
629	A	150	0	1432
643	A	146	0	874
605	B	168	0	2117
609.4-610.5	B	163	0	2572
611.5-612.35	B	147	0	1671
636-636.7	B	144	0	1384
628	C	145	0	1217
620	D	150	0	1556
630	D	132	0	702
649	D	146	0	1466
644.45-645.17	1W	141	0	784
649.5-650.9	1W	131	0	640
652	1W	144	0	319
666	1W	140	0	1351

TABLE A-3

UNCONFINED COMPRESSION TEST ON ROCK

SPECIMEN : A PENETRATION(FT) : 629.0

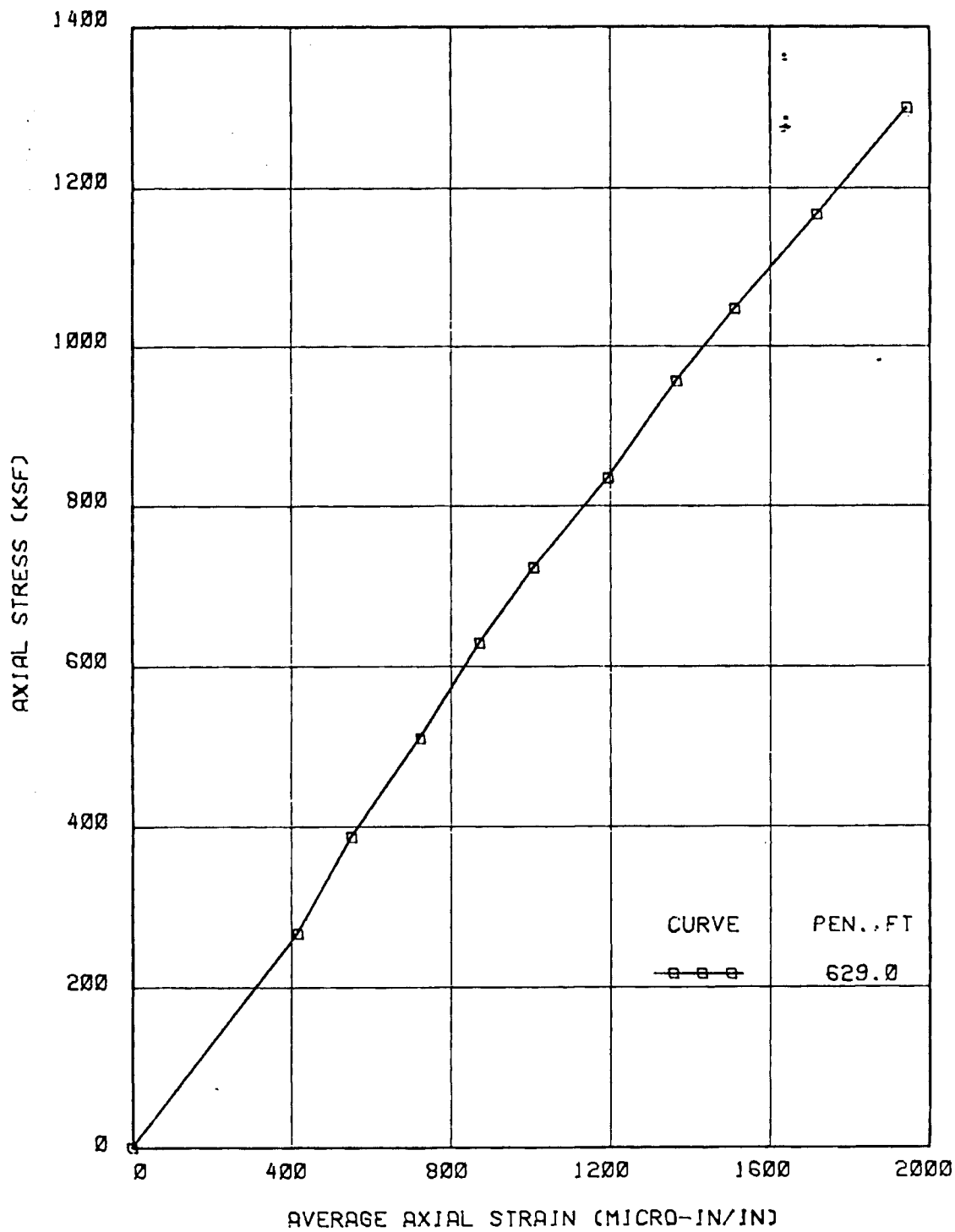
LENGTH (mm) = 190.54 DIAMETER (mm) = 89.15
 LOAD CONSTANT (lb-F/mv) = 9434

BULK DENSITY (pcf) = 150.1

VERT STRAIN (mIN/IN)				AXIAL STRAIN (mIN/IN)				LOAD (mv)	// (z)	// V STRAIN(mIN/IN)	A STRAIN(mIN/IN)	STRESS(ksf)
#1	#1(z)	#2	#2(z)	#1	#1(z)	#2	#2(z)					
23	0	34	0	-7	0	-19	0	-0.05	0.00	// 0.0	0.0	0.0
133	110	65	31	570	577	233	252	1.85	1.90	// 70.5	414.5	266.8
153	130	90	56	710	717	361	380	2.70	2.75	// 93.0	548.5	386.1
188	165	102	68	885	892	528	547	3.58	3.63	// 116.5	719.5	509.7
235	212	155	121	1024	1031	682	701	4.42	4.47	// 166.5	866.0	627.6
272	249	175	141	1165	1172	811	830	5.09	5.14	// 195.0	1001.0	721.7
339	316	218	184	1341	1348	1003	1022	5.88	5.93	// 250.0	1185.0	832.6
420	397	243	209	1492	1499	1192	1211	6.74	6.79	// 303.0	1355.0	953.3
492	469	290	256	1620	1627	1351	1370	7.39	7.44	// 362.5	1498.5	1044.6
583	560	310	276	1813	1820	1568	1587	8.24	8.29	// 418.0	1703.5	1163.9
705	682	305	271	1985	1992	1840	1859	9.18	9.23	// 476.5	1925.5	1295.9

MAXIMUM available STRESS (=) 1432 ksf

FIGURE A-1



STRESS-STRAIN CURVE

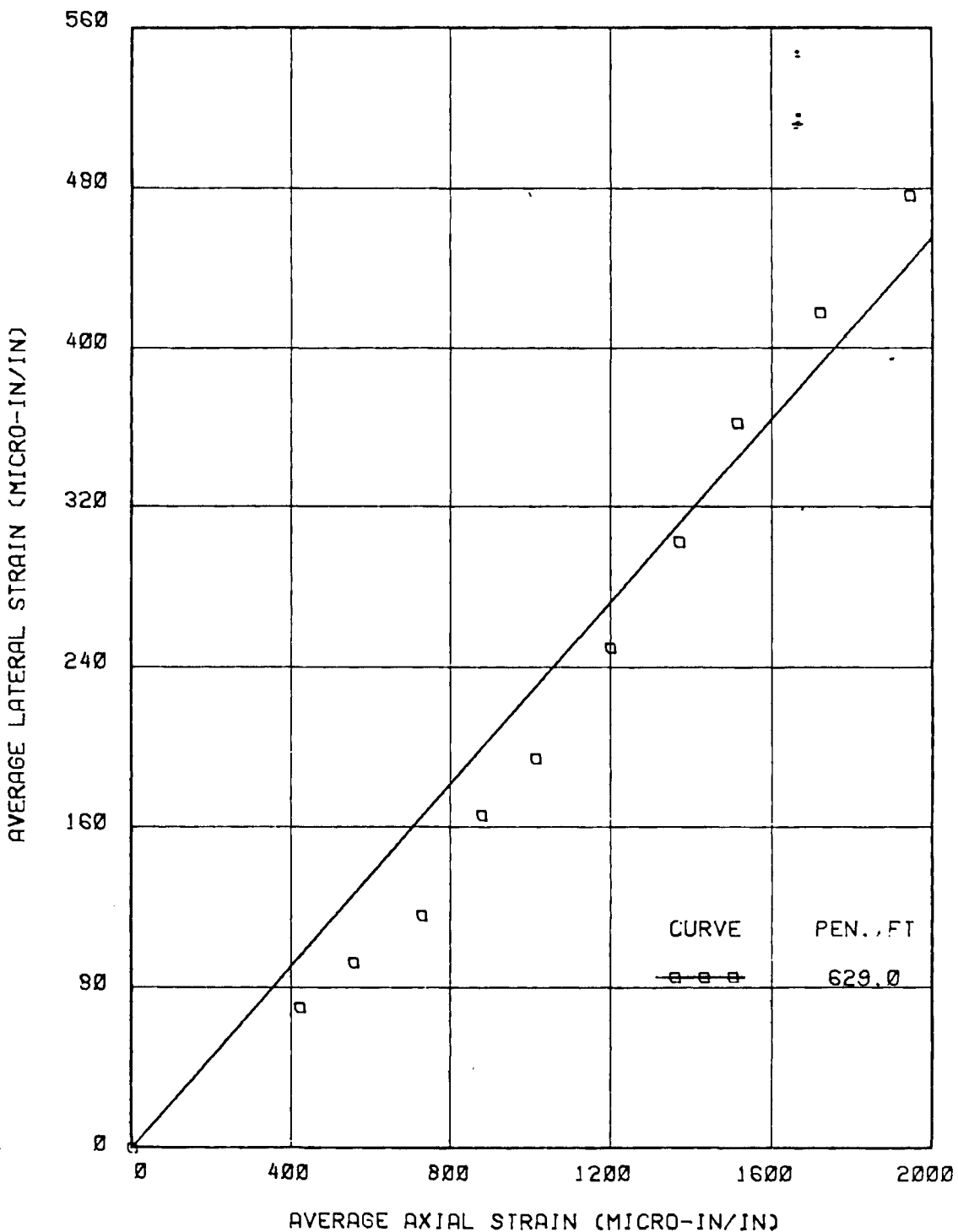
UNCONFINED COMPRESSION TEST

SAMPLE A

MAXIMUM STRESS = 1432 KSF

0181-04.17

FIGURE A-2



LATERAL VS AXIAL STRAIN
UNCONFINED COMPRESSION TEST

SAMPLE A
SLOPE = 0.228

TABLE A-4

UNCONFINED COMPRESSION TEST ON ROCK

SPECIMEN : A PENETRATION(FT) : 643.0

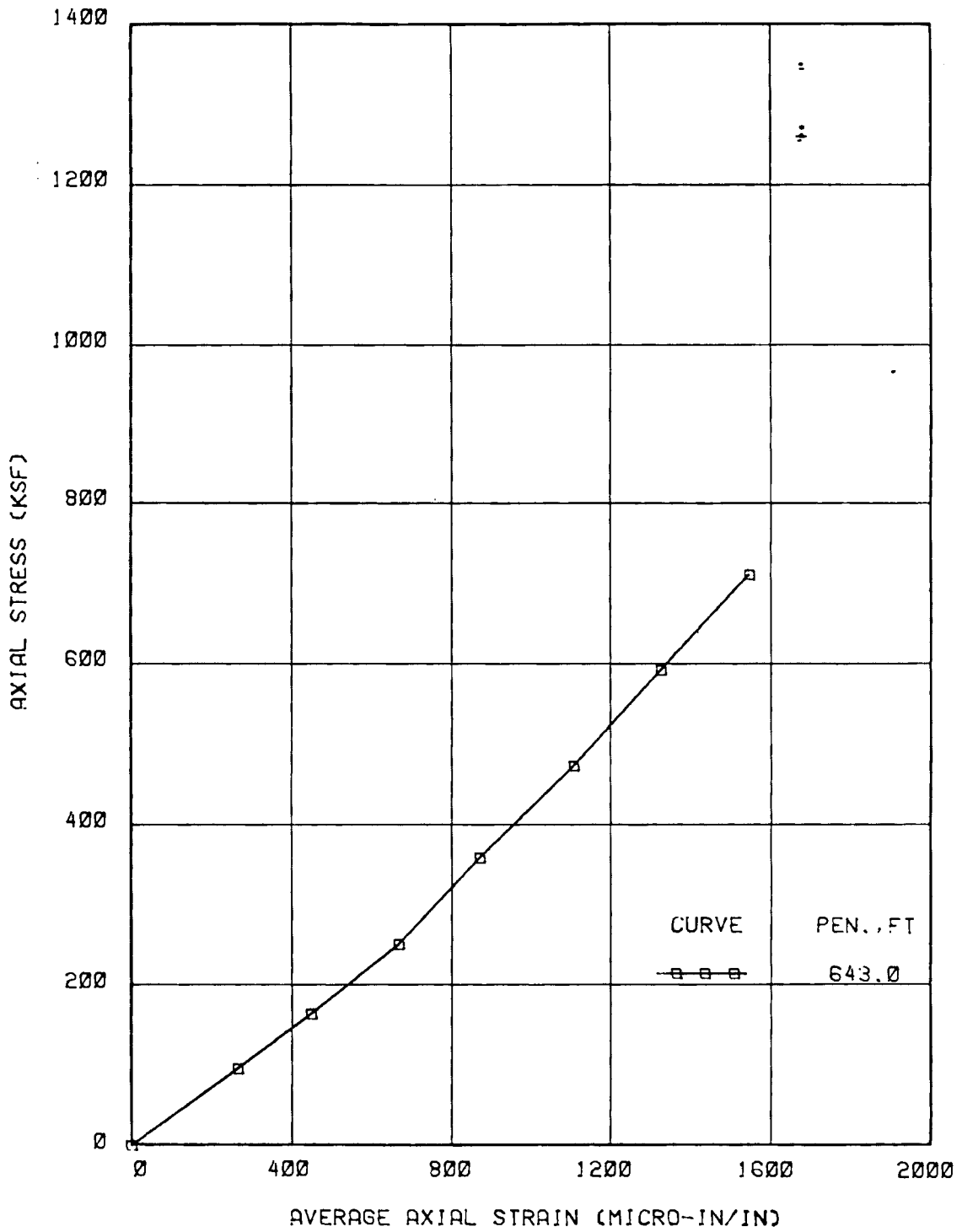
LENGTH (mm) = 189.75 DIAMETER (mm) = 89.38 BULK DENSITY (pcf) = 146
 LOAD CONSTANT (lb-F/mv) = 9434

VERT STRAIN (mIN/IN)				AXIAL STRAIN (mIN/IN)				LOAD (mv)	// V STRAIN(mIN/IN) (z) //	A STRAIN(mIN/IN) (av)	STRESS(ksf)
#1	#1(z)	#2	#2(z)	#1	#1(z)	#2	#2(z)				
2397	0	2370	0	-2300	0	-2480	0	-0.05	0.00 //	0.0	0.0
2403	6	2376	6	-2165	135	-2092	388	0.64	0.69 //	6.0	261.5
2416	19	2389	19	-1993	307	-1900	580	1.13	1.18 //	19.0	443.5
2445	48	2418	48	-1750	550	-1712	768	1.75	1.80 //	48.0	659.0
2425	28	2448	78	-1478	822	-1584	896	2.52	2.57 //	53.0	859.0
2472	75	2495	125	-1181	1119	-1415	1065	3.34	3.39 //	100.0	1092.0
2550	153	2534	164	-874	1426	-1288	1192	4.19	4.24 //	158.5	1309.0
2614	217	2572	202	-569	1731	-1156	1324	5.04	5.09 //	209.5	1527.5

A-7 ● ASSUMED

MAXIMUM available STRESS (=) 874 ksf

FIGURE A-3



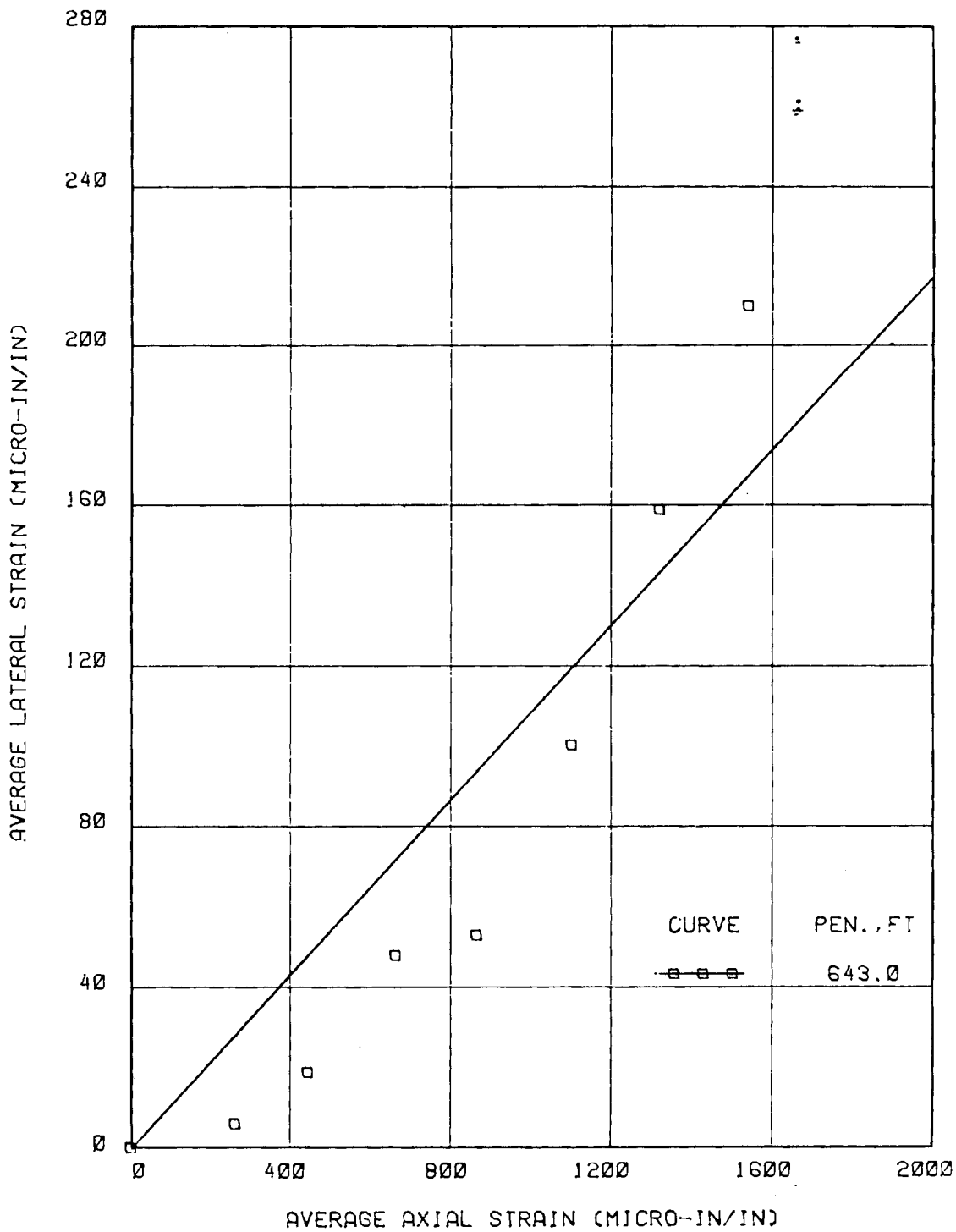
STRESS-STRAIN CURVE

UNCONFINED COMPRESSION TEST

SAMPLE A

MAXIMUM STRESS = 874 KSF

FIGURE A-4



LATERAL VS AXIAL STRAIN

UNCONFINED COMPRESSION TEST

SAMPLE A

SLOPE = 0.108

181-0411

TABLE A-5

UNCONFINED COMPRESSION TEST ON ROCK

SPECIMEN : B PENETRATION(FT) : 605.0

LENGTH (mm) = 189.9 DIAMETER (mm) = 89.45
 LOAD CONSTANT (lb-F/mv) = 9434

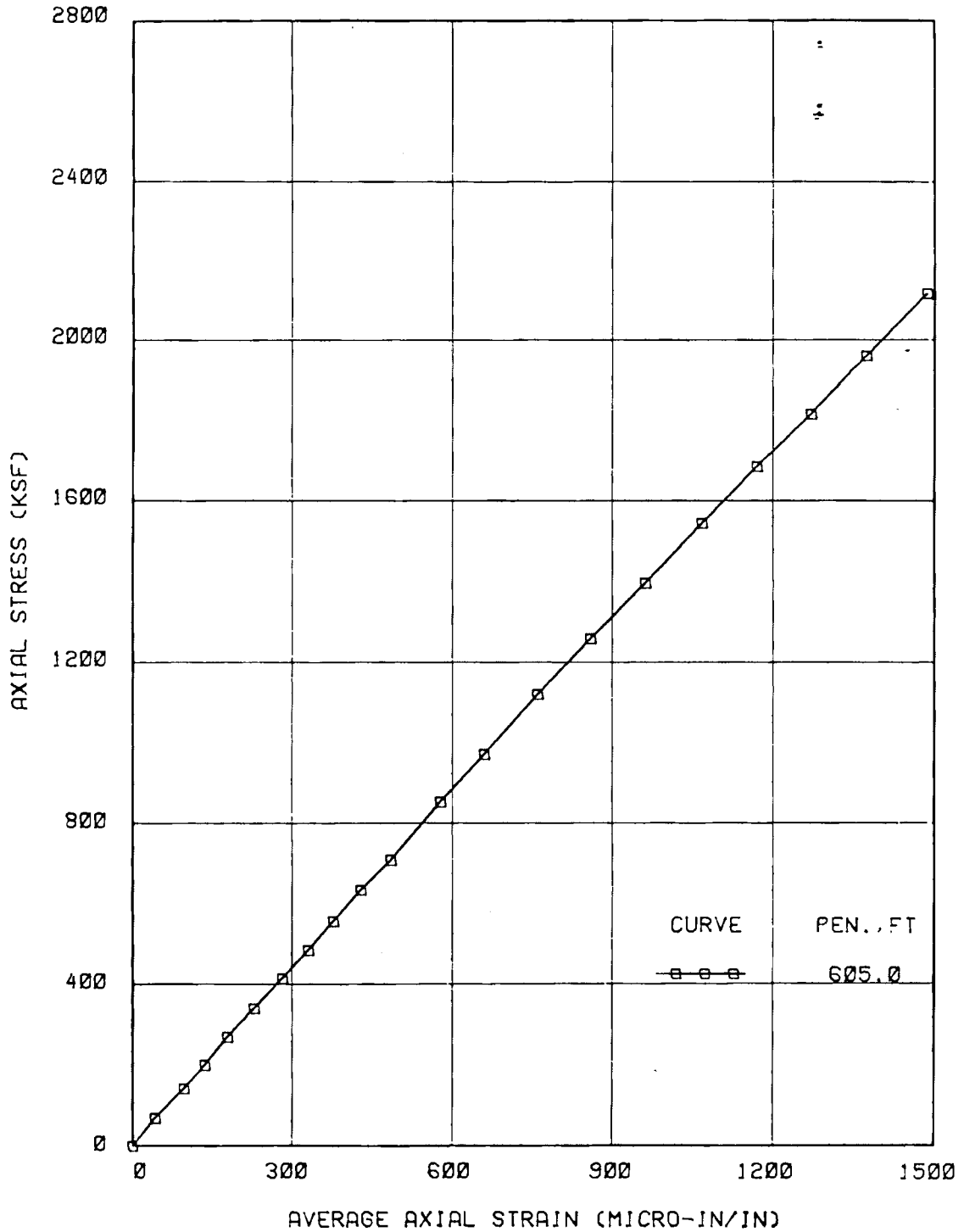
BULK DENSITY (pcf) = 167.6

A-10

VERT STRAIN (mIN/IN)				AXIAL STRAIN (mIN/IN)				LOAD (mv)	// (z)	// V STRAIN(mIN/IN)	A STRAIN(mIN/IN)	STRESS(ksf)
#1	#1(z)	#2	#2(z)	#1	#1(z)	#2	#2(z)					
0	0	3	0	-4	0	0	0	-0.05	0.00	// 0.0	0.0	0.0
16	16	32	29	0	4	81	81	0.45	0.50	// 22.5	42.5	69.7
16	16	57	54	10	14	178	178	0.97	1.02	// 35.0	96.0	142.3
24	24	82	79	22	26	244	244	1.39	1.44	// 51.5	135.0	200.8
30	30	96	93	35	39	315	315	1.89	1.94	// 61.5	177.0	270.6
41	41	118	115	64	68	387	387	2.40	2.45	// 78.0	227.5	341.7
48	48	136	133	92	96	463	463	2.93	2.98	// 90.5	279.5	415.6
60	60	156	153	113	117	538	538	3.43	3.48	// 106.5	327.5	485.3
64	64	178	175	141	145	604	604	3.95	4.00	// 119.5	374.5	557.8
81	81	202	199	170	174	676	676	4.51	4.56	// 140.0	425.0	635.9
94	94	211	208	203	207	754	754	5.04	5.09	// 151.0	480.5	709.9
118	118	252	249	260	264	880	880	6.06	6.11	// 183.5	572.0	852.1
140	140	284	281	319	323	984	984	6.91	6.96	// 210.5	653.5	970.7
161	161	323	320	385	389	1115	1115	7.97	8.02	// 240.5	752.0	1118.5
187	187	361	358	455	459	1240	1240	8.97	9.02	// 272.5	849.5	1257.9
207	207	388	385	542	546	1356	1356	9.95	10.00	// 296.0	951.0	1394.6
230	230	421	418	618	622	1491	1491	11.02	11.07	// 324.0	1056.5	1543.8
249	249	463	460	699	703	1614	1614	12.02	12.07	// 354.5	1158.5	1683.3
282	282	496	493	784	788	1731	1731	12.95	13.00	// 387.5	1259.5	1813.0
310	310	519	516	868	872	1850	1850	13.99	14.04	// 413.0	1361.0	1958.0
342	342	566	563	967	971	1977	1977	15.13	15.18	// 452.5	1474.0	2117.0

MAXIMUM available STRESS (=) 2117 ksf

FIGURE A-5



STRESS-STRAIN CURVE

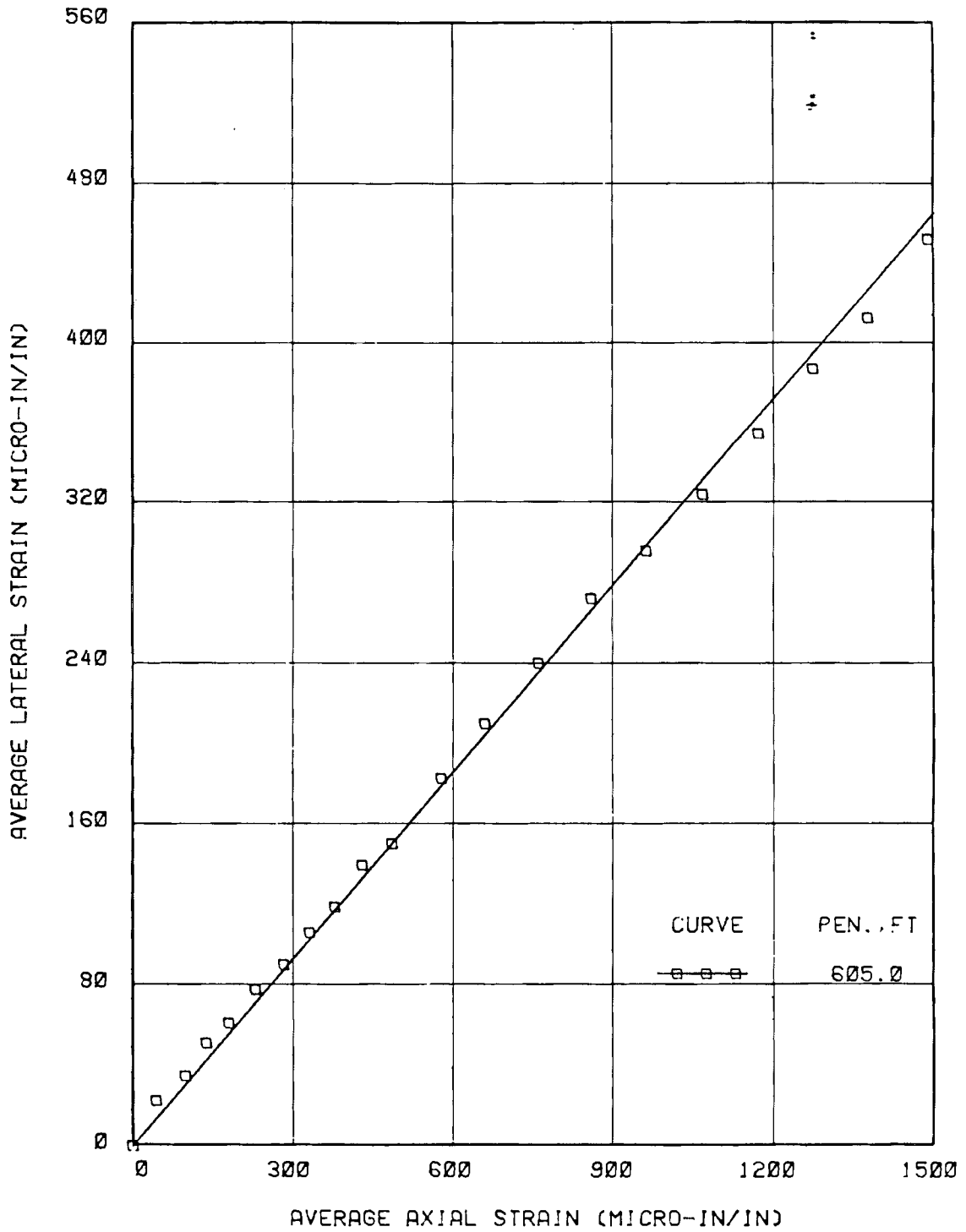
UNCONFINED COMPRESSION TEST

SAMPLE B

MAXIMUM STRESS = 2117 KSF

31-0411

FIGURE A-6



LATERAL VS AXIAL STRAIN

UNCONFINED COMPRESSION TEST

SAMPLE B

SLOPE = 0.310

UNCONFINED COMPRESSION TEST ON ROCK

SPECIMEN : B PENETRATION(FT) : 609.4-610.5

LENGTH (mm) = 179.02 DIAMETER (mm) = 89.47
LOAD CONSTANT (lb-F/mv) = 9434

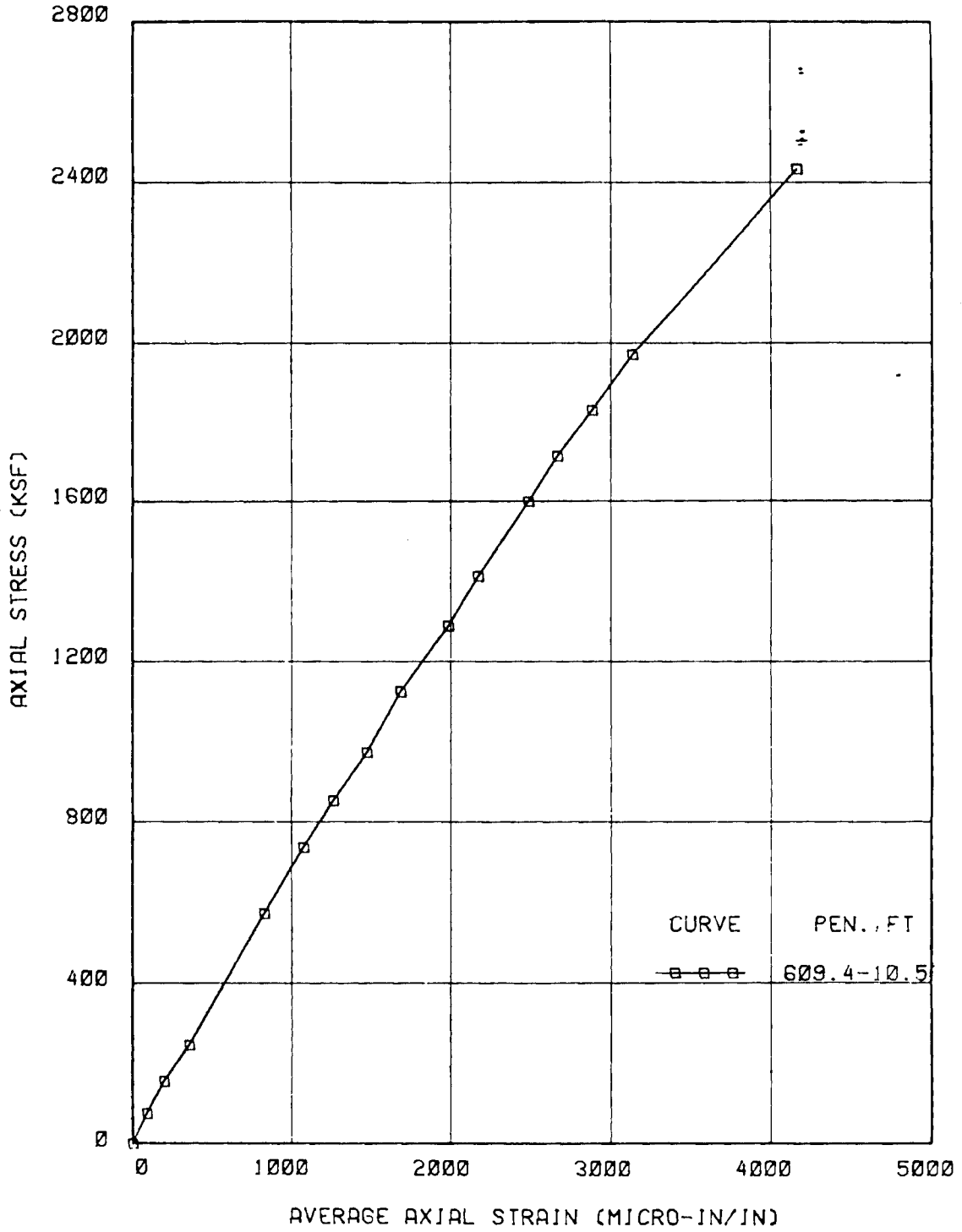
BULK DENSITY (pcf) = 163.3

VERT STRAIN (mIN/IN)				AXIAL STRAIN (mIN/IN)				LOAD (mv)	// V STRAIN(mIN/IN)	A STRAIN(mIN/IN)	STRESS(ksf)
#1	#1(z)	#2	#2(z)	#1	#1(z)	#2	#2(z)	(z)	// (av)	(av)	
-5	0	62	0	-8	0	-4	0	-0.05	0.00	// 0.0	0.0
28	33	86	24	158	166	0	4	0.50	0.55	// 28.5	85.0
47	52	205	143	310	318	66	70	1.08	1.13	// 97.5	194.0
57	62	289	227	494	502	192	196	1.72	1.77	// 144.5	349.0
157	162	186	124	1017	1025	608	612	4.07	4.12	// 143.0	818.5
181	186	167	105	1292	1300	821	825	5.25	5.30	// 145.5	1062.5
272	277	220	158	1716	1724	1183	1187	6.95	7.00	// 217.5	1455.5
314	319	268	206	1930	1938	1390	1394	8.03	8.08	// 262.5	1666.0
380	385	286	224	2264	2272	1651	1655	9.21	9.26	// 304.5	1963.5
532	537	463	401	2790	2798	2110	2114	11.43	11.48	// 469.0	2456.0
666	671	520	458	3215	3223	2474	2478	13.10	13.15	// 564.5	2850.5
745	750	575	513	3476	3484	2716	2720	14.10	14.15	// 631.5	3102.0
1116	1121	894	832	4376	4384	3860	3864	17.40	17.45	// 976.5	4124.0

A-13

MAXIMUM available STRESS (=) 2572 KSF

FIGURE A-7



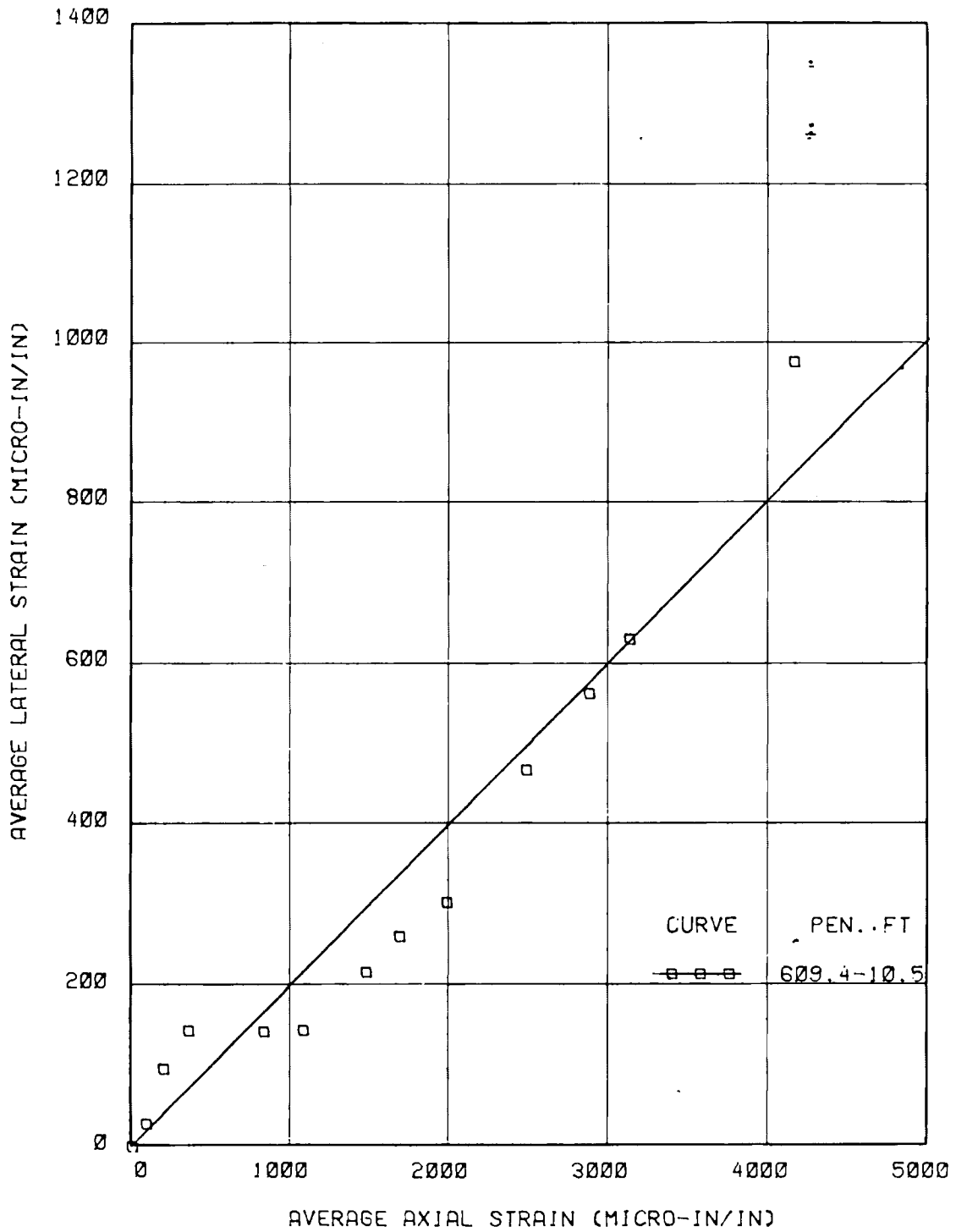
STRESS-STRAIN CURVE

UNCONFINED COMPRESSION TEST

SAMPLE B

MAXIMUM STRESS = 2572 KSF

FIGURE A-8



LATERAL VS AXIAL STRAIN

UNCONFINED COMPRESSION TEST

SAMPLE B

SLOPE = 0.203

TABLE A-7

UNCONFINED COMPRESSION TEST ON ROCK

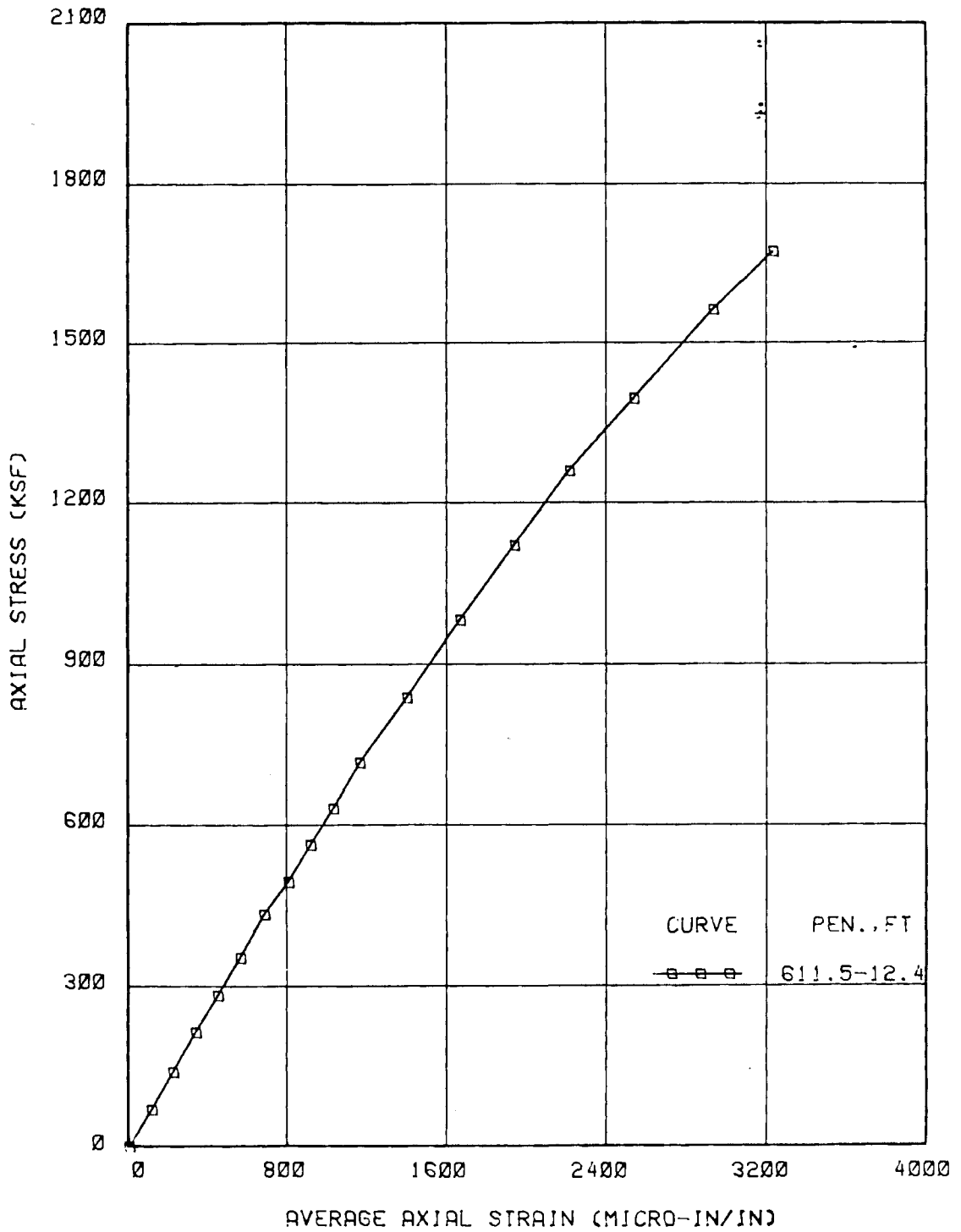
SPECIMEN : B PENETRATION(FT) : 611.5-612.4

LENGTH (mm) = 186.64 DIAMETER (mm) = 89.85 BULK DENSITY (pcf) = 147.4
 LOAD CONSTANT (lb-F/mv) = 9434

VERT STRAIN (mIN/IN)		AXIAL STRAIN (mIN/IN)				LOAD (mv)	// V STRAIN(mIN/IN)		A STRAIN(mIN/IN)	STRESS(ksf)		
#1	#1(z)	#2	#2(z)	#1	#1(z)	#2	#2(z)	(z)	(av)			
0	0	0	0	2	0	0	0	-0.05	0.00	// 0.0	0.0	0.0
15	15	24	24	120	118	99	99	0.45	0.50	// 19.5	108.5	69.1
38	38	45	45	235	233	200	200	0.96	1.01	// 41.5	216.5	139.6
50	50	69	69	358	356	302	302	1.50	1.55	// 59.5	329.0	214.2
81	81	87	87	490	488	396	396	2.00	2.05	// 84.0	442.0	283.4
106	106	115	115	627	625	486	486	2.50	2.55	// 110.5	555.5	352.5
130	130	142	142	767	765	586	586	3.09	3.14	// 136.0	675.5	434.0
160	160	154	154	913	911	675	675	3.52	3.57	// 157.0	793.0	493.5
188	188	189	189	1044	1042	759	759	4.02	4.07	// 188.5	900.5	562.6
231	231	219	219	1186	1184	847	847	4.51	4.56	// 225.0	1015.5	630.3
265	265	257	257	1344	1342	953	953	5.13	5.18	// 261.0	1147.5	716.0
340	340	310	310	1634	1632	1124	1124	6.01	6.06	// 325.0	1378.0	837.6
428	428	389	389	1963	1961	1321	1321	7.05	7.10	// 408.5	1641.0	981.4
521	521	468	468	2302	2300	1522	1522	8.06	8.11	// 494.5	1911.0	1121.0
660	660	560	560	2650	2648	1719	1719	9.06	9.11	// 610.0	2183.5	1259.2
783	783	649	649	3060	3058	1948	1948	10.04	10.09	// 716.0	2503.0	1394.7
1040	1040	815	815	3573	3571	2213	2213	11.25	11.30	// 927.5	2892.0	1561.9
1271	1271	1066	1066	4020	4018	2362	2362	12.04	12.09	// 1168.5	3190.0	1671.1

MAXIMUM available STRESS (=) 1671 ksf

FIGURE A-9



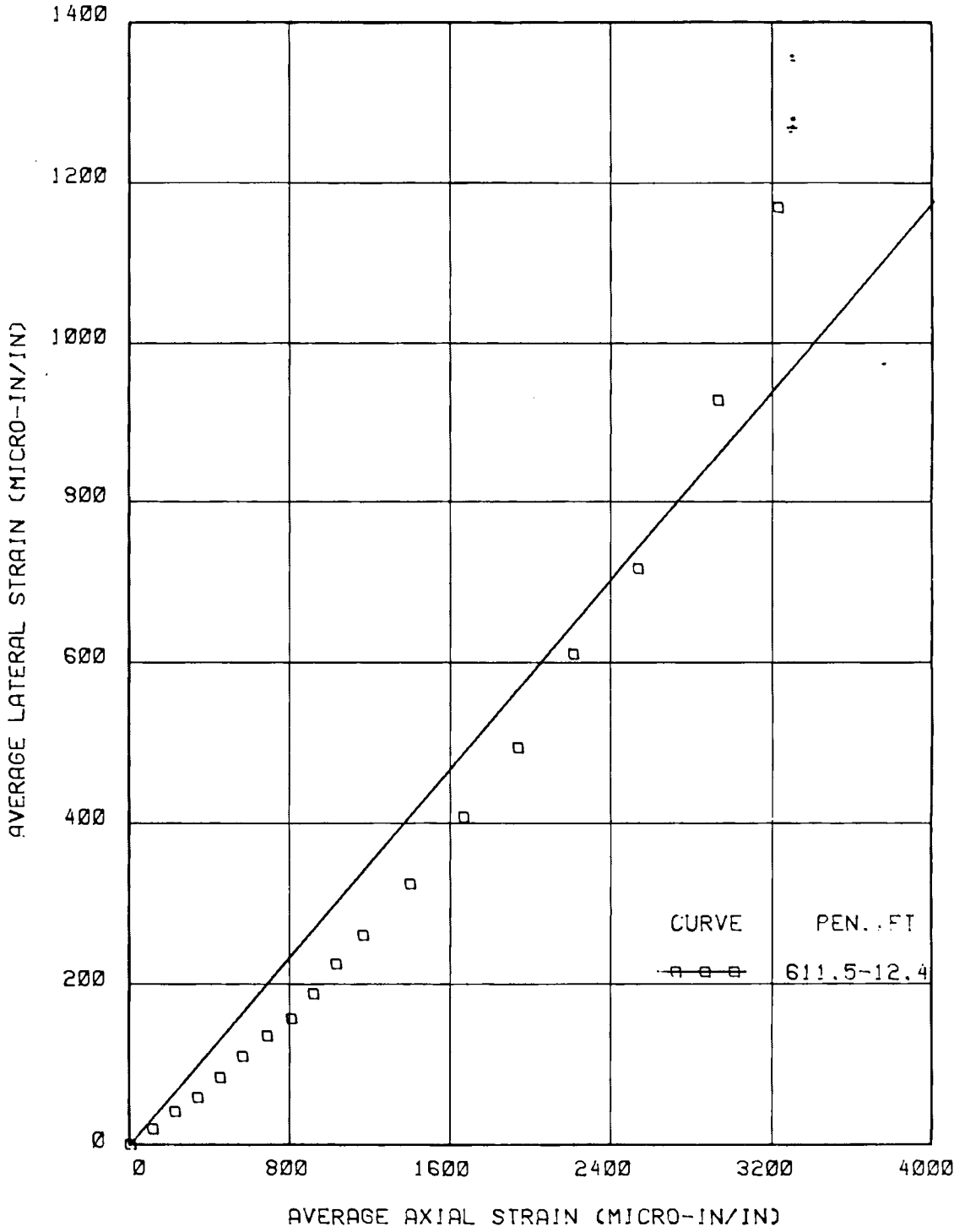
STRESS-STRAIN CURVE

UNCONFINED COMPRESSION TEST

SAMPLE B

MAXIMUM STRESS = 1671 KSF

FIGURE A-10



LATERAL VS AXIAL STRAIN

UNCONFINED COMPRESSION TEST

SAMPLE B

SLOPE = 0.296

TABLE A-8

UNCONFINED COMPRESSION TEST ON ROCK

SPECIMEN : B PENETRATION(FT) : 636.0-636.7

LENGTH (mm) = 177.13 DIAMETER (mm) = 89.38
 LOAD CONSTANT (lb-F/mv) = 9434

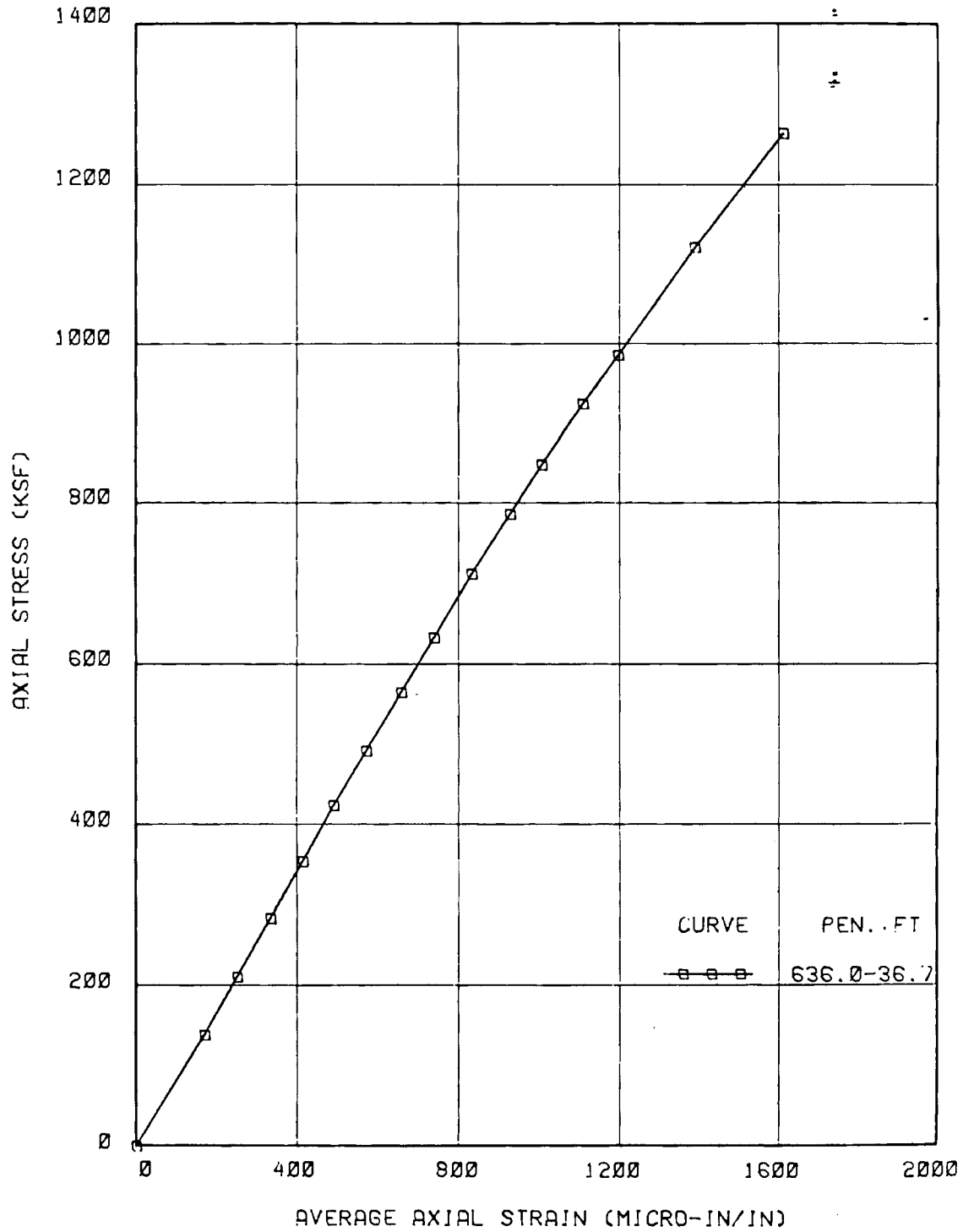
BULK DENSITY (pcf) = 144.4

A-19

VERT STRAIN (mIN/IN)				AXIAL STRAIN (mIN/IN)				LOAD (mv)	// V STRAIN(mIN/IN)		A STRAIN(mIN/IN)	STRESS(ksf)
#1	#1(z)	#2	#2(z)	#1	#1(z)	#2	#2(z)		(z)	// (av)		
-5	0	-5	0	0	0	-8	0	-0.05	0.00	// 0.0	0.0	0.0
8	13	69	74	0	0	326	334	0.94	0.99	// 43.5	167.0	138.3
18	23	100	105	30	30	455	463	1.46	1.51	// 64.0	246.5	210.9
33	38	135	140	74	74	575	583	1.98	2.03	// 89.0	328.5	283.6
49	54	165	170	124	124	686	694	2.49	2.54	// 112.0	409.0	354.8
61	66	194	199	173	173	788	796	2.98	3.03	// 132.5	484.5	423.2
79	84	218	223	230	230	891	899	3.47	3.52	// 153.5	564.5	491.7
105	110	250	255	290	290	1002	1010	3.99	4.04	// 182.5	650.0	564.3
115	120	278	283	353	353	1099	1107	4.48	4.53	// 201.5	730.0	632.8
132	137	302	307	424	424	1212	1220	5.04	5.09	// 222.0	822.0	711.0
150	155	330	335	499	499	1326	1334	5.57	5.62	// 245.0	916.5	785.0
164	169	357	362	560	560	1422	1430	6.01	6.06	// 265.5	995.0	846.5
190	195	393	398	640	640	1544	1552	6.56	6.61	// 296.5	1096.0	923.3
207	212	425	430	716	716	1645	1653	7.00	7.05	// 321.0	1184.5	984.7
250	255	477	482	860	860	1887	1895	7.97	8.02	// 368.5	1377.5	1120.2
290	295	533	538	1030	1030	2157	2165	8.98	9.03	// 416.5	1597.5	1261.3

MAXIMUM available STRESS (=) 1384 ksf

FIGURE A-11



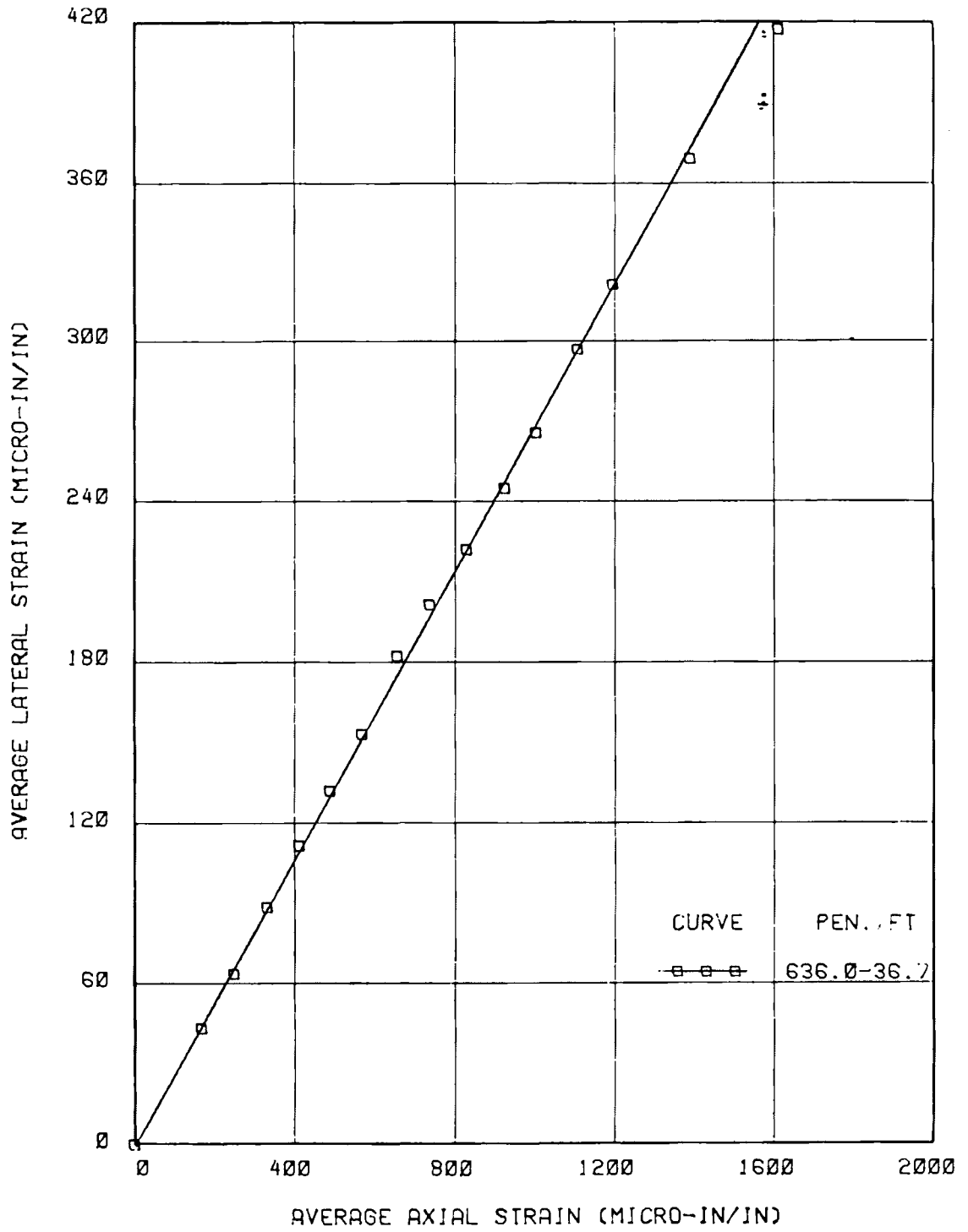
STRESS-STRAIN CURVE

UNCONFINED COMPRESSION TEST

SAMPLE B

MAXIMUM STRESS = 1384 KSF

FIGURE A-12



LATERAL VS AXIAL STRAIN

UNCONFINED COMPRESSION TEST

SAMPLE B

SLOPE = 0.268

TABLE A-9

UNCONFINED COMPRESSION TEST ON ROCK

SPECIMEN : C PENETRATION(FT) : 628.0

LENGTH (mm) = 186.4 DIAMETER (mm) = 89.1
 LOAD CONSTANT (lb-F/mv) = 9434

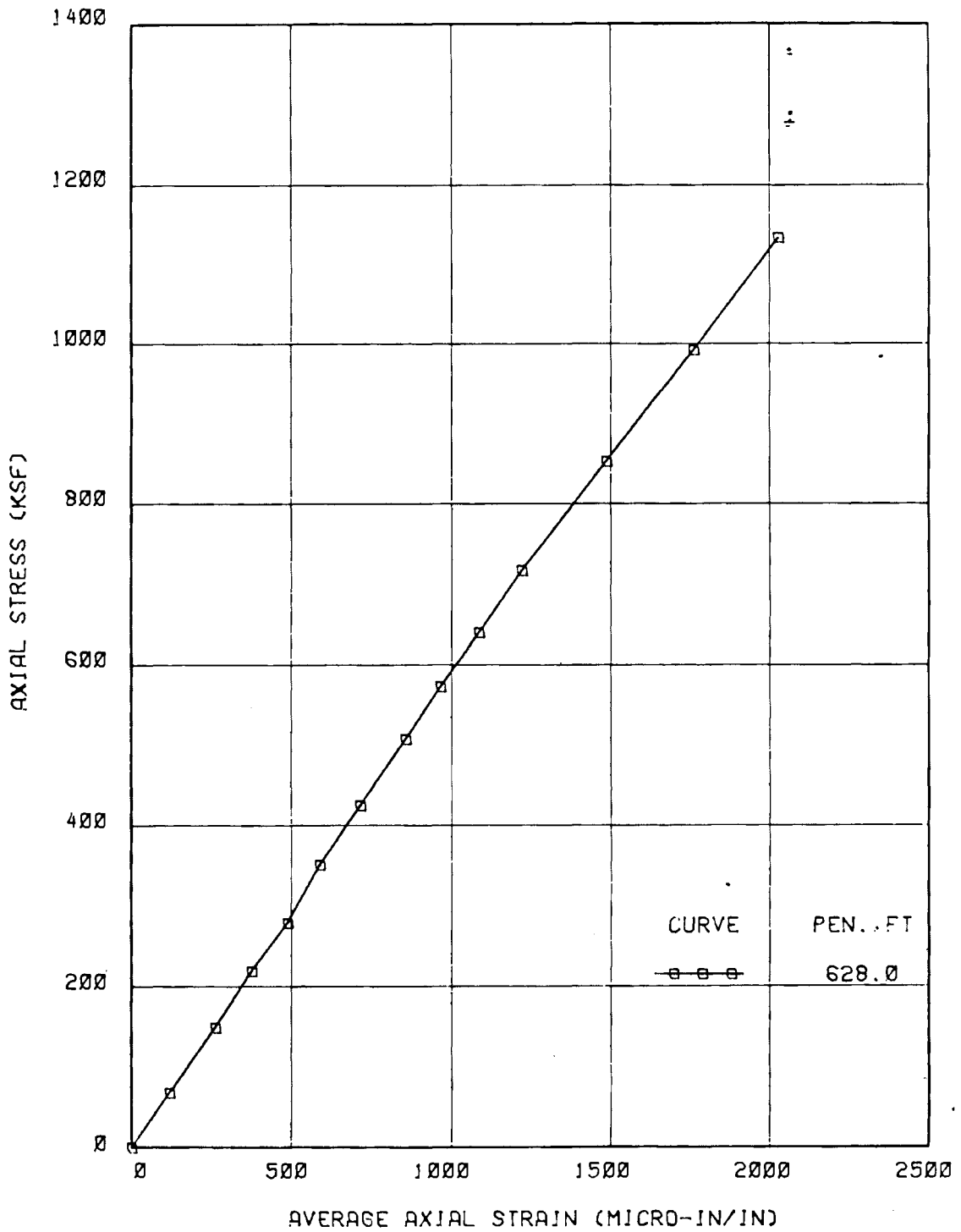
BULK DENSITY (pcf) = 144.8

A-22

VERT STRAIN (mIN/IN)				AXIAL STRAIN (mIN/IN)				LOAD (mv)	// (z)	// (av)	V STRAIN(mIN/IN) (av)	A STRAIN(mIN/IN) (av)	STRESS(ksf)
#1	#1(z)	#2	#2(z)	#1	#1(z)	#2	#2(z)						
-14	0	-10	0	0	0	-8	0	-0.05	0.00	//	0.0	0.0	0.0
0	14	21	31	99	99	132	140	0.44	0.49	//	22.5	119.5	68.9
23	37	42	52	238	238	277	285	1.01	1.06	//	44.5	261.5	149.0
57	71	68	78	355	355	383	391	1.51	1.56	//	74.5	373.0	219.3
88	102	82	92	472	472	493	501	1.94	1.99	//	97.0	486.5	279.7
133	147	116	126	581	581	584	592	2.45	2.50	//	136.5	586.5	351.4
184	198	148	158	717	717	696	704	2.98	3.03	//	178.0	710.5	425.9
244	258	182	192	873	873	819	827	3.56	3.61	//	225.0	850.0	507.4
316	330	206	216	996	996	912	920	4.02	4.07	//	273.0	958.0	572.1
398	412	244	254	1130	1130	1020	1028	4.50	4.55	//	333.0	1079.0	639.5
467	481	294	304	1283	1283	1132	1140	5.05	5.10	//	392.5	1211.5	716.9
720	734	386	396	1578	1578	1359	1367	6.01	6.06	//	565.0	1472.5	851.8
1048	1062	518	528	1903	1903	1580	1588	7.00	7.05	//	795.0	1745.5	990.9
1729	1743	704	714	2234	2234	1776	1784	8.00	8.05	//	1228.5	2009.0	1131.5

MAXIMUM available STRESS (=) 1217 ksf

FIGURE A-13



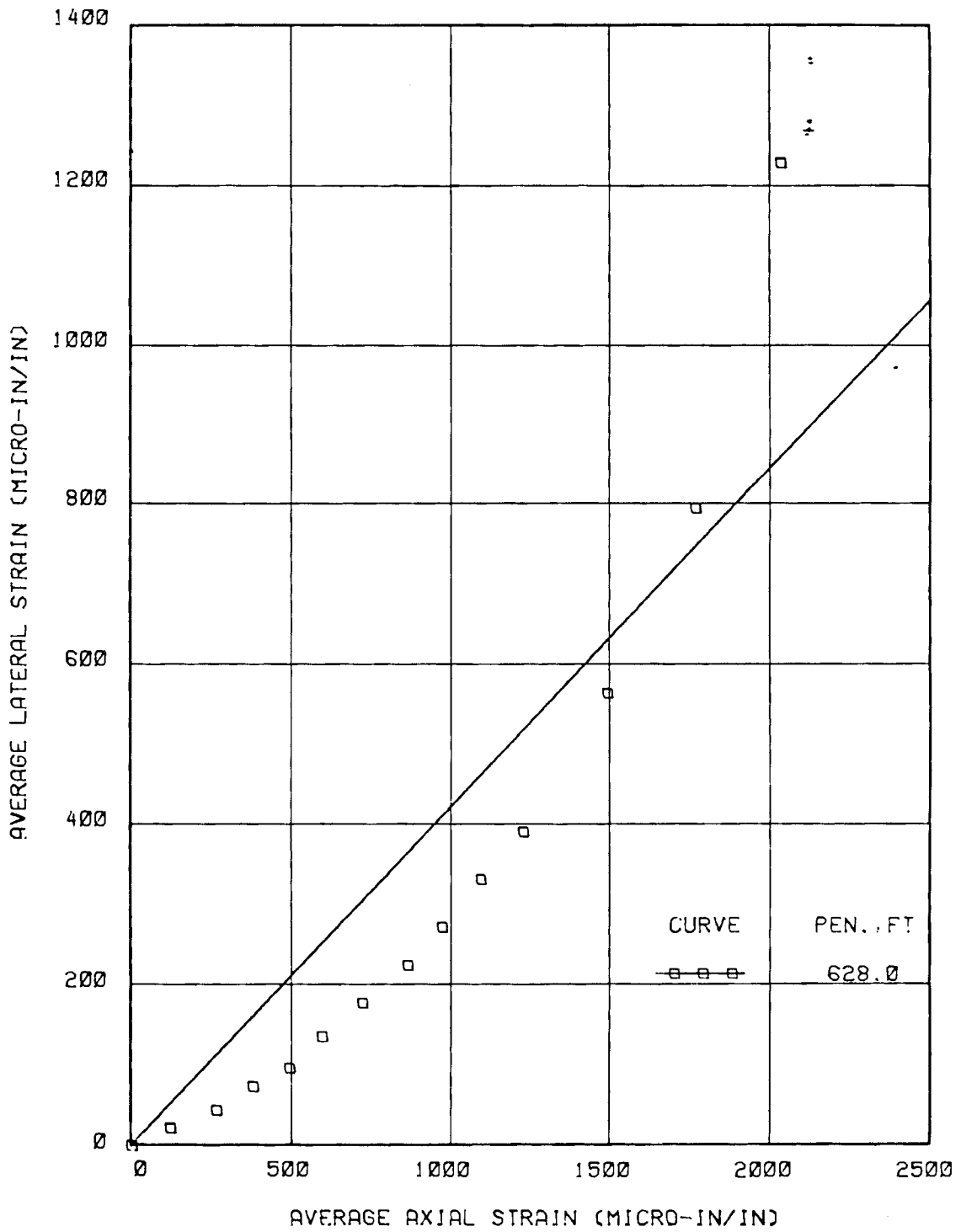
STRESS-STRAIN CURVE

UNCONFINED COMPRESSION TEST

SAMPLE C

MAXIMUM STRESS = 1217 KSF

FIGURE A-14



LATERAL VS AXIAL STRAIN

UNCONFINED COMPRESSION TEST

SAMPLE C

SLOPE = 0.423

TABLE A-10

UNCONFINED COMPRESSION TEST ON ROCK

SPECIMEN : D PENETRATION(FT) : 620.0

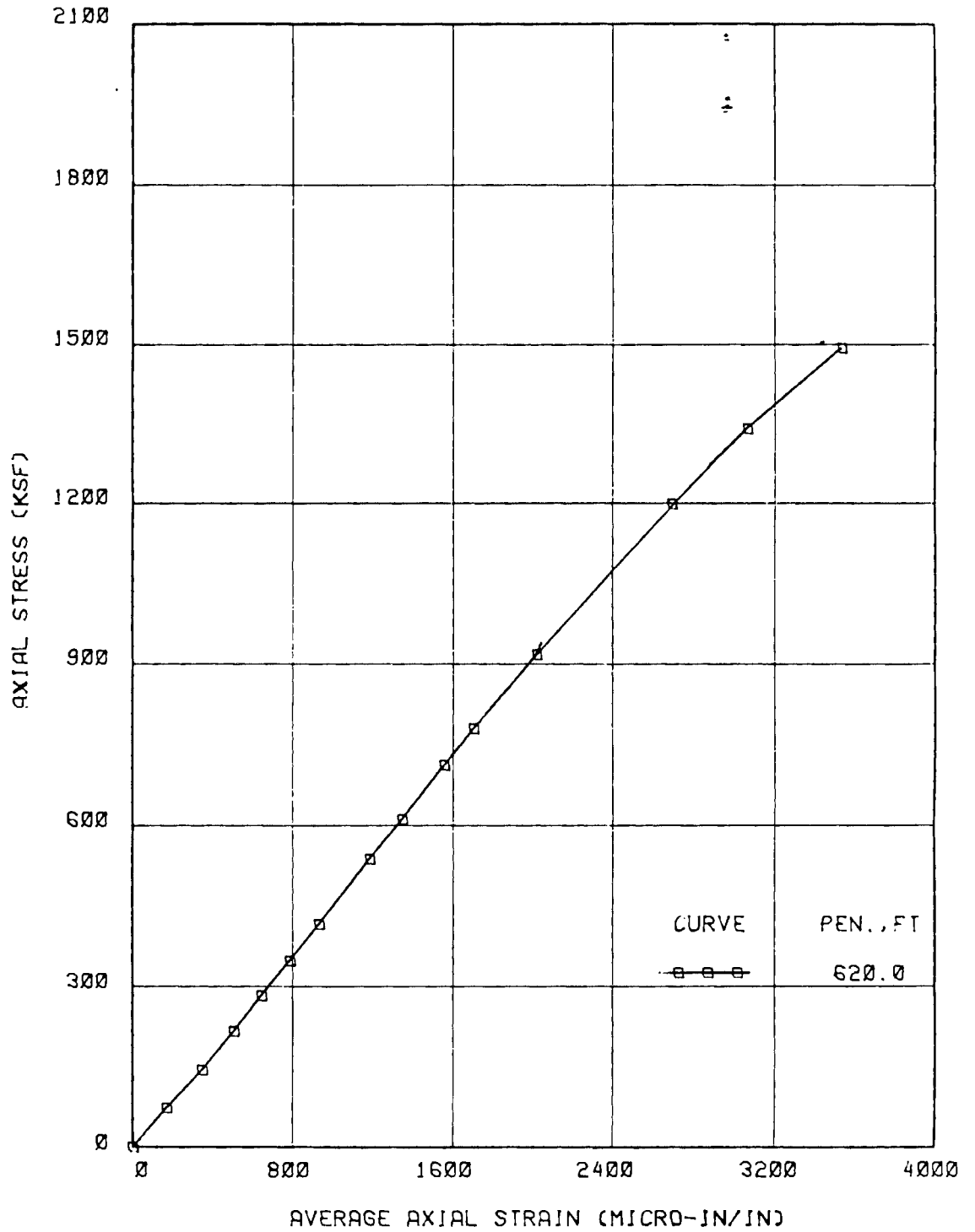
LENGTH (mm) = 188.3 DIAMETER (mm) = 89.5
LOAD CONSTANT (lb-F/mv) = 9434

BULK DENSITY (pcf) = 149.5

VERT STRAIN (mIN/IN)				AXIAL STRAIN (mIN/IN)				LOAD (mv)	// V STRAIN(mIN/IN)	A STRAIN(mIN/IN)	STRESS(ksf)
#1	#1(z)	#2	#2(z)	#1	#1(z)	#2	#2(z)	(z)	// (av)	(av)	
21	0	0	0	-1	0	-16	0	-0.05	0.00	// 0.0	0.0
58	37	26	26	192	193	131	147	0.48	0.53	// 31.5	170.0
84	63	46	46	377	378	298	314	0.99	1.04	// 54.5	346.0
112	91	67	67	539	540	444	460	1.51	1.56	// 79.0	500.0
155	134	87	87	687	688	570	586	1.98	2.03	// 110.5	637.0
186	165	119	119	832	833	708	724	2.44	2.49	// 142.0	778.5
234	213	148	148	993	994	831	847	2.93	2.98	// 180.5	920.5
323	302	205	205	1269	1270	1055	1071	3.80	3.85	// 253.5	1170.5
395	374	250	250	1446	1447	1193	1209	4.33	4.38	// 312.0	1328.0
487	466	307	307	1680	1681	1378	1394	5.05	5.10	// 386.5	1537.5
559	538	355	355	1842	1843	1501	1517	5.53	5.58	// 446.5	1680.0
746	725	464	464	2187	2188	1780	1796	6.51	6.56	// 594.5	1992.0
1014	993	595	595	2191	2192	2105	2121	7.68	7.73	// 794.0	2156.5
1328	1307	732	732	2943	2944	2352	2368	8.53	8.58	// 1019.5	2656.0
1790	1769	914	914	3373	3374	2665	2681	9.55	9.60	// 1341.5	3027.5
2710	2689	1187	1187	3920	3921	3044	3060	10.64	10.69	// 1938.0	3490.5

MAXIMUM available STRESS (=) 1556 ksf

FIGURE A-15



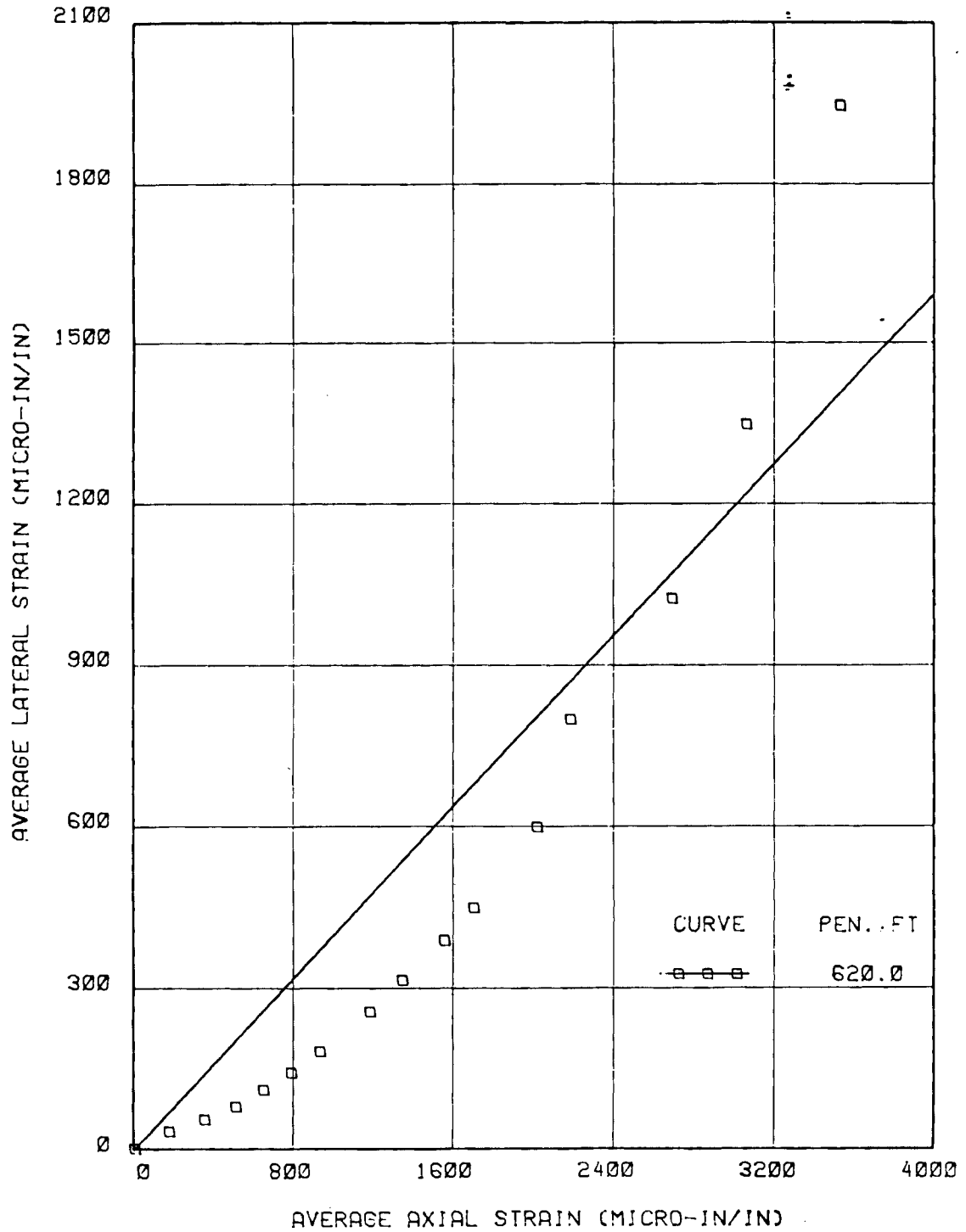
STRESS-STRAIN CURVE

UNCONFINED COMPRESSION TEST

SAMPLE D

MAXIMUM STRESS = 1556 KSF

FIGURE A-16



LATERAL VS AXIAL STRAIN

UNCONFINED COMPRESSION TEST

SAMPLE D

SLOPE = 0.397

6181-0411

TABLE A-11

UNCONFINED COMPRESSION TEST ON ROCK

SPECIMEN : D PENETRATION(FT) : 630.0

LENGTH (mm) = 188.88 DIAMETER (mm) = 89.15
 LOAD CONSTANT (lb-F/mv) = 9434

BULK DENSITY (pcf) = 132.3

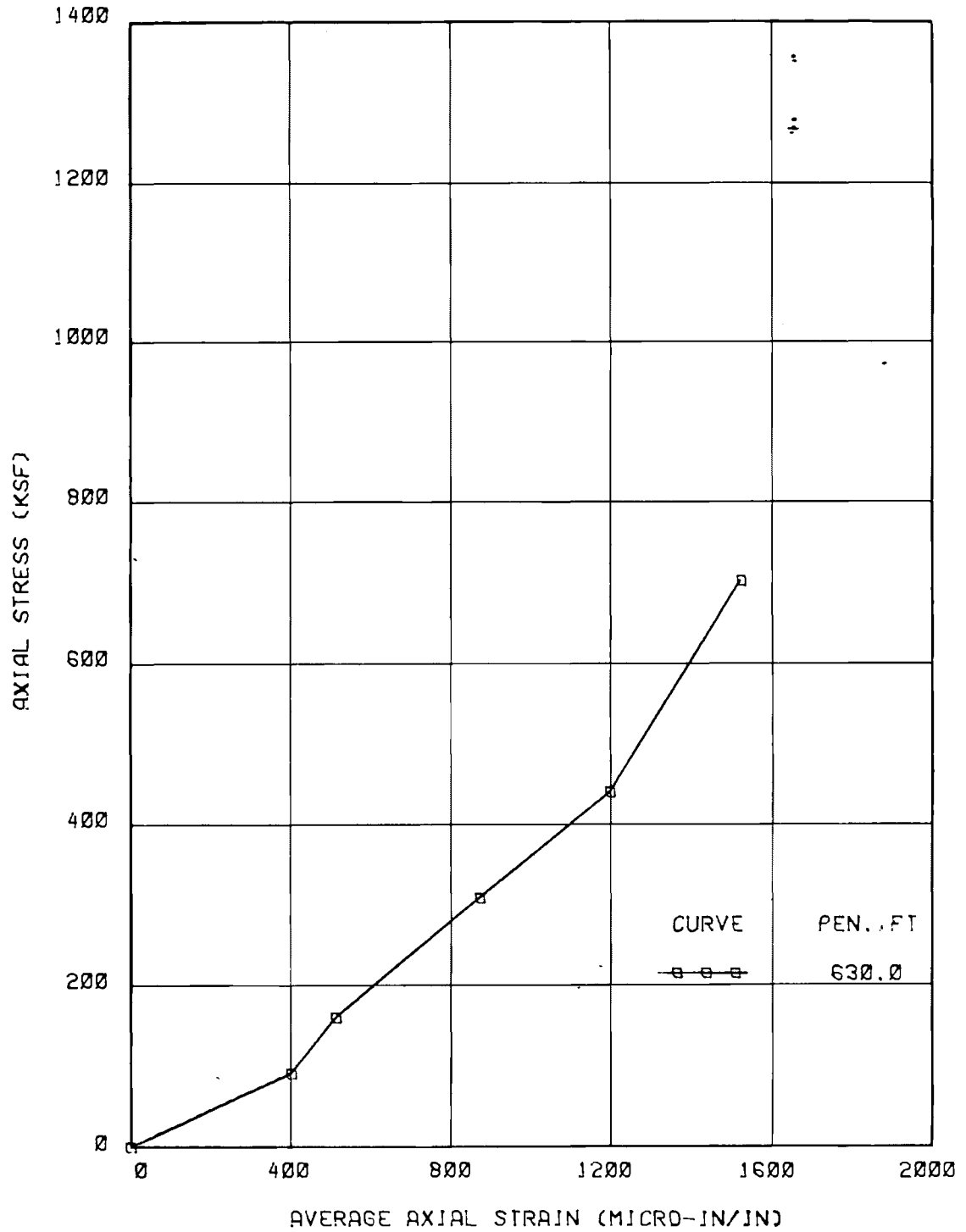
VERT STRAIN (mIN/IN)				AXIAL STRAIN (mIN/IN)				LOAD (mv)	// V STRAIN(mIN/IN)	A STRAIN(mIN/IN)	STRESS(ksf)
#1	#1(z)	#2	#2(z)	#1	#1(z)	#2	#2(z)	(z)	// (av)	(av)	
-120	0	-195	0	168	0	146	0	-0.05	0.00	// 0.0	0.0
-110	10	-185	10	482	314	626	480	0.60	0.65	// 10.0	397.0
28	148	-77	118	557	389	770	624	1.09	1.14	// 133.0	506.5
224	344	112	307	865	697	1169	1023	2.15	2.20	// 325.5	860.0
304	424	260	455	1158	990	1524	1378	3.09	3.14	// 439.5	1184.0
1804	1924	1180	1375	1229	1061	2100	1954	4.95	5.00	// 1649.5	1507.5

● ASSUMED

MAXIMUM available STRESS (=) 702 ksf

A-28

FIGURE A-17



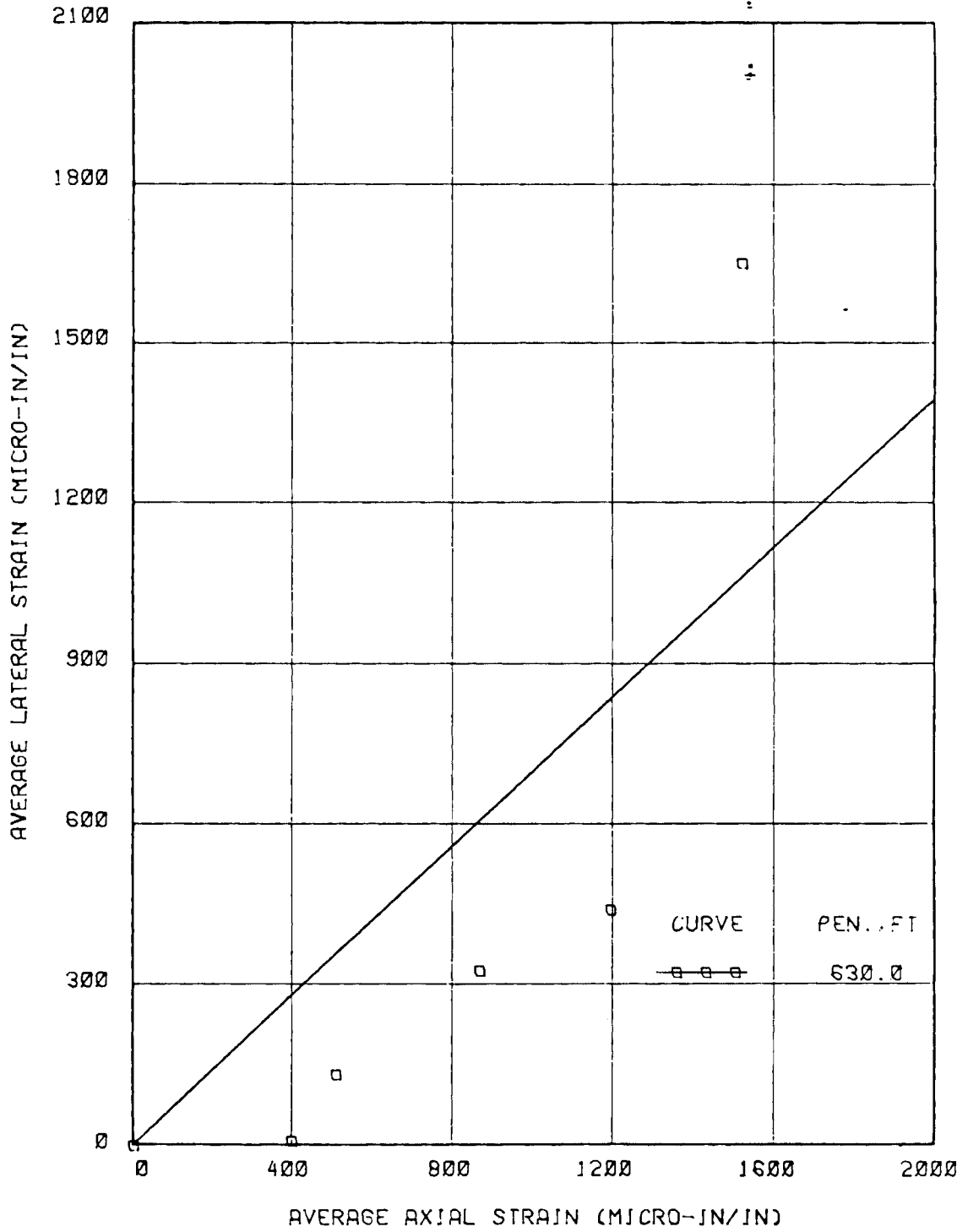
STRESS-STRAIN CURVE

UNCONFINED COMPRESSION TEST

SAMPLE D

MAXIMUM STRESS = 702 KSF

FIGURE A-18



LATERAL VS AXIAL STRAIN

UNCONFINED COMPRESSION TEST

SAMPLE D

SLOPE = 0.696

TABLE A-12

UNCONFINED COMPRESSION TEST ON ROCK

SPECIMEN : D PENETRATION(FT) : 649.0

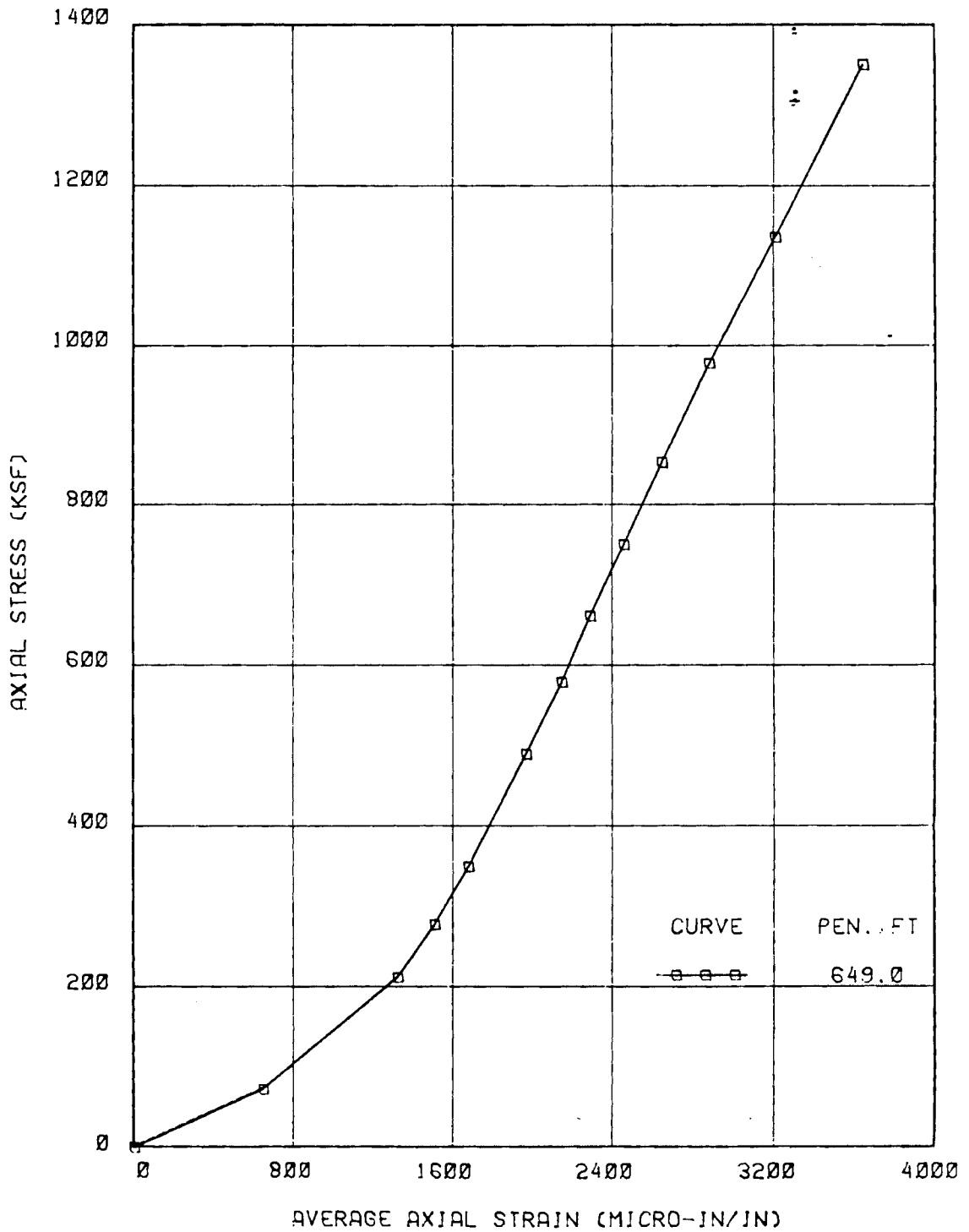
LENGTH (mm) = 189.15 DIAMETER (mm) = 89.6 BULK DENSITY (pcf) = 145.5
 LOAD CONSTANT (lb-F/mv) = 9434

A-31

VERT STRAIN (mIN/IN)				AXIAL STRAIN (mIN/IN)				LOAD (mv)	// V STRAIN(mIN/IN)	A STRAIN(mIN/IN)	STRESS(ksf)
#1	#1(z)	#2	#2(z)	#1	#1(z)	#2	#2(z)	(z)	// (av)	(av)	
268	0	209	0	1310	0	1571	0	-0.05	0.00	// 0.0	0.0
332	64	225	16	2007	697	2148	577	0.48	0.53	// 40.0	637.0
424	156	230	21	2598	1288	2906	1335	1.48	1.53	// 88.5	1311.5
462	194	279	70	2794	1484	3077	1506	1.95	2.00	// 132.0	1495.0
539	271	295	86	2982	1672	3225	1654	2.47	2.52	// 178.5	1663.0
666	398	335	126	3312	2002	3470	1899	3.48	3.53	// 262.0	1950.5
770	502	373	164	3517	2207	3619	2048	4.12	4.17	// 333.0	2127.5
874	606	394	185	3690	2380	3725	2154	4.71	4.76	// 395.5	2267.0
985	717	403	194	3889	2579	3862	2291	5.35	5.40	// 455.5	2435.0
1132	864	457	248	4112	2802	4013	2442	6.08	6.13	// 556.0	2622.0
1326	1058	555	346	4400	3090	4192	2621	6.98	7.03	// 702.0	2855.5
1740	1472	685	476	4810	3500	4430	2859	8.12	8.17	// 974.0	3179.5
2548	2280	928	719	5391	4081	4702	3131	9.65	9.70	// 1499.5	3606.0

MAXIMUM available STRESS (=) 1466 ksf

FIGURE A-19



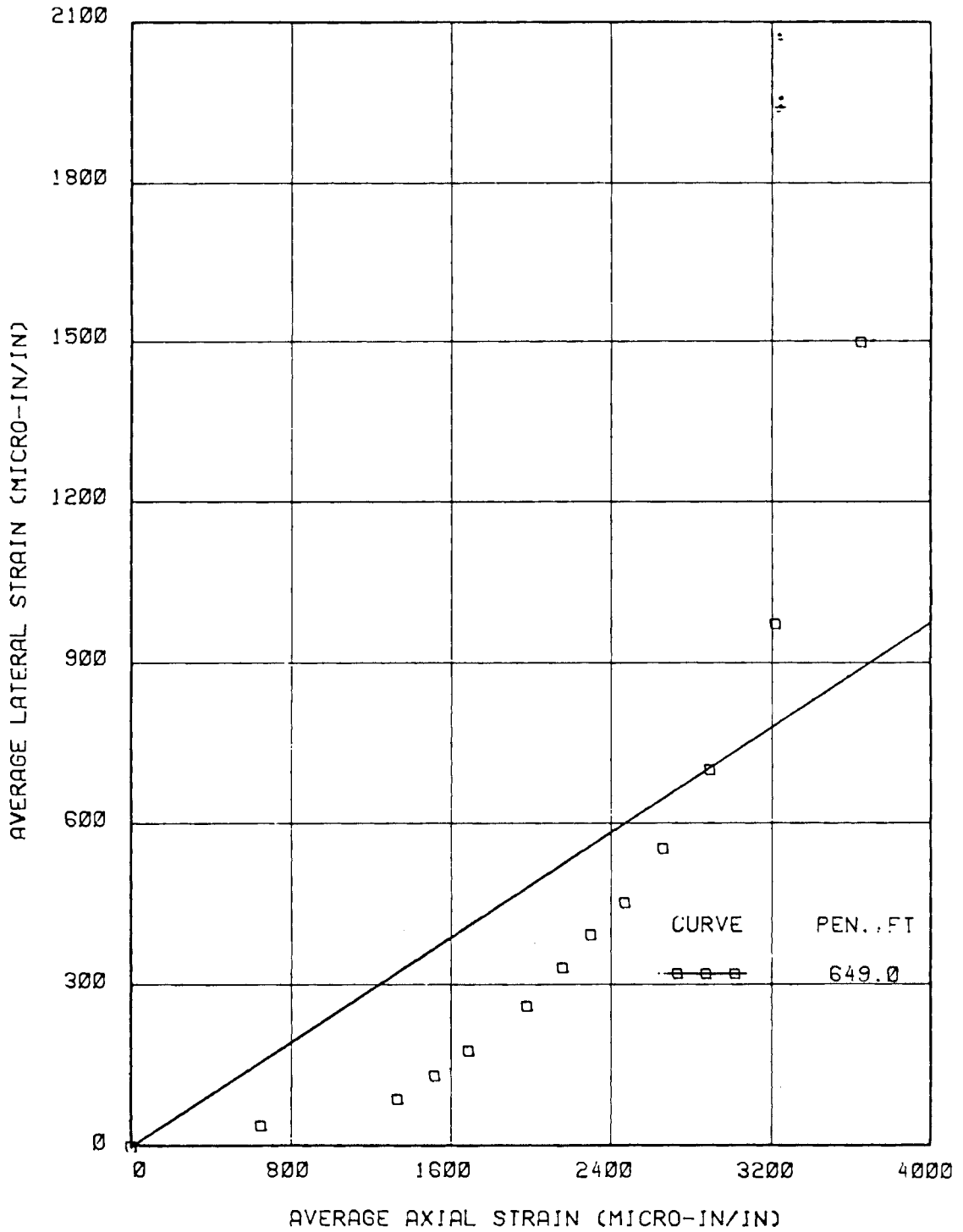
STRESS-STRAIN CURVE

UNCONFINED COMPRESSION TEST

SAMPLE D

MAXIMUM STRESS = 1466 KSF

FIGURE A-20



LATERAL VS AXIAL STRAIN

UNCONFINED COMPRESSION TEST

SAMPLE D

SLOPE = 0.245

TABLE A-13

UNCONFINED COMPRESSION TEST ON ROCK

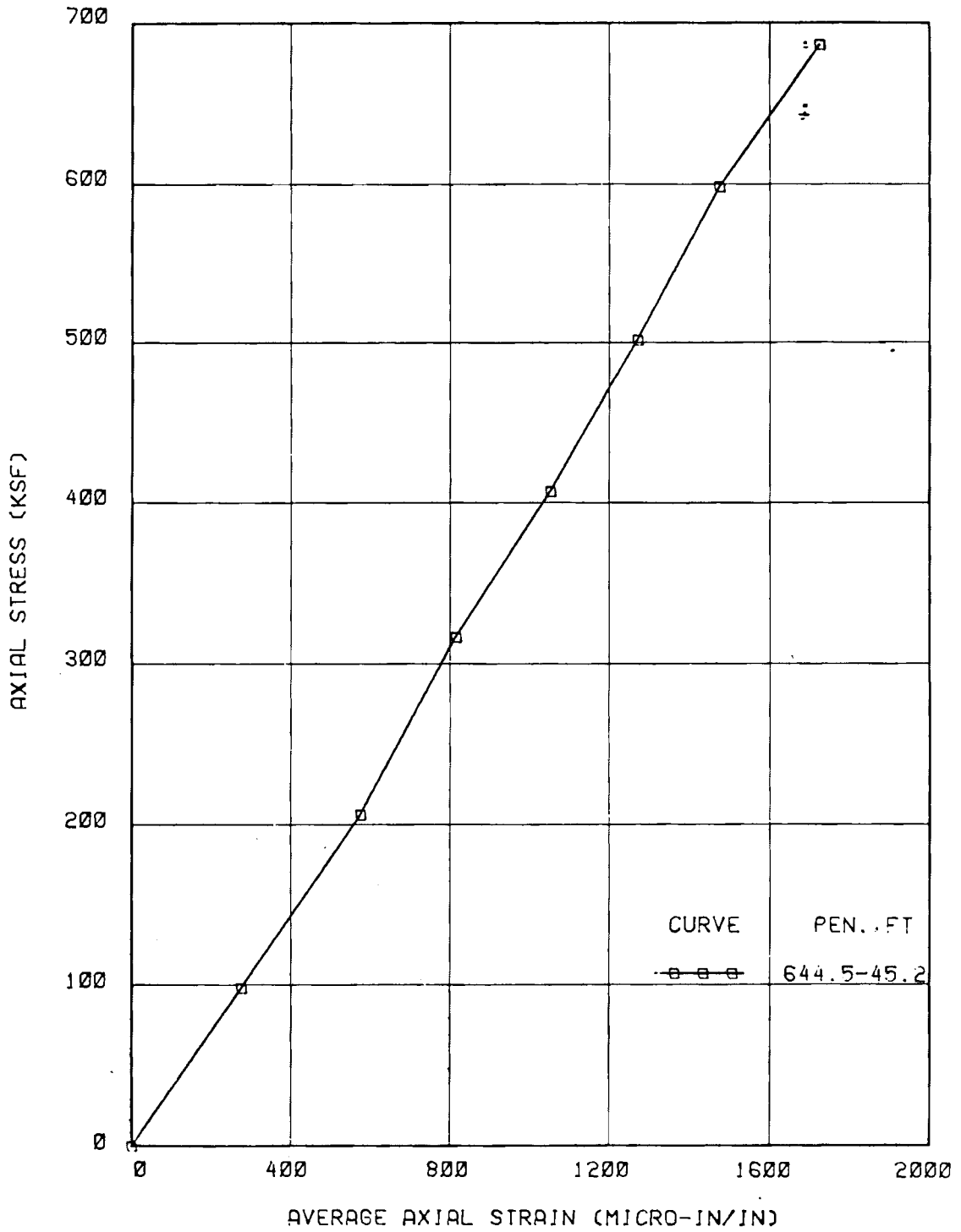
SPECIMEN : 1W PENETRATION(FT) : 644.5-645.2

LENGTH (mm) = 163.98 DIAMETER (mm) = 75.35 BULK DENSITY (pcf) = 141.3
 LOAD CONSTANT (1b-F/mv) = 9434

VERT STRAIN (mIN/IN)				AXIAL STRAIN (mIN/IN)				LOAD (mv)	// V STRAIN(mIN/IN)	A STRAIN(mIN/IN)	STRESS(ksf)
#1	#1(z)	#2	#2(z)	#1	#1(z)	#2	#2(z)	(z)	// (av)	(av)	
-18	0	-20	0	12	0	40	0	-0.05	0.00	// 0.0	0.0
8	26	15	35	212	200	384	344	0.45	0.50	// 30.5	272.0
58	76	49	69	436	424	752	712	1.00	1.05	// 72.5	568.0
115	133	86	106	596	584	1065	1025	1.56	1.61	// 119.5	804.5
204	222	156	176	809	797	1319	1279	2.02	2.07	// 199.0	1038.0
307	325	203	223	992	980	1570	1530	2.50	2.55	// 274.0	1255.0
409	427	262	282	1120	1108	1844	1804	2.99	3.04	// 354.5	1456.0
558	576	321	341	1367	1355	2094	2054	3.44	3.49	// 458.5	1704.5

MAXIMUM available STRESS (=) 784 ksf

FIGURE A-21



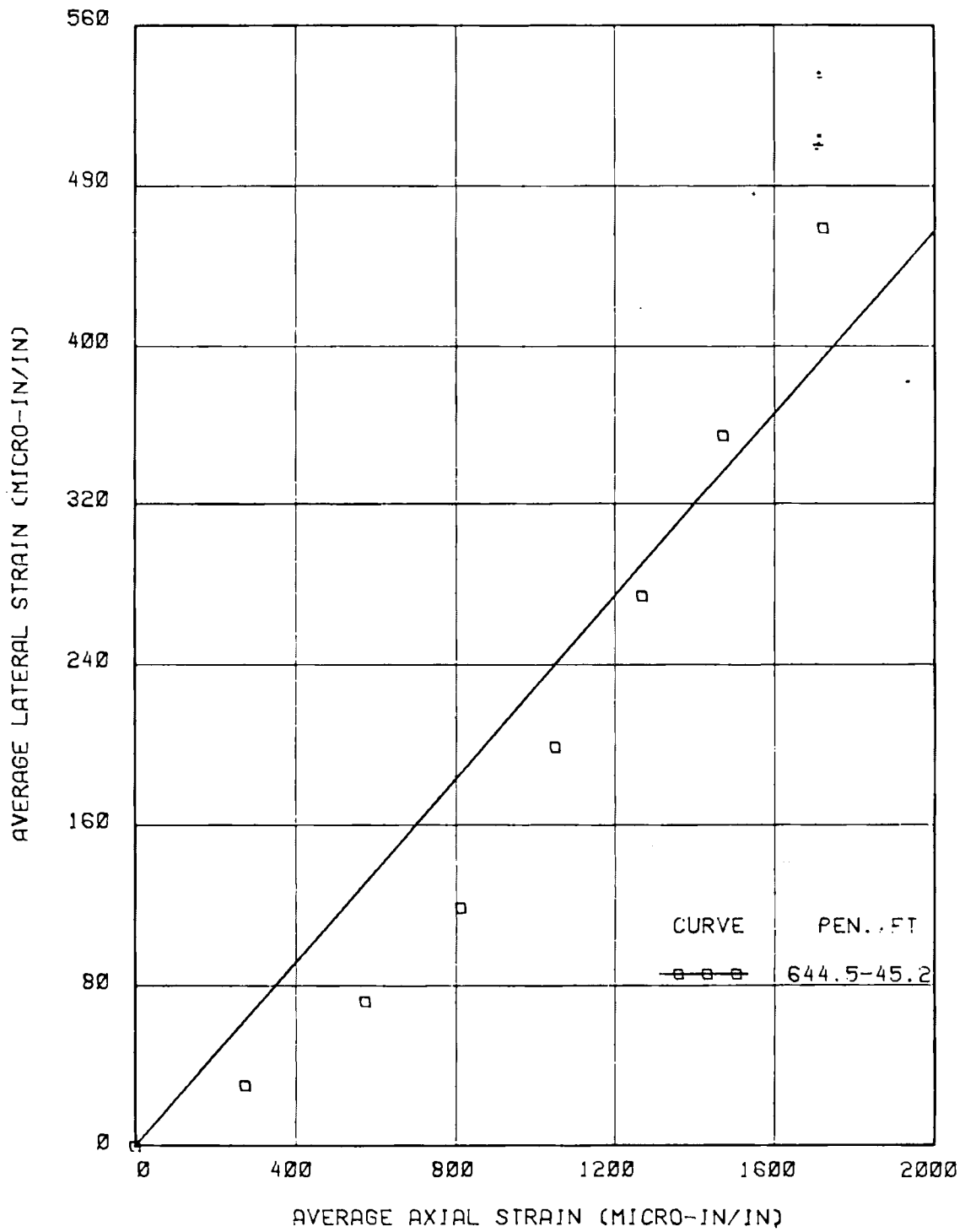
STRESS-STRAIN CURVE

UNCONFINED COMPRESSION TEST

SAMPLE 1W

MAXIMUM STRESS = 784 KSF

FIGURE A-22



LATERAL VS AXIAL STRAIN

UNCONFINED COMPRESSION TEST

SAMPLE 1W

SLOPE = 0.229

TABLE A-14

UNCONFINED COMPRESSION TEST ON ROCK

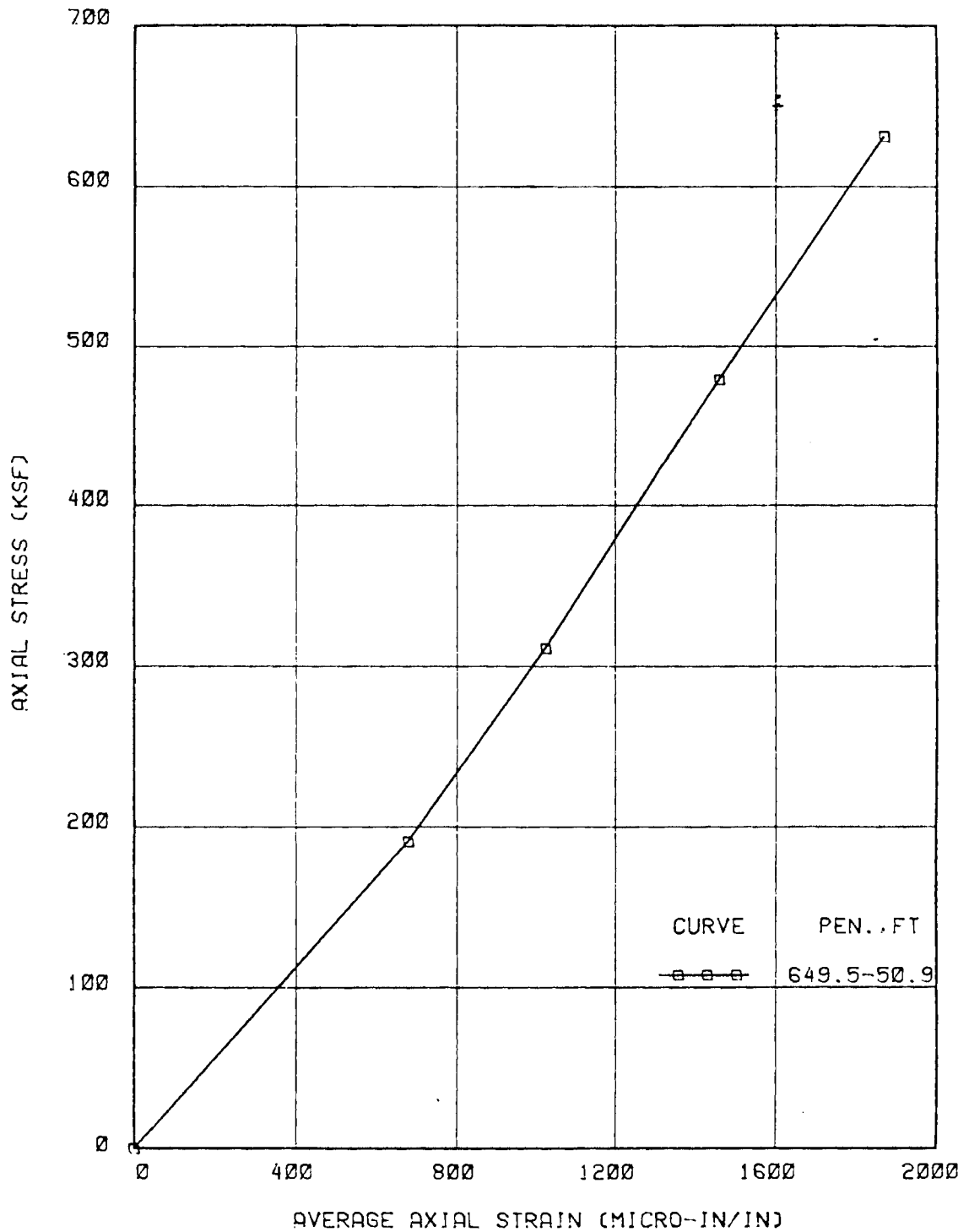
SPECIMEN : 1W PENETRATION(FT) : 649.5-650.9

LENGTH (mm) = 165.6 DIAMETER (mm) = 75.3 BULK DENSITY (pcf) = 130.9
 LOAD CONSTANT (lb-F/mv) = 9434

VERT STRAIN (mIN/IN)				AXIAL STRAIN (mIN/IN)				LOAD (mv)	// V STRAIN(mIN/IN)	A STRAIN(mIN/IN)	STRESS(ksf)
#1	#1(z)	#2	#2(z)	#1	#1(z)	#2	#2(z)	(z)	// (av)	(av)	
3290	0	930	0	-2028	0	-1594	0	-0.05	0.00 //	0.0	0.0
3389	99	1004	74	-1209	819	-1068	526	0.92	0.97 //	86.5	672.5
3416	126	1045	115	-853	1175	-740	854	1.53	1.58 //	120.5	1014.5
3496	206	1156	226	-415	1613	-314	1280	2.38	2.43 //	216.0	1446.5
3576	286	1290	360	0	2028	80	1674	3.15	3.20 //	323.0	1851.0

A-37
 MAXIMUM available STRESS (=) 640 ksf

FIGURE A-23



STRESS-STRAIN CURVE

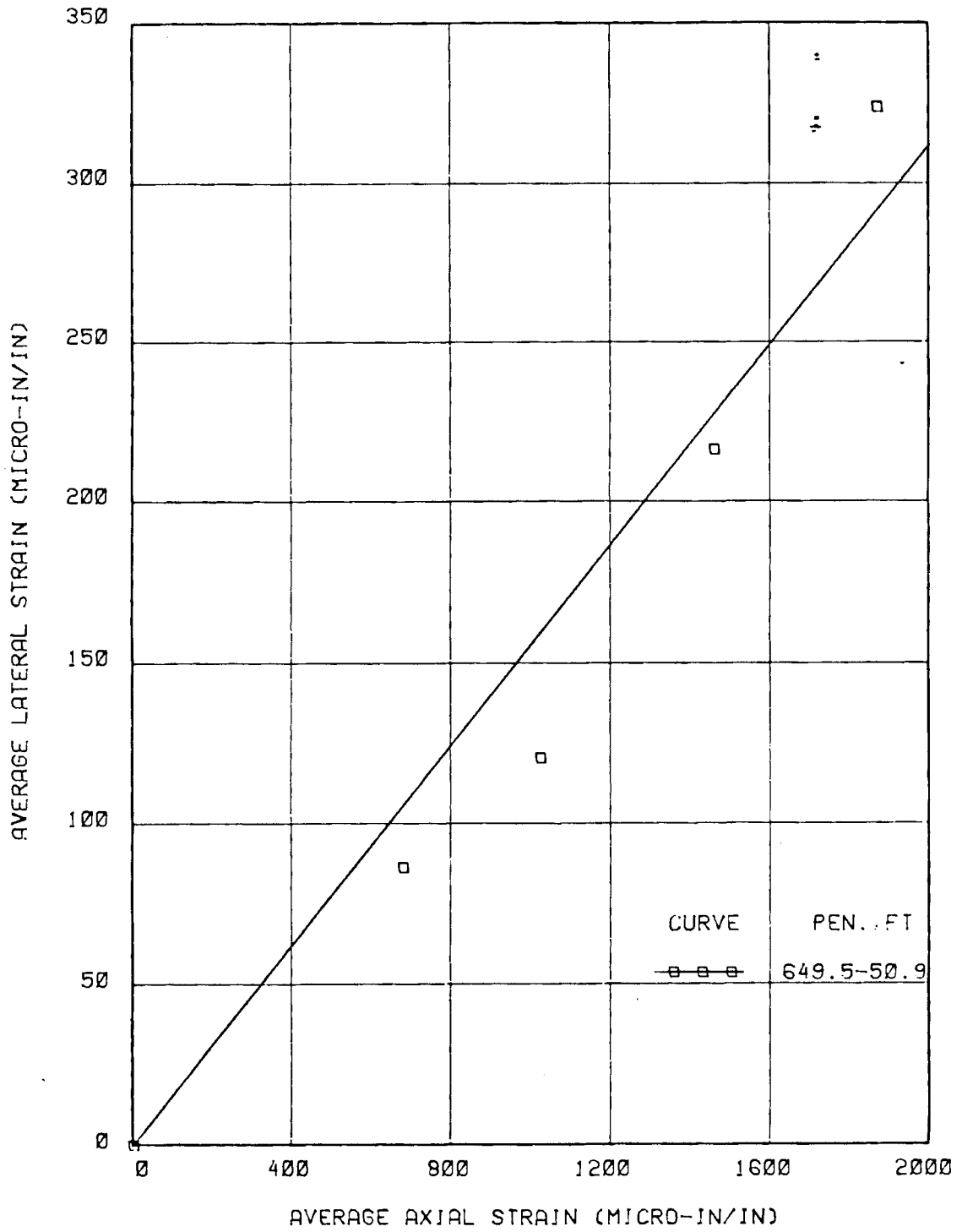
UNCONFINED COMPRESSION TEST

SAMPLE 1W

MAXIMUM STRESS = 640 KSF

0181-0411

FIGURE A-24



LATERAL VS AXIAL STRAIN

UNCONFINED COMPRESSION TEST

SAMPLE 1W

SLOPE = 0.156

TABLE A-15

UNCONFINED COMPRESSION TEST ON ROCK

SPECIMEN : 1W PENETRATION(FT) : 652.0

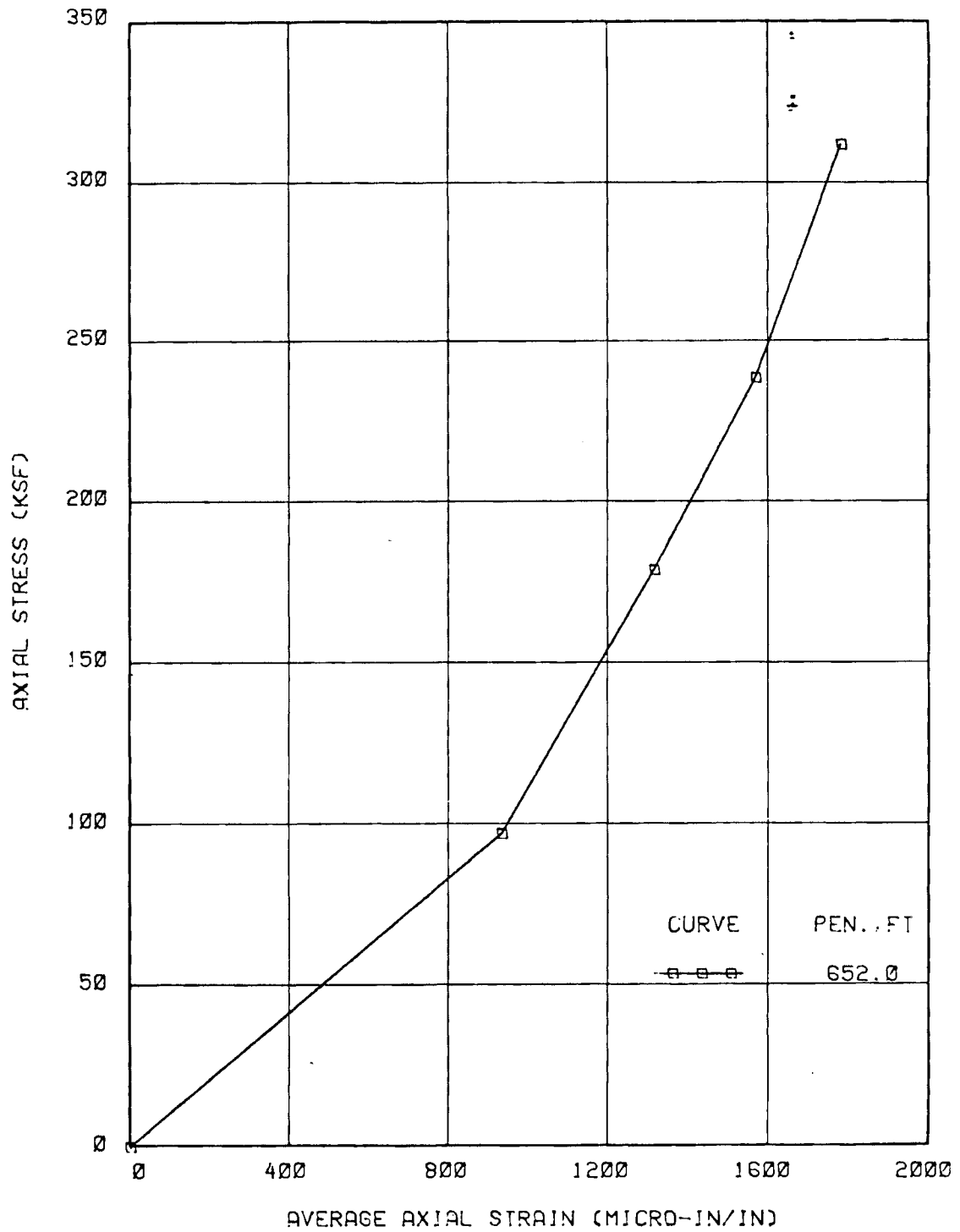
LENGTH (mm) = 149.72 DIAMETER (mm) = 75 BULK DENSITY (pcf) = 144.2
 LOAD CONSTANT (lb-F/mv) = 9434

VERT STRAIN (mIN/IN)				AXIAL STRAIN (mIN/IN)				LOAD (mv)	// V STRAIN(mIN/IN)	A STRAIN(mIN/IN)	STRESS(ksf)
#1	#1(z)	#2	#2(z)	#1	#1(z)	#2	#2(z)	(z)	// (av)	(av)	
-180	0	-813	0	-231	0	156	0	-0.05	0.00 //	0.0	0.0
-39	141	-506	307	548	779	1224	1068	0.44	0.49 //	224.0	923.5
79	259	-220	593	925	1156	1599	1443	0.85	0.90 //	426.0	1299.5
131	311	77	890	1175	1406	1847	1691	1.15	1.20 //	600.5	1548.5
268	448	522	1335	1423	1654	2018	1862	1.52	1.57 //	891.5	1758.0

MAXIMUM available STRESS (=) 319 ksf

81-0411

FIGURE A-25



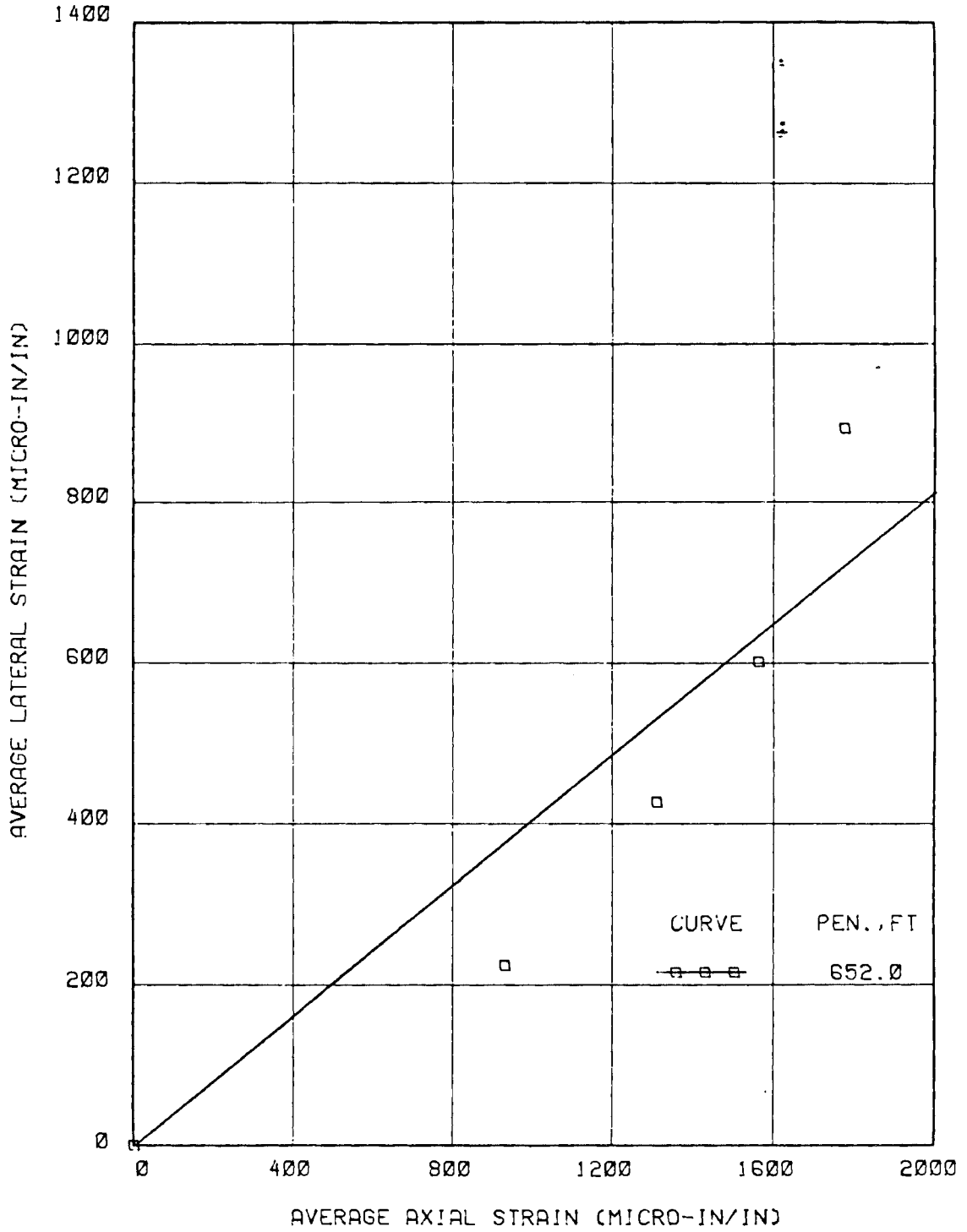
STRESS-STRAIN CURVE

UNCONFINED COMPRESSION TEST

SAMPLE 1W

MAXIMUM STRESS = 319 KSF

FIGURE A-26



LATERAL VS AXIAL STRAIN

UNCONFINED COMPRESSION TEST

SAMPLE 1W

SLOPE = 0.406

TABLE A-16

UNCONFINED COMPRESSION TEST ON ROCK

SPECIMEN : 1W PENETRATION(FT) : 666.0

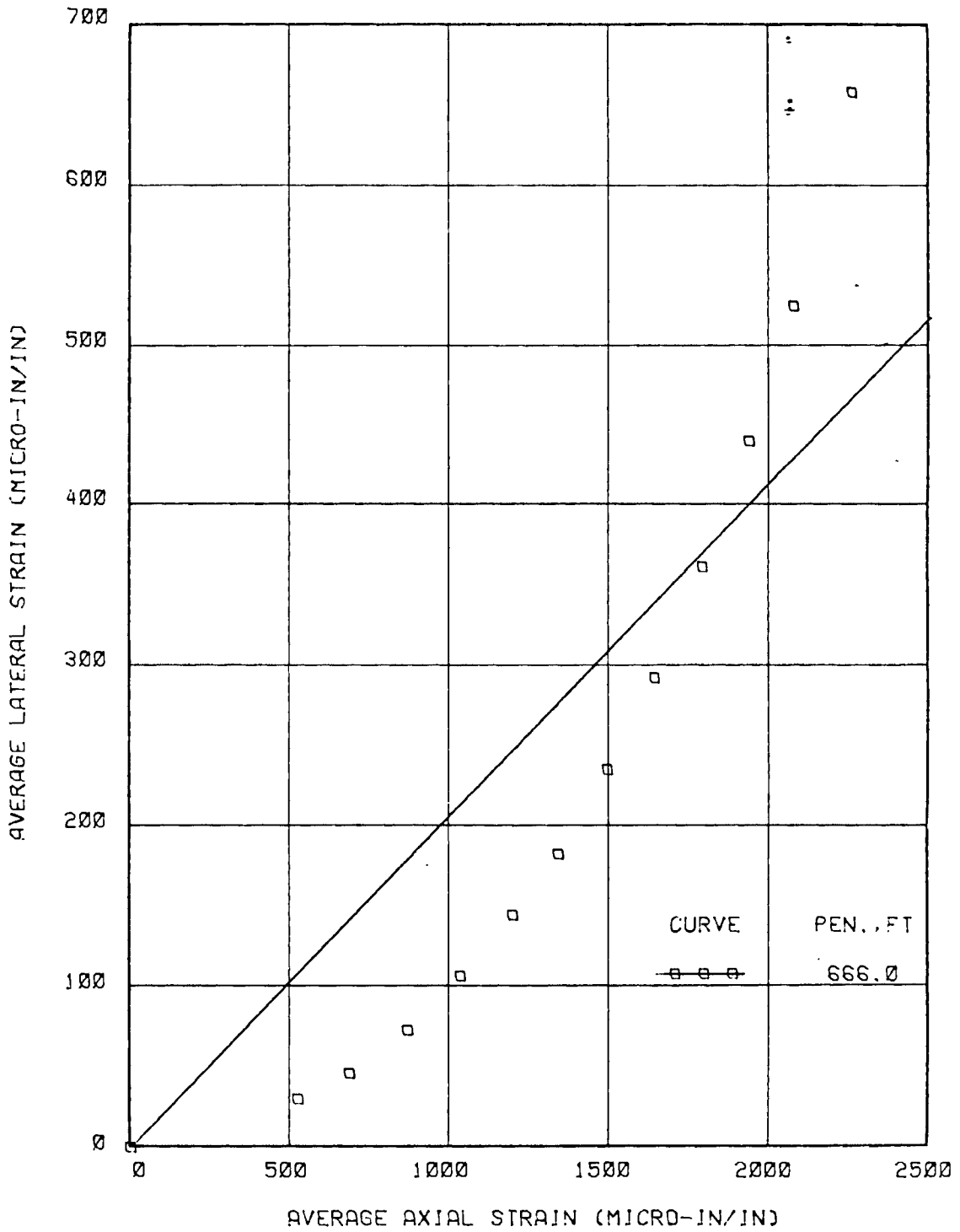
LENGTH (mm) = 162.84 DIAMETER (mm) = 75.5 BULK DENSITY (pcf) = 139.6
 LOAD CONSTANT (lb-F/mv) = 9434

VERT STRAIN (mIN/IN)				AXIAL STRAIN (mIN/IN)				LOAD (mv)	// V STRAIN(mIN/IN)	A STRAIN(mIN/IN)	STRESS(ksf)
#1	#1(z)	#2	#2(z)	#1	#1(z)	#2	#2(z)	(z)	// (av)	(av)	
0	0	-9	0	3	0	-2	0	-0.05	0.00 //	0.0	0.0
21	21	30	39	528	525	510	512	0.65	0.70 //	30.0	137.0
34	34	49	58	700	697	658	660	0.98	1.03 //	46.0	201.6
60	60	76	85	912	909	808	810	1.45	1.50 //	72.5	293.6
99	99	104	113	1103	1100	940	942	1.96	2.01 //	106.0	393.5
139	139	140	149	1289	1286	1072	1074	2.46	2.51 //	144.0	491.4
189	189	166	175	1462	1459	1187	1189	2.95	3.00 //	182.0	587.3
254	254	206	215	1643	1640	1306	1308	3.47	3.52 //	234.5	689.1
327	327	247	256	1817	1814	1420	1422	3.95	4.00 //	291.5	783.0
414	414	298	307	1998	1995	1537	1539	4.47	4.52 //	360.5	884.8
520	520	349	358	2181	2178	1642	1644	4.97	5.02 //	439.0	982.7
634	634	405	414	2350	2347	1748	1750	5.41	5.46 //	524.0	1068.8
819	819	485	494	2580	2577	1880	1882	6.00	6.05 //	656.5	1184.3

MAXIMUM available STRESS (=) 1351 ksf

A-43

FIGURE A-27



LATERAL VS AXIAL STRAIN

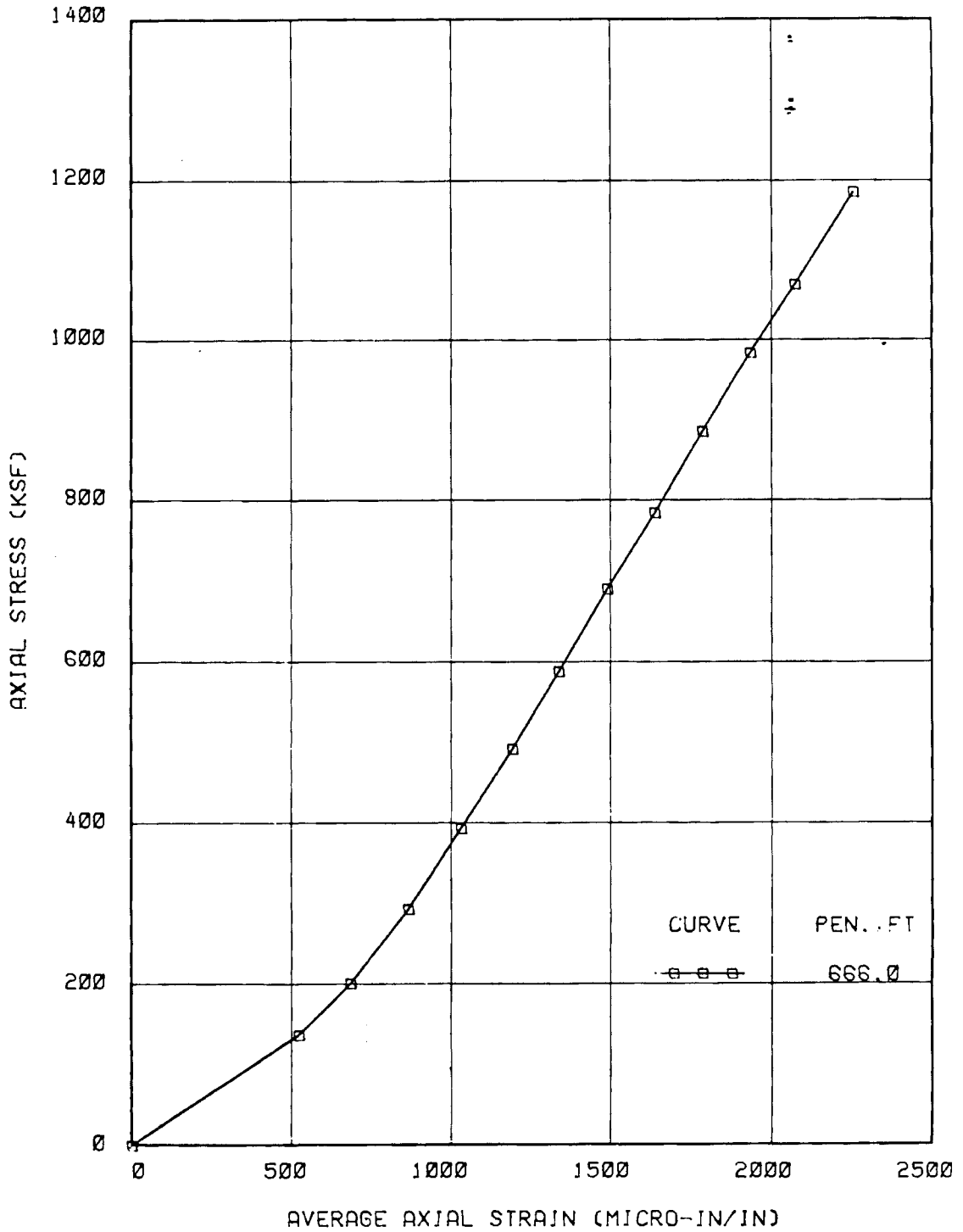
UNCONFINED COMPRESSION TEST

SAMPLE 1W

SLOPE = 0.207

181-0411

FIGURE A-28



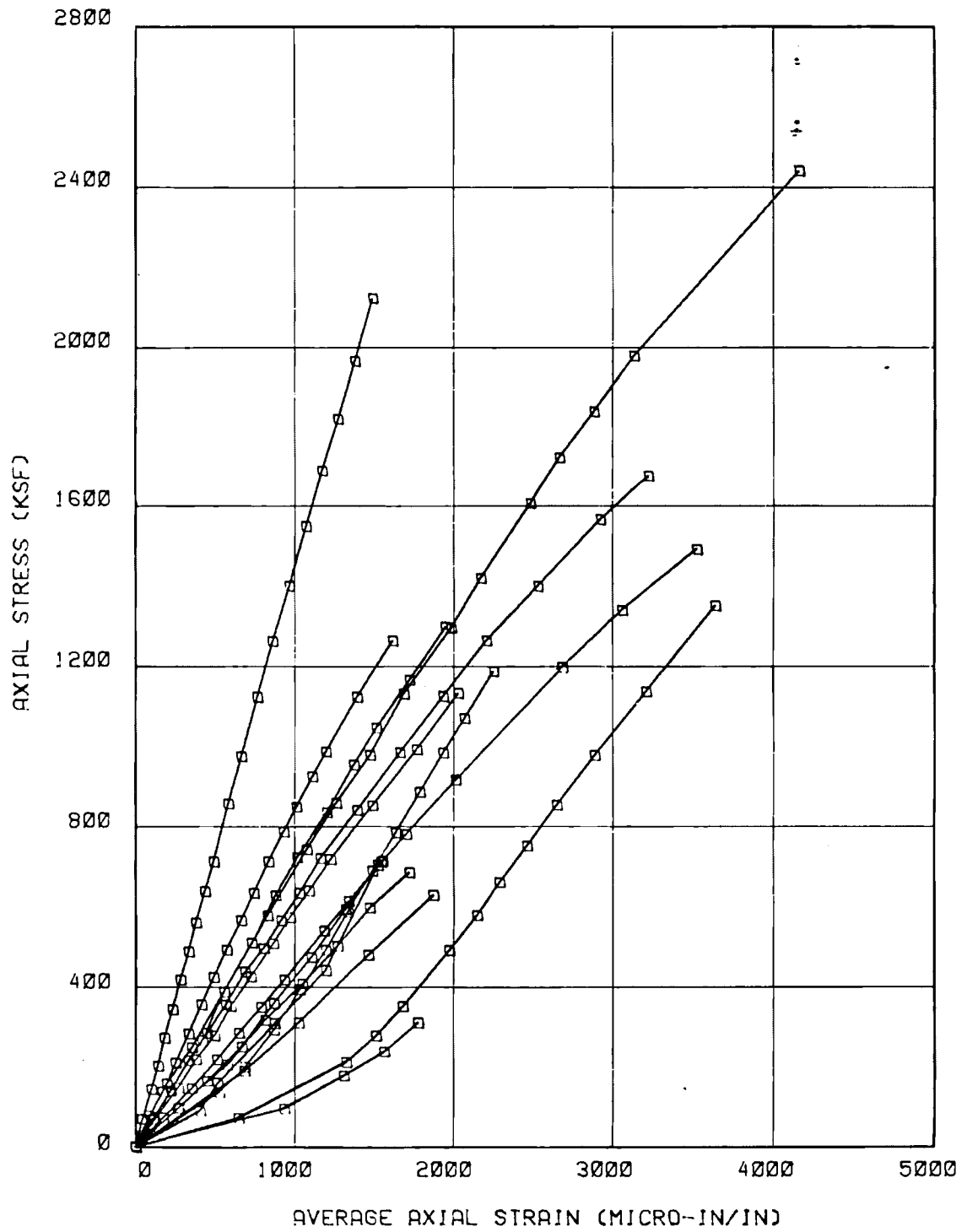
STRESS-STRAIN CURVE

UNCONFINED COMPRESSION TEST

SAMPLE 1W

MAXIMUM STRESS = 1351 KSF

FIGURE A-29



STRESS-STRAIN CURVES
UNCONFINED COMPRESSION TESTS

DISTRIBUTION

<u>No of Copies</u>		<u>No of Copies</u>	
	<u>OFFSITE</u>	2	PB-KBB Inc. Attn: J. Istvan PO Box 19672 Houston, TX 77024
	US Department of Energy Attn: I. Gyuk Office of Energy Systems Res. Forrestal Bldg., CE-141 5E-052 Washington, DC 20585		Potomac Electric Power Co. Attn: P. E. Schaub 1900 Pennsylvania Ave Washington, DC 20006
	US Department of Energy Attn: R. Shivers Office of Energy Systems Res. Forrestal Bldg., CE-141 5E-052 Washington, DC 20585		Public Service of Indiana Attn: T. W. McCafferty 1000 E. Main Street Plainfield, IN 46168
	US Department of Energy Attn: J. H. Swisher Office of Energy Systems Res. Forrestal Bldg., CE-141 5E-052 Washington, DC 20585		Sargent and Lundy Engineers Attn: W. C. Walke Project Manager 55 East Monroe Street Chicago, IL 60603
27	DOE Technical Information Center		Union Electric Co. Attn: H.C. Allen Vice President Research & Development PO Box 149 St. Louis, MO 63166
	Acres American, Inc. Attn: C. Driggs The Clark Building Suite 329 Columbia, MD 21044		University of Massachusetts Attn: O. C. Farquhar Dept. of Geology & Geography Morrill Science Center Amherst, MA 01003
	Electric Power Research Inst. Attn: R. B. Schainker 3412 Hillview Avenue PO Box 10412 Palo Alto, CA 94303		University of Michigan Attn: Donald L. Katz Dept. of Chemical Eng. 2042 E. Engr. Bldg. Ann Arbor, MI 48109
	Illinois Power Company Attn: G. E. Huck Manager of Planning 500 South 27th St. Decatur, IL 62525		

No of
Copies

University of Wisconsin
Attn: H. J. Pincus
Dept. of Geological Sciences
Sabin Hall and Greene Museum
PO Box 413
Milwaukee, WI 53201

Westinghouse Electric Corp.
Attn: W. F. Kobett
CAES Project Manager
Combustion Turbine Sys. Div.
Long Range Develop-Lab 100
PO Box 251
Concordville, PA 19331

ONSITE

DOE Richland Operations Office

H.E. Ransom/D.R. Segna

Pacific Northwest Laboratory

L.D. Kannberg (5)
Technical Information (5)
Publishing Coordination (2)